Optimization of Coalbed Methane Completion Strategies, Selection Criteria and Production Prediction: A Case Study in China's Qinshui Basin

Steven Anthony Keim

Dissertation submitted to the faculty of the
Virginia Polytechnic Institute and State University
in partial fulfillment of the requirements for the degree of

Doctor of Philosophy
In
Mining Engineering

Michael E. Karmis
Kramer D. Luxbacher
Gerald H. Luttrell
Claudio F. Santos
Erik C. Westman

August 18, 2011
Blacksburg, VA

Keywords: coalbed methane, reservoir modeling, Qinshui Basin

Optimization of Coalbed Methane Completion Strategies, Selection Criteria and Production Prediction: A Case Study in China's Qinshui Basin

Steven Anthony Keim

Abstract

Advanced three-dimensional reservoir modeling was used to determine the optimum strategy for coalbed methane production in China's Qinshui Basin. Multiple completion strategies were analyzed for pre-mining methane drainage on the bases of economic, environmental, and mining-safety-based factors. Effective degasification in the Qinshui Basin is crucial to enhance the health and safety of the underground mining workforce and to decrease carbon dioxide equivalent greenhouse gas emissions. Active, large-scale degasification wells in the region include hydraulically stimulated vertical fracture wells and multilaterally drilled horizontal patterns, with the latter much less common.

Reservoir modeling concludes that despite their limited implementation, horizontal coalbed methane drainage wells offer the benefits of faster reservoir depressurization, high gas production rates, and faster recovery times than traditional vertical fracture wells. Coupled with reservoir modeling results, discounted cash flow analyses show that high drilling density multilateral horizontal patterns are the most financially feasible degasification strategy in the Qinshui Basin, albeit a higher initial capital investment compared to traditional vertical fracture wells and lower drilling density horizontal patterns. Additionally, horizontal wellbore designs

can be altered to account for varying permeability, enhancing the productivity of methane from reservoirs exhibiting permeability values less than 1 millidarcy. Furthermore, modeling suggests that proper orientation of select horizontal wellbore patterns is crucial to optimize recoverable reserves.

Finally, a function was derived to represent the production rates of horizontal coalbed methane wells as a function of time. Analysis of the function's validity to actual production data and simulated production data suggest that it is most applicable in gassy coal seams up to 10 feet in thickness. The production rate curve was transformed to an analytical model, representing a function of well geometry and coal permeability as applied to other geological conditions of the Qinshui Basin.

Scientific contributions associated with this research include: An in depth study of degasification associated with the Qinshui Basin's low permeability coals; The methodology for assessing environmental, safety and economic benefits of coal degasification; The relationship between lateral spacing and permeability to maintain substantial gas production rates; An improved production model to describe the entire producing period of coalbed methane wells.

Acknowledgements

Without the support and influence of many other individuals, this work would not have been possible. I would like to thank my academic advisors, Dr. Kray Luxbacher and Dr. Michael Karmis for granting me the opportunity to continue my education. Both Dr. Kray Luxbacher and Dr. Michael Karmis have provided invaluable insight and advice over the course of the past several years, and for that, I am grateful. I would also like to acknowledge my other committee members, Dr. Jerry Luttrell, Dr. Erik Westman and Dr. Claudio Faria. These gentlemen have been very influential to me in my desire to pursue a doctorate degree and have been excellent role models for many years.

I would also like to thank Dr. Nino Ripepi and Steve Schafrik of the Virginia Center for Coal and Energy Research for technical insight and advice. Rhonda White, Ryan Belcher, Dave Arnold, George Oberlick, Charlie Schlosser, Matt Conrad and Mike Miller, all of Marshall Miller and Associates, have provided aid on many levels throughout the course of this work.

I also owe my friends a sincere thank-you for support throughout my education. Lastly, I would like to thank my family, Tom, Mom, and Dad. They have always believed in me and encouraged me to do my best.

Finally, I would like to acknowledge the United States Environmental Protection Agency for project funding. Pamela Franklin and Felica Ruiz of the EPA's Global Methane Initiative have been very supportive throughout this work.

Table of Contents

List of Figures

List of Tables

Chapter 1. INTRODUCTION

Preface

This dissertation contains three primary documents which have either been submitted to scholarly journals or are ready for submittal. Additionally, a literature review pertaining to fundamental coalbed methane concepts and background research directly related to the study area is included. Chapter 2, *A numerical study on optimization of multilateral horizontal wellbore patterns for coalbed methane production in Southern Shanxi Province, China*, has been accepted and published in the International Journal of Coal Geology. Dr. Michael Karmis and Dr. Kray Luxbacher served as co-authors in this work, and are acknowledged as such at the beginning of the chapter.

A contractual agreement between the United States Environmental Protection Agency (USEPA) and the Virginia Center for Coal and Energy Research (VCCER) necessitated the development of a document titled *A Regional Handbook for Coalbed Mehane Degasification in the Southern Shanxi Province, China.* A number of concepts and methodologies developed in this dissertation are also included in the aforementioned handbook.

1.1. Background

The Qinshui Basin's thick, high-methane-content coal seams necessitate innovative degasification strategies for effective gas drainage. While demonstrated production has occurred recently, ongoing research and development offers the potential to increase the Qinshui Basin's reserve base and provide a sustained, clean energy source for residential and commercial applications. Through a United States Environmental Protection Agency (USEPA) funded research project, a greenfield coalbed-methane-bearing property in the Southern Shanxi Province was analyzed. A portion of the research associated with this project was outlined in three individual manuscripts for submittal in peer-reviewed journals, one of which has been accepted and published. This dissertation includes the research objectives of the project, a literature review of fundamental coalbed methane concepts and previous published works related to coalbed methane in the Qinshui Basin, and the developed manuscripts for submittal to scholarly journals.

1.2. Research Objectives

Three primary research objectives were defined at the beginning of the research project. The objectives are designed such that outcomes of the research will benefit entities with interest in the development of the Qinshui Basin's coalbed methane resource. These objectives are listed below and outlined in detail in the following sections.

- Research Objective 1: Outline the selection criteria for well completion strategy as applied to pre-mining coalbed methane drainage wells.
- Research Objective 2: Investigate the impact of individual lateral spacing for multilaterally drilled horizontal coalbed methane wells in low permeability reservoirs.
- Research Objective 3: Develop an equation which describes the shape of a multilaterally drilled horizontal coalbed methane wells.

1.2.1. Research Objective 1

China's coalbed methane industry has grown significantly in the past 10 years. To date, more than 2,500 coalbed methane wells have been drilled, representing a tenfold increase in numbers from only a decade ago (Sang et al., 2009; Luo et al., 2009). Less than 30 multilaterally drilled horizontal wells have been completed, likely attributed to higher capital costs (Luo et al., 2009). The reported permeability figures in the Qinshui Basin, in the range of 0.1 to 2.0 millidarcies (md) (Su et al., 2005; Yao et al., 2008), reflect values where horizontal wells become applicable (Palmer, 2010).

The methodology for optimizing coalbed methane completions must be analyzed in accordance with environmental, economic, and mine-safety-based factors. While the ultimate goal is to increase production, pre-mining wells must drain the reservoir so no high-gas-content pockets or zones remain. When draining gas ahead of mining, poor gas recovery values decrease the safety conditions at the working face of a mine. Directly applied to Chinese coal mine

safety, the need for research in degasification technologies is crucial. China's reported mining fatality rate exceeds that of the United States by a factor of 100 (Wei, 2009; Lu and Li, 2011). This research identifies the optimum strategy to degasify coals ahead of mining, thus decreasing methane concentrations in underground coal mines.

Methane's heat-trapping capabilities are 23 times greater than those of carbon dioxide (Seinfeld and Pandis, 2006). A recent initiative by the United States Environmental Protection Agency has prompted research to help nations quantify, recover, and utilize their methane resources. A significant energy source exists in the coals of the Qinshui Basin. While recovering methane greatly enhances the health and safety of the underground workforce, a significant reduction in greenhouse gas emissions can also be accomplished while simultaneously providing communities with an economic energy source. As an outcome of this research, the reduction in carbon-dioxide equivalent emissions associated with coal degasification will be calculated in accordance with the coal geology of the Qinshui Basin. This represents a significant component of Research Objective 1.

1.2.2. Research Objective 2

Success has been noted in the Qinshui Basin through the use of herringbone and fishbone horizontal drilling patterns (Zhiming and Zhang, 2009). An endless number of horizontal patterns exist which can be optimized to account for varying geological conditions. Increasing the drilling density of horizontal laterals in coal seams offers the ability to recover gas from low permeability coal beds. A primary goal of this research involves defining the relationship between horizontal drilling density and coal seam permeability. This relationship will provide a measure of the viability of low permeability coals, as an economic cutoff exists where higher costs associated with increased drilling lengths are not offset by increased production.

Additionally, permeability values generally differ according to direction. Optimizing well orientation to take advantage of the higher directional permeability values can greatly increase the recoverable reserve base associated with horizontal well development. The research analyzes common horizontal wellbore patterns on a directional basis such that production can be optimized by proper orientation. Horizontal wellbore patterns are also analyzed in accordance with their risk for catastrophic borehole collapse. Great risks associated with multi-million dollar capital investments for horizontal well development exist, as wells can effectively be rendered inoperable by borehole collapse and failure.

1.2.3. Research Objective 3

Decline curve analysis focuses on production rates associated with petroleum production following a peak production rate. Coalbed methane wells must be dewatered to initiate gas flow. Generally production rate curves spike followed by a standard decline. Analysis of the decline portion of the curve does not incorporate any information pertaining to the early portion of coalbed methane production. A primary objective of this research is to develop a function which represents the entire producing period of a coalbed methane well over time. The function's applicability to real world data and simulated reservoir data is tested, pinpointing its range of applicability in various geological conditions. Additionally, the function's capability to serve as an analytical production model is investigated.

Chapter 1 References

Lu Y., Li., X. 2011. A study on a new hazard detecting and controlling method: The case of coal mining companies in China. Safety Science. 49. 279-285.

Luo, D., Chu, W., Wu, X., Li, W. 2009. Analysis of economic benefits of coalbed methane drilling technologies. Petroleum Exploration and Development. 36(3). 403-407.Sang et al., 2009

Seinfeld, J. and Pandis, S. 2006. Atmospheric chemistry and physics, 2nd edition. published by John Wiley & Sons, Hoboken, NJ.

Su, X., Lin, X., Liu, S., Zhao, M., Song, Y. 2005. Geology of coalbed methane reservoirs in the Southeast Qinshui Basin of China. International Journal of Coal Geology. 62. 197-210.

Yao, Y., Liu, D., Tang, D., Huang, W., Tang, S., and Che, Y. 2008. A Comprehensive Model for Evaluating Coalbed Methane Reservoirs in China. Acta Geol. Sin-Engl. 82 (6). 1253-1270.Wei, 2009

Zhiming, W., Zhang, J., 2009. CBM reservoir thickness affects production from horizontal wells. Oil and Gas Journal. 107(16). 42-46.

Chapter 2. LITERATURE REVIEW

2.1. Gas Storage and Transport Theory

2.1.1. Gas Storage in Coal

Methane is stored in coal as either a free gas or in the adsorbed state (McPherson, 1993). Harpalani (1984) determined that the overwhelming majority (up to 98 percent) of gas is stored via the adsorbed state. Dutta et al. (2007) outline the multiple models which are used to describe the adsorption of methane within the internal coal structure, including theoretical models (Langmuir Model, the BET multi-layer model, Dubinin's pore-filling model) and empirical models (Langmuir-Freundlich, Toth, UNILAN, and modified BET). Despite the multiple theoretically and empirically-derived models, the Langmuir-based theoretical models are generally applied in coalbed methane reservoir engineering (Pan and Connell, 2009).

As discussed by Garnier et al. (2011), the Langmuir Isotherm relationship assumes that coal surfaces are homogeneous, that adsorption is a reversible process, and that gas is stored as a single layer against the coal surface. Based on these assumptions, the Langmuir model as applied to a single gas can be derived from the original work of Irving Langmuir (1918) as outlined by Pan and Connell (2009):

$$V = \frac{V_L(BP)}{1+BP} \qquad \text{(Equation 2.1)}$$

In Equation 2.1, V represents the volume of gas which can be adsorbed to the coal at various pressures, P. B represents the Langmuir constant, and V_L represents the Langmuir Volume. Aminian and Ameri (2009) describe the physical meaning of the constants, including the Langmuir Volume and Langmuir Pressure. The Langmuir Volume (V_L) represents the maximum volume of gas which can be adsorbed to coal. The Langmuir Pressure (P_L) is

equivalent to the inverse of the Langmuir constant (*B*) described in Equation 2.1 and represents the pressure corresponding to one-half of the Langmuir Volume.

Pan and Connell (2009) discuss the extended Langmuir Isotherm for the simultaneous sorption of multiple gasses to a coal's surface. This relationship is shown below in Equation 2.2.

$$V_i = \frac{V_{L,i}(B_i P y_i)}{1+\sum_{j=1}^{N} B_j P y_j} \qquad \text{(Equation 2.2)}$$

In Equation 2.2, the subscripts *i* and *j* represent the gas components, and *y* represents the molar fraction of each constituent. *N* represents the number of gas components in the system.

2.1.2. Gas Transport in Coal

The flow of gas within coal beds is well understood to be two-phase process as verified by Griffin (1978), Creedy (1985), and Barker-Read (1984). Ahmed and McKinney (2005) describe the process as having four steps, including an initial dewatering phase and desorption phase, yet the latter two stages are the same as those commonly recognized by others. Following desorption, as outlined by Harris et al. (1996), a two-phase model developed by Airey (1968) describes gas flow in coal beds. The initial phase of Airey's model is based upon Fick's Law of Diffusion where gas migration is directly related to pressure gradients in the coal's pore structure. Airey's model is summarized below in Equation 2.3.

$$Q_t = Q_0 \left[1 - \frac{6}{\pi^2} \exp\left(-\frac{2\pi^2 Dt}{d^2}\right)\right] \qquad \text{(Equation 2.3)}$$

In Equation 2.3, Q_t represents the quantity of gas lost in the time, *t*, from a coal with an initial gas content Q_o. The diffusion constant is recognized by *D,* and *d* represents the mean diffusion distance. Recent variations of Airey's model based on Fick's Law of Diffusion simplify the

model into additional components which can easily be manipulated during modeling. Ziarani et al. (2011) state the matrix transport equation shown below in Equation 2.4.

$$\frac{dC_m}{dt} = \sigma D(C_E - C_m) \quad \text{(Equation 2.4)}$$

In Equation 2.4, dC_m/dt represents the gas flow rate through the matrix. The matrix shape factor is described by σ. D is the diffusion coefficient. C_E and C_m, respectively, represent the adsorbed gas concentration on the surface of micropores and the average gas concentration within the micropores. As stated by Ziarani et al. (2011), Equation 2.4 can be simplified to simultaneously account for the effects of geometry and the diffusion coefficient by substituting sorption time into the equation. Sorption time is shown in Equation 2.5.

$$\tau = \frac{1}{\sigma D} \quad \text{(Equation 2.5)}$$

As recognized by Ziarani et al. (2011), the sorption time (τ) corresponds with the amount of time for 63.2 percent of methane to desorb from a coal sample under constant pressure and temperature conditions. This calculation is best completed during gas-content canister testing where coal cores are placed in canisters to measure the amount of gas desorbing from the coal over time during exploratory coalbed methane drilling (Ahmed and McKinney, 2005). Smith and Williams (1984) developed a laboratory method for determining diffusion parameters in coal, eliminating the need for desorption canister testing.

Upon diffusing through the internal coal matrix and reaching the fracture system of the coal, gas flow is governed by Darcy flow (Darcy, 1856). Ahmed and McKinney (2005) describe the fracture system of coals as applied to coalbed methane, subdividing fractures into the inherent cleat system and tectonically-induced fractures. The face cleat is continuous throughout

the coal bed and serves as the primary mechanism for draining large areas. Butt cleats are discontinuous and cannot drain as large of an area as the face cleat system.

Darcy's Law (1856) describes the flow of fluids through porous media (Darcy, 1856). As stated by Pillalamarry et al. (2011), Darcy's Law is used to describe the flow of gas through a coal's cleat system. Darcy's Law, as applied to coalbed methane reservoirs, is presented below in Equation 2.6.

$$q = \frac{-kA}{\mu}\frac{dp}{dL} \qquad \text{(Equation 2.6)}$$

In Equation 2.6, q represents the volumetric flow rate through the coal's fractures. The coal's permeability is given by k, and μ represents the viscosity of the fluid. The pressure gradient per unit length is given by dp/dL.

Coal permeability varies spatially according to structural geology (Palmer, 2010) and with depth (Li et al., in press). Permeability values of targeted coal seams vary greatly, from values as high as 500 mD (Scott et al., 2004) to less than 0.1 mD (Clarkson and Bustin, 1997). The majority of coalbed methane production in the United States comes from reservoirs ranging between 3 and 30 mD (Palmer, 2008). Palmer (2010) argues that coal degasification strategy selection should be based on permeability.

There are two distinct competing mechanisms which can change the permeability of coal with a reduction in reservoir pressure. The release of gas from the internal coal matrix causes a collapse or shrinkage of the coal matrix, thus subsequently increasing the width of cleats and increasing permeability (St. George and Barakat, 2001). Competing with matrix shrinkage is an increase of the effective stress on the coal. As reservoir pressure is decreased, external stresses

dominate and cause the closure of flow paths for fluid flow, decreasing permeability (Harpalani and Schraufnagel, 1990).

Multiple analytical models have been published which describe permeability changes in coal during reservoir depletion (Pekot and Reeves, 2003; Palmer and Mansoori, 1996; Shi and Durucan, 2005; Cui et al., 2007; Siriwardane et al., 2009). This topic greatly interests researchers as permeability changes can be extremely large during production. The San Juan Basin exhibited a 100-fold change in permeability during production (Palmer, 2009). Palmer (2009) argues that analytical models are more transparent, less complicated, and more easily utilized in reservoir simulation programs than theoretical models.

Palmer (2009) offers a comparison and overview of well-recognized analytical permeability change models. The dynamic permeability modeled utilized in Advanced Resources International's (ARI) COMET3 reservoir simulator is based on the work of Pekot and Reeves (2003). This model is not based on a geomechanics framework, but rather incorporates matrix strain changes from a Langmuir curve of strain versus reservoir pressure. Matrix shrinkage is assumed to be proportional to a change in gas concentration, multiplied by a shrinkage compressibility factor. Pekot and Reeves (2003) determined that this model provides similar results as the Palmer and Mansoori (1996) model when applied to saturated coals. Palmer (2009) states that the Palmer and Mansoori (1996) model assumes that methane desorption changes volumetric strain, which in turn changes coal porosity and permeability. Additionally, this model assumes that desorption of methane changes the horizontal stress regime acting on the coal. A similar model developed by Shi and Durucan (2005) assumes that changes are stress based instead of strain based.

2.2. Coalbed Methane Based Geology of Study Area

2.2.1. Overview and Stratigraphy

A tectonic thermal event created the hydrocarbons within the Qinshui Basin (Su et al., 2005). Hu et al. (2007) state that the vitrinite reflectance of the Qinshui coals range between 2.6 to 3.7 percent, averaging 3.3 percent. The coals are anthracite in rank (Su et al., 2005).

The primary targeted coal beds in the southern Qinshui Basin are the No. 3 and No. 15 seams (Zou et al., 2010), with the depth of these seams ranging between 600 and 2,100 feet (Su et al, 2005). The No. 3 seam falls in the Permian Shanxi Formation with the No. 15 in the Pennsylvanian Taiyuan Formation (Su et al., 2005). The No. 15 coal seam is in direct contact with a calcium-rich mudstone and has proven difficult to dewater due to communication with the water-bearing bed (Zou et al., 2010). Coal Thickness

Coal thickness varies throughout the Qinshui Basin, as evidenced by differing stated thickness values in various publications. Wei et al. (2007) state that the thickness of the No. 3 seam in the Qinshui Basin varies from 1.6 to 23 feet. Zou et. al (2010) find that the thickness ranges from 16.6 to 23.7 feet, yet the clean coal section of the seam is generally between 15.8 and 23.7 feet with multiple layers of carbonaceous mudstone and mudstone in the coal bed.

2.2.2. Coal Permeability

Measurements of permeability in the Qinshui Basin vary over three orders of magnitude. Utilizing multiple exploration-based datasets, Su et al. (2005) find that the permeability of the southeast Qinshui Basin varies from 0.1 to 6.7 milidarcies, but is generally less than 2.0 milidarcies. Li et. al (in press) study two separate concession areas in the Qinshui Basin. They find the No. 3 seam permeability ranges from 0.017 milidarcies to 1.337 milidarcies. These calculations were made using geophysical logging data. Their correlations show a decrease in

permeability at increasing depths. They expect these values to be slightly lower than injection-falloff type results. Li et. al (in press) stress that permeability is a dominant reservoir parameter in the production of coalbed methane. Through COMET3 reservoir simulations as applied to the Qinshui Basin, Zou et al. (2010) find permeability to be less significant than reservoir pressure and gas content. Contrary to the findings of Zou et al. (2010), Palmer (2010) argues that degasification strategy selection is largely dependent on permeability.

2.2.3. Langmuir Coefficients

Su et al. (2005) state that the Langmuir Volume of the No. 3 coal bed in the Qinshui Basin ranges from approximately 1,060 to 2,010 cubic feet per ton. The same study finds the Langmuir Pressure coefficient values to range between 280 and 504 psi. In a carbon-sequestration-based study, Wong et al. (2007) report the Langmuir Volume and Langmuir Pressure of the No. 3 coal seam to be 926.2 cubic feet per ton and 143.1 psi, respectively. In a production-based case study of three separate wells, Zou et al. (2010) find the Langmuir Volume of the No. 3 seam to have values of 1,892, 1,638 and 1,459 cubic feet per ton. The corresponding Langmuir Volume for the samples were found to be 460, 422, and 467 psi. Jones and Bell (1987) provided a graphical depiction of adsorption isotherms based upon coal rank. Figure 2-1 displays their stated minimum and maximum isotherm curves for the adsorption of methane to anthracite coal with the aforementioned published values within the Qinshui Basin superimposed. As delineated in Figure 2-1, all published isotherm values underestimate the typical adsorption capacity of anthracite coals at low pressures (less than 300 psi). At higher pressures, some published isotherms underestimate, some overestimate, and some pinpoint the expected range published by Jones and Bell (1987).

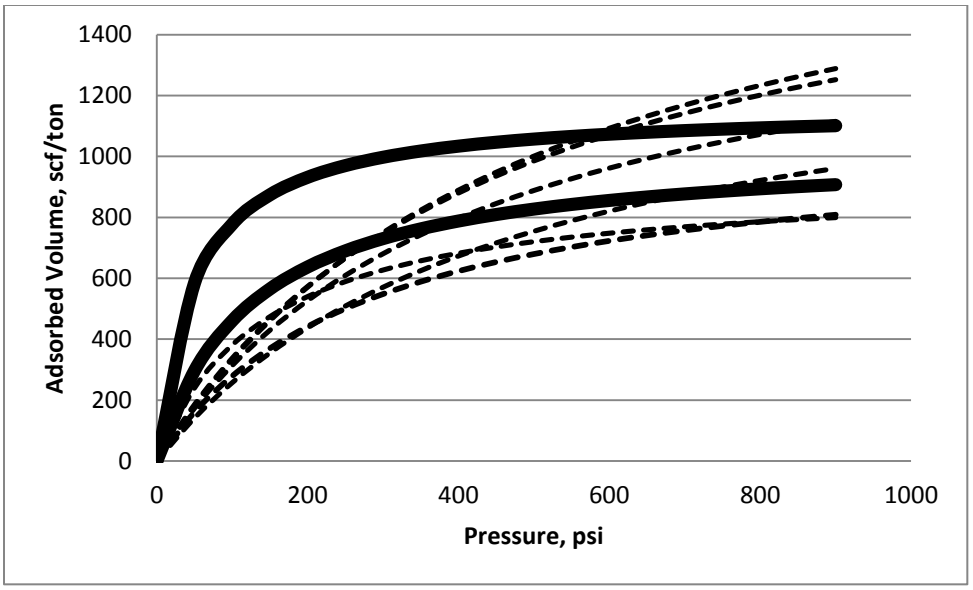

Figure 2-1: Ranges of anthracite isotherms (bold lines) with published isotherms in Qinshui Basin (dashed lines)

2.2.4. Gas Content and Reservoir Pressure

The No. 3 seam generally exhibits greater gas contents than the No. 15 seam, with gas contents in the range of 350 to 1300 cubic feet per ton (Su et al., 2005) with an average of approximately 750 cubic feet per ton (Hu et al., 2007). Pashin (2010) argues that gas saturation is as important of a parameter as gas content when analyzing the production potential of coalbed methane wells. Specific to the Qinshui Basin, Zou et al. (2010) state that reservoir pressure and gas content are the driving parameters in determining the productivity of coalbed methane wells. The combination of gas content and reservoir pressure are used to determine the degree of saturation; therefore, the findings of Zou et al. (2010) mirror those of Pashin (2010). Su et al. (2005) state the gas saturations of the Qinshui Basin to range from 56 to 100-percent with the higher values more conducive to faster dewatering and more economic gas production. Meng et al. (2011) determined that the fluid pressure gradient within the Qinshui Basin is generally hydrostatic, with some mild over-pressure and under-pressure instances between depths of 1,600 and 3,600 feet.

2.3. China CBM Industry

2.3.1. China CBM Reserve Base

The early 1990's brought the initial push for CBM development in China, fueled by 12 million dollars in funding to China from the United Nations. Through this funding, approximately 100 exploratory coalbed methane wells were drilled. Subsequent preliminary resource estimation showed a 30- to 35-trillion cubic meter resource of coalbed methane in China. More recent estimates of China's coalbed methane reserve base show nearly 1.3 quadrillion cubic feet of combined gas reserves and resources (Luo et al., 2011). In addition to a strong coalbed methane portfolio, China holds the third greatest coal reserves on a global scale, with nearly 115 trillion tons of proven reserves (EIA, 2007).

The Quinshui Basin is one of China's dominating CBM basins, along with the Odors, Junggar, Diandongqianxi, Erlian, Tuha, Tarim, Tianshan and Hailaer (Luo et al., 2011). The Qinshui Basin was the first commercially developed CBM play in China (Su et al., 2005) and has an estimated resource of 140 trillion cubic feet of gas (Luo et al., 2011).

2.3.2. Demonstrated Production and Modeling

Limited data has been published pertaining to demonstrated coalbed methane production data in the Qinshui Basin. Two specific coalbed methane degasification strategies have been used in China: namely, conventional vertical technology and multi-branch horizontal well technology (Luo et al., 2009). Additionally, underground (mine-level) drainage is often incorporated in Chinese mines. Mine-level horizontal wells tend to produce lower concentration methane and are generally used exclusively for safety reasons (Sang et al., 2010).

Prior to 2003, China had developed less than 250 coalbed methane wells. As of 2006, more than 1,183 CBM wells had been developed, 19 being multilateral horizontal wells (Sang et

al., 2009). By 2008, the number rose to nearly 2,500. Of these wells, less than 30 are of the multilateral type (Luo et al., 2009). As of 2007, five small-scale commercial development projects had been started (Luo and Dai, 2009). Luo et. al (2009) provide predicted production rates of four coalbed methane fields in the Qinshui Basin, outlined below in Table 2-1.

Table 2-1: Production prediction of Qinshui Basin CBM wells (Luo et al., 2009)

	Daily Production of Vertical Well (mscf/d)		Daily Production of Multi Branch Horizontal Well (mscf/d)	
Area	Peak	Average	Peak	Average
Hancheng	86.0	52.0	903.4	654.6
Ningwu	104.4	67.5	1,254.1	831.0
Jincheng	96.5	58.5	1,130.7	761.4
Dacheng	96.4	64.0	1,056.7	700.0

Zou et al. (2010) analyzed three producing wells in the Qinshui Basin, all of which are hydraulically fractured traditional vertical wells. Through a history-matching approach of the early-producing period of the vertical wells, they concluded that the vertical wells would continue to produce at average daily production rates of 40.3, 42.4, and 4.7 mscf/day. It should be noted that the permeability of the lowest-producing well was estimated to be 0.50 mD, with the other wells having respective permeability values of 1.50 and 2.10 mD. Su et al. (2005) state that 70 coalbed methane wells drilled by China United Coalbed Methane Co. Ltd. and China National Petroleum Corporation average between 70,000 and 140,000 cubic feet of production per day.

Chapter 2 References

Ahmed, T., McKinney, P. 2005. Advanced reservoir engineering. Published by Elsavier. Burlington, MA.

Airey, E. 1968. Gas emissions from broken coal, an experimental and theoretical investigation. International Journal of Rock Mechanics and Mining Sciences. 5. 475-494.

Aminian, K., Ameri, S. 2009. Predicting production performance of CBM reservoirs. Journal of Natural Gas Science and Engineering. 1. 25-30.

Barker-Read, G. 1984. A study of the gas dynamic behavior of coal measure straa, with particular reference to West Wales outburst prone seams. Ph.D. Thesis, University of Wales, Cardiff.

Clarkson, C., Bustin, R. 1997. Variation in permeability with lithotype and maceral composition of Cretaceous coals of the Canadian Cordillera. International Journal of Coal Geology. 33. 135-151.

Creedy, D. 1985. The orgin and distribution of firedamp in some British coalfields. Ph.D. Thesis, University of California Berkeley.

Cui, X., Busin, R., Chikatamarla, L. 2007. Adsorption-induced coal swelling and stress: Implications for methane production and acid gas sequestration into coal seams. Journal of Geophysical research. 112.

Darcy, H. 1856. Les Fontaines Publiques de la Ville de Dijon. Dalmont, Paris

Dutta, P., Harpalani, S., Prusty, B. 2008. Modeling of CO2 sorption on coal. Fuel. 87. 2023-2036.

EIA. 2007. International Energy Annual 2005. U.S. Energy Information Administration.

Garnier, C., Finqueneisel, G., Zimny, T., Pokryszka, Z., Lafortune, S., Defossez, P., Gaucher, E. 2011. Selection of coals of different maturities for CO2 storage by modeling of CH4 and CO2 adsorption isotherms. International Journal of Coal Geology. In Press.

Griffin, P. 1978. Methane sorption studies with particular reference to the outburst prone anthracites of West Wales. MSc. Thesis, University of California Berkeley.

Harpalani, S. 1984. Gas Flow through Stressed Coal. Ph.D. Thesis, University of California Berkeley.

Harpalani, S., Schraufnagel, R. 1990. Shrinkage of coal matrix with release of gas and its impact on permeability of coal. Fuel. 69. 551-556.

Harris, I., Davies, G., Gayer, R., Williams, K. 1996. Enhaned methane desorption characteristics from South Wales anthracites affected by tectonically induced fracture sets. Geological Society Special Publication No. 109. 181-196. Published by the Geological Society, London.

Hu, G., Li, J., Ma, C., Li, Z., Zhang, M., Zhou., Q. 2007. Characteristics and implications of the carbon isotope fractionation of desorbed coalbed methane in Qinshui coalbed methane field, China. Earth Science Frontiers. 14(6). 267-272.

Jones, H., Bell, G. 1987. Proceedings of the 1987 Coalbed Methane Symposium. Tuscaloosa, AL. 93-102.

Langmuir, I. 1918. The Adsorption of gases on plane surfaces of glass, mica, and platinum. Journal of American Chemistry Society. 40. 1361-1403.

Li, J., Liu, D., Yao, Y., Cai, Y., Qiu, Y. 2011. Evaluation of the reservoir permeability of anthracite coals by geophysical logging. International Journal of Coal Geology. In Press.

Luo, D., Dai, Y., Xia, L. 2011. Economic evaluation based policy analysis for coalbed methane industry in China. Energy. 36. 360-368.

Luo, D., Chu, W., Wu, X., Li, W. 2009. Analysis of economic benefits of coalbed methane drilling technologies. Petroleum Exploration and Development. 36(3). 403-407.

Luo, D., Dai, Y. 2009. Economic evaluation of coalbed methane production in China. Energy Policy. 37, 3883-3889.

McPherson, M. 1985. Mine Ventilation Society of South Africa. 28(8). 118.

McPherson, M. 1993. Subsurface Ventilation and Environmental Engineering. published by Chapman & Hall, London.

Meng, Z., Zhang, J., Wang, R. 2011. In-situ stress, pore pressure and stress-dependent permeability in the Southern Qinshui Basin. International Journal of Rock Mechanics & Mining Sciences. 48. 122-131.

Palmer, I. 2008. Coalbed methane wells are cheap, but permeability can be expensive. Energy Tribune.

Palmer, I. 2009. Permeability changes in coal: Analytical modeling. International Journal of Coal Geology. 77. 119-126.

Palmer, I. 2010. Coalbed methane completions: A world view. International Journal of Coal Geology. 82. 184-195.

Palmer, I., Mansoori, J. 1996. How permeability depends on stress and pore pressure in coalbeds: a new model. SPE Reservoir Evaluation and Engineering. 539-544.

Pan, Z., Connell, L. 2009. Comparison of adsorption models in reservoir simulation of enhanced coalbed methane recovery and CO2 sequestration in coal. International

Journal of Greenhouse Gas Controls. 3. 77-89.

Pashin, J. 2010. Variable gas saturation in coalbed methane reservoirs of the Black Warrior Basin: Implications for exploration and production. International Journal of Coal Geology. 82. 135-146.

Pekot, L., Reeves, S. 2003. Modeling the effects of matrix shrinkage and differential swelling on coalbed methane recovery and carbon sequestration. Proceedings of the 2003 International Coalbed Methane Symposium. Tuscaloosa, AL. Paper 0328.

Pillalamarry, M., Harpalani, S., Liu, S. 2011. Gas diffusion behavior of coal and its impact on production from coalbed methane reservoirs. International Journal of Coal Geology. 86. 342-348.

Sang, S., Liu, H., Li, Y., Li, M., Li, L. 2009. Geological controls over coal-bed methane well production in southern Qinshui Basin. Procedia Earth and Planetary Sciences. 1. 917-922.

Sang, S., Xu, H., Fang, L., Li, G., Huang, H. 2010. Stress Relief coalbed methane drainage by surface vertical wells in China. International Journal of Coal Geology. 82. 196-203.

Sawyer, W., Zuber, M., Kuuskraa, V. 1987. Proceedings of the 1987 Coalbed Methane Symposium. Tuscaloosa. AL. 295-307.

Scott, S., Anderson, B., Crosdale, P., Dingwall, J., Leblang, G. 2004. Revised Geology and coal seam characterstics of the Walloon subgroup - Surat Basin, Queensland. PESA Eastern Australasian Basins Syposium. II. Adelaide, Australia.

Shi, J., Durucan S. 2005. A model for changes in coalbed permeability during primary and enhanced methane recovery. SPE Reservoir Evaluation and Engineering. 291.

Siriwardane, H., Gondle,R., Smith, D. 2009. Shrinkage and swelling of coal induced by desorption and sorption of fluids: Theoretical model and interpretation of a field project. International Journal of Coal Geology. 7. 188-202.

Smith, D., Williams, F. 1984. Diffusion models for gas production from coal: Determination of diffusion parameters. Fuel. 63. 256-261.

St. George, J., Barakat, M. 2001. The change in effective stress associated with shrinkage from gas desorption in coal. International Journal of Coal Geology. 45. 105-113.

Su, X., Lin, X., Liu, S., Zhao, M., Song, Y. 2005. Geology of coalbed methane reservoirs in the Southeast Qinshui Basin of China. International Journal of Coal Geology. 62. 197-210.

Wei, C., Qin, Y., Wang, G., Fu, X., Jiang, B., Zhang, Z. 2007. Simulation study on evolution

of coalbed methane reservoir in Qinshui Basin, China. International Journal of Coal Geology. 72. 53-69.

Wong, S., Law, D., Deng, X., Robinson, J., Kadatz, B., Gunter, W., Jianping, Y., Sanli, F., Zhiqiang, F. 2007. Enhanced coalbed methane and CO2 storage in anthracitic coals-Micro-pilot test at South Qinshui, Shanxi, China. International Journal of Greenhouse Gas Controls. 1. 215-22.

Ziarani, A., Aguilera, R., Clarkson, C. 2011. Investigating the effect of sorption time on coalbed methane recovery through numerical simulation. Fuel. 90. 2428-2444.

Zou, M., Wei, C., Pan, H., Sesay., K.S., Cao, J. 2010. Productivity of oalbed methane wells in southern of Qinshui Basin. Mining Science and Technology. 20(5). 765-769.

Chapter 3. SELECTING DEGASIFICATION STRATEGIES FOR CHINA'S QINSHUI BASIN: ANALYSIS OF RESERVOIR MODELING RESULTS AS APPLIED TO MINE SAFETY, GREENHOUSE GAS EMISSIONS, AND ECONOMIC CRITERIA

Abstract

China's Qinshui Basin holds coals of significant thickness and gas content. Over the course of the past decade, substantial strides in the development of the Qinshui Basin's gas resource have been made. While several published works have analyzed the geology of the basin, very limited production data has been made public. Both hydraulically stimulated vertical fracture wells and multilaterally drilled horizontal wells have been used in the region, with the latter much less common. Although horizontal completions require a significantly higher capital investment, they provide the opportunity for higher production rates. This study serves as a framework in analyzing the production of multiple horizontal and vertical well completion strategies on mine safety, environmental, and economic bases. Three-dimensional reservoir modeling software shows that multilaterally drilled horizontal drainage patterns offer the most economic and environmentally friendly results when used in advance of mining. Based on the obtained modeling results, the high capital investment of horizontal wells is quickly offset by high initial gas production rates. Furthermore, high drilling density patterns with closely spaced laterals decrease the variability in seam gas content ahead of mining, providing the potential for increased health and safety of the underground workforce and increased coal production. From a greenhouse gas emission standpoint, a decrease in carbon dioxide equivalent emissions of 15-million metric tons can be noted over a 20-year mining period for high-capacity longwall operations in the Qinshui Basin through careful degasification planning. Although hydraulically fractured vertical wells have been used extensively, modeling concludes that horizontal completions are more effective from a production, economic, environmental and safety standpoint.

3.1. Introduction

3.1.1. Scope of Study

Multiple studies have been published to describe the coalbed-methane-related geology of the Qinshui Basin (Su et al., 2005; Sang et al., 2009; Wei et al., 2005). Limited information pertaining to actual production data in the Qinshui Basin has been made public, with the majority of published work being generalized and offering ranges of obtained production values. In lieu of production data, detailed 3-dimensional reservoir modeling offers the opportunity to predict the production capabilities of multiple degasification strategies. This paper serves as modeling

work which analyzes the benefits of degasification on safety, environmental and economic bases as related to multiple well completion strategies.

Modeling inputs for the work have been obtained from a greenfield concession area within the Qinshui Basin. In an effort to maintain confidentiality and protect the mineral lessee, specifics pertaining to the site location are withheld. Outcomes presented in this work can be used on an international basis as a framework for determining global degasification benefits.

3.1.2. Historical CBM Production in the Qinshui Basin

Surface-drilled completion strategies which have been effectively implemented in the Qinshui Basin include traditional hydraulically fractured vertical wells and multilaterally drilled horizontal wells (Luo et al., 2009). Over the course of the past decade, the number of coalbed methane wells in the Qinshui Basin has increased dramatically from less than 250 to over 2,500 (Sang et al., 2009; Luo et al., 2009). The majority of the wells are vertical wells with hydraulically fractured stimulation treatments. As of 2009, less than 30 multilaterally drilled horizontal wells have been developed, attributed to higher capital costs (Luo et al., 2009). Hydraulically fractured vertical wells in the Qinshui Basin produce gas at a rate between 70,000 and 140,000 cubic feet per day (Su et al., 2005). Modeling completed by Luo et al. (2009) estimates that horizontal wells in the basin should produce at rates around 700,000 cubic feet per day.

The primary coal beds targeted for mining and coalbed methane development in the Qinshui Basin are the No. 3 and No. 15 seams (Zou et al., 2005), both anthracitic in rank and formed from a tectonic thermal event (Su et al., 2005). The seam depths range from 600 to 2,100

feet (Su et al., 2005). An overlying aquifer causes difficulty in dewatering the No. 15 seam. Therefore, the No. 3 seam is used as the basis of modeling for this work.

3.2. Reservoir Modeling

3.2.1. Geological Modeling Inputs

Reservoir modeling utilizes Advanced Resources International's (ARI) *COMET3* reservoir simulator. Modeling inputs, as assumed or obtained from the greenfield property, are shown below in Table 3-1. Additionally, Table 3-1 contains ranges of values as found in published literature for the Qinshui Basin.

Table 3-1: Modeling inputs and associated ranges in Qinshui Basin

Parameter	As Modeled	Measured at Study Area?	Reported Regional Values	Regional Value Source(s)
Depth (ft)	2000	Yes	650 to 2300	Su et al., 2005
Coal Thickness (ft)	10	Yes	1.6 to 23	Wei et al., 2007
Water Saturation	85%			
Fluid Pressure Gradient (psi/ft)	0.3	Yes	0.30 to 0.48	Zou et al., 2010; Sang et al., 2009
Reservoir Pressure (psi)	600	Calculated		
Permeability	2.0	Yes	0.1 to 2.0	Su et al., 2005; Yao et al., 2008
Porosity	3%		1.15% - 7.69%	Zou et al., 2010
Langmuir Volume (ft^3/ton)	1000	Yes	1450 to 1870	Zou et al., 2010
Langmuir Pressure (psi)	300	Yes	422 to 467	Zou et al., 2010
Gas Content (ft^3/ton)	500	Yes	280 to 880	Lu et al., 2010; Yao et al., 2008; Su et al., 2005

As evident in Table 3-1, all obtained geological inputs from the greenfield property are representative of published values for the region with the exception of the Langmuir coefficients. The Langmuir isotherm curve and initial reservoir conditions are plotted in Figure 3-1. The initial reservoir pressure of 600 psi is calculated by multiplying the fluid pressure gradient (0.3 psi per foot) by the coal seam depth (2,000 feet). The coal seam is undersaturated with a degree of saturation of 75 percent. While the measured Langmuir coefficients are not within the range

of those published by Zou et al. (2010), the degree of saturation is within the general range stated by Su et al. (2005) who find the degree of saturation of Qinshui coals to range between 56 and 100 percent. Based on the obtained Langmuir coefficients, initial gas content, seam depth, and fluid pressure gradient, the critical desorption pressure is calculated to be 300 psi. This requires a decrease in reservoir pressure from 600 to 300 psi for gas to begin desorbing from the internal coal matrix.

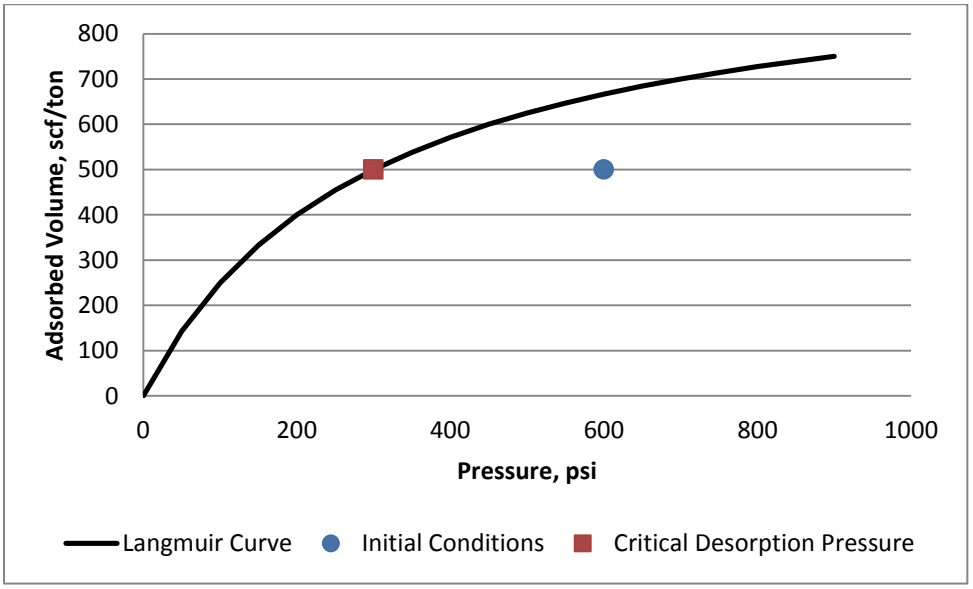

Figure 3-1: Langmuir isotherm with initial conditions and critical desorption pressure

Relative permeability curves obtained by the Kissell and Edwards' (1975) Bureau of Mines study were used in modeling. While the relative permeability curves were based on a Pocahontas No. 3 coal sample, the Qinshui reservoir exhibits similar geological qualities as the Pochahontas No. 3 seam, with a similar depth, fluid pressure gradient, methane concentration, and fracture network. Although relative permeability will vary by coal rank among other geologic parameters, no data has been published pertaining relative permeability within the Qinshui basin. The variations in coal rank between the Pocahontas No. 3 and Qinhsui coals could introduce error in modeling output. Still, the Kissell and Edwards (1975) Pocahontas No.

3 curves are included and considered representative based on the aforementioned geologic consistencies between the two basins. Data pertaining to matrix shrinkage and pore volume compressibility for the No. 3 Qinshui coal seam were unavailable. Therefore, these phenomena were assumed to offset each other and were excluded from modeling. Additionally, permeability anisotropy is excluded from modeling, with the face cleat and butt cleat directions modeled with the same permeability value of 2.0 md.

3.2.2. Modeled Well Geometry

An infinite number of horizontal wellbore patterns exist. Common drainage patterns include the single lateral, dual lateral, quadrilateral, and Pinnate (Maricic et al., 2008; Palmer, 2010). Pitchfork patterns, as analyzed by Keim et al. (2011), offer an alternative to Pinnate-style patterns with the opportunity for higher gas recovery. Success has been noted in the Shanxi Province through herringbone or fishbone patterns, which are geometrically similar to the Pinnate pattern (Zhiming and Zhang, 2009). To provide a comparative basis, the wellbore patterns depicted in Figure 3-2 are modeled. Their corresponding drainage areas and required in-seam drilling length are shown in Table 3-2.

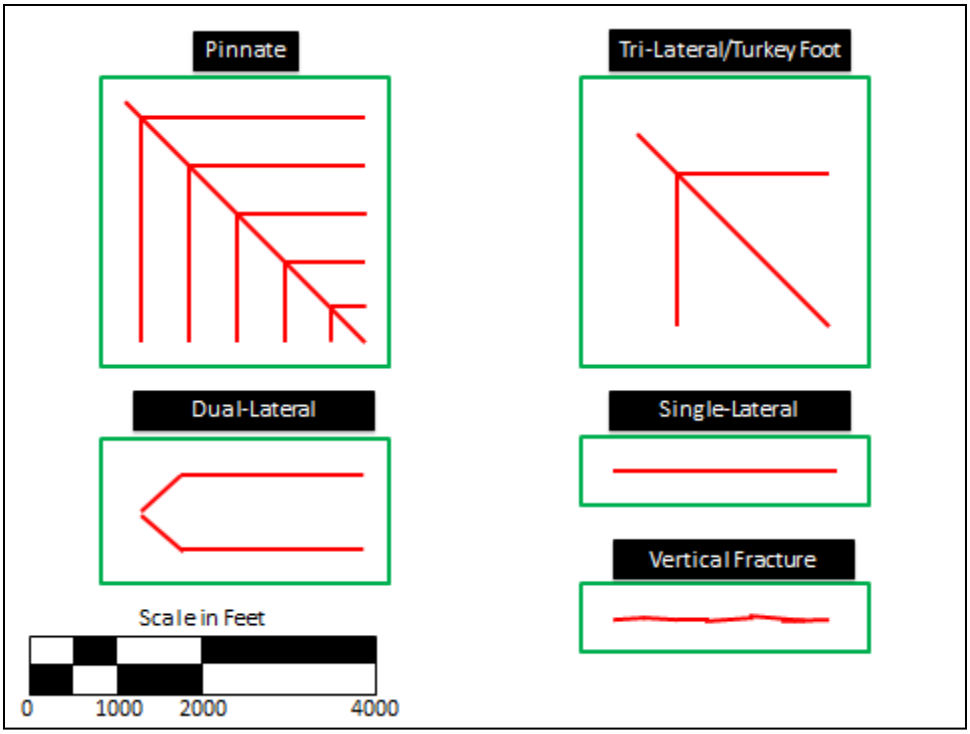

Figure 3-2: Plan view of modeled well geometry

Table 3-2: Drainage area and required in-seam drilling for modeled wells

Capital and Operating Expenses	Pinnate	Turkey Foot	Dual Lateral	Single Lateral	Vertical Fracture
In-Seam Drilling Length (ft)	20,000	7,100	6,800	3,200	-
Drainage Area (acres)	250	250	166	79	79
Drilling Density (in seam footage per acre drained) (ft/acre)	80	28	41	41	-

While a multitude of well configurations and drainage areas can be analyzed, the wells depicted in Figure 3-1 and Table 3-2 provide a comparative basis in terms of drainage area and drilling length. The modeled vertical fracture well can be compared to a single lateral well, as it is designed to drain the same area (79 acres). The single lateral and dual lateral wells both provide drilling densities of 41 feet per acre, with the dual lateral drilling doubling the acreage. The Turkey Foot and Pinnate-style patterns are modeled to drain 250 acres, with the Pinnate pattern requiring substantially more in-seam drilling footage. The presented wells allow for

multiple conclusions to be drawn with respect to drainage area, drilling density, and completion strategy when wells are analyzed on mining, environmental, and economic criteria.

Grids for the modeled wells utilize individual blocks which are 100 feet by 100 feet. The Pinnate and Turkey Foot grids are 33 blocks long by 33 blocks wide. The dual-lateral well incorporates a grid geometry of 38 blocks long by 19 blocks wide. The single lateral and fracture wells utilize grids which are 38 blocks wide by 9 blocks long.

As the vertical fracture well's production will be highly dependent on the stimulated fracture length, half fracture lengths were modeled as a worst (lowest), expected, and best (highest) case. Half fracture lengths for the vertical wells were arbitrarily set to 500 (worst), 700 (expected), and 900 (best) feet.

The model is governed based on water production limitations and well pressure constraints. All wells are assumed to produce water at a maximum rate of 250 barrels per day until each well's bottom hole pressure is reduced from the initial reservoir pressure to atmospheric pressure. Upon reaching the atmospheric conditions, water is continually pumped at a sufficient rate to maintain atmospheric conditions.

3.2.3. Modeling Results

Production rates over a 20-year period for the horizontal wells and the expected 700-ft half fracture length vertical well are displayed in Figure 3-3. Figure 3-4 displays the production rates for the worst-, expected-, and best-case vertical fracture wells. Cumulative production charts for the same well layouts are depicted in Figure 3-5 and Figure 3-6.

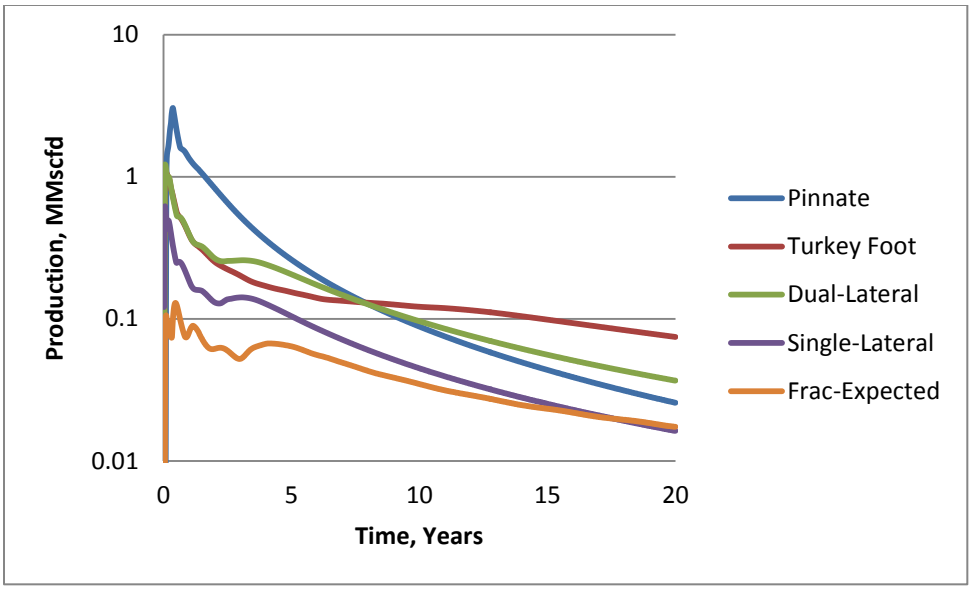

Figure 3-3: Production rates for horizontal well layouts and expected fracture well

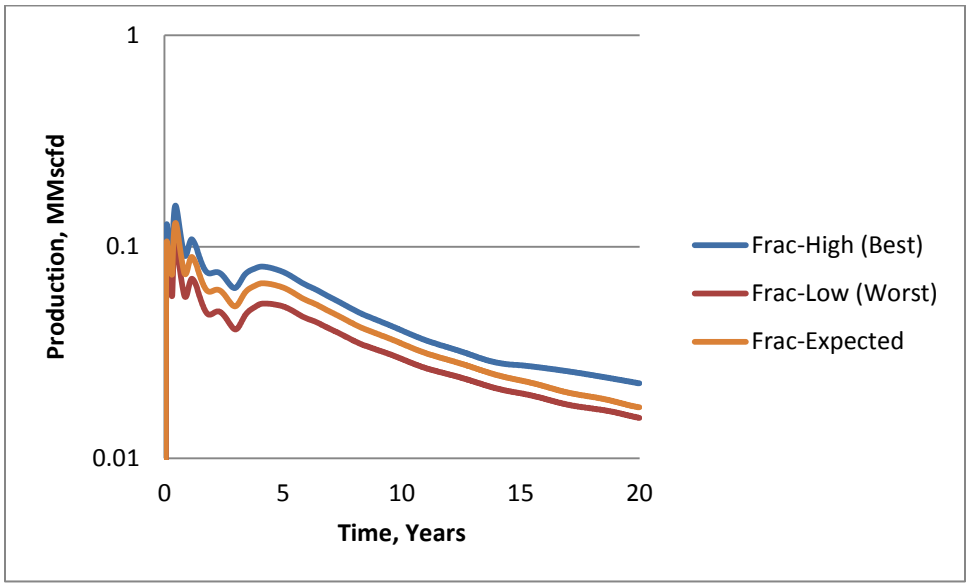

Figure 3-4: Production rate comparison for best, expected, and worst case vertical fracture completions

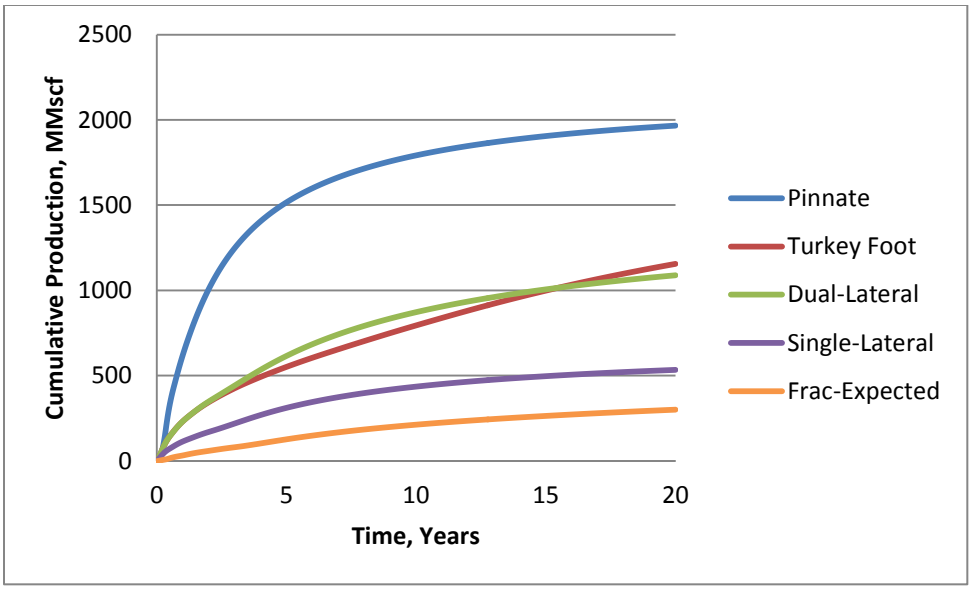

Figure 3-5: cumulative production for horizontal well layouts and expected fracture well

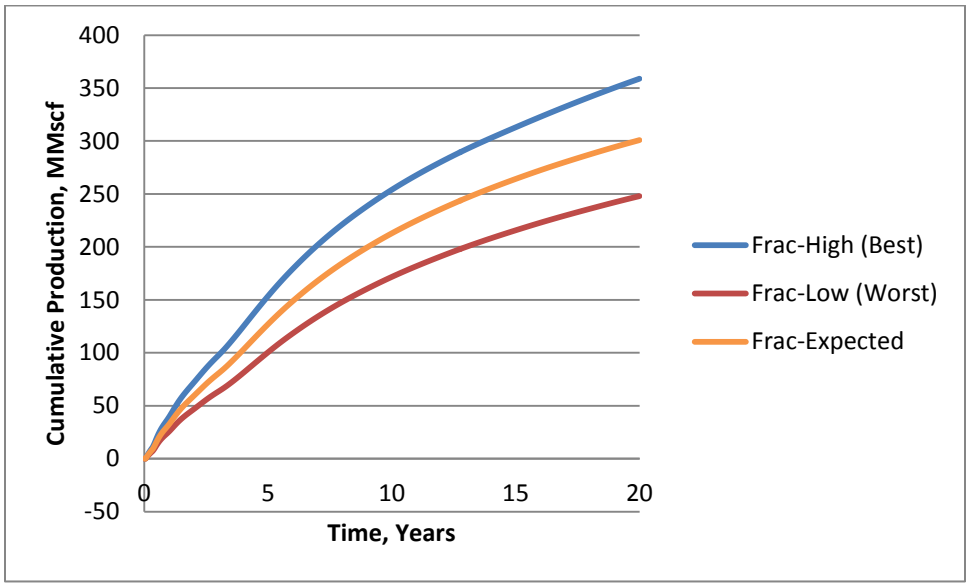

Figure 3-6: Cumulative production comparison for best, expected and worst case vertical fracture completions

As shown in Figure 3-3 and Figure 3-5, the Pinnate well out-produces all other horizontal wells in terms of production rate and cumulative production. The rapid reservoir depressurization from the high in-seam drilling length of the Pinnate pattern recovers methane faster than any other horizontal pattern. Compared to the Turkey Foot pattern which drains a similar area, the Pinnate produces nearly double the gas over a 20-year span. Modeling shows

that the gas production rate of the Turkey Foot pattern is more sustained over the 20-year span, albeit a lower total cumulative production figure. As expected, the dual lateral configuration produces roughly double the gas compared to the single lateral completion. Having the same drainage area, the single lateral well produces roughly 80 percent more gas than the expected case for the vertical fracture completion. Modeling shows that the half fracture length dictates both the production rate and cumulative production figure for hydraulically fractured vertical well treatments. The production rates and cumulative production curves are directly proportional to modeled half fracture length. Over a 20-year period, fracture length can be attributed to a nearly 150 million cubic foot increase in production when comparing the best-case and worst-case models.

While the production figures obtained from modeling provide a comparative basis to analyze well performance, additional aspects of each well layout must be analyzed to optimize performance. The following sections examine the obtained modeling results on a mining, greenhouse gas, and economic basis.

3.3. Mining Health and Safety

3.3.1. Overview

The impact of government regulations on the safety of the Chinese coal workforce has been an important issue in the literature over the past several decades (Shi, 2009). While the Chinese safety record has improved recently, grave numbers still exist in the reporting of coal-mining-related fatalities. Between 2000 and 2007, China's reported fatality rate per million tons of mined coal was found to be 3.04, over 100-times greater than the United States' 0.027 figure (Wei, 2009; Lu and Li, 2011). Methane-related explosions are the root cause of the majority of China's coal-related fatalities. The Chinese government analyzes fatal incidents by the number

of perished individuals. According to 2007 data, methane was linked to 51.2 percent of large incidents (3 to 9 fatalities) and 80.3 percent of extremely large accidents (more than 10 fatalities) (Cheng et al., 2011). Additional research and strides in degasification technology have the potential to greatly decrease the staggering coal-related fatality rates in China.

The following sections provide an overview of degasification strategy selection in relation to mine health and safety. Each well pattern is analyzed on a recovery basis in an effort to pinpoint potential positive and negative aspects of each well layout. Additionally, a brief review of the impact of degasification on production at a mine in the study area is presented.

3.3.2. Analysis from Reservoir Modeling

Regulatory standards require that the gas content of Chinese coal seams be lowered to a threshold value of 280 cubic feet per ton prior to mining. As applied to this work, 280 cubic feet per ton corresponds to a gas recovery rate of approximately 57 percent. When analyzing the recovery of coalbed methane, total recovery values for an entire drainage area can be skewed with large changes in recovery at varying distances from the producing wellbore. An average recovery of 57 percent actually represents a higher recovery proximal to the wellbore and significantly lower recoveries away from the wellbore. This creates a potential safety hazard, as a skewed recovery figure which suggests safe mining conditions could actually represent large variations in coal seam gas content. Areas away from a producing wellbore can hold dangerous volumes of explosive methane, albeit an acceptable average recovery across the drainage area. Figure 3-7 contains a schematic comparing the spatial variation in recoveries of Pinnate- and Turkey Foot-style patterns after two years of production. As evidenced in Figure 13, both wells display large variations in gas content. Figure 3-8 contains a similar diagram, but after 20 years of production. Figure 3-8 depicts much less variation in gas content for the Pinnate well, with

the entire drainage area exhibiting upwards of 90-percent recovery. Contrarily, the Turkey Foot-style well shows high recoveries proximal to the wellbore with significantly lower recoveries away from the wellbore. Based on these figures, the Pinnate-style pattern shows much more favorable characteristics for degasification ahead of mining, despite the added expense related to more in-seam drilling.

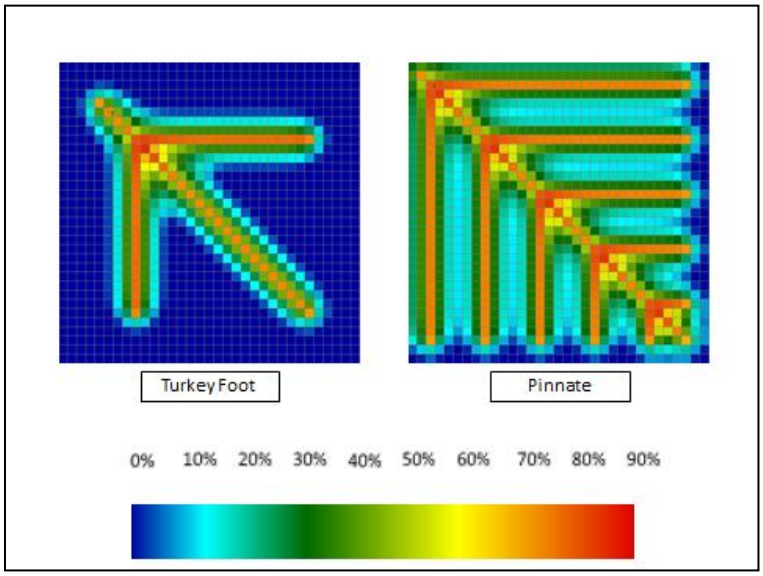

Figure 3-7: Spatial recovery comparison of Turkey Foot and Pinnate wells after 2 years of production

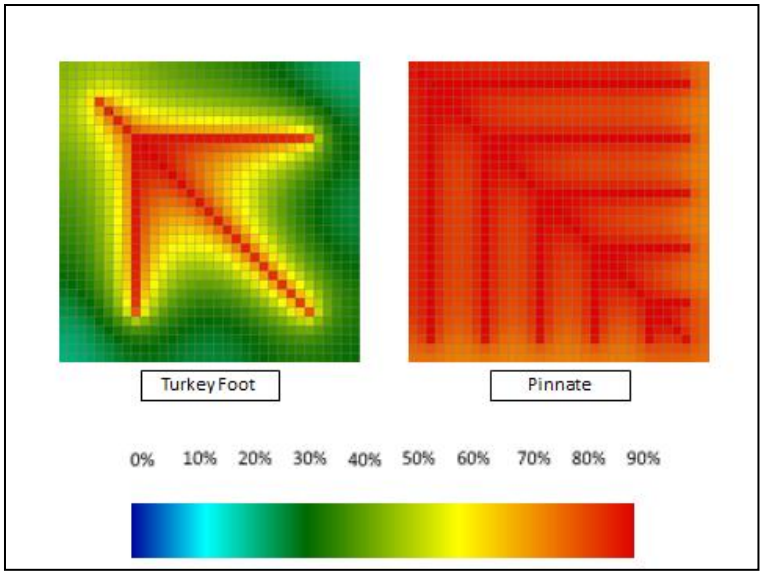

Figure 3-8: Spatial recovery comparison of Turkey Foot and Pinnate wells after 20 years of production

In an effort to compare the spatial recoveries of all modeled well layouts, a histogram was created which displays the percentage of modeled grid blocks for each well layout with specified gas recoveries after 20 years of production. Figure 3-9 displays the histogram.

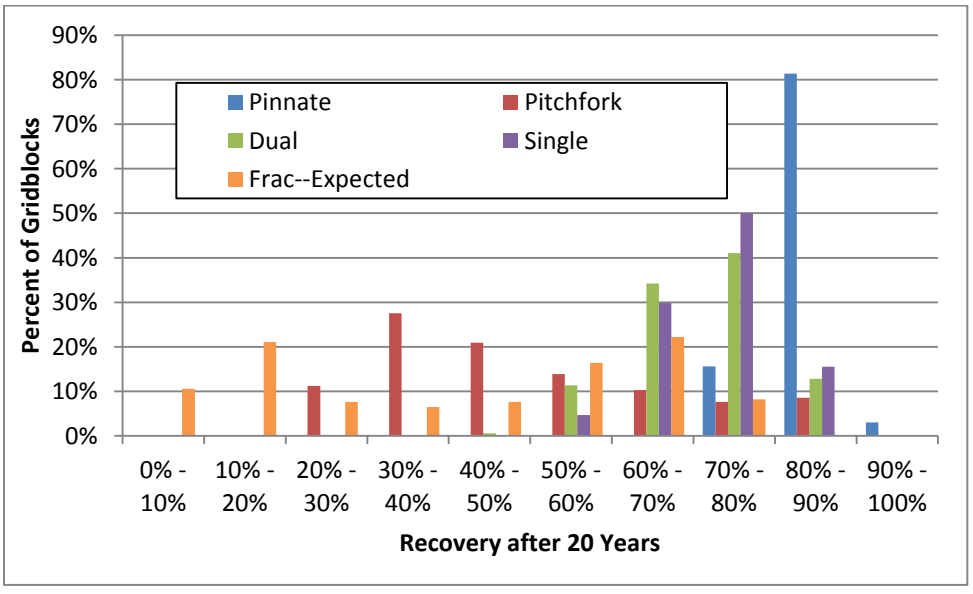

Figure 3-9: Recovery analysis by grid blocks after 20 years of production

As shown in Figure 3-9, the hydraulically fractured well exhibits a very large variation in gas recovery, similar in distribution to the Turkey Foot pattern. Gas recovery values for the hydraulically fractured well vary from 0 to 80 percent. The Turkey Foot pattern recovery values range from 20 to 90 percent. In both cases, there are large areas which are not effectively drained. By decreasing the drainage areas and subsequently increasing the number of wells in a given area, these distributions will shift to the right with more areas exhibiting higher recoveries. The single-lateral and dual-lateral wells show similar distributions, with at least 50-percent recovery across the entire drainage area. The close horizontal lateral spacing of the Pinnate well shows the most impressive performance. After a 20-year period, all targeted coal has been drained to at least 70-percent recovery, with the majority in the 80- to 90-percent range. Modeling results for the Qinshui's geological conditions suggest that multilaterally drilled horizontal patterns offer consistent recoveries across a drainage area. Alternate patterns can cause localized zones of higher gas content and do not offer the same safety benefits as Pinnate-style patterns.

Predictive graphs similar to those shown in Figure 3-9 provide a visual representation of the recovery distributions of wells and should be considered in coalbed methane recovery, especially in advance of mining. Pinpointing the location of high and low recovery zones through schematics similar to those shown in Figure 3-7 and Figure 3-8 provide the opportunity for improved health and safety of miners, less gas-offs, and increased productivity. Wells with a high drilling density per unit area, such as the modeled Pinnate well, exhibit the highest recoveries and smallest variations in recovery over the drainage area. As applied to China's Qinshui Basin, after a 20-year period, the Pinnate well is the only modeled well which drains all coal to the regulatory standard of 280 cubic feet per ton. In the instance that additional drainage

time is possible ahead of mining, other well layouts may be able to accomplish the same task. Still, modeling shows that the faster recovery time of the Pinnate is unquestionably the best method for degasification ahead of coal mining in the Qinshui Basin. Alternative variations of horizontal wells with closely spaced laterals should provide similar results.

3.3.3. Case Study of Degasification Ahead of Mining

While the results presented in Section 3.3.2. provide an overview of degasification as applied to regulatory-based gas content standards, they do not incorporate any analysis as applied to the methane concentration in the mine air. Karacan (2008) provides an excellent overview of modeling mine workings through the use of reservoir modeling software to determine methane emission rates and concentration of methane in the mine air. Using a similar methodology, the interactions and impacts of degasification wells on mine air can be determined. In lieu of an additional model to determine the impact of degasification on mine air and subsequent potential decreases in ventilation requirements, an analysis of a producing longwall mine in the Qinshui Basin is presented. To maintain confidentiality and protect the operator, specifics related to location of the operation are withheld. The case study serves as an example of a successful operation where degasification has greatly enhanced productivity.

Table 3-3 outlines the regulatory ventilation and air concentration standards set forth by China's Coal Mining Safety Regulation for continuous miner development sections and longwall sections.

Table 3-3: Chinese ventilation regulatory standards

Parameter	Value
Minimum Air Velocity	0.82 ft/s (0.25 m/s)
Maximum Air Velocity @ Working Face	13.12 ft/s (4 m/s)
Minimum Air Volume per Worker on Section	141 ft^3/min (4 m^3/min)
Maximum Methane Concentration @ Working Face and Returns	1%
Maximum Carbon Dioxide Concentration @ Working Face and Returns	1.5%
Maximum Methane and Carbon Dioxide Concentration in Intake Air	0.5%

The case study longwall operation has evolved greatly over the past decade, originally using very little degasification. Limited drainage time prior to mining necessitated a combination of in-mine longhole drainage in addition to surface drilled Pinnate-style patterns similar to those which have been modeled in this work. The in-mine longhole drainage technique uses 3-inch holes, approximately 2,500 feet in length to degasify development sections and longwall panels simultaneously. The closely spaced mine-level horizontal holes offer the advantage of faster recovery time, while the Pinnate-style wells are used to drain gas in areas encompassed by the long-term mine plan.

In accordance with the Coal Mining Safety Regulations of China, calculations of the required air volume to dilute methane to legal concentrations in gassy coal mines are based upon the methane emission rate in the mine. Determining the methane emission rate through theoretical calculations can prove difficult and is rather generally based upon neighboring mines with similar geology. The case-study longwall operation incorporates a blower ventilation system, moving 1.4 million cubic feet of air through the mine per minute. Approximately 25 percent of the air is directed to the longwall face. Development sections incorporate booster fans and use the remaining ventilation air. The continuous methane concentration at the exhaust shaft remains below the legal threshold value, generally hovering below 0.5 percent, but can spike to 0.75 percent.

In the presence of the degasification system, no significant changes have been noted to the methane concentrations in the mine air. However, significant improvements in mine productivity have been noted, with nearly a 10-fold increase in production over a six-year period. Coal is now produced at a rate of approximately 4 million tons per year. The reliance on the ventilation and degasification systems to maintain safe air concentrations is critical. The in-mine degasification system recovers approximately 35-million cubic feet of gas per day, with a methane concentration of around 50 percent.

3.4. Greenhouse Gas Considerations

3.4.1. Overview

The production and combustion of fossil fuels as an energy source releases large volumes of greenhouse gases to the atmosphere. Specifically, carbon dioxide and methane, both well-known greenhouse gases, have direct ties to the coal and coalbed methane industries. Carbon dioxide, formed from the combustion of fossil fuels, represents the largest anthropogenic greenhouse gas. Methane, the main constituent of natural gas, possesses radiative trapping capabilities roughly 23 times greater than that of carbon dioxide (Seinfeld and Pandis, 2006). Inherent within the coal's structure, methane desorbs from the coal's internal surfaces during the mining process, and then moves to the atmosphere through a mine's ventilation system. Gas contents of deep coal seams located in China's Quinsui Basin can exceed 500 cubic feet per ton (Su et al., 2005), resulting in significant volumes of methane being released through the atmosphere during the mining process. The United States Environmental Protection Agency (EPA) compiles CO_2 equivalent emissions statistics for coal-mine-related methane. Carbon dioxide equivalent methane emissions for the United States and China are respectively estimated to be 72,000 and 130,000 metric tons (USEPA, 2006). Recovering this methane prior to mining

provides a viable, clean-burning energy source which can be used in residential and commercial applications.

The following sections outline the potential carbon dioxide equivalent emission reductions associated with degasification ahead of a hypothetical coal operation in the Qinshui Basin. The methodology of determining equivalent emissions is presented as applied to the hypothetical case study. Feasible recovery figures are discussed based on reservoir modeling output.

3.4.2. Calculating and Forecasting Emission Reductions

Provided that either: a) detailed reservoir modeling has been used to predict well production; or b) good estimates of production for degasification wells can be made based on regional data where geologic conditions are consistent, emission reduction estimates can be made using a simple methodology. For the purpose of this study, carbon dioxide equivalent emission reductions are calculated on a coalbed methane recovery basis. Recovered methane will be combusted and released to the atmosphere in the form of carbon dioxide. Methane which is not recovered is vented to the atmosphere resulting in equivalent carbon dioxide emissions. In an effort to determine the true environmental impact of degasification as applied to a pre-mining situation, a hypothetical longwall mine is utilized.

Mining-based assumptions for the hypothetical Qinshui longwall mine are outlined in Table 3-4. Over a period of 20 years, clean coal is produced at a constant rate of 4 million tons per year. Coal is assumed to have a thickness of 10 feet, consistent with degasification modeling in Section 3.2.1. Clean coal specific gravity is estimated to be 1.55, higher than bituminous coals due to its higher anthracitic rank. Extraction ratio and plant yield are respectively assumed

to be 90 percent and 85 percent. Using these inputs, the longwall mine will encompass an area of nearly 5,000 acres over the 20-year study period. Within this 5,000-acre area, 52.3 billion cubic feet of gas will be exposed with the opportunity for recovery prior to mining or ventilation to the atmosphere during mining.

Table 3-4: Hypothetical Qinshui longwall mine model inputs

Study Period (years)	20
Coal Thickness (ft)	10
Clean Coal Annual Production (million tons/year)	4
Clean Coal Specic Gravity	1.55
Extraction Ratio	90%
Plant Yield	85%
Affected Area (acres)	*4964*
Total Affected Coal (million tons)	104.6
Total Affected Volume of Gas (bcf)	52.3

Calculations of equivalent carbon dioxide emissions on a recovery basis require knowledge of four significant factors. These are summarized below.

1. *Concentration of methane in produced gas.* The concentration of methane in produced gas for the Qinshui Basin is relatively high. For the purpose of this study, a methane concentration of 90 percent is utilized. The remaining 10 percent is comprised of constituents assumed to have an insignificant atmospheric heat-trapping impact. Of the four discussed significant factors, this is the only factor which will vary on a site-specific basis.
2. *Conversion factor to convert volume of methane (ft^3) to mass of methane (metric tons).* In accordance with the United State's Environmental Protection Agency's (USEPA) interactive units converter (2011), 1 cubic foot of methane has a mass of 1.93×10^{-5} metric tons.
3. *Global warming potential (GWP) of methane to convert mass of methane (metric tons) to mass of carbon dioxide (metric tons).* The global warming potential represents the heat trapping capabilities of a compound in relation to the heat trapping capabilities of an equivalent mass of carbon dioxide over a 100-year period. Seinfeld and Pandis (2006) find the GWP of methane to be 23, or 23 times as potent of a greenhouse gas than carbon dioxide over a 100-year period. The USEPA's interactive units converter (2011) states methane's GWP to be 21. For the purpose of this study, the USEPA's value of 21 is used.

4. *Stoichiometric conversion to convert combusted methane mass (metric tons) to carbon dioxide mass (metric tons).* The combustion of methane results in the creation of one molecule of carbon dioxide for each molecule of methane. Based on the molar masses of each molecule, 1 metric ton of combusted methane forms 2.75 metric tons of carbon dioxide.

The equivalent emissions of ventilated methane are outlined below in Equation 3.1.

$$\mathrm{CO_2E(CH_4)}_{vent} = V_{vent} C_{CH4} * 1.93 * 10^{-5} * 21 \qquad \text{(Equation 3.1)}$$

Where $CO_2E(CH_4)_{vent}$ represents the metric tons of equivalent carbon dioxide emissions by ventilating a volume of gas, V_{vent} (cubic feet) with a specified methane concentration, C_{CH4}. As previously discussed, the remaining constants convert the volume of methane to a mass of methane, then to an equivalent mass of carbon dioxide.

Recovered, combusted methane will emit the mass of carbon dioxide presented in Equation 3.2.

$$\mathrm{CO_2(CH_4)}_{combust} = V_{rec} C_{CH4} * 1.93 * 10^{-5} * 2.75 \qquad \text{(Equation 3.2)}$$

Where $CO_2(CH_4)_{combust}$ represents the metric tons of emitted carbon dioxide by combusting a specified volume of recovered gas, V_{rec} (cubic feet) at a given methane concentration (C_{CH4}).

By applying Equations 3.1 and 3.2 to the volume of exposed gas presented in Table 3-4, emission reductions based on various gas recoveries can be calculated. Figure 3-10 displays emission reductions in million metric tons of carbon dioxide equivalent emissions based on gas recoveries from zero to 100 percent for the hypothetical Qinshui longwall mine.

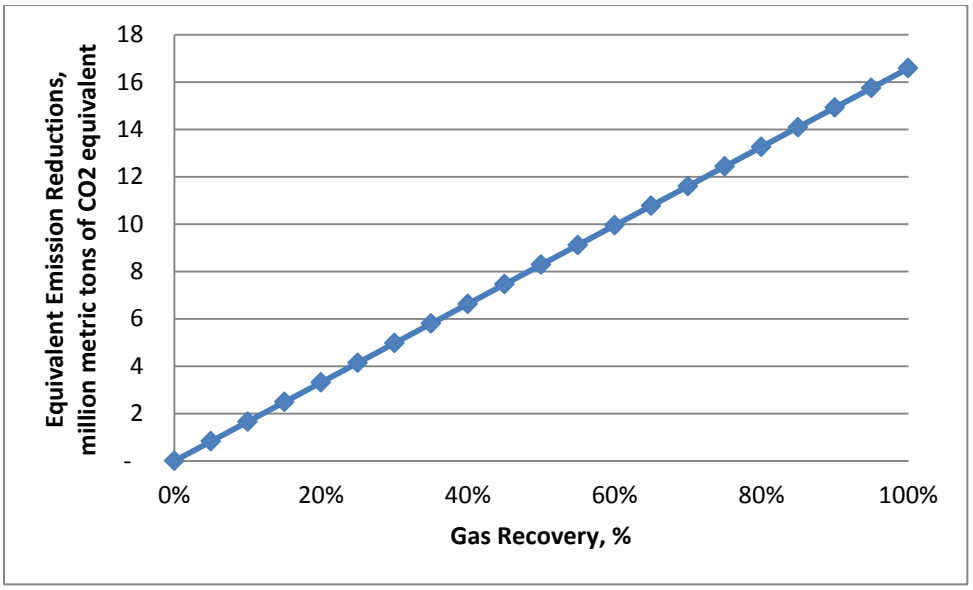

Figure 3-10: Emission reductions for hypothetical Qinshui longwall operation at various gas recoveries

While Figure 3-10 extends to 100-percent gas recovery, obtaining this figure would require substantial lead time and planning ahead of mining operations. Reservoir modeling was conducted over a 20-year period, during which each well layout reaches different levels of recovery. Figure 3-11 contains the required drainage time for wells to reach specified recoveries. This offers a planning tool, as cross referencing target emission reductions in Figure 3-10 with gas recoveries in Figure 3-11 show the range of potential drainage patterns which can be used.

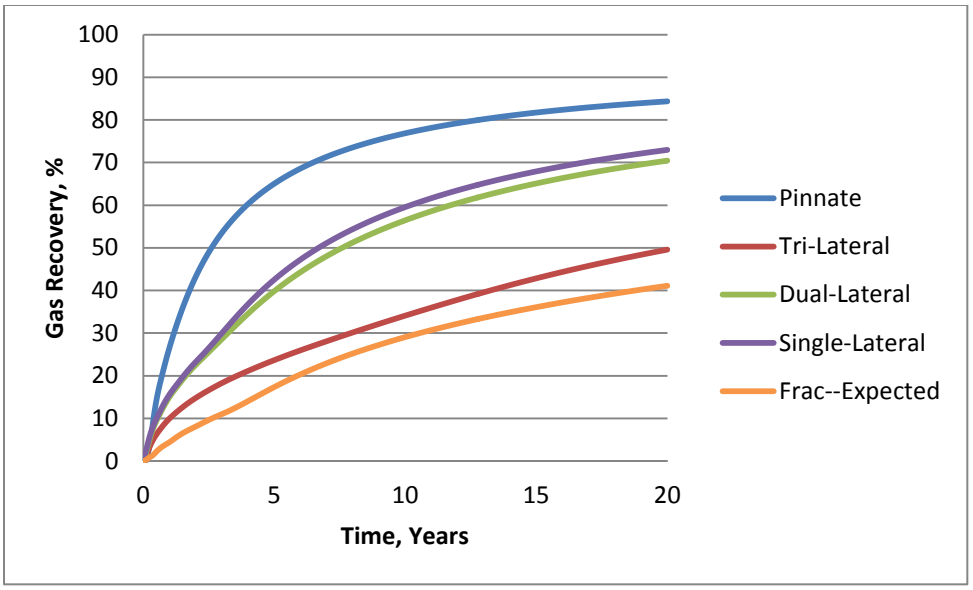

Figure 3-11: Recovery vs. time for horizontal and expected vertical fracture wells

The Pinnate-style well exhibits the highest recovery over a 20-year period, followed by the single-lateral, dual-lateral, tri-lateral, and vertical fracture well. Increasing the recovery of each well can be obtained by decreasing the drainage area, subsequently requiring more wells to be drilled on a per-unit-area basis. As evident in Figure 3-11, reaching 100-percent recovery is effectively impossible. The Pinnate-style well becomes asymptotic to a recovery value of nearly 90 percent. This corresponds to a decrease in carbon equivalent emissions of roughly 15 million metric tons when using multiple Pinnate wells ahead of a 20-year longwall mining plan in the Qinshui Basin.

A variety of wellbore patterns and degasification strategies can be implemented, as drainage time ahead of mining will vary on an individual well basis in accordance to the mine plan. For example, 50-percent recovery can be obtained in 20 years with a Turkey Foot-type pattern, 7 to 8 years with dual and single lateral setups, and in less than 3 years with a Pinnate-style well. A detailed financial analysis can be used to optimize this strategy. Section 3.5. includes the methodology to assess the economic feasibility of various wellbore patterns.

3.5. Financial Modeling

3.5.1. Overview

A detailed financial analysis represents a key factor in the design and selection of a wellbore pattern. The following sections outline the process in determining the economically optimum drainage pattern based on those patterns discussed in the preceding sections. Annual production values obtained through reservoir modeling in Section 3.2 are used in the discounted cash flow study. A sensitivity analysis is also included to identify those factors which have the most significant impact on the financial assessment. Additionally, a Monte-Carlo analysis is incorporated, placing a confidence interval on obtained results from the financial modeling.

3.5.2. Financial Model Inputs

Table 3-5 outlines the inputs as used for the financial modeling assessment. Cash flows are discounted over a 20-year project period at a rate of 10 percent. The financial model inputs are assumed to be accurate for the Qinshui Basin based on the authors' past affiliations with producing entities in the region. Gas prices start at a value of $5.60 per million BTU. Processed gas is assumed to have a heating value of 950 BTU per cubic foot. Gas prices escalate at a rate of 3 percent over the first 15 years of the project, and then become constant for the final 5 years. A gas shrinkage volume equivalent to 7 percent of the processed gas is incorporated to account for the lost produced gas utilized for gas compression and transmission. Gas gathering costs and overhead costs have respective values of $0.33 and $0.45 per thousand cubic feet, with costs escalating at an annual rate of 3 percent throughout the project life. The financial assessment represents a pre-tax and pre-royalty model.

Table 3-5: Financial modeling inputs

Cash Flow Discount Rate	10%
Initial Gas Price ($/MMbtu)	$ 5.60
Heating Value Adjustment (btu/scf)	950
Gas Price Escalation (Years 1-15)	3%
Gas Price Escalation (Years 16-20)	0%
Gas Shrinkage (Compressor Fuel)	7%
Gas Gathering Cost ($/mcf)	$ 0.33
Overhead Cost ($/mcf)	$ 0.45
Cost Escalation	3%

Required capital expenditures for each well configuration are summarized in Table 3-6. The Pinnate-style well requires 20,000 feet of in-seam drilling and is assumed to have a capital expenditure of $1.85 million. The remaining horizontal wells incorporate the baseline Pinnate cost and an incremental price reduction of $40 per linear foot of in-seam drilling. This reduction accounts for decreases in required capital expenditures for horizontal wells with lower in-seam drilling lengths, as they will require less drilling time. Vertical fracture wells are assumed to cost $400,000. Table 3-6 also includes operating costs and maintenance costs, which vary for horizontal and vertical wells.

Table 3-6: Capital and operating expenditures by well

	Pinnate	**Turkey Foot**	**Dual Lateral**	**Single Lateral**	**Fracture**
In-Seam Drilling Length (ft)	20,000	7,100	6,800	3,200	X
Drainage Area (acres)	250	250	166	79	79
Base Capital (million $)	$ 1.185	$ 1.185	$ 1.185	$ 1.185	$ 0.4
Capital Adjustment ($/ft)	$ 40	$ 40	$ 40	$ 40	X
Capital Adjustment	$ -	$ 516,000	$ 528,000	$ 672,00	X
Adjusted Capital (million $)	*$ 1.85*	*$ 1.334*	*$ 1.322*	*$ 1.178*	*$ 0.4*
Year 1 Fixed Operating Expenses ($/Month)	$ 7,500	$ 7,500	$ 7,500	$ 7,500	$ 4,000
Year 2 Fixed Operating Expenses ($/Month)	$ 5,000	$ 5,000	$ 5,000	$ 5,000	$ 2,500
Year 3+ Fixed Operating Expenses ($/Month)	$ 2,000	$ 2,000	$ 2,000	$ 2,000	$ 1,500

3.5.3. Financial Modeling Results

Incorporating the discussed financial modeling inputs with production values obtained from reservoir modeling results yield the cash flows summarized in Table 3-7. Each well configuration's internal rate of return (IRR) and net present value (NPV) are also included as calculated over the 20-year project period.

Based upon the financial assessment of each well, the Pinnate well provides the highest level of economic feasibility. While the Pinnate configuration shows the highest NPV, project IRR is the governing parameter in investment decision making assuming that compared projects have a similar scale and duration. The IRR depicts the quality of an investment, while the NPV is an indicator of the magnitude of a project. In addition to having the most favorable IRR, the Pinnate well provides the fastest project payback. The project payback period represents the amount of time required to recover the initial project capital expenditures. The high gas production rates associated with the Pinnate well allow a payback period of less than 1 year, largely contributing to its high IRR.

While the Pinnate-style configuration shows the best economic investment criteria, it requires a significantly larger investment than the other wells. Still, it should be noted and understood that the Pinnate-style configuration drains an equivalent area of the Turkey Foot, 50-percent more area than the dual-lateral configuration, and double the area of the discussed single lateral and vertical fracture wells. In analyzing the capital costs associated with drilling additional wells of the alternate configurations, the Pinnate well requires the least capital per unit area, making it more financially attractive.

Table 3-7: Annual cash flow, project NPV and IRR by well

Year	Pinnate	Turkey Foot	Dual Lateral	Single Lateral	Frac (Low)	Frac (Expected)	Frac (High)
0	$(1,850,000)	$(1,334,000)	$(1,322,000)	$(1,178,000)	$(400,000)	$(400,000)	$(400,000)
1	$2,500,583	$879,792	$879,509	$386,548	$58,664	$87,264	$115,863
2	$1,598,605	$421,624	$438,019	$179,964	$60,770	$85,321	$109,872
3	$1,039,033	$336,820	$390,418	$194,811	$56,318	$76,252	$96,185
4	$692,827	$279,224	$396,709	$202,992	$61,910	$83,783	$105,650
5	$496,716	$252,236	$358,276	$173,471	$73,351	$95,205	$117,054
6	$375,778	$235,085	$308,142	$142,120	$68,210	$87,325	$106,442
7	$295,583	$223,571	$264,792	$117,364	$60,571	$77,119	$93,670
8	$239,211	$222,459	$230,178	$98,237	$53,399	$67,855	$82,314
9	$197,848	$222,855	$202,274	$83,260	$47,342	$60,093	$72,850
10	$166,462	$221,600	$179,496	$71,360	$43,339	$54,708	$66,088
11	$141,996	$221,987	$160,713	$61,741	$39,101	$49,353	$59,616
12	$122,504	$222,475	$145,043	$53,849	$36,113	$45,447	$54,798
13	$106,680	$220,055	$131,809	$47,267	$33,984	$42,547	$51,124
14	$93,616	$215,330	$120,510	$41,711	$31,467	$39,379	$47,363
15	$82,686	$209,444	$110,786	$36,970	$29,749	$37,108	$45,976
16	$70,084	$195,462	$97,980	$30,921	$27,073	$33,709	$43,994
17	$59,468	$182,196	$86,869	$25,710	$23,935	$29,945	$41,596
18	$50,443	$169,697	$77,169	$21,187	$21,552	$27,022	$39,011
19	$42,701	$157,960	$68,639	$17,233	$19,818	$24,698	$36,283
20	$35,229	$144,727	$59,981	$13,260	$17,126	$21,345	$32,858
NPV	*$4,142,627*	*$1,421,528*	*$1,469,992*	*$56,700*	*$35,733*	*$179,260*	*$328,447*
IRR	*100%*	*34%*	*38%*	*11%*	*12%*	*18%*	*24%*

3.5.4. Sensitivity Analyses

The financial modeling inputs which have the most significant influence on project NPV and IRR are determined through a sensitivity analyses. For the purpose of this study, financial parameters with the highest likelihood of variation were discretely changed to analyze their impact on each well's project NPV and IRR. Through this process, the framework of the financial model remained the same as discussed in Sections 3.5.2 and 3.5.3. As with the initial financial analysis, gas price escalation is only assumed to occur over the first 15 years of the project. Similarly, well maintenance and operating costs only vary during the initial 3 years of

production. Table 3-8 outlines those parameters which are altered and their respective likely minimum and maximum values as incorporated in the sensitivity study. For simplicity in displaying the sensitivity results, gathering and operating costs were combined and changed simultaneously. The same methodology was applied to well operating and maintenance expenses for different project years: for example, the expenses for all project years were changed by a factor of 50-percent simultaneously as opposed to an independently varying expense for individual years.

Table 3-8: Sensitivity study parameters

Parameter	Percent-Adjustment	Baseline Value	Adjustment
Initial Gas Price	+/- 40%	$5.60	+/- $2.24
Gas Price Escalation (Years 1 - 15)	+/- 50%	3%	+/- 1.5%
Costs (Gathering and Overhead) ($/mcf)	+/- 50%	$0.78	+/- $0.39
Cost Escalation	+/- 50%	3%	+/- 1.5%
Capital (Horizontal and Vertical Wells)	+/- 20%	varies	+/- varies
Vertical Well Operating Expenses (Year 1)	+/- 50%	$4,000	+/- $2,000
Vertical Well Operating Expenses (Year 2)	+/- 50%	$2,500	+/- $1,250
Vertical Well Operating Expenses (Year 3)	+/- 50%	$1,500	+/- $750
Horizontal Well Operating Expenses (Year 1)	+/- 50%	$7,500	+/- $3,750
Horizontal Well Operating Expenses (Year 2)	+/- 50%	$5,000	+/- $2,500
Horizontal Well Operating Expenses (Year 3)	+/- 50%	$2,000	+/- $1,000

A graphical depiction of the sensitivity analysis results is shown in Figure 3-12 and Figure 3-13. The column charts contain the baseline respective NPV and IRR values for each well pattern as obtained in Section 3.5.3 and displayed in Table 3-7. Error bars are included to represent the impact of the anticipated maximum differences of the financial modeling inputs as displayed in Table 3-8.

As expected, initial gas price data plays the most significant role in the financial analyses for both the NPV and IRR calculations. While gas price escalation shows a much lesser impact than initial gas price, the sensitivity analysis only analyzes gas price escalation on a positive

basis with gas prices increasing through the life of the project. A downturn in gas prices could pose a more significant impact, especially in the early years of a well's life.

After initial gas price, the relative significance of financial modeling inputs on NPV vary based on well pattern. For all well patterns, cost escalation shows the least significance. Gas price escalation, gathering and overhead costs, capital expenditures, and operating expenses demonstrate varying importance depending on the well pattern. Still, the impact of these parameters is miniscule in comparison to the impact of initial gas price.

Based on the sensitivity analysis results, second to initial gas price, project IRR is most sensitive to capital expenditures, followed by gathering and overhead costs, operating expenses, gas price escalation and cost escalation. The early years of a project's life largely dictate the IRR, making gas price escalation and cost escalation hold the least significance of all input parameters. At a small incremental annual increase, price and cost escalation do not become significant until the later years of the well's producing life. Discounting the later years of a cash flow yields a much lesser impact than the early years. The Pinnate wellbore pattern is the only configuration which maintains a financially viable IRR value at the least anticipated initial gas price of $2.24 per MMBTU, with a corresponding IRR of 35 percent.

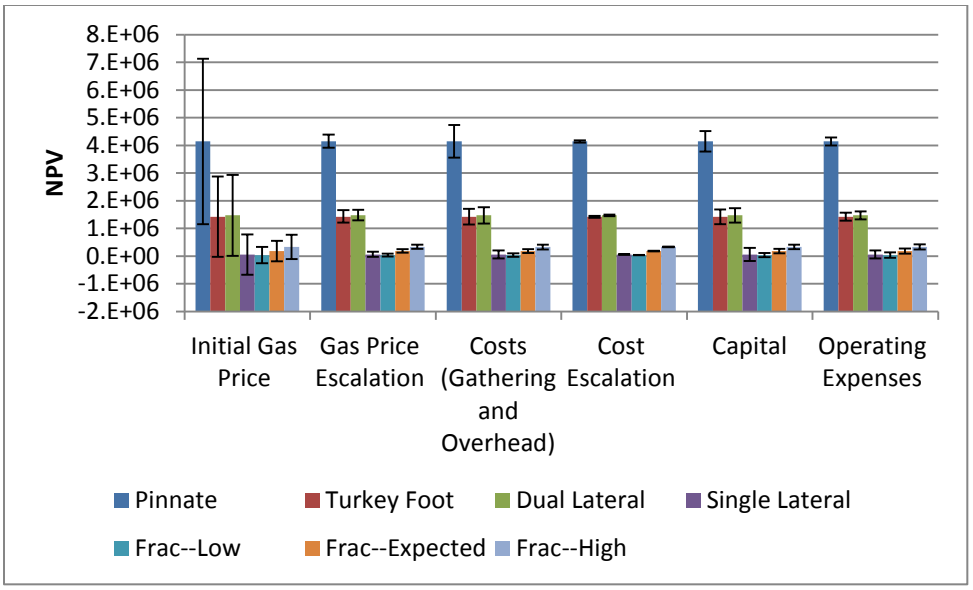

Figure 3-12: NPV sensitivity analysis results

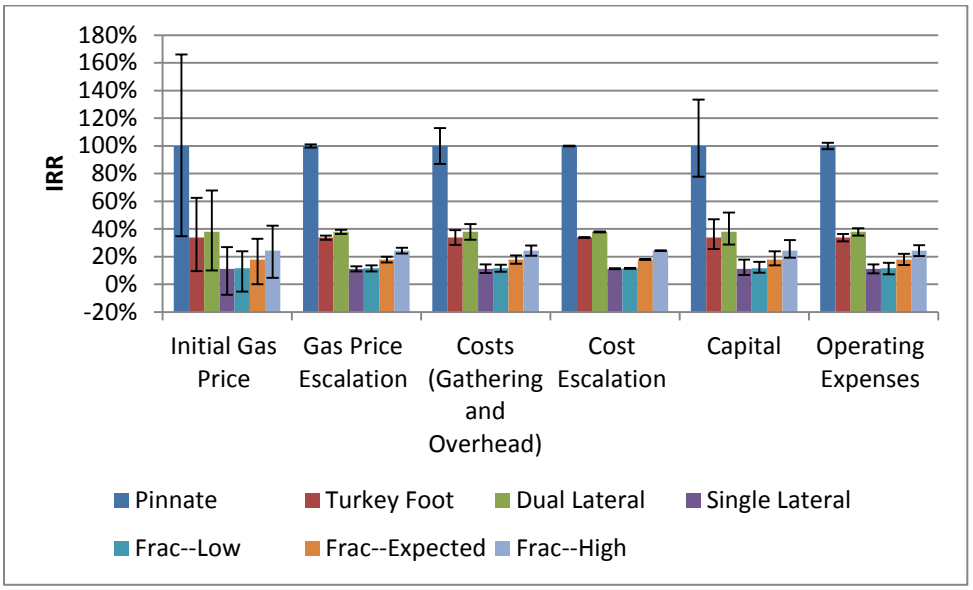

Figure 3-13: IRR sensitivity analysis results

3.5.5. Monte Carlo Simulation

While the sensitivity analysis presented in the preceding section determines the relative significance of selected financial modeling inputs, their respective roles are analyzed on an independent basis. Simultaneous changes in financial model inputs can result in a more significant impact than the discrete changes already presented. A probabilistic analysis through a

Monte Carlo simulation relates the interactions of multiple financial input parameters to help better understand their expected combined impact on project profitability.

Stermole and Stermole (2006) provide an excellent overview of Monte Carlo simulations as applied to discounted cash flow analyses. They state that the use of a range of values to describe input parameters as opposed to single values greatly enhances the quality of a financial study. The sensitivity analysis presented above describes a best-, expected- and worst-case scenario but does not adequately quantify the complete range of values between the best and worst cases. By applying a probability distribution to each financial model input parameter, multiple financial model iterations can be executed to determine a likely range of financial model outputs. Each financial model iteration uses randomly generated data for each input parameter which is matched to a pre-determined probability distribution. Stermole and Stermole (2006) recommend using at least 1,000 iterations for accurate results. The Monte Carlo-type study allows a decision maker to understand the effects of risk and uncertainty in a better manner than any other analysis approach (Stermole and Stermole, 2006). Furthermore, a confidence interval can be placed on output parameters.

As stated by Stermole and Stermole (2006), the greatest weakness of the Monte Carlo-type study involves the subjective nature in assigning probabilities of occurrence to input parameters. For the purpose of this study, the financial parameters listed in Table 3-8 are modeled with normal probability distributions. The normal distribution represents a bell-shaped curve. The baseline values presented in Table 3-8 are modeled as the mean values in the normal probability distribution. The anticipated minimum and maximum values are assumed to fall two standard deviations (σ) from the mean baseline value. In accordance with statistical theory, 95 percent of the data for each input parameter will fall within the anticipated minimum and

maximum values. Figure 3-14 displays a normal probability bell-shaped curve as applied to this study's Monte Carlo analysis. As with any normal distribution, 68 percent of the data falls within 1 standard deviation of the mean, 95 percent within 2 standard deviations and 99.7 percent within 3 standard deviations.

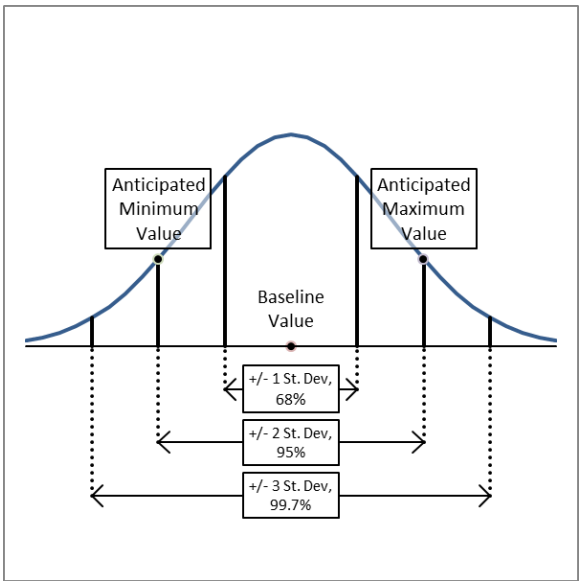

Figure 3-14: Normal distribution as applied to input parameters for Monte Carlo study

Data for the input parameters was generated through the use of Microsoft Excel's random number generator in the Data Analysis Toolpak. For each input parameter shown in Table 3-8, 10,000 numbers were randomly generated such that their mean value was equivalent to the baseline value, and the data sets' standard deviations were equivalent to one-half of the adjustment value. The same process was also applied to the production values associated with the worst-, expected-, and best-case half-fracture lengths for the vertical fracture wells obtained through reservoir modeling. For the vertical fracture well production data, 95 percent of the data will fall between the worst- and best-case production scenarios. This eliminates the need to describe the vertical well production on worst, expected, and best case while quantifying the data continuously throughout the range of production values.

In analyzing statistical financial data, Stermole and Stermole (2006) stress that project IRR can lead to dual solutions and inconsistent measures of performance. Therefore, in determining the profitability and associated confidence intervals for the 10,000 iterations discussed above, project NPV and Benefit to Cost (B/C) ratios are utilized. B/C ratios are calculated by dividing the discounted present value of positive cash flows at a specified discount rate (10 percent this study) by the maximum capital exposure (occurring at year zero for this case). As B/C ratios increase, projects become more profitable and attractive. A B/C ratio of 1 represents the economic breakeven point where discounted income is equivalent to capital exposure at year zero. B/C ratios greater than 1 are considered profitable, with those less than 1 not economically satisfactory (Stermole and Stermole, 2006).

Project NPV and B/C ratios were calculated for the 10,000 combinations of input parameters for each well layout. A graphical analysis was performed to determine if the 10,000 output NPV and B/C ratios follow similar bell-shaped normal distribution as the input parameters. Figure 3-15 and Figure 3-16 display histograms of the NPV and B/C ratios for the Pinnate-style well. The x-axis values are plotted with respect to the calculated distributions' mean and standard deviation values. In Figure 3-15 and Figure 3-16, x respecively represents NPV and IRR values calculated within varying standard devisations, σ, from the mean value. As is evident in the histograms, the distributions are normal and bell shaped. Therefore, confidence intervals can be applied using a z-score system which rates the probability of occurrence based on relative distance from the mean with respect to standard deviation. *Note: The remaining well layouts provide normal distributions for NPV and B/C ratios, but their histograms are not included in the interest of brevity.*

Table 3-9 contains the expected NPV and B/C ratios as calculated from the baseline financial model inputs. In addition, the mean NPV and B/C ratios are included from the 10,000 iterations obtained by the Monte Carlo analysis. In reporting the confidence intervals, the expected calculated value from baseline inputs is included in lieu of the mean Monte Carlo values, as the expected value from baseline inputs is more accurate and some error is introduced in the Monte-Carlo simulation. The 95-percent confidence interval is represented by 2 standard deviations of the 10,000 outputs for each well layout. These results are presented graphically in Figure 3-17 and Figure 3-18. The dot on the graphs represents the expected value while the vertical bars depict the 95-percent confidence interval.

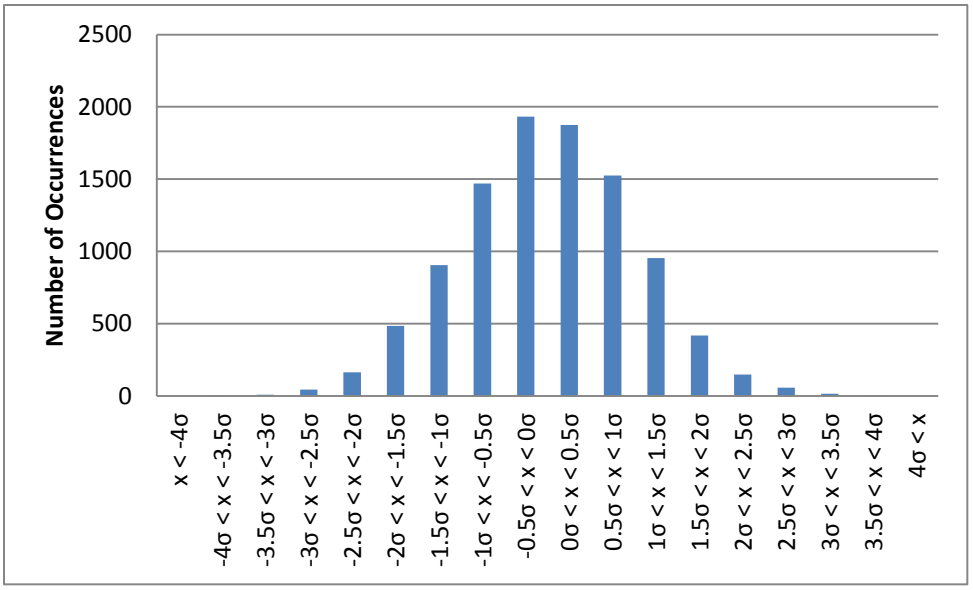

Figure 3-15: Monte Carlo results: NPV histogram for Pinnate style well

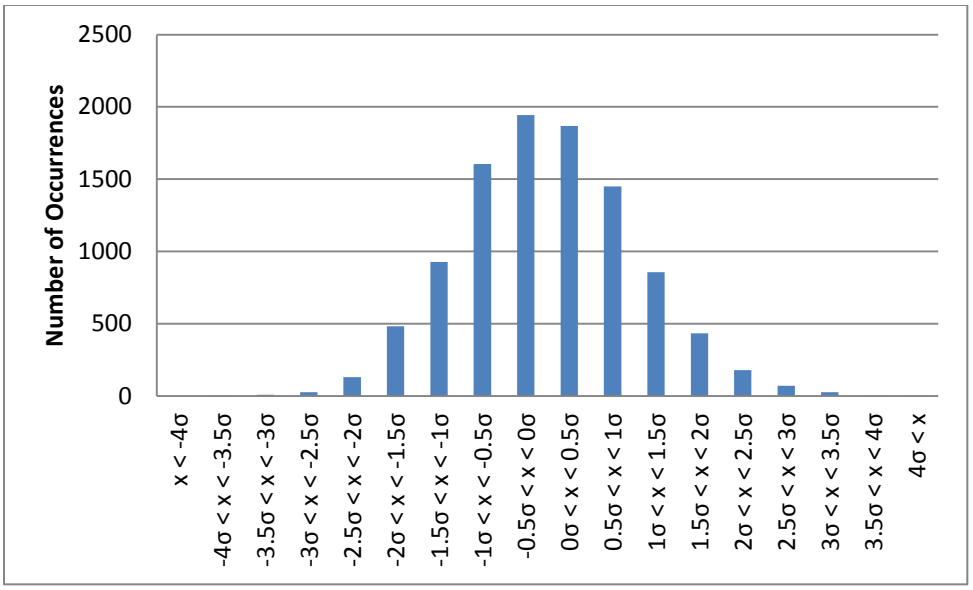

Figure 3-16: Monte Carlo results: B/C ratio histogram for Pinnate style well

Table 3-9: Monte Carlo output summary

	Pinnate	Turkey Foot	Dual Lateral	Single Lateral	Vertical
Expected NPV (Calculated from Baseline Inputs)	$4,142,627	$1,421,528	$1,469,992	$56,700	$179,260
Monte Carlo Mean NPV	$4,144,737	$1,424,483	$1,472,164	$57,720	$180,127
Percentage Difference	-0.05%	-0.21%	-0.15%	-1.80%	-0.48%
Expected B/C (Calculated from Baseline Inputs)	3.24	2.07	2.11	1.05	1.45
Monte Carlo Mean B/C	3.27	2.09	2.13	1.06	1.46
Percentage Difference	-1.03%	-1.10%	-1.07%	-1.08%	-1.12%
95-Percent Confidence Interval (NPV)	$4,142,627 +/- $3,077,759	$1,421,528 +/- $1,526,869	$1,469,992 +/- $1,537,409	$56,700 +/- $795,374	$179,260 +/- $432,667
95-Percent Confidence Interval (B/C)	3.24 +/- 1.80	2.07 +/- 1.22	2.11 +/- 1.24	1.05 +/- 0.69	1.45 +/- 1.12

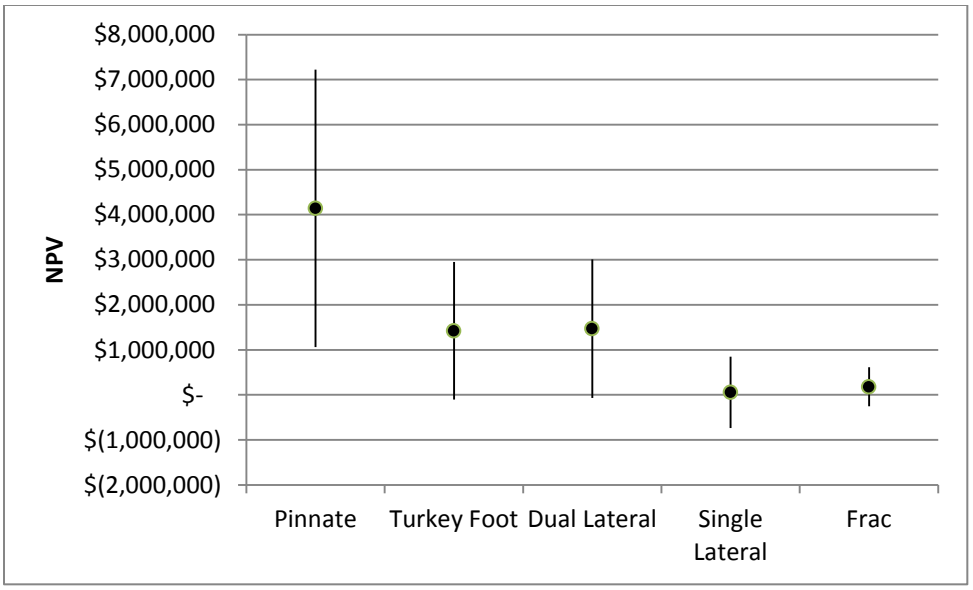

Figure 3-17: NPV 95% confidence interval from Monte Carlo results

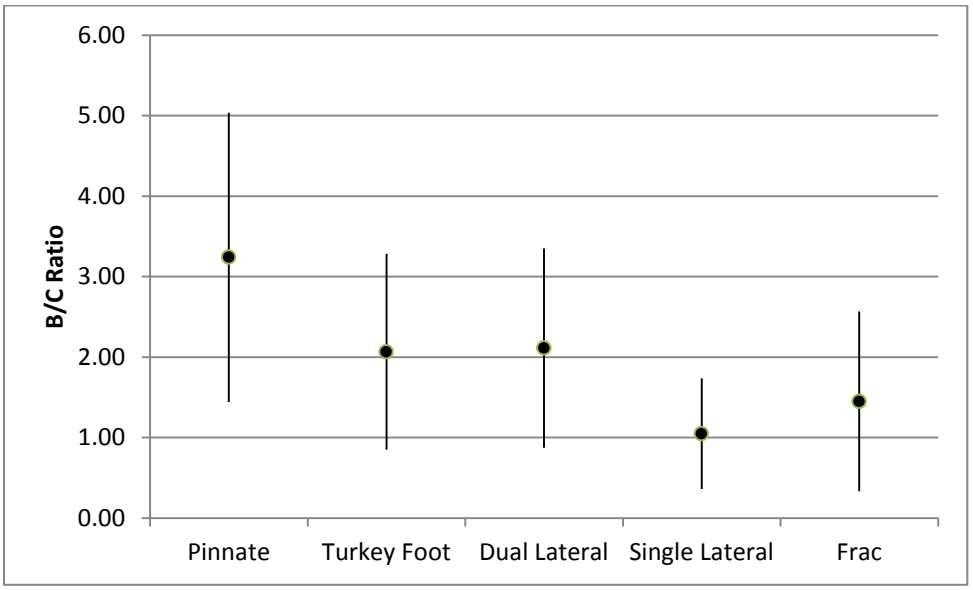

Figure 3-18: B/C ratio 95% confidence interval from Monte Carlo results

As shown in Figure 3-17 and Figure 3-18, the Pinnate well is the only modeled horizontal well pattern which shows a 95-percent confidence interval of being profitable. The other horizontal patterns exhibit potential benefit to cost ratios of less than 1.0. Discounting cash flows at a rate of 10-percent, Monte Carlo simulations suggest that Pinnate wells are the only modeled completion strategy which provide positive project net present values when varying

financial modeling inputs over expected ranges. Single-lateral and vertical fracture wells demonstrate the lowest likelihood of profitability.

3.6. Conclusions

The preceding sections serve as a framework for determining the optimum degasification pattern based on coalbed methane drainage ahead of mining, greenhouse gas emissions, and economic criteria. Of the analyzed well patterns, Pinnate-style wells provide the best characteristics for economic production while simultaneously decreasing greenhouse gas emissions and offering the potential for increased mine productivity. While the Pinnate pattern is the only studied multilaterally drilled design, variations of this design should provide similar results.

Reservoir and financial modeling show that maximizing drainage areas and in-seam drilling footage from a single well platform offer the best return on capital investment. The required increase in capital of drilling additional in-seam footage is quickly offset by increased production. The closely spaced laterals of a Pinnate-style pattern quickly recover methane, boosting the project's internal rate of return, benefit-to-cost ratio, and project net present value. Contrarily, while traditional hydraulically fractured vertical wells require a significantly lower capital investment, they do not effectively drain CBM from coal ahead of mining and result in a lower project rate of return. In the event that the required capital is not available to develop large Pinnate-style patterns, single-lateral and dual-lateral configurations provide the next best economic return but result in lower recoveries than the Pinnate-style wells. Additionally, to successfully develop Pinnate wells, higher operator skill and state-of-the-art drilling technology is required. The multiple branches and associated geometry can be difficult to drill without technically advanced drilling equipment.

As carbon dioxide equivalent emission reductions are directly proportional to the volume of produced gas by a well or series of wells, Pinnate wells offer the best option of drainage in advance of mining to decrease greenhouse gas emissions. Gas recoveries of upwards of 80-percent are feasible through the use of Pinnate wells when operated over a 20-year period. As applied to a longwall operation in the Qinshui Basin, an 80-percent recovery corresponds to a decrease in carbon dioxide equivalent emissions of approximately 15 million metric tons over a 20-year mine plan. The remaining modeled well layouts cannot reach a recovery of 80-percent over a 20-year period. To boost recovery values for the remaining wells, drainage area can be decreased, subsequently increasing the number of required wells to drain a given area.

Raw recovery values are useful in assessing the effectiveness of a well as applied on an economic and greenhouse gas emission basis. Spatial distributions of recovery across a drainage area offer a better analysis method for determining the impact of a degasification well on mine safety. Minimizing the variation in recovery will result in more consistent conditions during mining and minimizes isolated gassy zones. The closely spaced laterals of Pinnate-style wells help maintain a consistent recovery across the drainage area. The minimal drilling footage per unit area of Turkey Foot-style patterns results in a large variation, similar to the variation exhibited by hydraulically fractured wells. Single lateral and dual lateral configurations provide a fairly consistent distribution of recoveries, albeit lower recoveries than that of the Pinnate well. A case study analysis of a producing longwall in the Qinshui Basin serves as an example of successful drainage through surface-drilled horizontal and in-mine horizontal drainage. Production has increased 10-fold throughout the evolution of the degasification system at this operation.

In conclusion, increasing production of coalbed methane is the key factor to enhancing the profitability of drainage wells and improving reductions in equivalent carbon dioxide emissions. Larger drainage patterns make the best use of capital. The high initial production rates of larger drainage patterns help offset capital investment and increase a project's internal rate of return. Further, closely spaced laterals decrease variability in recovery across a drainage area, enhancing mine safety and potentially boosting productivity. While this work is applied to China's Qinshui Basin, the framework for assessing the effectiveness of coalbed methane drainage wells is applicable on a global scale. The discussed results are applicable for coalbed methane basins exhibiting similar geologic characteristics to those of the Qinshui Basin, including those with low permeability, gassy, thick coal seams.

Chapter 3 References

Cheng, Y., Wang, L., Zhang., X. 2011. Environmental impacts of coal mine methane emissions and responding strategies in China. International Journal of Greenhouse Gas Control. 5. 157-166.

Karacan, C. 2008. Evaluation of the relative importance of coalbed methane reservoir parameters for prediction of methane inflow rates during mining of longwall development entries. Computers and Geosciences. 34(9). 1039-1114.

Keim, S., Luxbacher, K., Karmis, M. 2011. A numerical study on optimization of multilateral horizontal wellbore patterns for coalbed methane production in Southern Shanxi Province, China. International Journal of Coal Geology. 86(4). 306-317.

Lu Y., Li., X. 2011. A study on a new hazard detecting and controlling method: The case of coal mining companies in China. Safety Science. 49. 279-285.

Lu, Y., Liu, Y., Li, X., and Kang, Y. 2010. A new method of drilling long boreholes in low permeability coal by improving its permeability. International Journal of Coal Geology. 84. 94-102.

Luo, D., Chu, W., Wu, X., Li, W. 2009. Analysis of economic benefits of coalbed methane drilling technologies. Petroleum Exploration and Development. 36(3). 403-407.

Maricic, N., Mohaghegh, S.D., and Artun, E. 2008. A Parametric Study on the Benefits of Drilling Horizontal and Multilateral Wells in Coalbed Methane Reservoirs. SPE Reservoir Evaluation and Engineering. 11 (6). 976-983.

Palmer, I. 2010. Coalbed methane completions: A world view. International Journal of Coal Geology. 82. 184-195.

Sang, S., Liu, H., Li, Y., Li, M., Li, L. 2009. Geological controls over coal-bed methane well production in southern Qinshui Basin. Procedia Earth and Planetary Sciences. 1. 917-922.

Seinfield, J., Pandis, S. 2006. Atmospheric Chemistry and Physics, 2nd Edition. published by John Wiley & Sons, Inc., Hoboken, NJ.

Shi, X. 2009. Have government regulations improved workplace safety? A test of the asynchronous regulatory effects on China's coal industry, 1995-2006. Journal of Safety Research. 40. 207-213.

Stermole, F., Stermole, M. 2006. Economic Evaluation and Investment Decision Methods, 11th Edition. Published by Investment Evaluations Corporation, Lakewood, CO.

Su, X., Lin, X., Liu, S., Zhao, M., Song, Y. 2005. Geology of coalbed methane reservoirs in the Southeast Qinshui Basin of China. International Journal of Coal Geology. 62. 197-210.

U.S. Environmental Protection Agency. 2006. Global anthropogenic non-CO_2 greenhouse gas emissions: 1990-2020.

U.S. Environmental Protection Agency. 2011. Coal Mine Outreach Program. Interactive Units Converter. <http://www.epa.gov/cmop/resources/converter.html>.

Wei, C., Qin, Y., Wang, G., Fu, X., Jiang, B., Zhang, Z. 2007. Simulation study on evolution of coalbed methane reservoir in Qinshui Basin, China. International Journal of Coal Geology. 72. 53-69.

Yao, Y., Liu, D., Tang, D., Huang, W., Tang, S., and Che, Y. 2008. A Comprehensive Model for Evaluating Coalbed Methane Reservoirs in China. Acta Geol. Sin-Engl. 82 (6). 1253-1270.

Zhiming, W., Zhang, J., 2009. CBM reservoir thickness affects production from horizontal wells. Oil and Gas Journal. 107(16). 42-46.

Zou, M., Wei, C., Pan, H., Sesay., K.S., Cao, J. 2010. Productivity of coalbed methane wells in southern of Qinshui Basin. Mining Science and Technology. 20(5). 765-769.

Chapter 4. A NUMERICAL STUDY ON OPTIMIZATION OF MULTILATERAL HORIZONTAL WELLBORE PATTERNS FOR COALBED METHANE PRODUCTION IN SOUTHERN SHANXI PROVINCE, CHINA

Steven A. Keim[1], Kramer D. Luxbacher[2], Michael Karmis[1]
[1]Virginia Center for Coal and Energy Research, Virginia Tech, Blacksburg, Virginia
[2]Department of Mining and Minerals Engineering, Virginia Tech, Blacksburg, Virginia

This work is published in the International Journal of Coal Geology, Volume 86, pages 306-317

Abstract

China's southern Shanxi Province contains thick, gassy coals of anthracite rank. These high-methane-content (higher than 500 cubic feet per ton) coals necessitate pre-mining methane drainage to enhance the health and safety of underground coal workers. Both traditional vertical wells and multilateral horizontal wells, which were shown to perform better, have been drilled in the area in order to effectively reduce the gas content of coals. However, optimization of well drilling patterns is crucial to improve the gas drainage by boosting well performance and resulting in significant additional recovered gas in a cost-effective manner. In this study, exploration borehole data from an undeveloped coalbed methane field in China's Qinshui Basin was obtained where permeability is expected to range from 0.1 to 10 md.

Reservoir modeling conducted in this study concludes that in the presence of low permeability coals (less than 1.0 md) well patterns can be optimized to maintain high methane production rates. In this work, relationships to determine combinations of horizontal lateral spacing and permeability that yield similar production curves were developed in order to maximize production. Pinnate wells with laterals spaced at 600-ft intervals in reservoirs with 2.0 md permeability performed similar to those with 200-ft lateral intervals in 0.5 md reservoirs. Additional similar relationships were drawn for reservoirs ranging from 0.1 to 8.0 md. Furthermore, because of the Qinshui Basin's potential high stress regime, Pitchfork and Pinnate horizontal well patterns were analyzed based on their potential for catastrophic wellbore failure at well junctions and producing well branches. Analyses concluded that Pitchfork wells had a significantly lower risk for significant wellbore loss due to borehole collapse, while providing the opportunity for higher gas recovery in reservoirs exhibiting directional permeability.

4.1. Introduction and Background

There are three main benefits of methane drainage in gassy coal seams: an improvement in health and safety for the underground workforce, a decreased environmental impact, and the production of a relatively clean-burning energy source. The accurate modeling of coalbed methane drainage helps to predict the effectiveness of a degasification strategy prior to drilling of

costly production wells. Coalbed methane reservoirs vary globally and locally in terms of geologic parameters and reservoir parameters, and thus must be modeled accordingly. Governing factors for the production of coalbed methane include, but are not limited to, isotherm data, gas content, hydrological data, seam structure, and permeability. This work focuses on variations in permeability, and its effect on gas production. Extraction of ample volumes of gas from low permeability coal seams requires one of three specific strategies (Palmer 2008).

1. Locate a high-producing zone within a property through structural geological maps, coal thickness maps, or trial and error.
2. Opt to produce gas through the use of horizontal wells.
3. Develop advanced stimulation techniques, thus enhancing the limited natural fracture system of the coal to be developed.

This paper will examine the second option, as multilateral horizontal wells have successfully produced gas both domestically and internationally.

Coalbed methane drainage technology has seen vast improvements over the past half century. Degasification of coal from surface boreholes for the express purpose of improving mining conditions began in the mid-1930s in the U.S. The first in-seam horizontal drainage holes were completed in the late 1950s by Consolidation Coal Company in the Pittsburgh coal seam, and the effectiveness of these wells was highly dependent on well orientation and well length (Spindler, 1960). Only in the 1970s was coalbed methane recognized as a marketable fossil fuel, separate from coal (Flores, 1998). In China, commercial drilling of CBM reservoirs began in the 1980s, but success has been limited (Yao et al., 2008). Today, many different drilling techniques are used to produce methane from unmineable coal beds, as well as economically viable coal reserves. Modern wells may be vertical, vertical-to horizontal, or horizontal from in-seam mine workings. They can be stimulated, or rely solely on the natural

fracture system to transport gas and water to the producing well. Wells can target multiple coal seams, including virgin seams. This work concentrates on optimizing vertical-to-horizontal multilateral wells, which have many advantages over more traditional techniques, including the drainage of a larger area from a single drill site, and the ability to effectively increase anisotropic permeability by the drilling and orientation of laterals.

Presently, horizontal wells drilled from both the surface and from internal mine workings provide the opportunity for higher levels of methane recovery in less time compared to traditional vertical fracture wells. Logistically, vertical-to-horizontal wells may be advantageous, because in-mine horizontal drainage techniques require an extensive pipeline system which must constantly be moved and maintained. Additionally, drill rig movement and short lead times ahead of coal production make in-mine drainage less attractive, because entries must be developed for drill rig access. Surface-to-horizontal techniques can begin well ahead of mining, and do not interfere with underground mining practices. Also, gateroads and longwall panels can be degasified simultaneously (Thakur, 2003). Additionally, because surface-to-horizontal holes increase the drainage area significantly, as compared to vertical wells, they may not require stimulation by hydraulic fracturing. This is an advantage in pre-mining situations as hydraulic stimulation can cause fractures to propagate into overlying strata and cause ground control issues (Colmenares and Zoback, 2007; Ross et al., 2009). Vertical-to-horizontal wells are generally capital intensive, but they also tend to result in long-term, sustained production of methane, with a smaller surface footprint.

Strictly from a coal-mining perspective, coal degasification greatly enhances the health and safety of underground miners. As shallow coal reserves are depleted, mining of deep and gassy coal seams is becoming standard practice for coal companies worldwide. Under these

circumstances, typical ventilation practices and only gob-gas ventholes often do not sufficiently eliminate gas methane concentration build-ups, requiring in-seam horizontal methane drainage to maintain lower gas emissions in mine workings. Due to varying geological conditions and mine planning, horizontal borehole designs must be adjusted on a site-by-site basis to successfully extract methane from coal seams prior to mining (Karacan, 2007).

4.1.1. Vertical to Horizontal Degasification Patterns

The U.S. Bureau of Mines began evaluating vertical to horizontal degasification techniques for coalbeds in the late 1970s, and conducted field trials with limited success; they recognized that horizontal holes should be drilled perpendicular to face cleats to yield the most gas (Diamond et al., 1977), because permeability is generally anisotropic and already enhanced in the face cleat direction (Pashin, 1998; Deimbacher et al., 1992). Furthermore, in most cases, hydraulic fracturing will generally continue to enhance permeability in the face cleat direction (Deimbacher et al., 1992) while horizontal drilling allows for enhancement in the butt cleat direction. Estimates for production yield of horizontal wells compared to traditional vertical wells are increased anywhere from 2 to 10 times (Diamond et al., 1977), while costs for horizontal holes range from only 1 to 4 times as much (Palmer, 2010; Gentzis, 2009). Horizontal holes are generally deemed most appropriate for thick coal seams, while stimulated vertical holes may be used to degasify multiple thin seams. However, steerable drilling bits can now effectively degasify seams which are less than one foot thick (Lightfoot et al., 2009), demonstrating that horizontal drilling is becoming increasingly practical. Horizontal completions are also recommended in lower permeability seams, less than 3 md (Palmer, 2010).

Vertical-to-horizontal well patterns generally include single lateral, dual lateral, trilateral, quadrilateral or Pinnate (Palmer, 2010; Maricic et al., 2008). For the purpose of this paper,

pitchfork patterns will refer to multilateral horizontal patterns in which all laterals are branched from a single junction and turned parallel to each other, while a Pinnate pattern refers to two sets of laterals drilled perpendicular to each other, all joined to a single main lateral.

4.1.2. Simulation of Horizontal Multilateral Well Production

A multitude of parameters must be considered during the optimization of horizontal multilateral wells. Studies presenting reservoir simulation of production from these wells have ranged from analysis of specific parameters, such as drilling fluid utilization, to more general analyses including sensitivity studies varying reservoir parameters and wellbore patterns and parameters.

In an early simulation study of horizontal wells, many features of the reservoir and wellbore were examined to determine influence on gas production, and the role of each discussed. Additionally, orientation of patterns was examined for the anisotropic permeability generally found in CBM reservoirs (Ertekin et al., 1988). Gentzis and Bolen (2008) used numerical simulation to examine CBM production from vertical and horizontal wells in Canada, and were able to determine optimal well spacing and water production rates. The study area was a low permeability reservoir (<1 md), and the authors found that lateral spacing (they modeled multiple single leg wells) was a function of permeability and was especially important in low permeability settings. Subsequent studies by Gentzis and others coupled geomechanical modeling and reservoir simulation to examine influence of wellbore stability (Gentzis et al., 2009a; Gentzis et al., 2009b). Another study compared several different horizontal multilateral patterns, varying spacing, permeability and lateral length using a reservoir simulator and determined optimum lateral spacing, pattern, and well length based on net present value (Maricic et al., 2008).

4.1.3. Horizontal Wellbore Stability

Horizontal wellbore stability is an important component of horizontal multilateral well design. Horizontal multilateral wells are capital intensive and careful consideration of stability is imperative to protecting investments. Several researchers have examined wellbore stability based on characteristics of the wellbore (Gentzis, 2009), the mechanical properties of the reservoir (Deisman et al., 2010; Hawke, 2007; Whittles et al., 2007), and drilling design (Gentzis et al., 2009a; Gentzis et al., 2009b). However, there is little evidence of work examining probability of wellbore collapse based on the geometry of the drilling pattern alone, which can provide valuable guidance in reservoirs that are highly heterogeneous or poorly characterized.

4.1.4. Historical CBM Development in Southern Shanxi Province, China

Specific to China, CBM development increased significantly throughout the past decade. Prior to 2003, less than 250 documented CBM wells existed. Five years later, a shift towards safer mining practices and a need for additional energy reserves increased the number of producing wells almost ten-fold. Of these nearly 2,500 wells, less than 30 are of the multilateral horizontal type. The lack of extensive horizontal well development is attributed to high capital costs and limited technology (Luo et al., 2009; Sang et al., 2010). Most multilateral horizontal wells in China are referred to as a herringbone or fishbone pattern, and are similar to the Pinnate pattern (Zhiming and Jian, 2009).

Many of the coal reservoirs in China are characterized by low permeability, soft coal, generally relatively thick and laterally continuous, with gas contents ranging from 8-10 m^3/ton in the majority of mining areas (Su et al., 2005; Lu et al., 2010; Yao et al., 2008). The low permeability values, typically less than 1 md to 6 md, make the reservoirs good candidates for horizontal drilling. However, the soft coal can cause wellbore instability and drilling problems.

Coals in China's Shanxi Province consist of high-rank anthracites. Contrary to pressure-formed anthracite coals, the Shanxi Province anthracites were heated by an igneous intrusion, thus leaving a cleat system which can transport gas and water. Targeted coal seams for degasification in the Southern Shanxi Province extend to depths upwards of 2,000 feet with gas contents greater than 20 m^3/ton (Su et al., 2005). Like many other coals in China, this area generally has a low permeability, 0.1 to 2.0 md (Su et al., 2005; Yao et al., 2008), but the anthracites are much more competent than many of the other basins referenced in China, allowing for improved wellbore stability for horizontal drilling.

4.1.5. Reservoir Overview

4.1.5.1. Coal Bed Geology of Southeastern Qinshui Basin

China's southern Shanxi Province (southeastern Qinshui Basin) contains thick, gassy coals targeted both as a coal and coalbed methane resource. Figure 4-1 displays a map of the Qinshui Basin and generalized location of the study area analyzed in this paper. The primary coalbed for economic gas and coal production is the No. 3 seam, located at the base of the Lower Permian system. Depths for the No. 3 seam range from outcropping to several thousand feet. The No. 3 seam is well explored, and high thicknesses, greater than 20 feet in some areas, permit exploration of the seam via seismic exploration strategies. Figure 4-2 displays a generalized stratigraphic column for the region.

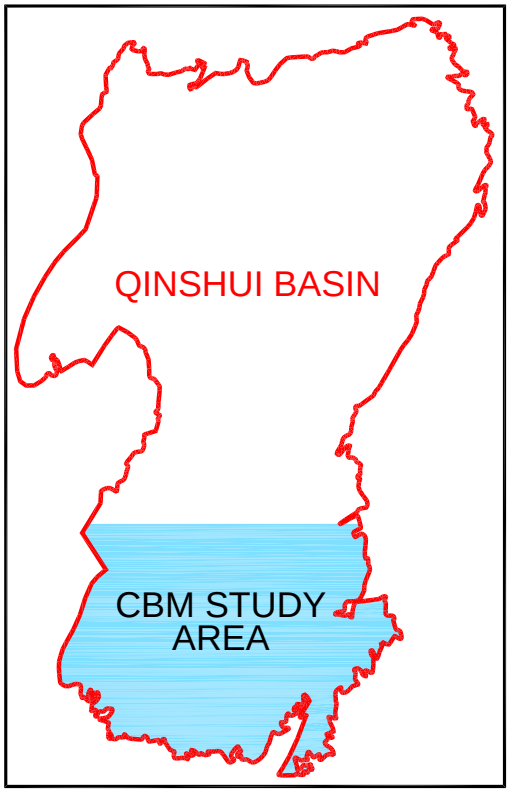

Figure 4-1: Qinshui Basin and CBM study area

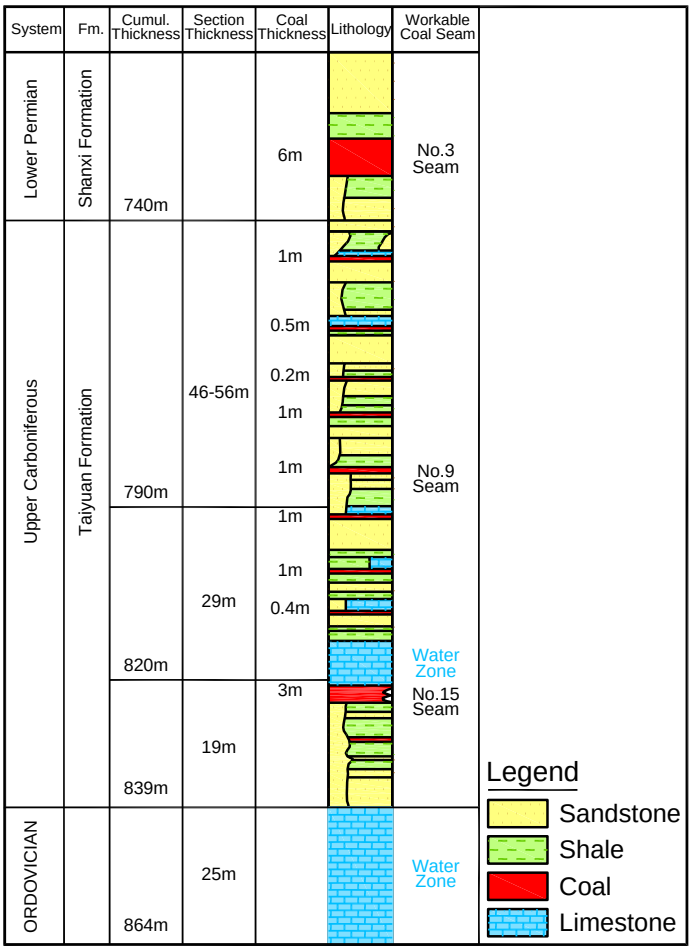

Figure 4-2: Generalized stratigraphic column of study area

Structurally, the region is characterized by many north-trending anticlines and synclines. Faulting is also prominent, with normal and reverse faults of substantial throw and displacement. Again, seismic exploration strategies can pinpoint faulting and discontinuities within targeted coalbeds prior to the mining or drilling process. In complex structural settings such as this, a detailed exploration program is key to success prior to the capital investment of well development, especially expensive multilateral horizontal borings.

Exploration programs have not noted significant water-bearing aquifers proximal to the No. 3 seam. Still, the seam is saturated with water which must be removed prior to the initiation of gas flow. The No. 3 seam is overlain and underlain by both shales and sandstones, some of

which are carboniferous. Overall, the structural setting of the basin is favorable for horizontal well development. More than 20 multilateral horizontal wells have been completed in the region. Confidentiality issues restrict the publishing of production data for these wells, yet initial findings suggest that horizontal wells perform significantly better than vertical wells in the region. The importance of degasification in the region is significant, from a mine-safety standpoint, a greenhouse gas emission standpoint, and the potential value of the gas as a local energy provider.

4.1.5.2. Reservoir Modeling Inputs

In this study, *COMET3* reservoir modeling software was used. COMET3 incorporates a three-dimensional, dual porosity simulator which models fluid flow through coal to a producing wellbore. For the purpose of this study, a single gas component sorption model was utilized, assuming pure methane in the coal seam.

Reservoir parameters are modeled to match those of China's Southern Shanxi Province, where permeability is believed to vary from 0.1 to 10.0 md. Cleats are generally calcite filled and do not contribute to permeability which is primarily controlled by shear fractures. Additionally, tectonic deformation of coal is variable, and in areas of extreme deformation, the coal contains myolithic structures and very low permeabilities, while in more lightly deformed areas higher permeabilities are noted (Su et al., 2005).

Reservoir modeling parameters were obtained from exploration drilling at a greenfield coalbed methane site, characterized by high gas contents and thick coal seams. Based on the obtained exploration borehole data including gas content, coal thickness and permeability, the coal is representative of other coals in the region. These reservoir parameters are outlined in Table 4-1. According to the obtained Langmuir coefficients, depth, pressure gradient, and initial

gas content, the coal is undersaturated. At the initial reservoir pressure conditions, the coal's sorption capacity for methane is 667 standard cubic feet per ton; the coal only contains 500 standard cubic feet per ton.

Table 4-1: Some of the coal reservoir data used in the models

Parameter	Value
Depth (ft)	2000
Coal Thickness (ft)	10
Water Saturation	85%
Fluid Pressure Gradient (psi/ft)	0.3
Permeability—Scenario 1 (md)	0.1 to 8
Permeability Anisotropy Ratio--Scenario 1	1:1
Permeability—Scenario 2 (md)	4, 1
Permeability Anisotropy Ratio—Scenario 2	4:1
Fracture Porosity	3%
Langmuir Volume (ft^3/ton)	1000
Langmuir Pressure (psi)	300
Gas Content (ft^3/ton)	500
Water Saturation (%)	85%
Cleat Spacing (inches)	2
Sorption Time (days)	50

Provided permeability data from injection falloff tests show a wide range of measured values, ranging from less than 0.1 to 10 md. Data pertaining to permeability anisotropy was unavailable. Therefore, to account for both the wide ranges of potential permeability across the study area and the impact of anisotropy, two separate modeling cases were analyzed. The first focuses on the effect of varying permeability without anisotropy and the effects of altering horizontal lateral spacing on production. The second analyzes the impact of wellbore orientation with respect to cleat structure and the associated gains and losses in production associated with proper and improper well orientation assuming an average face-cleat-to-butt-cleat permeability ratio of 4:1.

Relative permeability curves for the modeled reservoir were unavailable. Therefore, relative permeability is assumed to be similar to that of the permeability curves obtained by a 1975 Bureau of Mines Study, and were used to represent the reservoir, as depicted below in Figure 4-3 (Kissell and Edwards, 1975). The Bureau of Mines study focused on relative permeability in the Pocahontas 3 coalbed, which exhibits similar geologic characteristics to the modeled reservoir. Geologically, both coal seams exhibit a similar vertical fluid pressure gradient, depth, high methane content, and similar fracture networks.

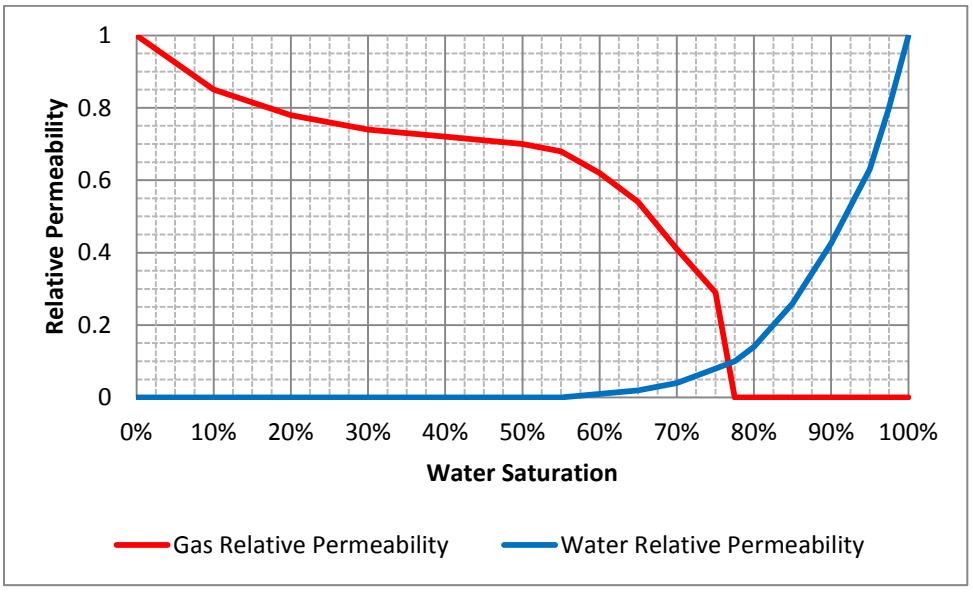

Figure 4-3: Relative permeability curves (modified from Kissell and Edwards, 1975)

All reservoir models incorporate two constraints to govern gas production. A maximum water producing constraint represents water pumping limitations and was assumed to be 250 barrels per day. Additionally, a minimum bottom-hole pressure constraint of atmospheric pressure is incorporated.

4.2. Modeling Scenarios

The following sections contain an overview of the two analyses modeled to examine the effect of horizontal wellbore patterns on permeability and the associated impacts on production. The initial study investigates the interactions of permeability, horizontal lateral spacing, and gas production. The second study focuses on the optimization of well patterns in reservoirs exhibiting directional permeability. The potential gains and losses in well production will be analyzed based on well orientation with respect to cleat structure.

4.2.1. Scenario 1: Z-Pinnate Pattern: Analysis of Lateral Spacing, Permeability and Production

The Z-Pinnate horizontal drainage pattern has proven effective in the central Appalachian Basin. Large drainage patterns greater than 300 acres require less road construction and result in a smaller collective surface footprint than vertical fracture wells. Pinnate patterns have been noted to recover more than 85 percent of in-place gas within a 2-year period (Zupanick, 2006). The proceeding section describes a relationship between permeability, production, and lateral spacing of Pinnate wells as applied in China's southern Shanxi Province. A derived relationship will illustrate combinations of permeability values and lateral spacings which yield similar production curves.

In this work, wells were modeled at lateral spacings of 200, 400, 600, and 800 feet. Side laterals spur from a main lateral at angles of 45 degrees. Similar to current drilling practices in the southern Shanxi Province, drainage areas are modeled as 1-square kilometer zones (247 acres). Table 4-2 displays the total length of drilling (in coal seam) corresponding to each lateral spacing.

Table 4-2: Lateral spacing and in-seam drilling lengths of modeled boreholes

Lateral Spacing (ft)	Total Length of Drilling (ft)
200	46,000
400	27,000
600	20,000
800	17,000

In the models, square grid blocks with 100-ft sides were used to create a total of 1089 grids in the simulated area. Reservoir parameters similar to those of the No. 3 coal seam in China's southern Shanxi Province were modeled as displayed in Table 4-1. It should also be noted that dynamic permeability data pertaining to pore volume compressibility and coal matrix shrinkage was unavailable. Therefore, these two phenomena were assumed to offset each other and were excluded from modeling.

Base model runs were conducted for Pinnate wells with lateral spacings of 600 feet giving a total in-seam drilling length of 20,000 feet in the model in a coal with 1-md permeability. Four independent models of the permeability values for the 600-ft-spaced wells were set to 4.0, 2.0, 1.0, and 0.5 md. Permeability values for the remaining lateral spacings were adjusted until the cumulative production curves for the 200-, 400- and 800-ft spaced wells closely matched those of the 600-ft spacing scenarios with cumulative production values within 5 percent at years 10, 15, and 20. This provides a comparative relationship between permeability, lateral spacing, and production; i.e., a Pinnate well drilled at X-ft spacing in a Y-md reservoir will yield a similar cumulative production curve as a Pinnate well with 600-ft lateral spacing in a Z-md reservoir. In this study, the X-values (lateral spacing) are constrained to 200 ft, 400 ft, and 800 ft. The permeability values (Y) range from 0.1 to 8.0 md. Permeability values for the 600-ft spacing reservoirs, represented by "Z" above, are 4.0, 2.0, 1.0, and 0.5 md.

4.2.2. Scenario 2: Comparison of the Z-Pinnate and Pitchfork Patterns

An additional option for optimizing well production involves completely altering the well geometry and pattern. The proceeding sections compare the previously discussed Pinnate pattern with a Pitchfork pattern. The modeled Pitchfork pattern represents a multilateral horizontal well where all laterals spur apart at the producing well and are then turned parallel to each other. The advantages and disadvantages of both patterns will be analyzed in the presence of reservoirs that display moderate directional permeability and those with the potential of borehole collapse. A diagram of the directional permeability analysis is shown in Figure 4-4. Each modeled well has a lateral spacing of 700 ft, and both Pinnate and Pitchfork wells require similar total drilling lengths of approximately 17,500 feet. Modeled coal reservoir parameters are equivalent to those discussed in previous sections, shown in Table 4-1. To accommodate the well geometry of Pinnate 1 and Pinnate 2 as depicted in Figure 4-4, modeled grids were extended to cover approximately 600 acres. The same grid size was utilized for Pinnate 3 and both modeled Pitchfork wells. Due to the diagonal nature of Pinnate wells 1 and 2, their lateral spacing is actually 707 ft. This represents a 1-percent difference compared to the lateral spacing values of Pinnate 3, Pitchfork 1, and Pitchfork 2.

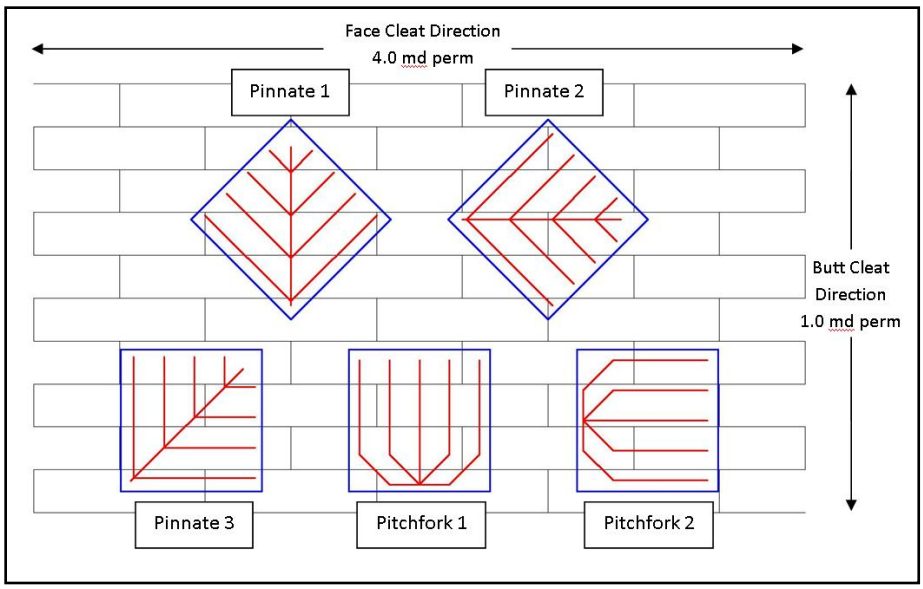

Figure 4-4: Schematic depicting orientation of Scenario 2 modeled wells in reservoir with directional permeability

4.2.2.1. Borehole Collapse Assessment

As coalbed methane wells extend into deeper coal seams, high in-situ stresses pose the risk of borehole collapse. Worst-case-scenario borehole collapses can cause permanent entrapment of drilling equipment, resulting in millions of lost dollars for drilling companies in costs associated with lost equipment or for fishing operations. On the other hand, during gas production, a borehole collapse near the producing well can effectively terminate the entire well's production.

When comparing the Pinnate and Pitchfork drilling patterns, each exhibit advantages and disadvantages with respect to lost footage from a borehole collapse. It should be noted that the results sections do not provide an analysis of borehole stresses, but rather a comparison of the effect of borehole collapses in Pinnate and Pitchfork-style wells and lost footages. Probability bar graphs were created to illustrate comparisons of expected lost footage from single horizontal borehole collapses for each discussed well pattern as shown in Figure 4-16 and Figure 4-17.

4.2.2.2. Analysis of Pitchfork and Pinnate Pattern Orientation with Respect to Cleat Structure

The naturally fractured cleat structure of coal can cause large variations in permeability in the face cleat and butt cleat directions. General accepted horizontal drilling practices involve intersecting the face cleat with the horizontal well whenever possible, thus taking advantage of the higher permeability value (Karacan, 2007). The ratio of the face cleat direction permeability to the butt cleat direction permeability can range from 1.8:1 to 17:1, with an average value of approximately 4:1 (Massarotto et al., 2003). The discussed Pinnate and Pitchfork drilling patterns with lateral spacings of 700 feet were modeled in a reservoir exhibiting respective face cleat and butt cleat permeabilities of 4 md and 1 md. Well orientation was also varied with respect to the face cleat and butt cleat, thus demonstrating the most advantageous pattern and orientation given an average directional permeability ratio. Figure 4-4 displays a schematic of the modeled wells and their orientations. The continuous horizontal lines represent the face cleat direction, and the discontinuous lines represent the butt cleat directions. It should be noted that these lines are provided only for visual aid and are not to scale. Each blue box represents a 1-square kilometer (248-acre) drainage area.

4.3. Results and discussion

4.3.1. Scenario 1: Z-Pinnate Pattern: Analysis of Lateral Spacing, Permeability and Production

Figure 4-5 contains a graphical summary of combinations of permeability values and lateral spacings which yield similar production data. An exponential relationship was fit to each set of data. Table 4-3 contains the combinations of lateral spacings and permeabilities which are plotted in Figure 4-5. For example, Combination 1 contains an 800-ft spaced model at 8 md, a 600-ft model at 4 md, a 400-ft model at 2 md, and a 200-ft model at 1 md. These models all

produce similar cumulative production curves over a 20-year period. The same holds true for Combinations 2, 3, and 4.

Table 4-3: Scenario 1 results--lateral spacing and permeability values (md)

Lateral Spacing (ft)		**800**	**600**	**400**	**200**
Combination 1	Permeability (md)	8	4	2	1
Combination 2		3.5	2	1	0.5
Combination 3		1.6	1	0.6	0.22
Combination 4		0.8	0.5	0.3	0.1

As previously discussed, permeability values for the 800-, 400-, and 200-ft-spacing well configurations were adjusted such that their cumulative production values were within 5 percent of the 600-ft spacing scenarios at years 10, 15, and 20. Figure 4-6 contains the averaged production rates for each combination shown in Figure 4-5 and Table 4-3. Figure 4-7 contains the ranges of obtained cumulative production curves for each combination of permeability values and lateral spacings shown in Figure 4-5 and Table 4-3. This is not depicted as a finite line, as the various combinations of permeability values and spacing scenarios do not create identical curves.

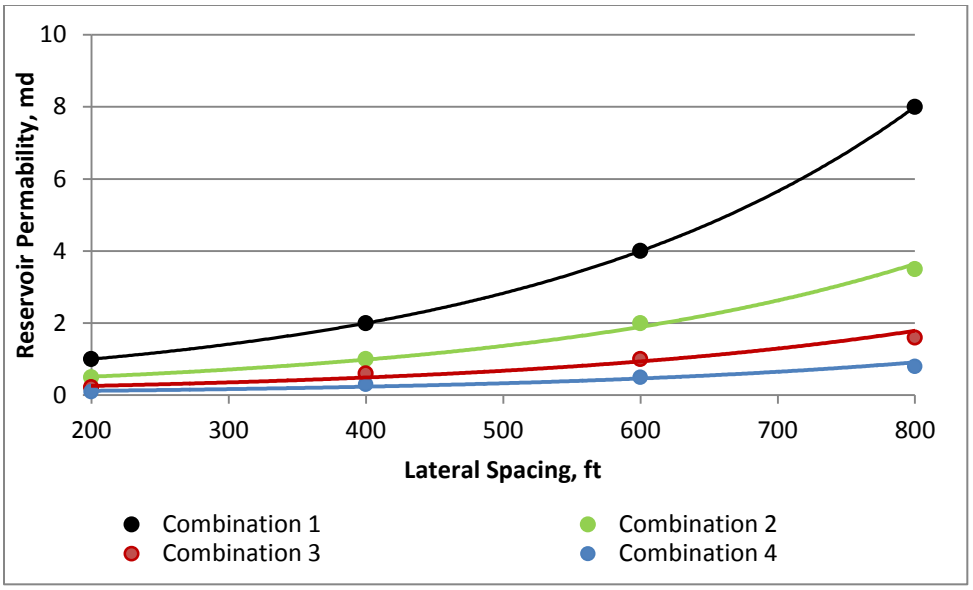

Figure 4-5: Lateral spacing and permeability combinations which yield similar cumulative production curves

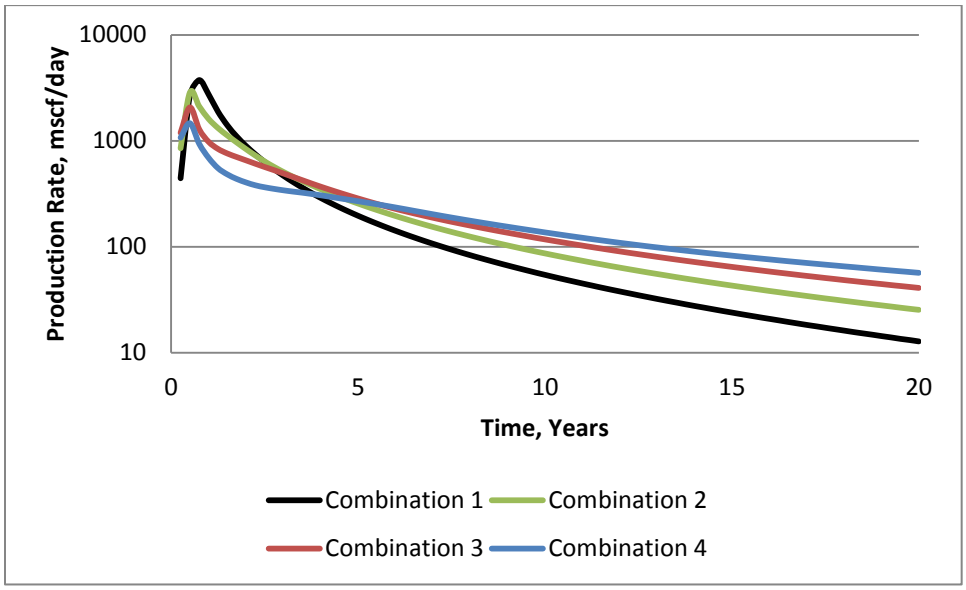

Figure 4-6: Averaged production rate curves for combinations of permeability and lateral spacing values

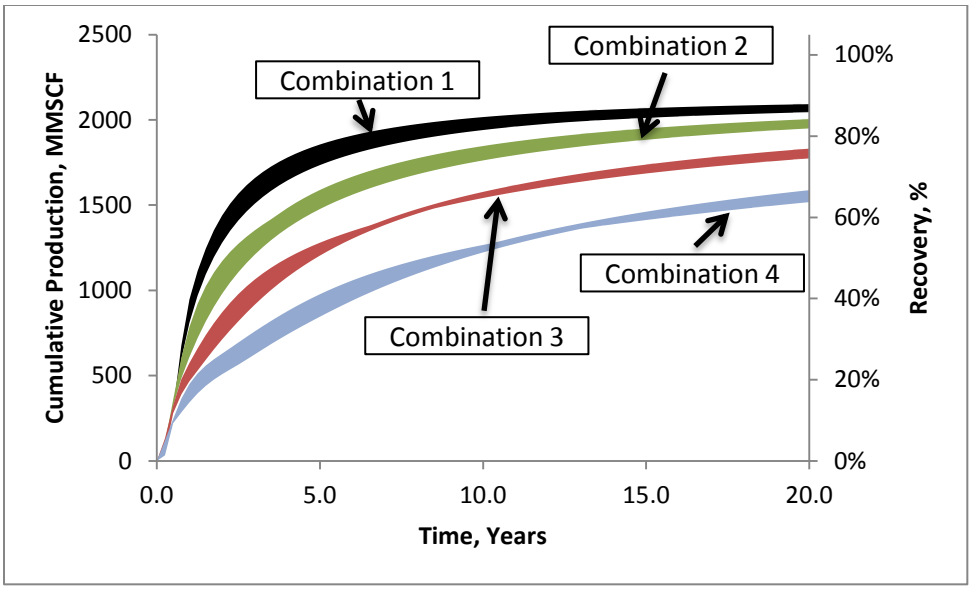

Figure 4-7: Ranges of cumulative production curves obtained by combinations of lateral spacing and permeability values

The average production rates (Figure 4-6) depict a steeper production decline for the lower combinations with higher peak production rates. Average peak production rates for Combinations 1, 2, 3, and 4 are respectively 3.7, 2.9, 2.1, and 1.4 million cubic feet per day. After a 20-year production period, Combinations 1 through 4 produce at respective average rates of 13, 25, 41, and 57 thousand cubic feet per day. As expected, the higher permeability models which correspond to the lower combinations produce more gas over the 20-year period. Combinations 1 through 4 produce respective cumulative production values of 2.07, 1.98, 1.83, and 1.52 billion cubic feet of methane. These cumulative production values correspond with recovery values of 87, 73, 77, and 64 percent of original gas in place.

As is evident in Figure 4-6 and Figure 4-7, low permeability coal seams can be offset by additional drilling and decreased lateral spacing. An economic limit exists where it is impractical and prohibitively expensive to drill additional footage. Decreasing lateral spacing from 600 ft to 200 ft more than doubles the drilled in-seam footage of a well, posing a potential

threat to the financial feasibility of the well. While this study does not focus on the financial aspects of well drilling, Table 4-4 contains a summary of the 20-year cumulative production per foot of in-seam drilling for each model.

Table 4-4: Lateral spacing and cumulative produced gas per unit of drilling length (mcf/ft) after 20 years of production

Lateral Spacing (ft)		800	600	400	200
Combination 1	production per drilling length (mcf/ft)	123.1	103.6	76	44.5
Combination 2		117.9	99	72.2	42.5
Combination 3		107.7	90.8	67.7	38.6
Combination 4		93.3	78.3	58.8	33

4.3.1.1. Sensitivity of Results to Grid Geometry

In an effort to determine the influence of the modeled grid cell geometry on simulation output, additional simulations were run to determine the effect of grid cell size and the proximity of grid boundaries to modeled horizontal laterals. Sensitivity results for both parameters are presented and discussed below.

To examine the effect of the position of laterals proximal to grid boundaries, simulations were executed on a 9-square kilometer grid, maintaining the 100-squre foot grid block geometry while utilizing the same well geometry. It should be noted that the large modeled grid could actually contain 9 multilateral horizontal wells based on the original assumptions that gas is only targeted in the 1 square kilometer zone. While it is expected that the original 1-square kilometer model will demonstrate a faster reservoir depressurization than the 9-square kilometer model, this is not entirely unrealistic. Similar fast depressurizing would occur if wells were placed side by side (Gentzis and Bolen, 2008). Although the Gentzis and Bolen (2008) work concentrates on depressurization between individual laterals, the same phenomenon will occur for separate

wells spaced closely together. Ultimately, the 1-square kilometer model is designed to closely represent a Pinnate well surrounded by other producing horizontal wells, while the 9-square model is more accurate for a lone producing single Pinnate.

Simulations were conducted on the large grid for the following lateral spacing and permeability combinations: 800-ft spacing at 8 md, 800-ft spacing at 0.8 md, 200-ft spacing at 1 md, and 200-ft spacing at 0.1 md. Note that these are the extreme combinations of lateral spacing and permeability values reported in Table 4-3. Figure 4-8 through Figure 4-11 display comparisons of production curves for the large and originally modeled grid drainage areas.

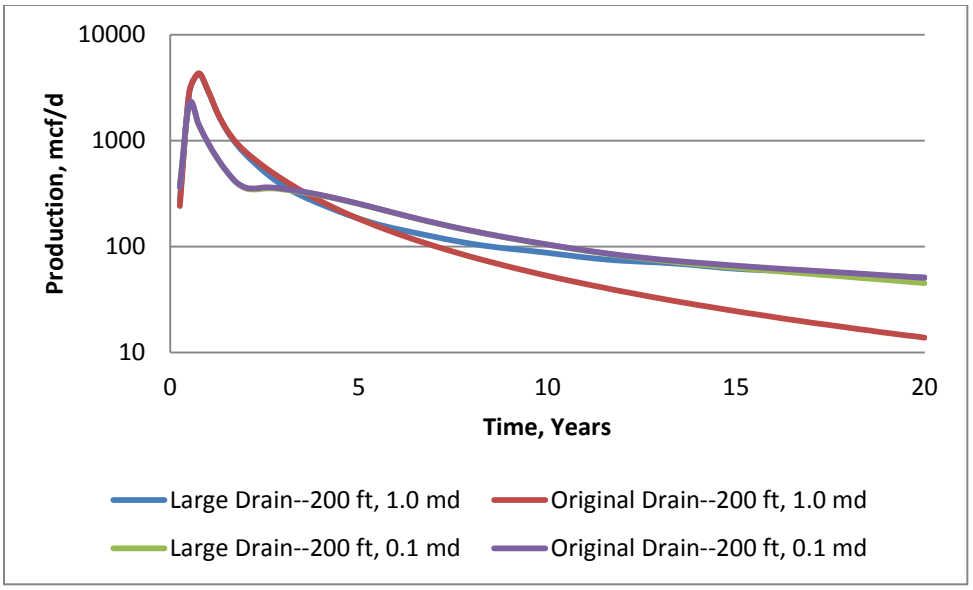

Figure 4-8: The effect of modeled grid drainage area on production rate for 200-ft lateral spacing models in 1.0 and 0.1 md reservoirs

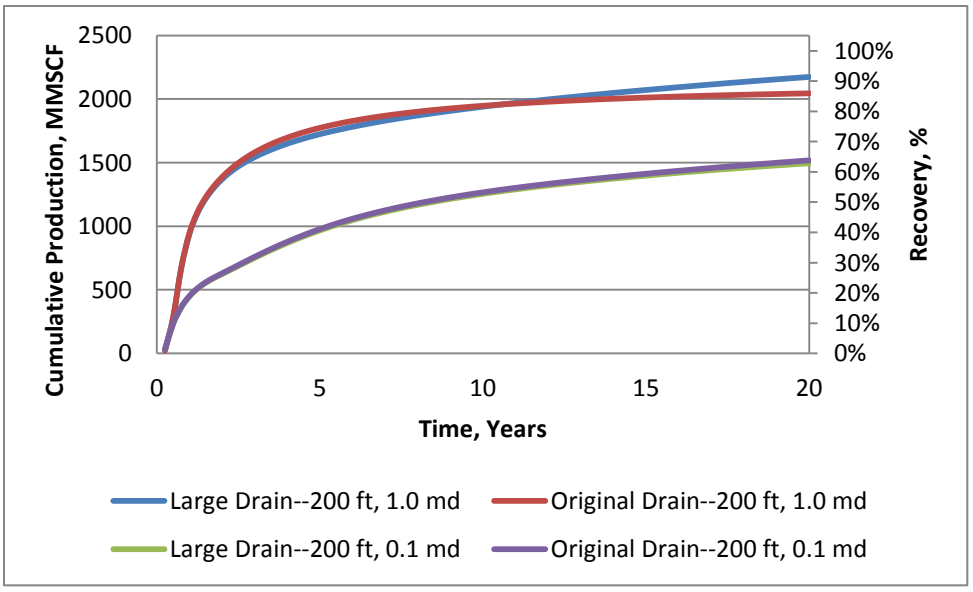

Figure 4-9: The effect of modeled grid drainage area on cumulative production for 200-ft lateral spacing models in 1.0 and 0.1 md reservoirs

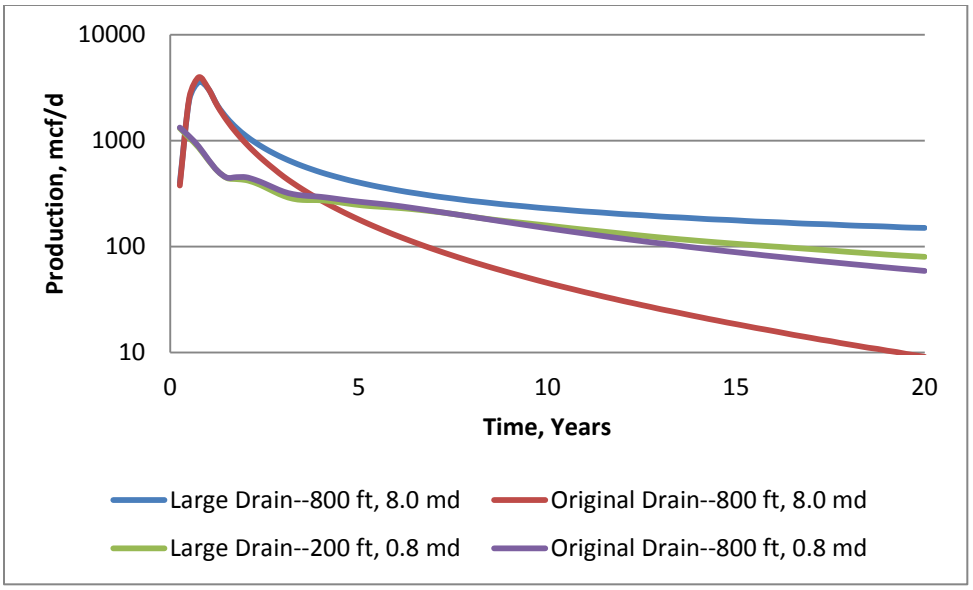

Figure 4-10: The effect of modeled grid drainage area on production rate for 800-ft lateral spacing models in 8.0 and 0.8 md reservoirs

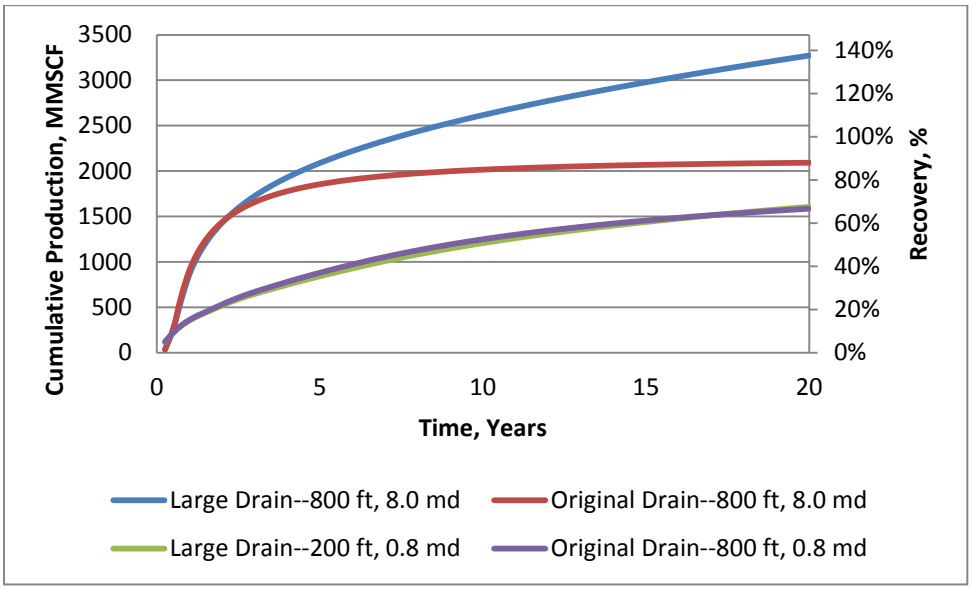

Figure 4-11: The effect of modeled grid drainage area on cumulative production for 800-ft lateral spacing models in 8.0 and 0.8 md reservoirs

As evident in the above figures, the modeled grid drainage area becomes more significant in higher permeability applications, in which case the pressure transients arrive at the boundaries in a shorter time period. The 200-ft spacing, and the lowest 0.1 md permeability case provides a maximum cumulative production difference of 1 percent when comparing the larger grid area

with the originally modeled grid. The highest permeability (1.0 md) 200-ft spacing scenario demonstrates the significance of grid size. The larger grid model produces 13 percent more gas than the originally modeled grid after a 20-year period. If the simulation were to continue, this difference would increase, as production rates at the end of the 20-year period are 2.7 times higher for the larger grid with the rate difference continuing to increase.

Similar trends are noted in the 800-ft lateral spacing models. The lower permeability (0.8 md) provides minimal (1 percent) cumulative production difference after the 20-year period. This 1-percent difference would grow if the simulations were continued to run after the 20-year period, as the larger grid model produces more gas on a rate basis and the 20-year time mark. The 800-ft spacing, 8.0 md (highest permeability) provides the most significant comparison and largest cumulative and rate difference of all compared models. After the 20-year producing period, the larger grid cumulatively out-produces the original grid by 56 percent. More significant is the difference in rate; the large grid produces 15 times more gas per unit time than the original grid at the 20-year mark, illustrating the significant impact of grid boundary proximity to modeled wellbores in high permeability applications. In summary, the effective drainage area is governed by permeability.

Grid cell size was also analyzed by executing additional simulations with smaller (20-ft by 20-ft) grid blocks. As lateral spacing decreases, grid cell size is anticipated to become more relevant and significant for accurate modeling due to averaging of solutions in a smaller area. Therefore, the smallest lateral spacing (200-ft) model was analyzed to determine the impact of grid cell size on simulation results. Simulations were run for the 1.0 and 0.1 md scenarios and results were compared to the originally modeled grid cell size of 100 feet by 100 feet. Production rate and cumulative production curves are shown below in Figure 4-12 and Figure

4-13, respectively. Results show that cumulative production is relatively stable based on altering grid cell size. Yet, the time-dependent solution can be refined by reducing grid cell size. A tradeoff exists between grid cell size, the subsequent simulation time, and simulation accuracy. Similar results would be expected for all other scenarios if grid size was to be decreased. A detailed analysis of the 200-ft spacing model is shown below.

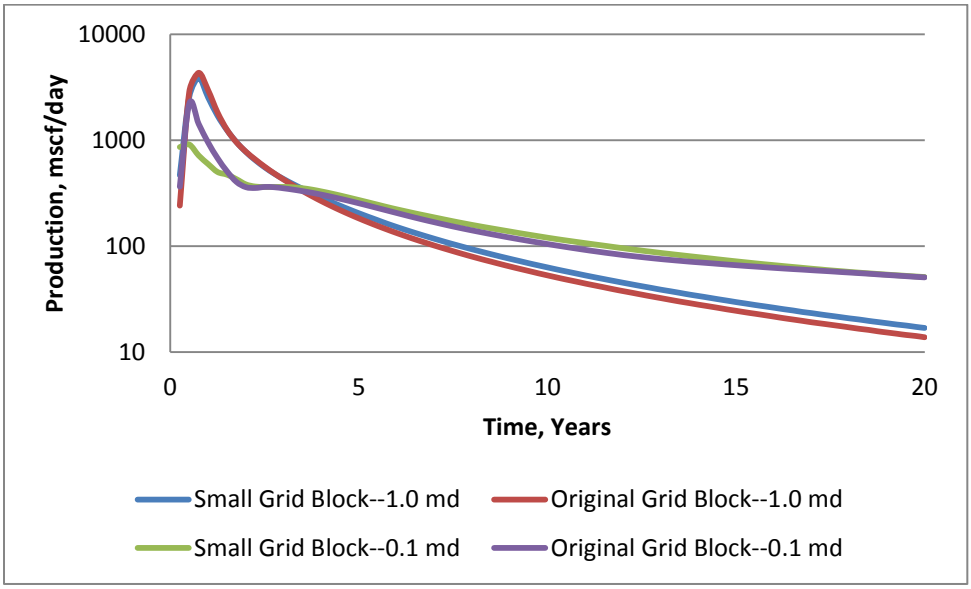

Figure 4-12: The effect of modeled grid block size on production rate for 200-ft lateral spacing models in 0.1 and 1.0 md reservoirs

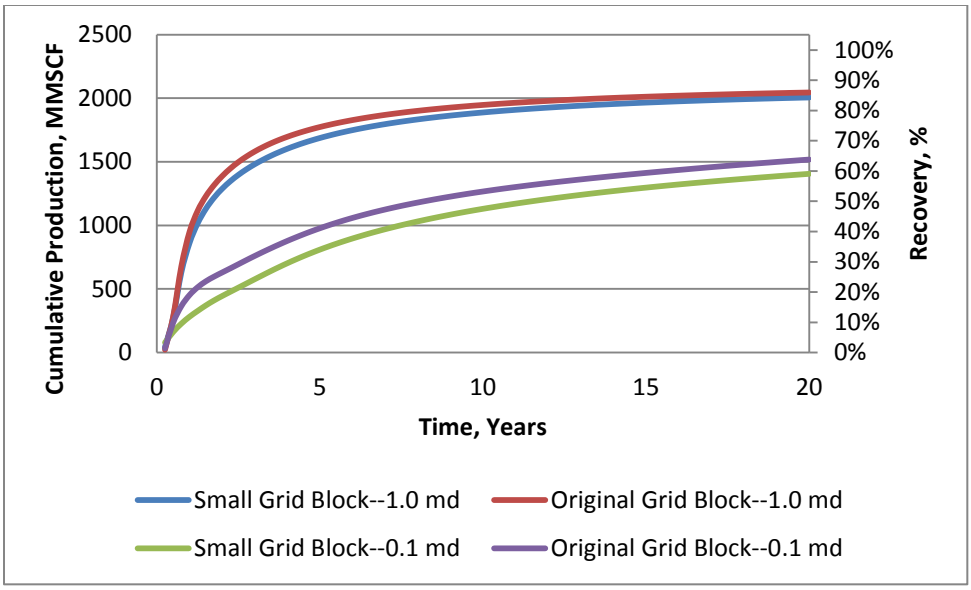

Figure 4-13: The effect of modeled grid block size on cumulative production for 200-ft lateral spacing models in 0.1 and 1.0 md reservoirs

A comparison of modeling results for the originally modeled 100-ft by 100-ft grid blocks with 20-ft by 20-ft grid blocks implies that grid cell size becomes more significant at lower permeability values. The cumulative production curves for the 200-ft lateral spacing, 1.0 md model begin 9-percent smaller (after 1 year of production) for the smaller grid block model when compared to the original grid block model. Cumulative production for the smaller grid block does not exceed the original grid block model, but the difference in the cumulative production curves decreases continually throughout the 20-year producing period. After 20 years, the cumulative production difference drops to 2 percent.

Similar trends can be noted for the 0.1 md case with a higher magnitude difference. Cumulative production values begin 38-percent smaller for the smaller grid block model after 1 year of production. The difference decreases to 7 percent after the 20-year period. The larger differences for the lower-permeability comparison (0.1 md vs. 1.0 md) demonstrate that grid cell dimensions become increasingly more important as permeability decreases. Regardless of

permeability, the small grid block (20 feet by 20 feet) models produce less gas over the 20-year producing period than the originally modeled 100 feet by 100 feet models.

The original methodology to determine if combinations of lateral spacings and permeability yield similar production curves involves cumulative production comparison to the 600-ft lateral spacing baseline as discussed in Section 3.2.1. If cumulative production curves are within 5 percent of the 600-ft lateral spacing baselines at years 10, 15, and 20, production curves are considered similar. The smaller grid block models were compared to the 600-ft spacing baselines to determine if the small grid model results are consistent with the original grid block models. The 200-ft lateral spacing and 1.0 md small block grid model produces cumulative production values within the 5-percent threshold of the 600-ft lateral spacing, 4.0 md baseline (Combination 1 in Table 4-3). The 200-ft lateral spacing, 0.1 md case does not fit the discussed criteria of producing a similar production curve. Compared to the 600-ft spacing, 0.5 md permeability model (Combination 4 in Table 4-3), the 200-ft, 0.1 md case produces values 7.5-percent, 9.5-percent, and 10.2-percent different than the respective 10-, 15-, and 20-year values of the baseline case. To maintain uniformity of all models and maintain consistency, the results from the original 100-ft by 100-ft are presented. Still, the impact of grid cell size should be noted, and especially taken into account in instances of very low permeability and low lateral spacing levels.

4.3.2. Scenario 2: Comparison of the Z-Pinnate and Pitchfork Patterns

4.3.2.1. Borehole Collapse Assessment

In analyzing the chance of borehole collapse for Pitchfork and Pinnate wells, each pattern was discretized into individual sections. The discussed Pinnate pattern contains 13 individual sections with 8 side lateral branches, and five individual sections within the main lateral, while

the Pitchfork well only contains a total of five separate sections. The maximum and minimum lost footage corresponding to a collapse in each section was then determined. Given everything else is constant, the statistical probability of a wellbore collapse being located in a given section is equivalent to that section's length divided by the total length of a well. However, the probability of a particular length of well rendered unproductive due to wellbore collapse is equivalent to the length of the section disconnected from the production well divided by the total length, which also gives the percentage of unproductive section of the wellbore. Table 4-5 and Table 4-6 represent the discussed well section lengths, minimum and maximum lost footage for a collapse corresponding to the section, and the statistical odds that a failure will occur in that section for the respective Pinnate and Pitchfork designs. Figure 4-14 and Figure 4-15 display the discretized sections of each well corresponding with the data in Table 4-5 and Table 4-6. Note that the highlighted rows in Table 4-5 and Table 4-6 represent the sections of borehole shaded in red in Figure 4-14 and Figure 4-15.

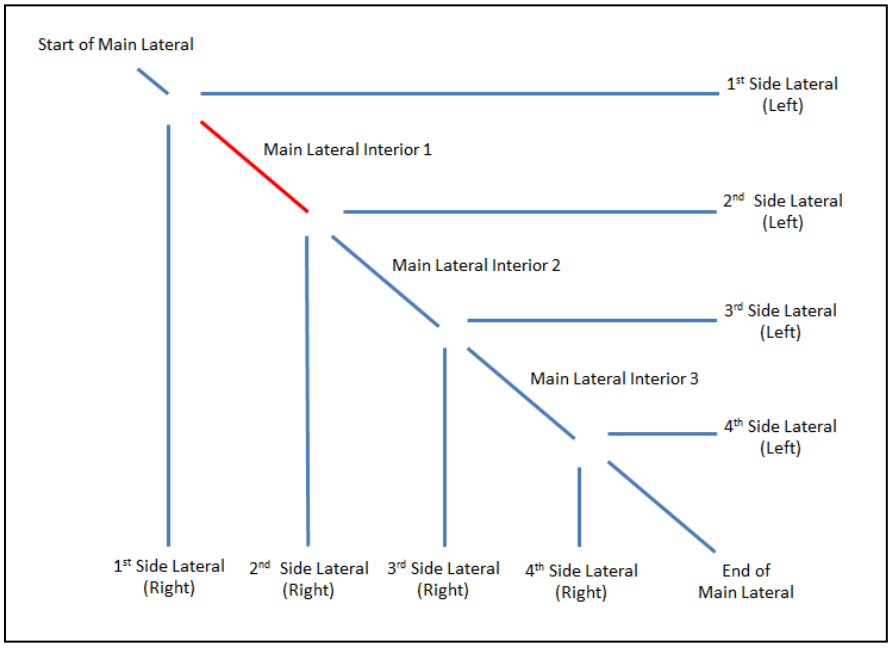

Figure 4-14: Pinnate well discretized into individual sections for borehole collapse analysis

Table 4-5: Analysis of wellbore failure for sections of Pinnate well

Section	Description	Length of Section (ft)	Max. Lost Length if Collapse Occurs in Section (ft)	Min. Lost Length if Collapse Occurs in Section (ft)	Probability of Collapse Occurring in this Section
1	Start of Main Lateral	100	17842	17742	0.56%
2	Main Lateral Interior 1	1000	12085	11085	5.60%
3	Main Lateral Interior 2	1000	6843	5843	5.60%
4	Main Lateral Interior 3	1000	3014	2014	5.60%
5	End of Main Lateral	600	600	0	3.36%
6	1st Side Lateral (Left)	2828	2828	0	15.85%
7	1st Side Lateral (Right)	2828	2828	0	15.85%
8	2nd Side Lateral (Left)	2121	2121	0	11.89%
9	2nd Side Lateral (Right)	2121	2121	0	11.89%
10	3rd Side Lateral (Left)	1414	1414	0	7.93%
11	3rd Side Lateral (Right)	1414	1414	0	7.93%
12	4th Side Lateral (Left)	707	707	0	3.96%
13	4th Side Lateral (Right)	707	707	0	3.96%
	Total Length:	*17842*			

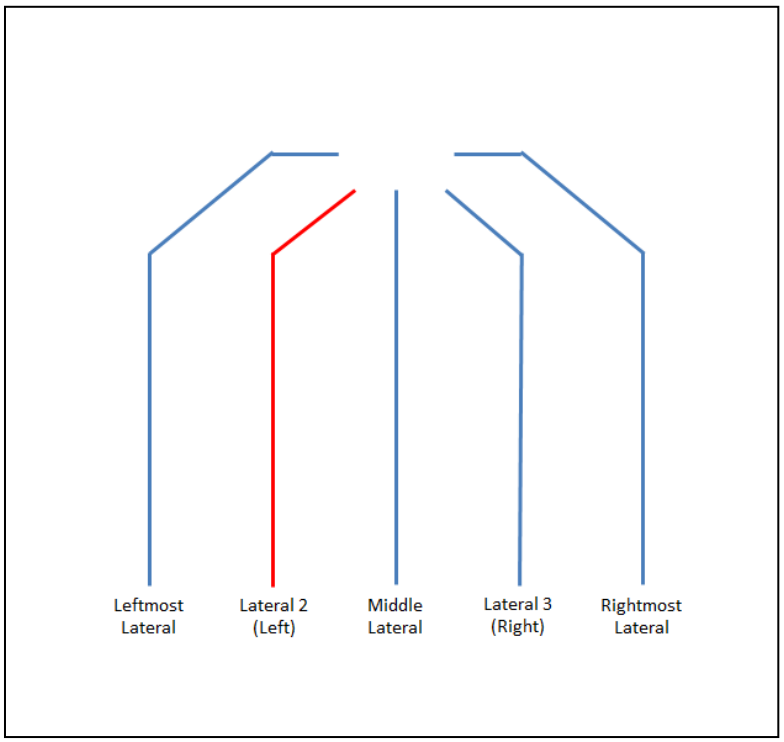

Figure 4-15: Pitchfork well discretized into individual sections for borehole collapse analysis

Table 4-6: Analysis of wellbore failure for sections of a Pitchfork well

Section	Description	Length of Section (ft)	Max. Lost Length if Collapse Occurs in Section (ft)	Min. Lost Length if Collapse Occurs in Section (ft)	Probability of Collapse Occurring in this Section
1	Leftmost Lateral	3990	3990	0	22.72%
2	Lateral 2 (Left)	3290	3290	0	18.74%
3	Middle Lateral	3000	3000	0	17.08%
4	Lateral 3 (Right)	3290	3290	0	18.74%
5	Rightmost Lateral	3990	3990	0	22.72%
	Total Length:	*17560*			

As the probability for failure is assumed to be constant anywhere within a section, the odds of failure can be divided between pre-determined boundaries based on a weighting function. For this example, boundaries were placed at even intervals of 1,000 feet between zero and 18,000 feet. Figure 4-16 and Figure 4-17 display respective probability bar graphs for lost footage from a single borehole collapse and a cumulative probability chart.

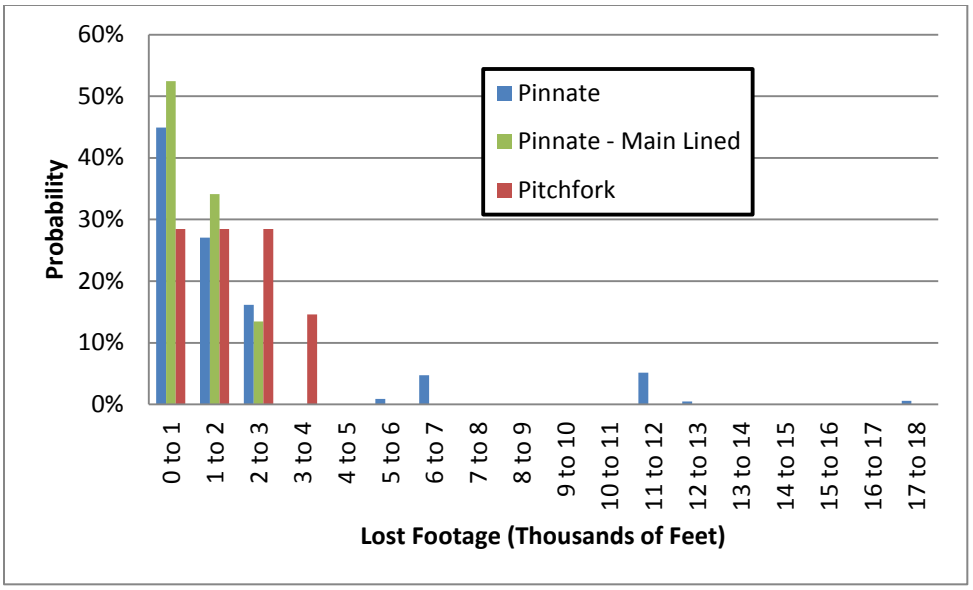

Figure 4-16: Comparison of the probabilities of lost wellbore footage for an unlined Pinnate, a Pinnate with its main lateral lined, and an unlined Pitchfork well from a single borehole collapse

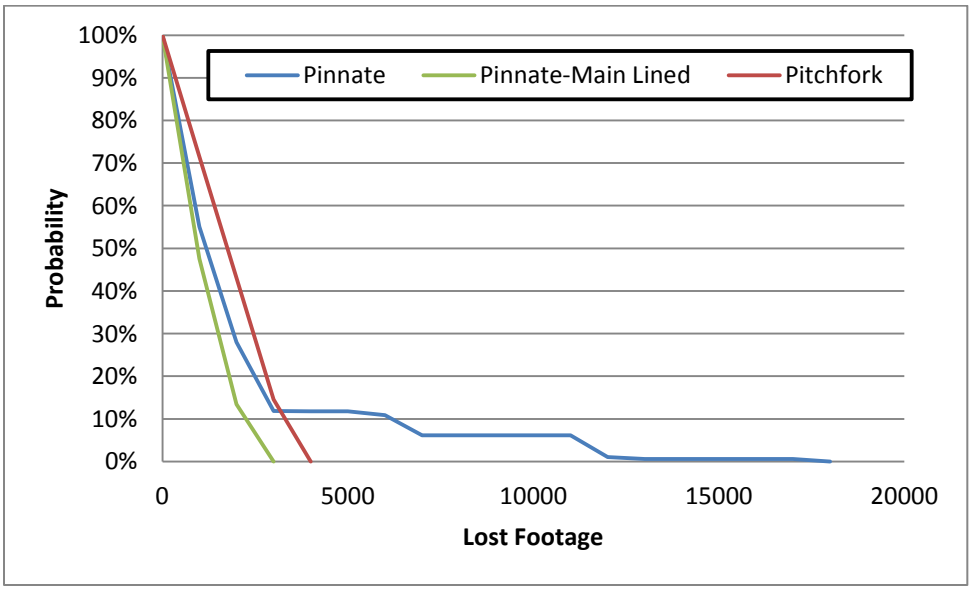

Figure 4-17: Comparison of the cumulative probabilities of lost wellbore footage for an unlined Pinnate, a Pinnate with its main lateral lined, and an unlined Pitchfork well from a single borehole collapse

Figure 4-16 demonstrates a constant probability of losing between zero and 3,000 feet of wellbore from a single collapse in a Pitchfork pattern, with a slight decrease in probability between 3,000 and 4,000 feet. The independent branches of a Pitchfork pattern eliminate the

potential for catastrophic failure of a well from a single collapse, as the maximum lost footage from a single borehole collapse is approximately 4,000 feet (the maximum length of a single horizontal leg). Alternatively, a Pinnate pattern offers a higher probability of minimal lost footage from a collapse with a gradual decrease from zero to 6,000 feet. Yet, the geometric nature of a Pinnate well with a main lateral linked to side branches poses the potential risk for extreme well failure, because the side laterals are dependent on the integrity of the main lateral. Figure 4-17 displays a cumulative probability chart for each well pattern, which represents the probability of losing greater than a specified length of wellbore from a single borehole collapse. For example, the probability of losing greater than 1,000 ft is approximately 70 percent in a Pitchfork pattern.

Mitigating the risk of borehole collapse can be accomplished by inserting liners within boreholes. More than three miles of liner are required to completely line well patterns presented here. Very little information pertaining to perforated linings in horizontal coalbed methane wells exists in the literature, yet success has been noted in the San Juan Basin. There, linings were utilized in horizontal wells where coal fines and dust created plugging issues, requiring extensive well cleaning after production started. Over 9,000 feet of well were successfully lined to maintain clean boreholes (Malkewicz Hueni Associates, Inc., 2004) and eliminate plugging issues. The utilized liner type and strength is unknown, only demonstrating that liner installation is possible, not denoting liner strength, although Gentzis recommends liners to increase borehole stability in a case study in southeast British Columbia (2009).

The relative ease of lining Pitchfork and Pinnate Patterns varies greatly. The well's length, junctions, and depth determine the complexity of fully lining a well. Fully lining the discussed Pinnate pattern would require 9 separate liner sections (main lateral and eight side

laterals), while the Pitchfork pattern would only require 5. Additionally, the measured distance from the surface to the wellbore junctions in a Pinnate pattern greatly increases the difficulty of inserting liners. The proximity of the junction of the five separate laterals within the discussed Pitchfork pattern makes it easier to line than a Pinnate pattern.

While a Pinnate pattern poses more difficulty with respect to liners than a Pitchfork pattern, a great decrease in risk associated with well failure from borehole collapses can be obtained from lining only the main lateral of a Pinnate well. Figure 4-16 and Figure 4-17 include probability charts for lost wellbore footage for a Pinnate pattern with a lined main lateral.

Figure 4-16 and Figure 4-17 display a significant reduction in lost footage risk associated with borehole collapse in a Pinnate pattern when mining the main lateral. This would only require lining roughly 20 percent of the total well length, roughly 3,700 feet. Unlined, Pitchfork patterns offer more protection from catastrophic well failure than Pinnate patterns. Yet, risk can be offset in Pinnate patterns by lining the main lateral.

4.3.2.2. Analysis of Pitchfork and Pinnate Pattern Orientation with Respect to Cleat Structure

Figure 4-18 and Figure 4-19 display the production rate and cumulative production curves corresponding to the wells depicted in Figure 4-4. Table 4-7displays a summary of the cumulative production values for years 1, 5, and 10.

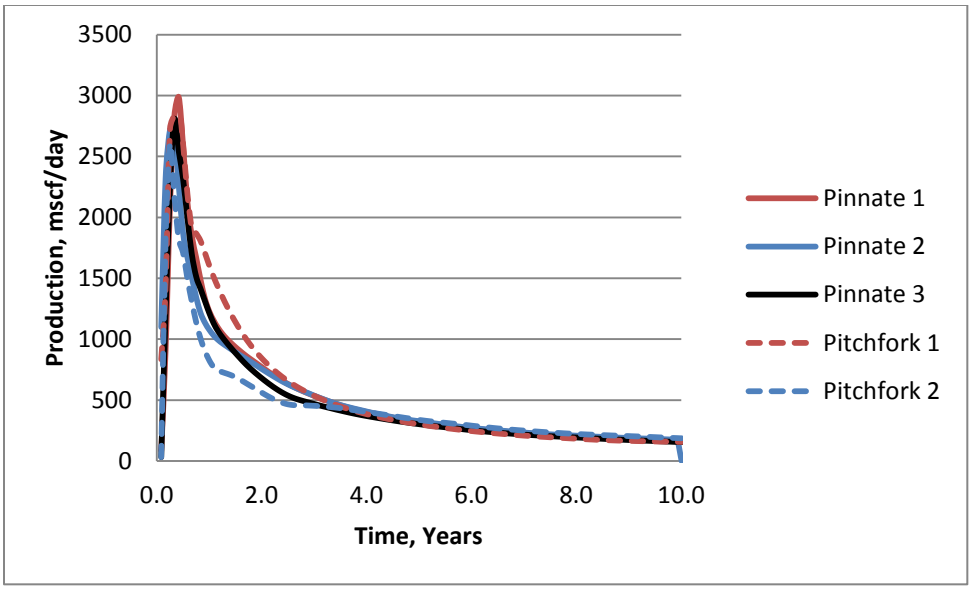

Figure 4-18: Production rate comparisons of Pinnate and Pitchfork wells based on orientation in directional permeable reservoirs

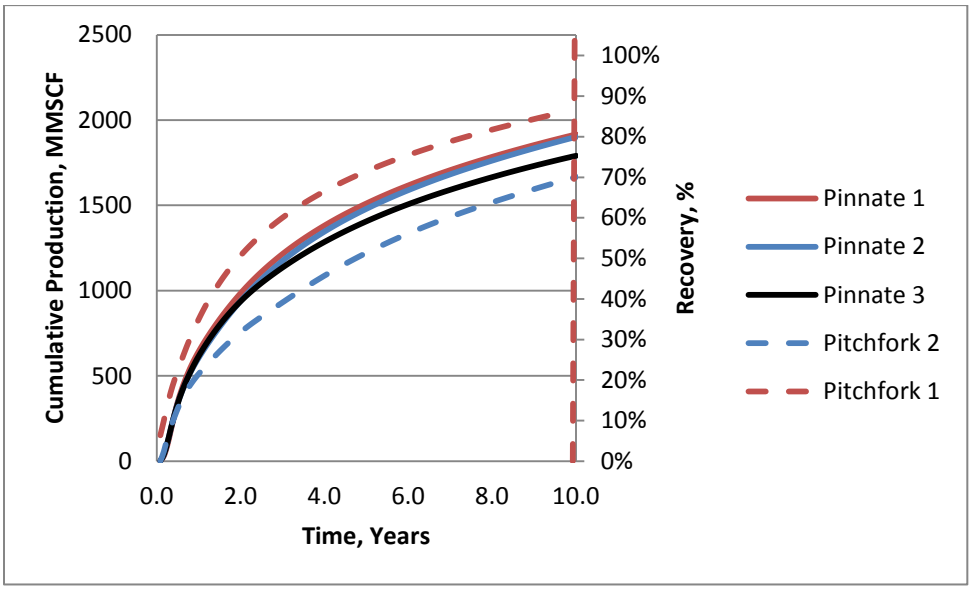

Figure 4-19: Cumulative production rate comparisons of Pinnate and Pitchfork wells based on orientation in directional permeable reservoirs

Table 4-7: Summary of cumulative production values for various well pattern orientations

Well	Description	1-Year Total Production (bcf)	5-Year Total Production (bcf)	10-Year Total Production (bcf)
Pinnate 1	Main Lateral Intersects Face Cleats	0.644	1.51	1.92
Pinnate 2	Main Lateral Parallel to Face Cleats	0.607	1.48	1.90
Pinnate 3	Main Lateral Intersects Face and Butt Cleats	0.606	1.40	1.78
Pitchfork 1	Laterals Intersect Face Cleats	0.695	1.67	2.05
Pitchfork 2	Laterals Parallel to Face Cleats	0.513	1.22	1.67

Comparing the production rates of both the Pitchfork and Pinnate models at all orientations, all differences exist within the first 4 years of production. After the initial 4-year producing period, the production rates in all cases are relatively similar. This can also be noted by the cumulative production curves. The differences in cumulative values remain relatively constant after the initial 4-year period, suggesting a faster return on investment, with the major benefit on proper well orientation occurring early in the well's producing life.

As shown in Figure 4-18 and Figure 4-19, Pinnate wells show little sensitivity to directional orientation with respect to coal cleats. Model results show that the most favorable drilling orientation for Pinnate wells is to intersect the face cleat with the main lateral, Pinnate 1 scenario. This provides negligible additional production to drilling the main lateral parallel to the face cleat, Pinnate 2 scenario. Directly comparing the two scenarios, Pinnate 1 provides the highest benefit after one year of production, with a cumulative advantage over Pinnate 2 of 6 percent. This advantage gradually drops to 1 percent after 10 years of production. Alternatively, the main lateral of a Pinnate can be drilled to intersect both the face and butt cleats, Pinnate 3 scenario, which provides a 7-percent reduction in cumulative production after 10 years.

The similarity in production between the Pinnate 1 and Pinnate 2 scenarios involves the orientation of the side laterals. In both situations, all side laterals intersect face cleats. The

negligible additional production from Pinnate 1 over Pinnate 2 is due to the orientation of the main lateral. The main lateral of Pinnate 1 takes advantage of the higher permeability of the face cleats. The significant drop in production of Pinnate 3 compared to Pinnate 1 and Pinnate 2 also involves the side laterals. Only half of the side laterals of Pinnate 3 intersect face cleats, thus hindering well production.

Pitchfork patterns exhibit greater sensitivity to cleat structure drilling orientation than Pinnate patterns, but provide the opportunity for higher gas production. As all laterals of Pitchfork patterns are drilled parallel to one another, the entire well can take advantage of directional permeability, as in Pitchfork 1. Incorrect orientation of Pitchfork drainage patterns, illustrated by Pitchfork 2, results in a substantial decrease in gas production. After 10 years of production, modeling concludes that drilling Pitchfork patterns parallel to the face cleat results in a total gas production decrease of 19 percent when compared to drilling the Pitchfork pattern perpendicular to face cleats.

includes the 1-, 5-, and 10-year cumulative production values for the discussed drainage patterns in the presence of directional permeability at a 4:1 ratio. As previously discussed, Pitchfork patterns offer the best potential for high gas production compared to Pinnate patterns, but are more susceptible to significant decreases in production due to improper orientation.

Although outside the scope of this paper, seam dip represents an additional important consideration for proper multilateral wellbore orientation. Whenever possible, wells should be drilled in an up-dip direction from the producing well to allow water to flow downhill to the producing well. Failure to do so can result in significant lost gas reserves, as water must be pushed through the wellbore by a buildup of gas pressure.

4.3.2.3. Summary of Results: Pitchfork vs. Pinnate

Technological developments in steerable drilling equipment allow precise drainage patterns to be drilled in coal seams. Regardless of the accuracy of the drilling equipment, the difficulty associated with well development is directly proportional to the number of branch junctions in a well, and the distance of those junctions from the base of the producing well. The geometric nature of a Pinnate pattern with multiple junctions located at varying distances from the producing well results in a more complex and difficult design compared to a Pitchfork pattern. By limiting the number of junctions, and moving those junctions closer to the producing well, a great decrease in drilling difficulty is achieved. Further, when inserting liners to protect boreholes from catastrophic collapse, the complexity of liner insertion is directly related to the number and location of junctions.

The limited well junctions and interconnected branches in a Pitchfork pattern also pose a significantly decreased risk with respect to catastrophic wellbore failure. The production of a Pinnate well is highly dependent on the structural integrity of the main lateral, thus increasing the risk of losing the majority of the well from a single borehole collapse. This risk can be mitigated through the use of perforated liners in the main lateral. For example, there is a 43-percent probability that greater than 2,000 feet of borehole will be lost with an unlined Pinnate well in a single wellbore failure. This probability drops to 28 percent with a Pitchfork well. The risk can be mitigated in Pinnate wells by utilizing a perforated liner in the main lateral, dropping the probability of losing greater than 2,000 feet of wellbore from 43 percent to 13 percent.

While well pattern selection and drilling density both considerably affect the production capacity of the well, proper wellbore orientation also provides a significant variable in the ability of the well to produce large volumes of gas. Wells should always be drilled in an up-dip manner,

utilizing gravity to promote water flow to the producing well. Additionally, face cleats should be intersected whenever possible, taking advantage of their higher permeability values. Modeling concludes that Pinnate patterns exhibit little sensitivity to orientation in the presence of moderate directional permeability, with a 4:1 face-cleat-to-butt-cleat ratio. Conversely, Pitchfork patterns require proper orientation with respect to cleat fractures to produce at their maximum potential. Improper orientation of Pitchfork patterns, orienting the laterals parallel to face cleats, results in nearly a 20-percent reduction in produced gas.

4.4. Conclusions

China's southern Shanxi Province contains thick coal seams with high gas contents, yet low permeability values threaten the economic viability of coalbed methane projects. Three-dimensional reservoir modeling indicates that through the alteration of typical horizontal drilling patterns, these coals can produce ample volumes of gas. By roughly doubling the drilled length of Pinnate drainage patterns, high gas production can be maintained, even with a tenfold decrease in permeability. Although these wells require significant capital investment, this work indicates that they are also capable of high production rates even in low permeability coals with the optimization of lateral spacing and well orientation. Through the use of *COMET3* reservoir modeling software, simulations were executed to investigate the influence of well pattern and orientation at a greenfield site in the southern Shanxi Province of China with an anthracitic, low permeability, deep reservoir. A permeability range was examined, along with the required lateral spacing to maintain a given production, and the data indicate that high production rates can be achieved in low permeability reservoirs by decreasing lateral spacing and increasing total drilling length. A number of combinations of scenarios examining varied lateral spacing and

permeability may serve as rule-of-thumb in preliminary consideration of low permeability reservoirs.

Additionally, two common MLD patterns were studied to determine the associated probability of borehole collapse for each and the effect of orientation with regard to cleat on production. It was determined that the probability of collapse is far less for Pitchfork patterns because the flow of gas from the lateral legs is not dependent on a single main lateral. Although the Pitchfork pattern was at much lower risk of catastrophic borehole collapse, proper orientation of this pattern was found to be crucial to production. Improper orientation of the Pitchfork pattern, with the main lateral parallel to the face cleat, resulted in a 19-percent reduction in total gas production over 10 years, while the same improper orientation of the Pinnate pattern resulted in only a 7-percent reduction in production over 10 years. In conclusion, this modeling indicates that, although the Pinnate presents a higher risk of borehole collapse, it may be the favorable pattern in a reservoir that demonstrates high directional permeability, especially if the nature of the anisotropy is not well characterized.

Offsetting low permeability values can be achieved by altering typical multilateral horizontal well patterns, increasing drilling density, and properly orienting wells. As global energy demands increase and easily accessed high permeability reservoirs are depleted, low permeability reservoirs will become the standard for coalbed methane production. Well patterns must be adjusted accordingly. Modeling concludes that these reservoirs hold promise for the future of coalbed methane development.

Chapter 4 References

Colmenares, L., Zoback, M. 2007. Hydraulic fracturing and wellbore completion of coalbed methane wells in the Powder River Basin, Wyoming: Implications for water and gas production. AAPG Bulletin. 91(1). 51-67.

Diamond, W., Oyler, D., Fields, H., 1977. Report of Investigations 8277: Directionally Controlled Drilling to Horizontally Intercept Selected Strata, Upper Freeport Coalbed, Green County, Pa. US Bureau of Mines, 1-20.

Deimbacher, F., Economides, M., Heinemann, Z., Brown, J. 1992. Comparison of Methane Production From Coalbeds Using Vertical or Horizontal Fractured Wells. Journal of Petroleum Technology. 44 (8). 930-935.

Deisman, N., Mas Ivars, D., Darcel, C., and Chalaturnyk, R.J. 2010. Empirical and numerical approaches for geomechanical characterization of coal seam reservoirs. International Journal of Coal Geology. 82. 204-212.

Ertekin, T., Sung, W., and Schwerer, F. 1988. Production Performance Analysis of Horizontal Drainage Wells for the Degasification of Coal Seams. Journal of Petroleum Technology. 40 (5). 625-632.

Flores, R., 1998. Coalbed Methane; from hazard to resource. International Journal of Coal Geology. 35(1-4). 3-26.

Gentzis, T., 2009. Stability analysis of a horizontal coalbed methane well in the Rocky Mountain Front Ranges of southeast British Columbia, Canada. International Journal of Coal Geology. 77. 328-337.

Gentzis, T. and Bolen, D. 2008. The use of numerical simulation in predicting coalbed methane producibility from the Gates coals, Alberta inner Foothills, Canada: Comparison with Mannville coal CBM production in the Alberta Syncline. International Journal of Coal Geology. 74. 215-236.

Gentzis, T., Deisman, N., and Chalaturnyk, R.J. 2009a. A method to predict geomechanical properties and model well stability in horizontal boreholes. International Journal of Coal Geology. 78. 149-160.

Gentzis, T., Deisman, N., and Chalaturnyk, R.J. 2009b. Effect of drilling fluids on coal permeability: impact on horizontal wellbore stability. International Journal of Coal Geology. 78. 177-191.

Hawke C., 2007. Assessing the mechanical stability of horizontal boreholes in coal. Canadian Geotechnical Journal. 44 (7). 797-813 (17).

Karacan, C., Diamond, W., Schatzel, S., 2007. Numerical Analysis of the Influence of In-Seam Horizontal Methane Drainage Boreholes on Longwall Face Emission Rates. International Journal of Coal Geology. 72(1). 15-32.

Kissell, F., Edwards, J. 1975. Two-Phase Flow in Coal Beds. Report of Investigations - United States, Bureau of Mines. 8066.

Lightfoot, J., McLaughlin, S. and Toothman, R., 2009. Development and Case Study of 3-3/4 Slim Hole Logging While Drilling Motor (LWDM) for 4-3/4 Coalbed Methane Multilateral Horizontal Wells in the Northern Appalachian Operations. Proceedings of the International CBM Symposium, University of Alabama, Tuscaloosa, USA.

Lu, Y., Liu, Y., Li, X., and Kang, Y. 2010. A new method of drilling long boreholes in low permeability coal by improving its permeability. International Journal of Coal Geology. 84. 94-102.

Luo, D., Chu, W., Wu, X., Li, W. 2009. Analysis on Economic Benefits of Coalbed Methane Drilling Techniques. Petroleum Exploration and Development. 36(3). 403-07.

Malkewicz Hueni Associates, Inc., 2004. Evaluation of Coalbed Methane Well Types in the San Juan Basin. Prepared for The Bureau of Land Management.

Maricic, N., Mohaghegh, S.D., and Artun, E. 2008. A Parametric Study on the Benefits of Drilling Horizontal and Multilateral Wells in Coalbed Methane Reservoirs. SPE Reservoir Evaluation and Engineering. 11 (6). 976-983.

Massarotto, P., Golding, S.D., Rudolph, V., 2003. Anisotropic Permeability Characterization of Permian Coals. Proceedings of the International CBM Symposium, University of Alabama, Tuscaloosa, USA.

Palmer, I., 2010. Coalbed Methane Completions: A World View. International Journal of Coal Geology. 82. 184-95.

Palmer, I., 2008. Coalbed Methane Wells are Cheap, but Permeability Can Be Expensive. Energy Tribune, 19 Mar. 2008. Accessed online: 14 June 2010.

Pashin, J. 1998. Stratigraphy and structure of coalbed methane reservoirs in the United States: An overview. International Journal of Coal Geology. 35. 209-220.

Ross, H., Hagin, P., and Zoback, M. 2009. CO2 storage and enhanced coalbed methane recovery: Reservoir characterization and fluid flow simulations of the Big George Coal, Powder River Basin, Wyoming, USA. International Journal of Greenhouse Gas Control. 3(6). 773-786.

Sang, S., Xu, H., Fang, L., Li, G., and Huang, H. 2010. Stress relief coalbed methane drainage by surface vertical wells in China. International Journal of Coal Geology. 82. 196-203.

Spindler, G., Poundstone, W., 1960. Experimental Work in the Degasification of the Pittsburgh Coal Seam by Horizontal and Vertical Drilling. Trans. AIME. 220. 37-46.

Su, X., Lin, X., Liu, S., Zhao, M., and Song, Y. 2005. Geology of coalbed methane reservoirs in the Southeast Qinshui Basin of China. International Journal of Coal Geology. 62. 197-210.

Thakur, P., 2003. Optimum Methane Drainage in Gassy Coal Mines. 2003 SME Annual Meeting and Exhibit, February 24-26, Cincinnati, Ohio. Preprint 03.116.

Whittles, D., Lowndes, I., Kingman, S., Yates, C., and Jobling, S. 2007. The stability of methane capture boreholes around a longwall coal panel. International Journal of Coal Geology. 71. 313-328.

Yao, Y., Liu, D., Tang, D., Huang, W., Tang, S., and Che, Y. 2008. A Comprehensive Model for Evaluating Coalbed Methane Reservoirs in China. Acta Geol. Sin-Engl. 82 (6). 1253-1270.

Zhiming, W., Zhang, J., 2009. CBM reservoir thickness affects production from horizontal wells. Oil and Gas Journal. 107(16). 42-46.

Zupanick, J., 2006. Coal Mine Methane Drainage Using Multilateral Horizontal Wells. Mining Engineering. 58(1). 50-521.

Chapter 5. DERIVATION OF AN ANALYTICAL COALBED METHANE PRODUCTION MODEL FOR MULTILATERALLY DRILLED HORIZONTAL WELLS

Abstract

The hyperbolic decline curve model only accurately describes the shape of coalbed methane well production following the peak production rate. The versatility of the hyperbolic model to describe both exponential and harmonic decline make it the best candidate to describe the widest range of declining gas production data. A modified form on the Morse Potential function utilizes the same equation inputs as the hyperbolic decline model and can be used to describe gas production prior to and immediately following a coalbed methane well's peak production rate. Merging the modified Morse Potential function with the hyperbolic function yields an equation which accurately describes the shape of coalbed methane production curves from dewatering to reservoir depletion. The applicability of the merged model was verified through analysis of production data from multilaterally drilled horizontal coalbed methane wells in the central Appalachian Basin. With the exception of several wells that provided inconsistent production data, the coefficients of determination calculated when comparing the best fit merged production model to sample datasets all exceeded 0.90. The locations of the analyzed wells in the central Appalachian Basin were clustered such that coal thickness, permeability, reservoir pressure, and gas content were generally consistent, limiting the ability to link the model to multiple geologic parameters. The model was analyzed on a wider range of geologic inputs through production data generated with advanced reservoir modeling software. Permeability varied from 0.2 to 8.0 millidarcies, gas content from 100 to 600 cubic feet per ton, reservoir pressure from 50 to 1,500 psi, and coal thickness from 2 to 25 feet to create 832 production datasets for analysis. Finally, the merged functions were used to derive an analytical production model, linking permeability and horizontal drilling density to gas production rates in the presence of geologic conditions specific to China's Qinshui Basin.

5.1. Introduction

Decline curve models exist which describe the shape of petroleum production curves following the maximum production rate. Coalbed methane wells require dewatering to initiate the flow of methane from the internal coal matrix. During this period, gas production rates rise to a peak value, then decline in accordance to the existing decline models. Therefore, common production curves only describe the production rates of coalbed methane wells after the dewatering period. The following work creates a production model based on the same equation inputs as industry- and academia-accepted decline curves to describe the entire producing period of multilaterally drilled horizontal coalbed methane wells. This provides the opportunity to

describe a coalbed methane well's production rate from dewatering to depletion with a single function. The early period of coalbed methane well production is key to financial feasibility, as quick investment return boosts the attractiveness of startup coalbed methane operations worldwide.

The work is applied to China's Qinshui Basin, where rapid development of gassy coalbeds through vertical and horizontal well development is ongoing (Sang et al., 2009; Luo et al., 2009). Limited production data specific to the Qinshui Basin has been made publically available for a production rate assessment. Therefore, publically available data from the central Appalachian Basin is initially used to verify the validity of the production model with real world data. A multitude of datasets created using advanced 3-dimensional reservoir simulation software provide the opportunity to determine the applicability of the model to varying levels of geologic parameters specific to China's Qinshui Basin.

5.1.1. Decline Curve Models

Three main formulas exist which relate petroleum production to time. As outlined by Koederitz et al. (1989), the exponential, hyperbolic, and harmonic decline curves are recognized by industry and academia, with the former two curves being much more common. The decline curve models were first developed by Arps (1945). Equation 5.1 represents the exponential decline formula.

$$q = q_i e^{-Dt} \qquad \text{(Equation 5.1)}$$

In Equation 5.1, q represents a production rate, in units of volume per time. The initial production rate is represented by q_i. D represents the nominal decline fraction ($^1/_{\text{time}}$). Lastly, the independent variable, time, is represented by t. The decline rate, D, in the exponential model is

assumed constant throughout the well's life. Hook et al. (2009) stress that the exponential decline model is simplistic and fits oil production data well, but can underestimate long term production rates.

The hyperbolic decline equation predicts a longer well life with more sustained production than the exponential model. The decline rate is assumed to decrease over time. In practical applications, the hyperbolic decline model best describes tight reservoirs, such as organic shale formations (Markes, 2010). Coalbed methane reservoirs are also classified as tight due to their low permeability values. The general form of the hyperbolic decline equation is presented in Equation 5.2.

$$q = q_i(1 + bD_i t)^{-1/b} \qquad \text{(Equation 5.2)}$$

The inputs and associated units for q and q_i are the same as those recognized by Equation 5.1. D_i represents the initial nominal decline fraction, with units of $^{1}/_{\text{time}}$. The hyperbolic exponent, b, is a constant without units which describes how fast production rates approach zero. The hyperbolic exponent is constrained to values between zero and one.

The harmonic decline model is a specialized form of the hyperbolic model, where the hyperbolic exponent (b) is equivalent to a value of 1. Equation 5.3 outlines the harmonic decline curve.

$$q = q_i(1 + D_i t)^{-1} \qquad \text{(Equation 5.3)}$$

Although the harmonic model is not commonly used, fitting the hyperbolic model to production data can result in a harmonic curve. Therefore, the harmonic model is still considered a significant decline analysis model.

5.1.1.1. Applicability of Decline Curve Models to Coalbed Methane Wells

Coalbed methane production in the Black Warrior Basin in the southeastern United States can be characterized by exponential decline. Water production curves for the same coals are classified as hyperbolic (Pashin, 2007). Gentzis and Bolen (2008) analyzed the production of horizontal wells in the Gates coals in Canada. Their findings show that following peak production rates, both gas and water decline at a hyperbolic rate. Using a hyperbolic decline model, Yang et al. (2008) assessed the economic feasibility of coalbed methane wells in China's Qinshui Basin.

While exponential and hyperbolic models have both been used to describe the productivity of coalbed methane wells, it should be noted that a hyperbolic exponent (*b*) value of zero represents exponential decline (Li and Horne, 2003). Therefore, the hyperbolic model offers the widest range and broadest applicability to various shapes of decline curves and is used in modeling for this work.

5.1.1.2. Introduction of Modified Morse Potential Curve

The Morse potential energy function describes the potential energy of a diatomic molecule. A transformed version of the Morse potential function, shown below in Equation 5.4, can be used to describe the early producing period of coalbed methane wells.

$$P = -P_{max}\left(1 - e^{D_i(t_p - t)}\right)^2 + P_{max} \qquad \text{(Equation 5.4)}$$

In Equation 5.4, P represents the production rate of a coalbed methane well (volume per unit time) as a function of time, t. P_{max} represents the maximum production rate, while t_p represents the time at which the peak production rate occurs. The rate at which the production spikes and subsequently declines is given by D_i. Figure 5-1 displays a graph of the modified Morse

Potential function (MMP) as applied to sample coalbed methane well production data from the Central Appalachian Basin.

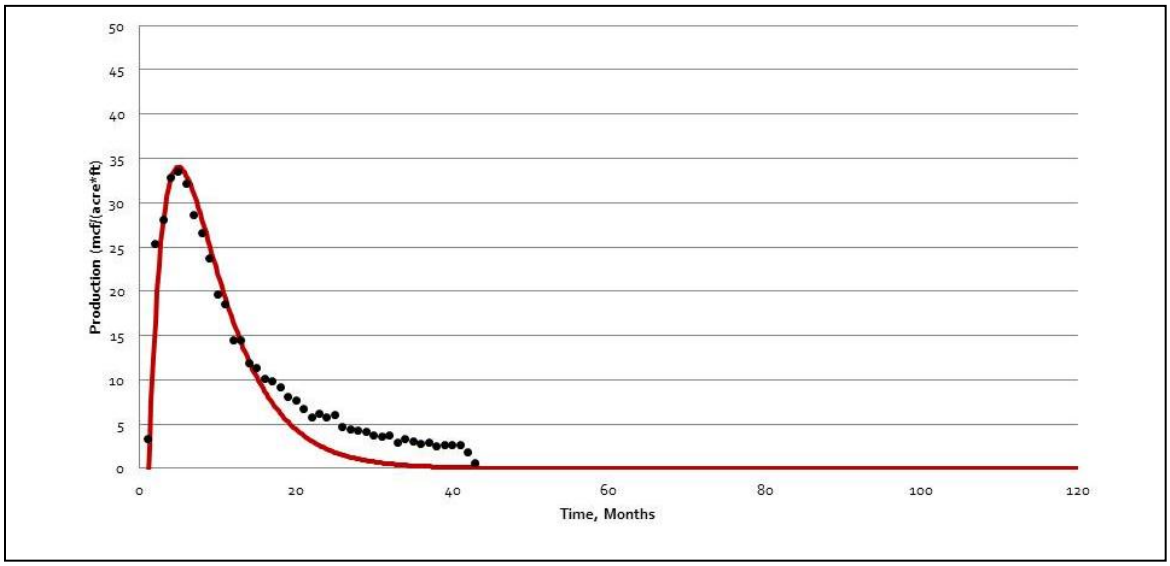

Figure 5-1: MMP curve with sample data

As presented in Figure 5-1, the MMP curve provides for a good data fit early in the well's life. Equation 5.5 outlines a form of the hyperbolic decline equation, with an additional parameter (t_p) to shift the curve laterally on the x-axis.

$$P = P_{max}\left(1 + bD_i\left(t - t_p\right)\right)^{-1/b} \qquad \text{(Equation 5.5)}$$

In Equation 5.5, t_p represents the time at which the maximum production value occurs. The initial nominal decline fraction, D_i, and hyperbolic exponent, b, represent the same parameters as described in Equation 5.2. Equation 5.2's q_i value has been renamed P_{max} to maintain consistency with the constants expressed in Equation 5.5. Equation 5.4 utilizes the same constants and Equation 5.5, with the exception of not having a b constant. Figure 5-2 displays the same sample production data used in Figure 5-1 with the hyperbolic function fit to the data.

The same equation inputs have been utilized for the MMP function in Figure 5-1 and the hyperbolic function in Figure 5-2.

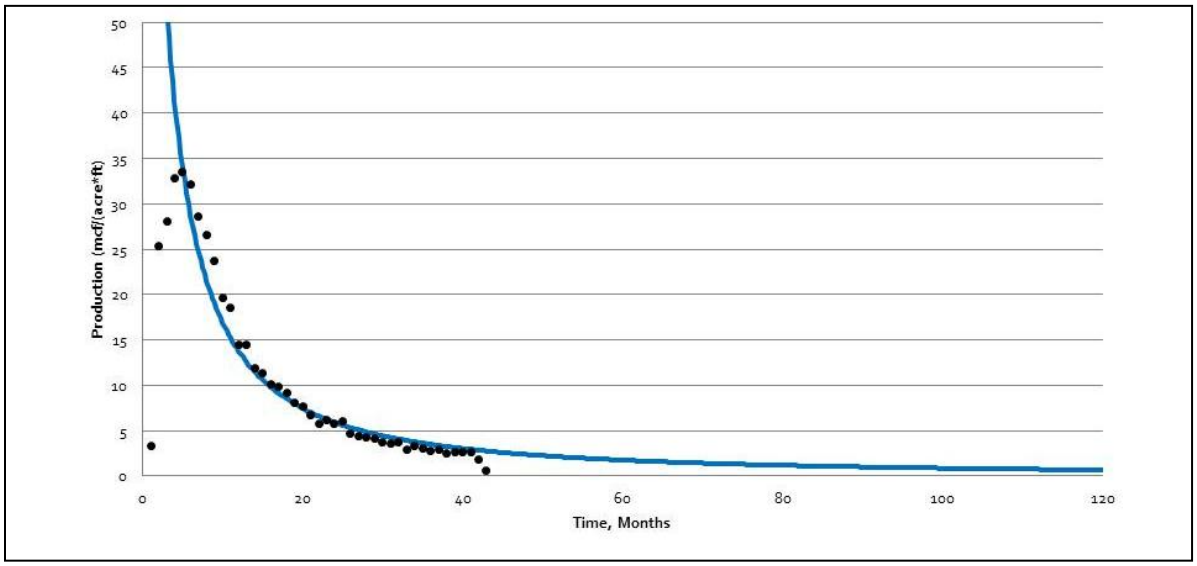

Figure 5-2: Hyperbolic curve with sample data

5.1.2. Merging Functions

As the MMP curve provides for a good data fit during a well's early producing period and the hyperbolic decline curve better fits production data later in a well's life, a combination of the two curves yields a function that accurately describe a well's production rate from dewatering to reservoir depletion. The respective periods when each curve is considered accurate are depicted in Figure 5-3. The time at which the hyperbolic function becomes applicable is denoted by t^*, the second intersection of the curves.

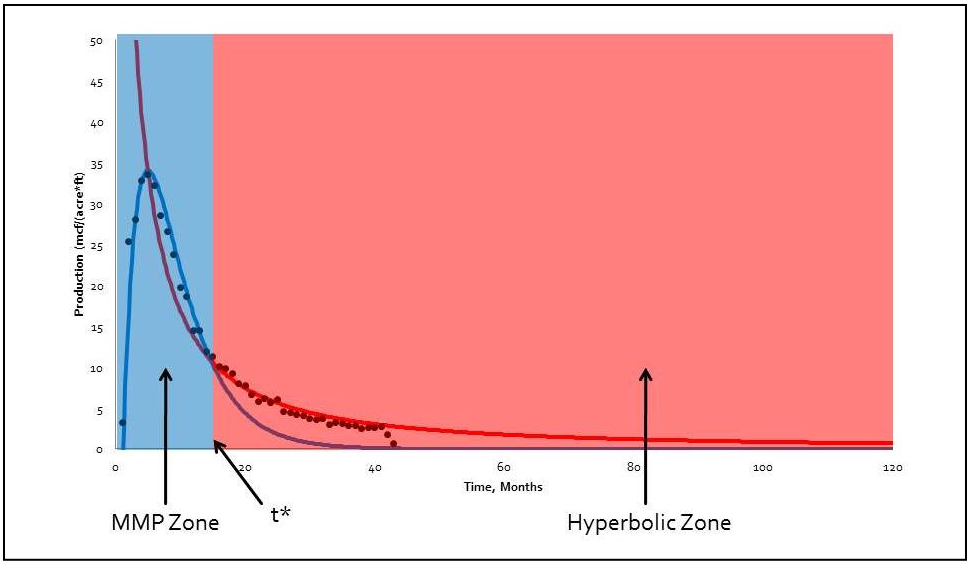

Figure 5-3: Depiction of applicable time ranges for each curve

Calculation of *t** is required to determine the point at which the curve's shape shifts from the MMP function to the hyperbolic function. In calculating *t**, the equations for both the MMP and hyperbolic decline curves are set equivalent to each other (Equation 5.6), solving for the independent variable, *t*.

$$-P_{max}\left(1-e^{D_i(t_p-t)}\right)^2+P_{max}=P_{max}\left(1+bD_i\left(t-t_p\right)\right)^{-1/b} \qquad \text{(Equation 5.6)}$$

Dividing Equation 5.6 by P_{max} and performing algebraic transformations simplifies Equation 5.6 to Equation 5.7, as shown below.

$$e^{D_i(t_p-t)}\left(2-e^{D_i(t_p-t)}\right)-\left(1+bD_i\left(t-t_p\right)\right)^{-1/b}=0 \qquad \text{(Equation 5.7)}$$

Due to the mathematical complexity of the relationship outlined in Equation 5.7, an approximation of the time (*t*) at which the functions are equivalent must be carried out. Equation 5.7 is further simplified by substitution of a new variable, *A*, as shown below in Equations 5.8 and 5.9.

$$A = D_i(t_p - t) \quad \text{(Equation 5.8)}$$

$$e^A(2 - e^A) - (1 - bA)^{-1/b} = 0 \quad \text{(Equation 5.9)}$$

As discussed in Section 5.1.1, both variables D_i and b are constrained between the values of zero and one. Additionally, a review of the previously discussed Pinnacle production data shows that the time at which the MMP and hyperbolic curves intersect is within 10 months of the time corresponding with the peak production rate. Therefore, the value of A can be constrained between the values of negative ten and zero, as these are the minimum and maximum possible values which can be calculated by Equation 5.8 corresponding with A. A graphical depiction of A as a function of b and the associated sixth order polynomial best-fit line are shown below in Figure 5-4. The sixth order polynomial function is shown in Equation 5.10.

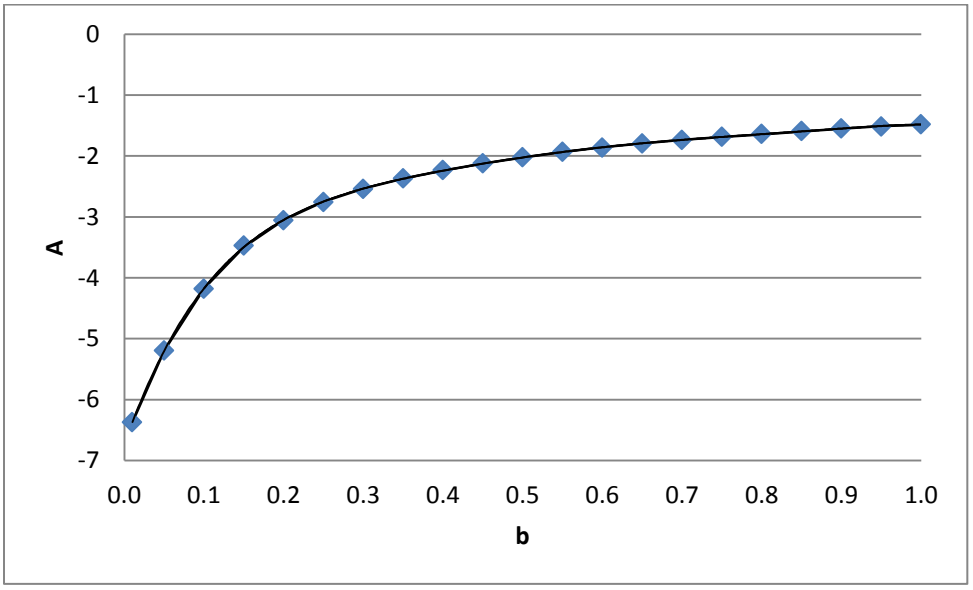

Figure 5-4: A as a function of b which can be used to determine t*

$$A = -66.6b^6 + 253.0b^5 - 389.8b^4 + 313.7b^3 - 142.0b^2 + 37.0b + 6.7 \quad \text{(Equation 5.10)}$$

Rearranging Equation 8 and substituting the above expression for *A*, the time at which the curves intersect, can be approximated by Equation 5.11.

$$t^* = t_p - \frac{-66.6b^6+253.0b^5-389.8b^4+313.7b^3-142.0b^2+37.0b+6.7}{D_i} \quad \text{(Equation 5.11)}$$

Two separate methods were considered for merging the equations at the approximated value of *t**. Initially, a piecewise function was considered. While a piecewise function minimizes the mathematical complexity of the calculation, it does not guarantee a smooth and continuous function. As *t** is an approximation of the curves' intersections and not necessarily the exact intersecting value, the production rates calculated by the MMP and hyperbolic functions are not guaranteed to be equivalent to each other. Additionally, the slope of the MMP and hyperbolic functions will be different at *t**, reducing the smoothness of the transition from function to function. Due to the potential lack of continuity associated with a piecewise function, an arctangent-based weighting function was used to merge the MMP curve with the hyperbolic decline curve.

The utilized arctangent-weighting function multiplies the MMP and hyperbolic curves by respective weighting factors and adds the curves together. During the early producing period, the MMP weighting factor is nearly 100-percent, while the hyperbolic weighting factor is nearly zero percent. Therefore, the function is dominated by the MMP curve prior to *t**. As time approaches the approximated value of *t**, the MMP weighting factor decreases while the hyperbolic weighting factor increases. At *t**, each weighting factor is 50-percent. In the later-producing period, the MMP weighting factor drops and the hyperbolic weighting factor increases, with the hyperbolic curve representing the data. Figure 5-5 displays a graphical depiction of the MMP and hyperbolic weighting functions with respect to t*. The blue dotted

line represents the MMP weighting factor and the red line represents the hyperbolic weighting factor. It should be noted that the actual shift from the MMP curve to the hyperbolic curve is much more abrupt, with Figure 5-5 denoting a more gradual change and lesser slope at t^* for comprehensive purposes and to depict the transformed arctangent functions.

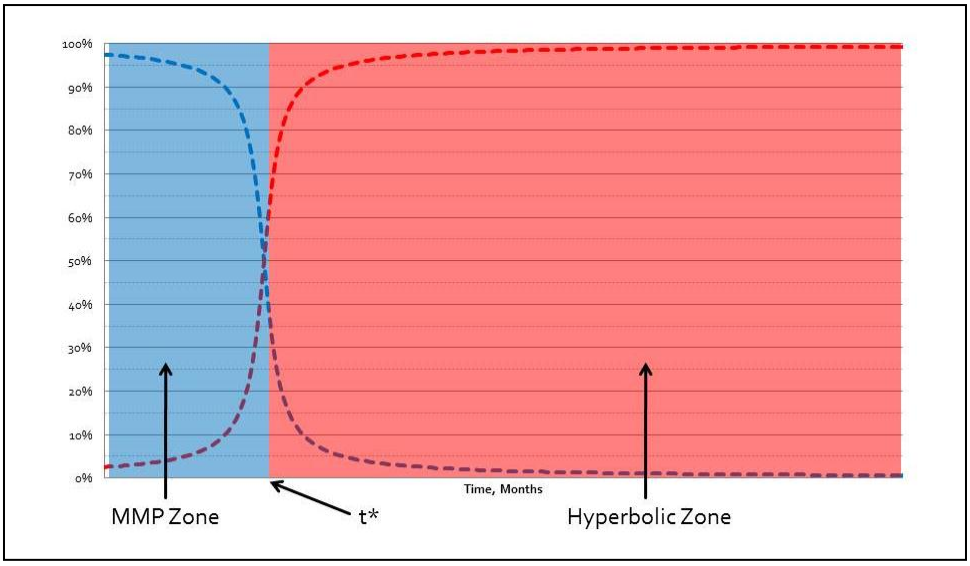

Figure 5-5: Depiction of arctangent-weighting function

The mathematical relationships for the MMP weighting factor (W_{MMP}) and hyperbolic weighting factor (W_{Hyp}) are shown below in Equations 5.12 and 5.13.

$$W_{MMP} = \frac{-\text{atan}\left[\frac{t-t^*}{t^*-t_p}*\tan(0.5\pi)\right]}{\pi} + 0.5 \qquad \text{(Equation 5.12)}$$

$$W_{Hyp} = 1 - \left(\frac{-\text{atan}\left[\frac{t-t^*}{t^*-t_p}*\tan(0.5\pi)\right]}{\pi} + 0.5\right) \qquad \text{(Equation 5.13)}$$

While the arctangent function outputs values between $-½\pi$ and $+½\pi$, the weighting factor requires output values between 0 and 1. Therefore, as shown in Equations 5.12 and 5.13, the resultant arctangent function is divided by π and increased by a value of 0.5. Combining Equations 5.12 and 5.13 with the hyperbolic and MMP functions, the finalized equation

describing the full production period of multilateral horizontal coalbed methane wells is outlined in Equation 5.14.

$$P = W_{MMP} * \left[-P_{max}\left(1 - e^{D_i(t_p - t)}\right)^2 + P_{max}\right] + W_{Hyp}\left[P_{max}\left(1 + bD_i\left(t - t_p\right)\right)^{-1/b}\right]$$

(Equation 5.14)

Although the above equation contains additional parameters beyond the four constants originally discussed, both W_{MMP} and W_{Hyp} are also functions of the original four constants. Therefore, the final equation presented above is a function of time, *t* and the four constants, P_{max}, T_p, D_i, and *b*.

5.2. Applicability of Equation to Real World Pinnacle Data

Production data corresponding to 50 multilaterally drilled horizontal coalbed methane wells used to degasify coal ahead of mining at the Pinnacle operation in southern West Virginia were used to determine the applicability of the production equation shown in Equation 14 to multiple datasets. The following sections provide an outline of the obtained data, associated geology of the area, and strengths and weaknesses of the equation's shape. Figure 5-6 displays a schematic of the studied wells.

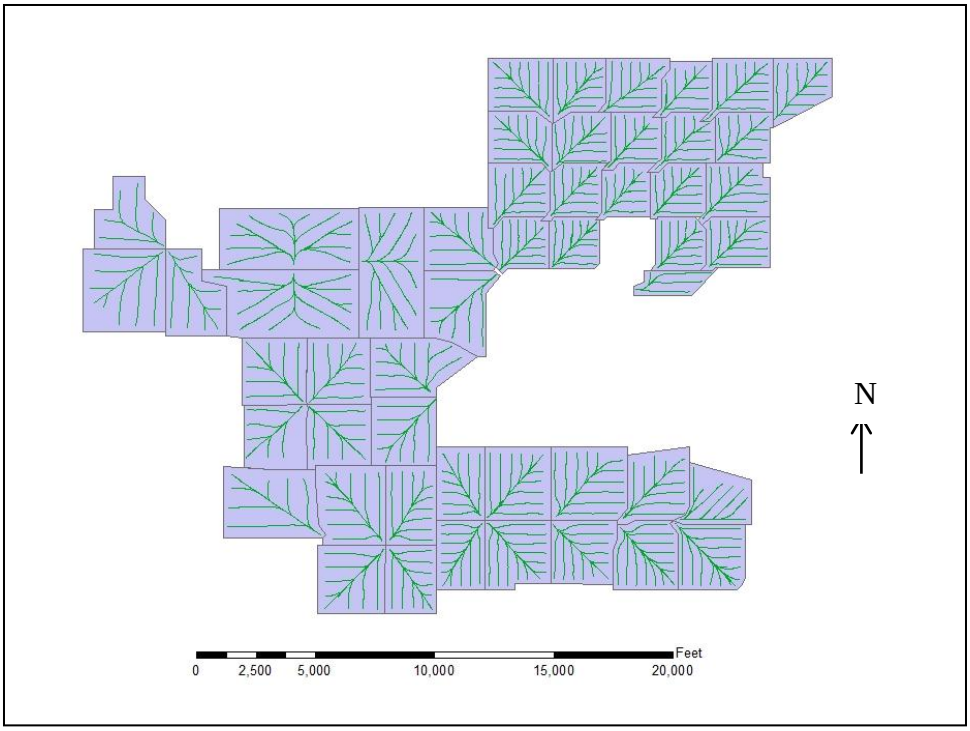

Figure 5-6: Plan view of Pinnacle coalbed methane wells

5.2.1. Overview of Data

The Pinnacle Mining Operation, located in Pineville, WV, utilizes multilaterally drilled horizontal coalbed methane wells to drain methane from the Pocahontas No. 3 coal bed ahead of longwall mining. In addition to draining the Pocahontas No. 3 coal bed, several of the horizontal wells have been completed in both the Pocahontas No. 3 and Pocahontas No. 4 coal beds, utilizing a configuration of vertically stacked horizontal patterns to simultaneously produce gas from both seams. Because the majority of the wells were only completed in the Pocahontas No. 3 coal bed, the Pocahontas No. 3 seam serves as the primary focus for this work.

Production data corresponding to the wells was obtained from the West Virginia Department of Environmental Protection through an online database (WVDEP). Marshall Miller and Associates provided geological information of the region, including seam depth, structure, and thickness information. Additionally, drilling patterns as permitted were obtained online

from the West Virginia Geological and Economic Survey for both the Pocahontas No. 3 and Pocahontas No. 4 coal beds.

Throughout the study area, the Pocahontas No. 3 seam ranges in thickness from 3 to 6 feet, generally averaging between 4 and 5 feet. A series of anticlines and synclines intersect the study area, trending in a northeast-southwest direction. The No. 3 coal bed gradually dips to the west. The coal seam depth in the study area ranges between 800 and 1,300 feet.

5.2.2. Pinnacle Case Study Data Processing

Raw data obtained from the WVDEP online database was transformed to normalize the data by well drainage area and seam thickness. Production values were analyzed on a per-acre-foot basis, where original production values were divided by both the well's calculated drainage area and the drainage area's average seam thickness. Normalizing the data in this manner transforms production rates to read as production rate per unit volume of targeted coal. This provides a standard baseline allowing a potential relationship between horizontal well drilling density and well production to be drawn. Drilling density, in units of feet per acre, is defined as the total in-seam drilling footage for well divided by the drainage area of the well. For the purpose of this study, gas content and permeability are assumed to be consistent through the area as data pertaining to these parameters was unavailable. Drainage areas corresponding with each well (depicted by purple-outlined boxes in Figure 5-6) and in-seam drilling lengths (green lines in Figure 5-6) were calculated using GIS software. Additionally, the average seam thickness for each well's drainage area was determined by gridding measured coal thickness values through GIS software.

Table 5-1 includes each well's drainage area, in-seam drilling density, and thickness as calculated by GIS software. Both original production values as obtained from the WVDEP online database and standardized production rates on a per-acre-foot basis are shown in Appendix A. Because total well production for wells completed in both the Pocahontas No.3 and No. 4 seams is reported through the WVDEP online database, production data for wells which were completed in both the Pocahontas No. 3 and No. 4 coal beds were adjusted such that the data is representative of production from only the Pocahontas No. 3 seam. Production from the Pocahontas No. 3 seam was assumed to be proportional to the ratio of in-seam drilling footage in the Pocahontas No. 3 seam to the sum of the in-seam drilling footages of the Pocahontas No. 3 and No. 4 seams.

Table 5-1: Pinnacle well drilling footage, seam thickness, drainage area, and drilling density

Well No.	In Seam Drilling Length (ft)	Average Poca-3 Seam Thickness (ft)	Drainage Area (acres)	Drilling Density (ft/acre)	Well No.	In Seam Drilling Length (ft)	Average Poca-3 Seam Thickness (ft)	Drainage Area (acres)	Drilling Density (ft/acre)
1	17474	5.1	277.6	62.9	26	19864	4.7	164.2	120.9
2	9916	5.1	155.7	63.7	27	16778	4.8	137.8	121.8
3	16820	4.8	263.6	63.8	28	16699	4.1	135.8	123.0
4	11511	5.2	162.5	70.8	29	14215	3.9	115.3	123.3
5	27149	5.0	381.0	71.3	30	21948	4.6	177.6	123.6
6	13346	5.3	177.0	75.4	31	15652	4.4	126.4	123.8
7	26788	5.3	345.9	77.4	32	16631	5.0	132.9	125.1
8	15232	5.4	195.2	78.0	33	13575	4.3	106.5	127.5
9	27224	4.6	344.9	78.9	34	16346	4.2	127.3	128.4
10	14604	5.3	173.6	84.1	35	17673	4.2	135.4	130.5
11	16974	4.9	201.0	84.4	36	14648	4.3	111.3	131.6
12	13857	4.8	163.3	84.9	37	15552	4.5	117.3	132.5
13	18648	4.7	216.9	86.0	38	15256	4.6	114.6	133.1
14	15730	4.5	181.1	86.8	39	23645	4.8	172.6	137.0
15	16185	4.9	185.7	87.2	40	15398	4.3	112.2	137.2
16	14921	5.0	169.0	88.3	41	24555	5.1	178.4	137.7
17	16741	5.2	174.5	95.9	42	16396	4.6	118.8	138.0
18	13565	4.7	137.6	98.6	43	9070	4.2	65.5	138.4
19	17633	4.4	165.1	106.8	44	14162	4.2	102.1	138.8
20	24089	4.7	225.3	106.9	45	14473	4.3	103.8	139.4
21	18800	4.7	175.3	107.3	46	16237	4.1	115.7	140.3
22	15496	4.4	141.8	109.3	47	19143	4.0	136.4	140.3
23	15885	5.1	143.1	111.0	48	19158	4.2	135.8	141.0
24	21885	4.4	196.1	111.6	49	15400	4.3	105.8	145.6
25	17248	4.7	144.4	119.5	50	16518	4.3	104.2	158.5

5.2.3. Pinnacle Data Analysis

Equation 5.14 was fit to each of the 50 Pinnacle coalbed methane well production datasets using a Microsoft Excel based algorithm. Curve fitting was optimized using Microsoft Excel's Solver tool. The Solver tool computes the coalbed methane well's production rate in accordance with Equation 5.14 as a function of the independent variable, time, and four equation constants (P_{max}, T_p, b, D_i) on a monthly basis. The difference between the dataset's production

value and the curve's predicted value is calculated, representing the relative error in the Equation 5.14's predicted production rate. The squared error for all times is calculated and summed to determine the sum of the squared error (*SSQ*), serving as a factor which represents effectiveness of the curve's fit. Lower *SSQ* values represent a better curve fit than higher *SSQ* values. The solver tool iteratively adjusts equation inputs to minimize the *SSQ* value. Microsoft Excel's Solver tool requires initial estimates of equation inputs prior to their automatic adjustment to best fit Equation 5.14's production curves to sample data. The following list outlines the process of obtaining initial equation input estimates, constraints placed on equation inputs in the Solver tool, and additional programming statements used in the curve-fitting algorithm.

1. *Initial Estimate for P_{max}.* The initial estimate for the curve's peak production rate is represented by the dataset's maximum production rate, calculated using a maximum value function in Microsoft Excel.
2. *Initial Estimate for t_p.* The initial value used by the Solver tool which represents the time corresponding with the peak production rate is set to the time corresponding with the original estimate for P_{max}. This is determined using a match formula.
3. *Initial Estimates for b and D_i.* As the hyperbolic exponent (*b*) and initial nominal decline fraction (D_i) are constrained between the values of zero and one, their initial estimates in the solver routine are set to 0.5. Additionally, the Solver tool is set such that the values of *b* and D_i cannot exceed 1 or be equivalent or less than zero.
4. *Correcting Negative Values*. Equation 5.14 outputs negative values prior to the initial intersection with the time axis. All output negative calculated production rates by Equation 5.14 are set to values of zero through an if-statement.
5. *Number Errors*. Because negative values cannot be raised to a negative exponent, an if-statement was placed in the program to eliminate this possibility in the hyperbolic decline equation. If the expression denoted below in Equation 5.15 holds true, Equation 5.14's value at time *t* is set to zero.

$$1 + bD_i\left(t - t_p\right) < 0 \qquad \text{(Equation 5.15)}$$

Table 5-2 and Table 5-3 contain a summary of the initial estimates for P_{max} and T_{max}, the converged best fit equation inputs, the *SSQ* values, and coefficient of determination (r^2) values for the 50 Pinnacle production datasets. Highlighted rows represent datasets which provide a best fit equation coefficient of determination less than 0.90. Appendix B contains graphs which display the best fit curves for each dataset with the sample data. Additionally, Appendix B contains graphs which show the error values as a function of time, displaying potential trends in the error curves.

Table 5-2: Summary of best fit curve parameters (wells 1 – 25)

Well No.	Actual P_{max} (mcf/month)/ (acre*ft)	Actual T_p (months)	Best Fit P_{max} (mcf/month)/ (acre*ft)	Best Fit T_p (months)	Best Fit b	Best Fit d_i (1/month)	SSQ	R^2
1	28.2	4	27.9	4.3	1.00	0.19	98.1	0.97
2	23.4	4	21.0	5.8	1.00	0.14	186.6	0.93
3	51.5	4	56.5	4.0	1.00	0.22	257.8	0.97
4	43.0	2	44.1	3.8	1.00	0.22	410.1	0.93
5	17.9	5	12.4	6.9	0.79	0.09	188.3	0.81
6	33.6	5	34.6	4.3	1.00	0.24	345.3	0.93
7	17.7	4	15.2	6.7	0.64	0.12	139.6	0.90
8	43.9	3	41.8	3.8	0.61	0.32	107.5	0.98
9	17.9	3	16.5	6.9	1.00	0.12	277.9	0.80
10	62.6	4	64.7	3.2	1.00	0.31	396.7	0.97
11	40.4	3	42.2	3.1	1.00	0.32	573.9	0.87
12	55.3	5	53.8	3.9	0.69	0.21	270.8	0.97
13	71.8	3	67.9	3.0	0.72	0.32	66.4	0.99
14	81.3	4	75.4	3.9	0.63	0.27	180.3	0.99
15	46.2	6	43.3	5.2	0.63	0.21	196.6	0.97
16	58.0	4	59.7	2.1	0.80	0.22	101.7	0.99
17	35.1	3	34.5	3.7	0.73	0.40	164.6	0.94
18	35.6	3	35.6	3.4	0.98	0.27	126.2	0.96
19	51.4	2	51.0	3.6	0.72	0.24	432.6	0.95
20	43.1	4	40.5	4.7	0.65	0.17	269.6	0.97
21	41.2	3	39.2	3.6	1.00	0.23	230.7	0.96
22	68.0	3	64.8	2.9	1.00	0.34	404.0	0.96
23	45.3	3	43.6	4.4	0.93	0.24	355.4	0.94
24	10.9	4	10.1	2.7	0.50	0.09	12.9	0.97
25	35.0	4	35.2	3.4	0.68	0.25	53.2	0.99

Table 5-3: Summary of best fit curve parameters (wells 26 – 50)

Well No.	Actual P_{max} (mcf/month)/ (acre*ft)	Actual T_p (months)	Best Fit P_{max} (mcf/month)/ (acre*ft)	Best Fit T_p (months)	Best Fit b	Best Fit d_i (1/month)	SSQ	R^2
26	50.3	3	51.0	3.2	0.75	0.28	132.9	0.98
27	58.3	2	58.5	2.6	0.68	0.27	90.3	0.99
28	49.9	3	48.1	3.2	0.58	0.26	68.3	0.99
29	70.5	3	69.0	3.1	0.74	0.31	1167.8	0.90
30	77.9	3	74.3	3.2	0.47	0.33	179.8	0.99
31	61.6	4	64.5	2.9	0.49	0.32	356.3	0.97
32	50.2	3	49.3	2.5	0.69	0.29	58.3	0.99
33	71.8	3	71.5	3.3	0.42	0.28	165.7	0.99
34	58.2	3	56.9	3.0	0.63	0.28	32.4	1.00
35	60.1	6	63.3	6.3	1.00	0.43	3803.3	0.65
36	83.0	2	80.7	2.3	0.40	0.32	282.7	0.98
37	61.6	2	64.5	2.5	0.56	0.44	93.7	0.99
38	86.6	3	88.6	2.9	0.36	0.39	329.1	0.98
39	38.9	3	39.2	3.4	0.74	0.28	90.0	0.98
40	68.7	2	65.6	2.8	0.26	0.24	96.3	0.99
41	33.5	5	33.8	4.6	0.67	0.18	41.6	0.99
42	57.4	3	58.7	3.8	0.45	0.24	88.1	0.99
43	67.9	3	71.7	2.6	0.77	0.76	3077.5	0.46
44	72.2	2	72.9	3.0	0.49	0.32	306.7	0.98
45	63.5	3	65.2	3.0	0.72	0.31	90.6	0.99
46	70.8	3	73.7	2.9	0.30	0.33	83.9	0.99
47	72.2	2	68.5	2.8	0.62	0.27	161.7	0.99
48	54.2	2	51.4	2.3	1.00	0.34	79.6	0.97
49	76.9	2	77.4	2.2	0.70	0.43	253.6	0.97
50	71.7	3	67.6	2.5	0.86	0.35	270.0	0.97

Analyzing the production data corresponding with the highlighted wells in Table 5-2 and Table 5-3 suggests operating challenges during gas production, causing poorer quality curve fits. Well numbers 5 and 35 both display multiple abrupt increase and decreases in production rate prior to and following the peak production value. This suggests potential water pumping issues where the coal bed was not continuously dewatered, likely causing rapid increases and decreases in bottom-hole pressure. Inconsistent bottom-hole pressure results in a series of gas production spikes and drops. Well number 43 contains similar trends, in addition to no production data after a period of 10 months. This minimizes the available data for an accurate curve fit, decreasing the coefficient of determination. Well number 9 shows zero production before to the peak rate, providing no data for curve fitting prior to the maximum production rate.

The remaining datasets' coefficients of determination values make a strong case in favor of the applicability of Equation 5.14 to describe the shape of the production rate curve of multilaterally drilled horizontal coalbed methane wells. An analysis of the error graphs in Appendix B shows inconsistent error trends between datasets. Although individual production datasets can show some trends of overestimating and underestimating production rate, the trends are not reproduced from dataset to dataset and are often reversed.

Figure 5-7 displays a graph containing the maximum production values as obtained from the datasets plotted against the best fit P_{max} values. The black line denotes the expected 1:1 relationship. As displayed in Figure 5-7, the Solver algorithm converges with P_{max} values similar to the true peak production values of the data. Figure 5-8 contains a similar graph, but reflects the true and best fit T_p values. T_p values must undergo a larger transformation than P_{max} values to optimize the curve fit.

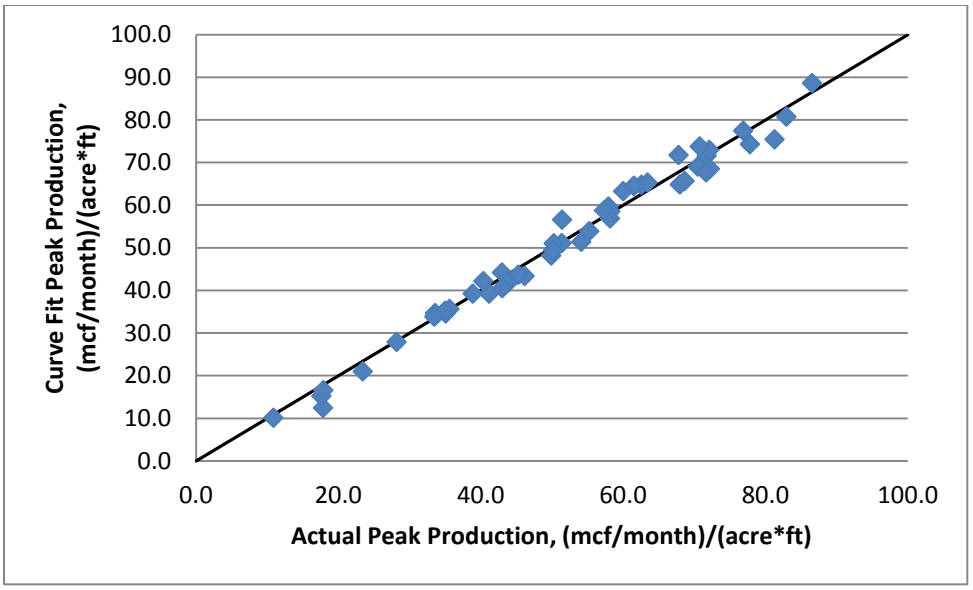

Figure 5-7: Comparison of actual peak production rates and P_{max} values obtained from curve fitting

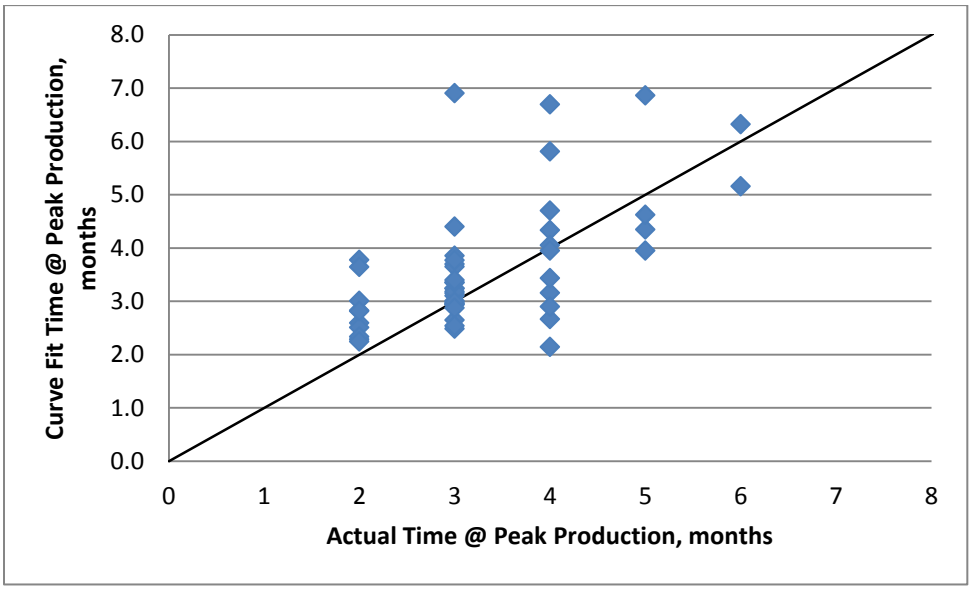

Figure 5-8: Comparison of actual peak production time and t_p values from curve fitting

Based on the favorable results in the goodness-of-fit analysis, the 50 production datasets can be analyzed on a drilling density basis. The obtained curve fitting parameters from the Solver algorithm were plotted against horizontal drilling density to determine if a relationship exists between equation inputs and drilling density. These results are displayed in Figure 5-9

through Figure 5-12. In an effort to determine positive or negative correlation of the equation inputs with respect to drilling density, a best fit linear regression line was imposed on each graph.

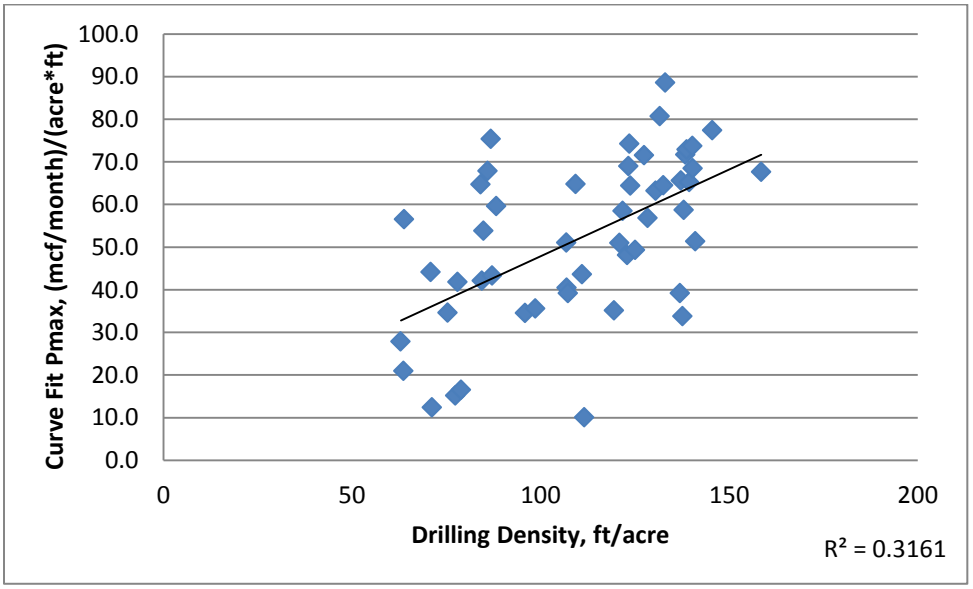

Figure 5-9: Curve fit P_{max} vs. drilling density

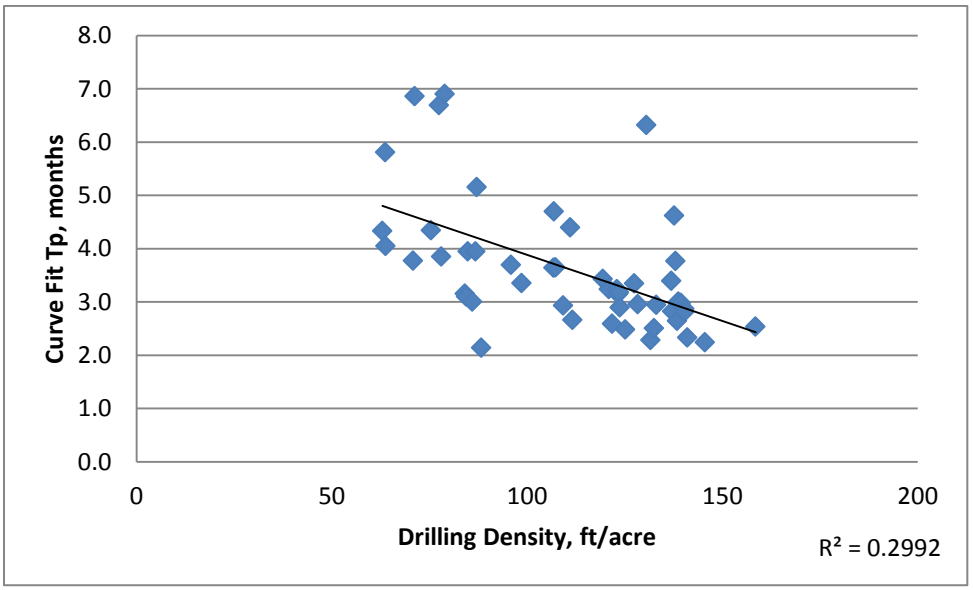

Figure 5-10: Curve fit T_p vs. drilling density

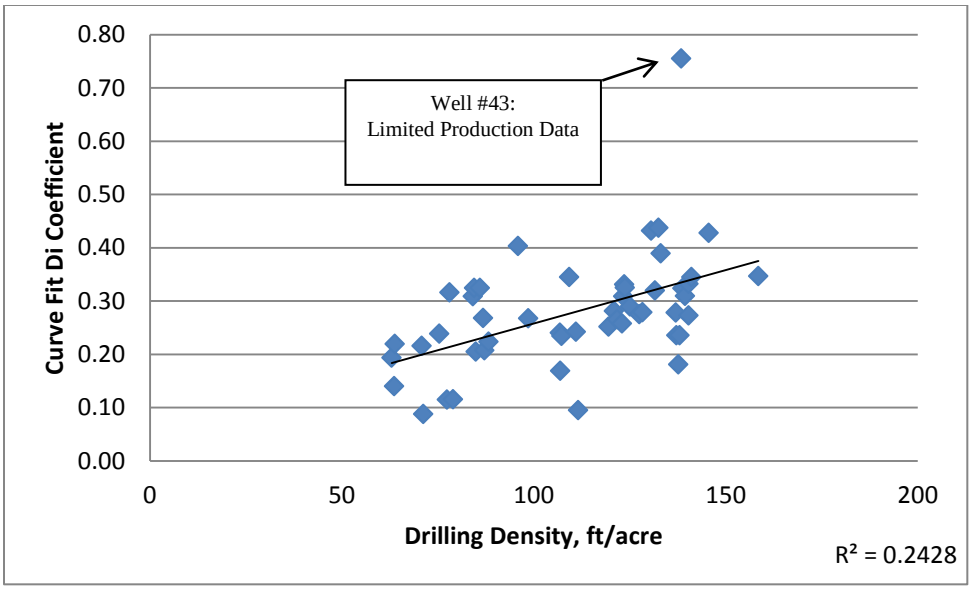

Figure 5-11: Curve fit D_i vs. drilling density

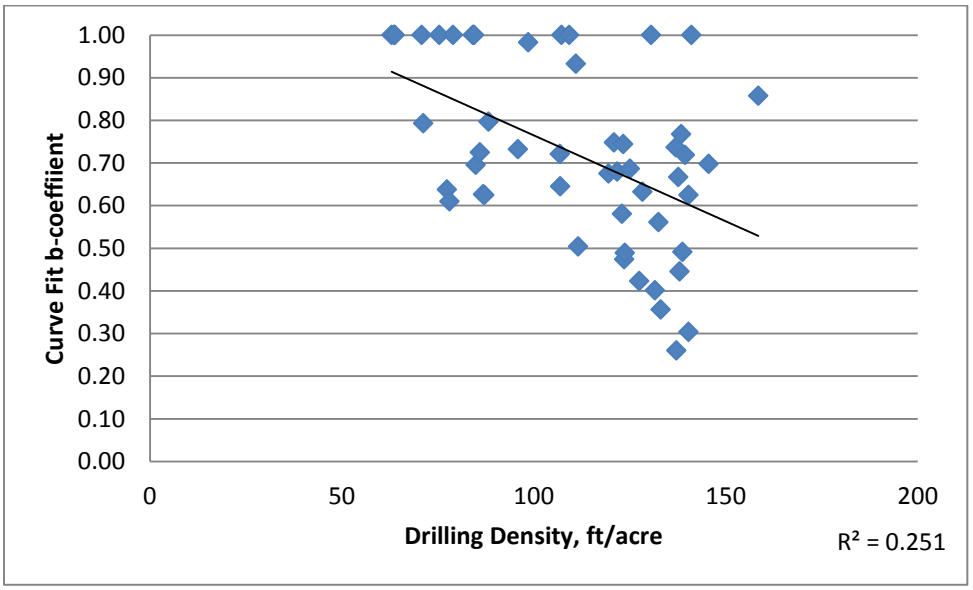

Figure 5-12: Curve fit b vs. drilling density

The weak coefficients of determination presented in Figure 5-9 through Figure 5-12 suggest additional geologic and operating factors or combinations of factors influence the curve-fitting parameters. These factors likely include, but are not limited to, seam structure, permeability, Langmuir coefficients, liniments, depth, pressure, proximity of producing wells to mine workings, proximity of producing wells to other producing and abandoned wells,

dewatering rates, and operating pressure. While pinpointing the relationships of these factors with the equation constants is beyond the scope of the Pinnacle case study, several important and expected conclusions can be drawn from Figure 5-9 through Figure 5-12.

Rapid depressurization of a hydrocarbon reservoir can be expected with increased drilling density. Fast depressurization yields higher gas production rates and faster recovery. Higher gas production rates (P_{max}) with increased drilling density are recognized by the positive correlation in Figure 5-9. Early peak production rates (T_p) and steep decline (D_i) resulting from an increased drilling density are suggested in Figure 5-10 and Figure 5-11. Figure 5-12 shows a curve's hyperbolic exponent should decrease as drilling density increases. This is expected, as higher *b* values result in slower recovery and sustained production.

The sample Pinnacle coalbed methane well data shows that the combined MMP and hyperbolic curve outlined in Equation 5.14 accurately describes real world coalbed methane production data. High coefficients of determination and random error trends show that the curve is applicable across multiple datasets. Normalizing the wells' production rates on a per-acre-foot basis show expected trends when comparing the equation inputs of Equation 5.14 to horizontal drilling density.

5.3. Production Equation Applicability for Different Geological Settings

The preceding section proves the ability of Equation 5.14 to accurately describe the shape of production curves associated with real world data. The Pinnacle production data used for the analysis was assumed to be geologically consistent in terms of seam thickness, reservoir pressure, permeability, and seam gas content. Because of the consistency of the geology associated with the production data, well geometry was the only parameter which could be

linked to variations in equation inputs and the associated shape of the production curve. This section aims to determine the applicability of Equation 5.14 to a broader range of geologic inputs by generating production curves with advanced 3-dimensional reservoir modeling software over various combinations of geologic parameters. Ultimately, equation inputs will be tied to selected geologic parameters to transform Equation 5.14 to a predictive analytical production model.

5.3.1. Modeled Reservoir

China's Qinshui Basin serves as an emerging coalbed methane basin with significant reserve development occurring over the past decade (Sang et al., 2009; Luo et al., 2009). While multiple studies have outlined the coalbed-methane-based geology of the basin (Su et al., 2005; Sang et al., 2009; Wei et al., 2005), limited production data and production modeling has been made public through international journals. Keim et al. (2011) describes the relationships between lateral spacing and permeability for multilaterally drilled coalbed methane wells in the Qinshui Basin through reservoir modeling. This work builds on the findings of Keim et al. (2011) to further determine the relationships of additional geologic parameters and well geometry and their associated impact on production by analyzing simulated production curves and relating modeled curves to Equation 5.14.

Advanced Resources International's COMET3 reservoir simulator was used to model coalbed methane production curves across a range of geologic parameters and differing well geometries. Grid geometry and well geometry were based on the work of Keim et al. (2011) with grids modeled as square blocks with dimensions of 100 feet by 100 feet. The well drainage area was held constant for all simulations, modeled as 250 acres. This requires 33 grids in both the X- and Y-directions. Figure 5-13 contains a 3-dimensional depiction of the modeled wells and the well geometry which is held constant or varied for simulations. Individual lateral

spacing was modeled at values of 200, 400, 600, and 800 feet. Table 5-4 contains the required in-seam drilling length for modeled lateral spacing values in addition to their associated drilling density at a constant drainage area of 250 acres. Note that the drilling density for wells used in the Pinnacle analysis varies from 63 to 159 feet per acre.

Table 5-4: Simulated well geometry lateral spacing, in-seam drilling length and drilling density

Lateral Spacing (ft)	Total In-Seam Drilling Length (ft)	Drilling Density (ft/acre)
200	46,000	184
400	27,000	108
600	20,000	80
800	17,000	68

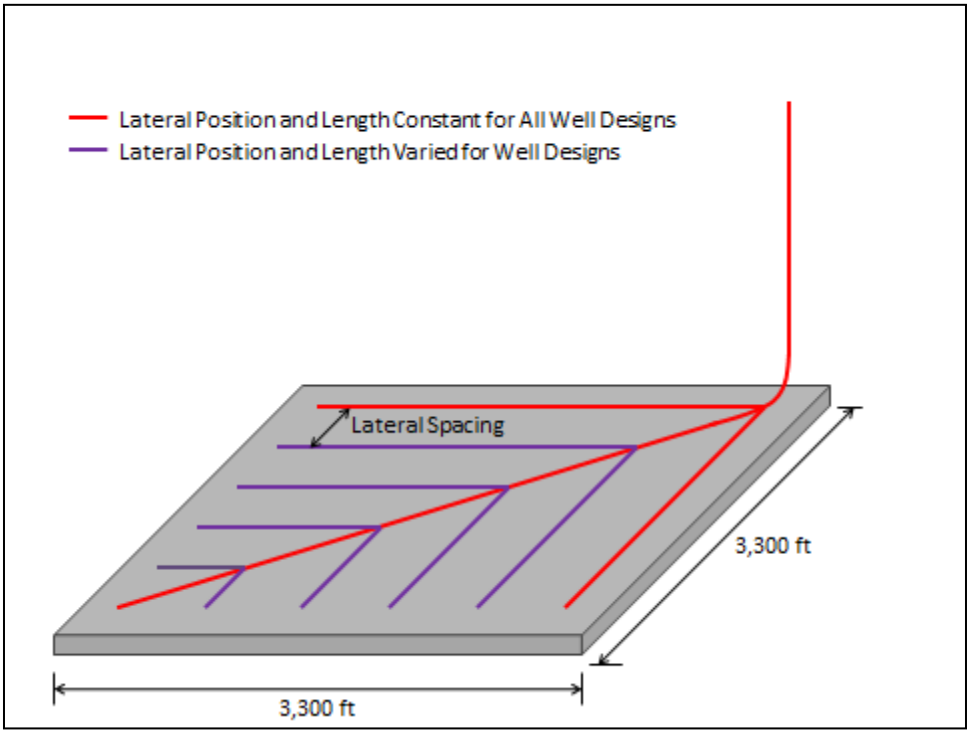

Figure 5-13: Depiction of modeled well geometry

Table 5-5 contains an overview of the modeling inputs which were held constant for all simulations. Table 5-6 displays the geologic inputs which were varied for simulations.

Table 5-5: Modeling inputs held constant for all simulations

Parameter	Value
Water Saturation	85%
Permeability Anisotropy Ratio	1:1
Fracture Porosity	3%
Langmuir Volume (ft^3/ton)	1000
Langmuir Pressure (psi)	300
Water Saturation (%)	85%
Cleat Spacing (inches)	2
Sorption Time (days)	50

Table 5-6: Geologic parameters varied in simulations

	Seam Thickness (ft)	Seam Permeability (md)	Reservoir Pressure (psi)	Gas Content (scf/ton)
Level 1	1.21	0.2	50	100
Level 2	8.91	0.7	500	267
Level 3	16.6	2.5	1000	433
Level 4	24.3	8	1500	600

The COMET3 reservoir simulator does not have the ability to model oversaturated coalbed methane reservoirs. Oversaturated reservoirs are defined as reservoirs which have initial gas contents greater than the gas content calculated by the Langmuir relationship at the initial reservoir pressure. As applied to this work, the combinations of gas contents and reservoir pressures outlined in Table 5-6 are undersaturated with the exception of the Level 1 reservoir pressure and Level 2, 3, and 4 gas contents. These combinations of reservoir pressure and gas content yield oversaturated conditions and cannot be accurately modeled with the COMET3 simulator; therefore, these combinations of gas content and reservoir pressure are discarded and not simulated or analyzed. Disregarding these combinations of reservoir pressure and gas content, all remaining variations of geologic inputs yield 832 COMET3 simulations.

5.3.2. Data Analysis

Utilizing the same methodology outlined in Section 5.2.2, a best-fit curve was applied to the 832 simulation datasets to determine the applicability of Equation 5.14 to the range of geologic parameters in Table 5-6. Output simulation data was matched to the same format as the Pinnacle data to maintain consistency in analysis. Data is outputted from the COMET3 simulator in the form of standard cubic feet per day. The data was transformed to average production rate per month and analyzed on a monthly basis. Appendix C contains tables which include the best fit equation inputs and coefficients of determination for each of the simulations.

Figure 5-14 through Figure 5-18 display plots of the coefficients of determination of the best-fit curves with respect to the simulation data for the varied geologic and well-operating parameters. Through analysis of these graphs, the combinations of simulation input parameters which result in good data fit can be pinpointed.

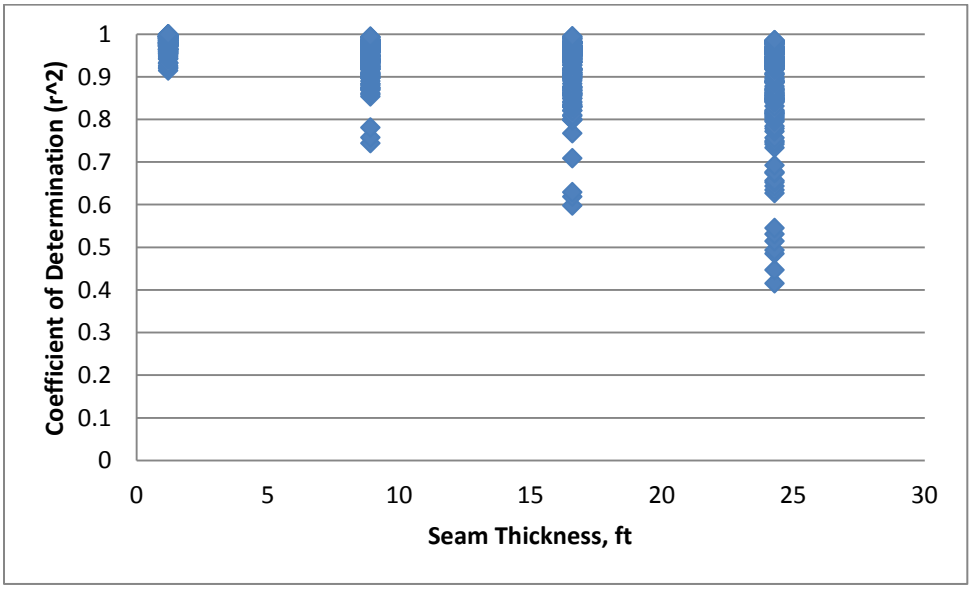

Figure 5-14: Seam thickness vs. coefficient of determination

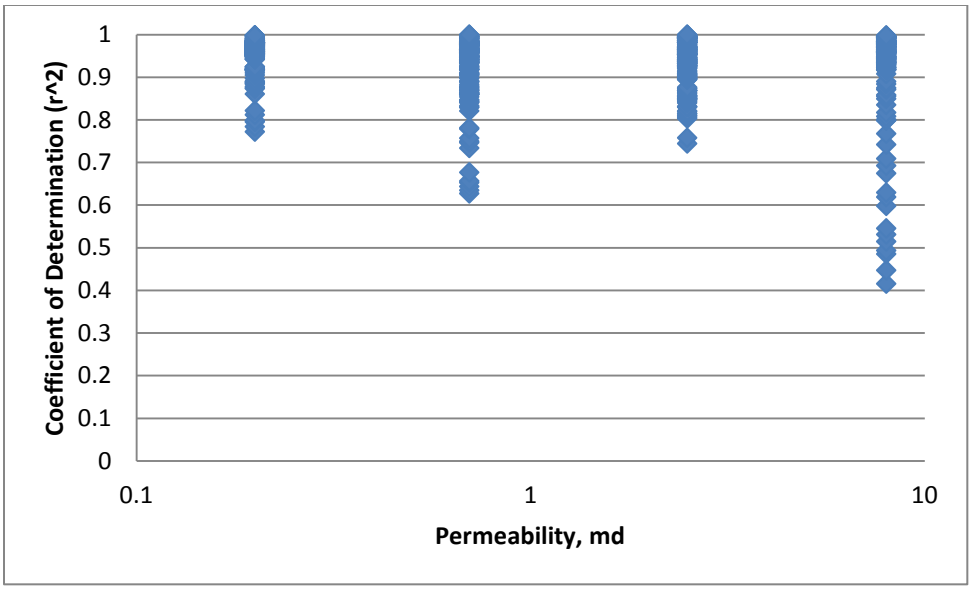

Figure 5-15: Permeability vs. coefficient of determination

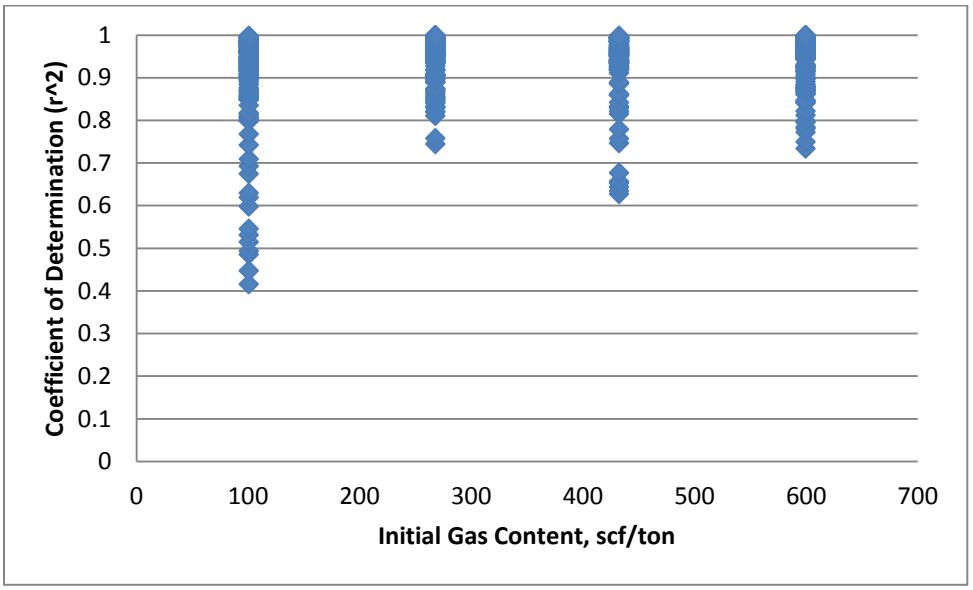

Figure 5-16: Initial gas content vs. coefficient of determination

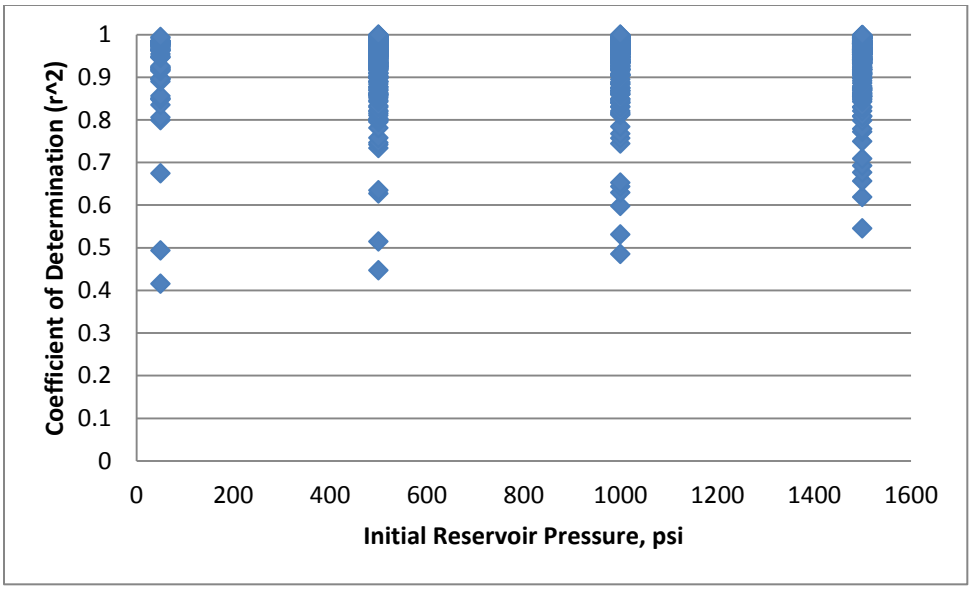

Figure 5-17: Initial reservoir pressure vs. coefficient of determination

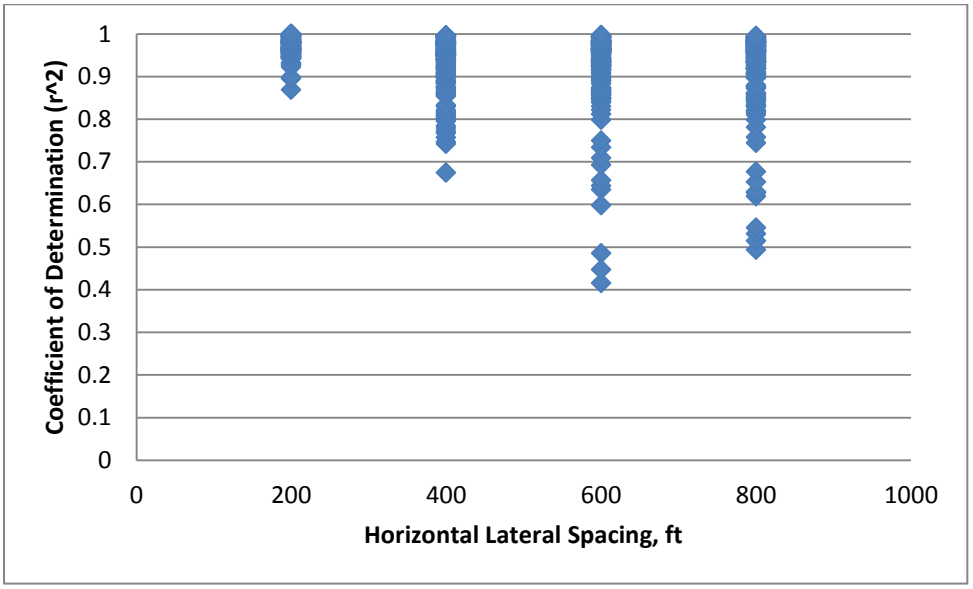

Figure 5-18: Horizontal lateral spacing vs. coefficient of determination

The trends in Figure 5-14 through Figure 5-18 and the corresponding reference data (see Appendix C) allow several significant conclusions about the applicability of Equation 5.14 to various well geometry and geological parameters to be drawn. First, no simulations modeled at a seam thickness of 1.21 feet provide for a coefficient of determination of less than 0.9. This

suggests that the production equation represented in Equation 5.14 fits production curves across the range of geologic parameters presented in Equation 5.14, provided that the coal seam thickness is relatively thin, approximately 1 foot. Further, the ability of the curve to fit production data is most largely governed by thickness. As shown in Figure 5-14, as seam thickness increases, the span of the coefficient of determination increases faster than any of the remaining varied modeling inputs.

In analyzing the reference data for Figure 5-14 through Figure 5-18, the higher permeability models (8 md) combined with the thick seam models provide for the lowest coefficients of determinations. All coefficients of determination less than 0.6 are represented by 24.3-ft and 16.6-ft seam thickness models coupled with permeability values of 8 md. Additionally, these models all utilize initial gas contents of 100 standard cubic feet per ton. Based on these results, Equation 5.14 is not applicable in high permeability, low gas content, thick coal seams. Certain areas within the San Juan Basin exhibit high permeability, thick, low gas content coals. Therefore, coalbed methane production curves associated with these areas within the San Juan Basin would not accurately be described by Equation 5-14. Contrarily, the coals of the central Appalachian Basin are summarized by thin to moderate thickness, low to moderate permeability and moderate to high gas contents. As verified by the analysis of Pinnacle sample data, production data from the Central Appalachian Basin is well represented by Equation 5-14.

Figure 5-18 suggests that the 200- and 400-ft lateral spacing models fit Equation 5.14 better than the 600- and 800-ft simulations. Only 3 of the 200-ft spacing models provided best fit equation coefficients of determination less than 0.9, all of which were modeled at a seam

thickness of 24.3 feet. Finally, Figure 5-17 suggests that the ability of Equation 5.14 to fit data is least sensitive to initial reservoir pressure.

In summary, Equation 5.14 tends to best fit production curves with low to moderate seam thicknesses, in the range of approximately 1 to 10 feet. Moderate to high gas contents, approximately 270 to 600 cubic feet per ton also help provide the best data fit in this thickness span. Lateral spacing between 600 and 800 feet, coupled with low permeability (less than 2.5 md), hinders the ability of Equation 5.14 to fit production data in the presence of seam thicknesses of around 9 feet. Initial reservoir pressure has little influence on the applicability of Equation 5.14 to fit production data in this thickness range. Although Equation 5.14 fits certain combinations of geologic parameters better than others, it serves as a viable expression which can be used to describe the overall shape of production curves throughout a well's entire producing period.

5.3.3. Converting Production Equation to Analytical Model

As discussed in Section 5.3.2, Equation 5.14 accurately describes the shape of production curves over various ranges of geological features. In an effort to determine the applicability of Equation 14 as a predictive analytical model, the four equation inputs were analyzed as functions of varying permeability and lateral spacing. This ultimately transforms Equation 5.14 to read as functions of a geologic factor, permeability, a well geometry parameter, and horizontal lateral spacing.

For this analysis, reservoir pressure, seam thickness, and gas content were set constant as values typically reported in the literature for methane-bearing coal seams targeted for development in the Qinshui Basin. Initial reservoir pressure was assumed to be 1,000 psi. Seam

thickness and gas content were respectively assumed to be 8.91 feet and 430 cubic feet per ton. Holding these geologic parameters constant, the average coefficient of determination calculated for the 16 combinations of lateral spacing and permeability was found to be 0.96 when analyzed in the preceding section through the best-fit curve analysis. The minimum and maximum coefficients of determination were respectively found to be 0.92 and 0.99. Therefore, this dataset represents a good candidate for deriving an analytical model, as the simulated production curves in this pressure, gas content, and thickness span are accurately represented by Equation 5.14.

Figure 5-19 presents the general methodology associated with linking constants found in Equation 5.14 to lateral spacing and permeability. The steps in determining the constants c_1, c_2, c_3, c_4, c_5, and c_6 in Figure 5-19 are outlined below. The remaining constants are determined in the same manner.

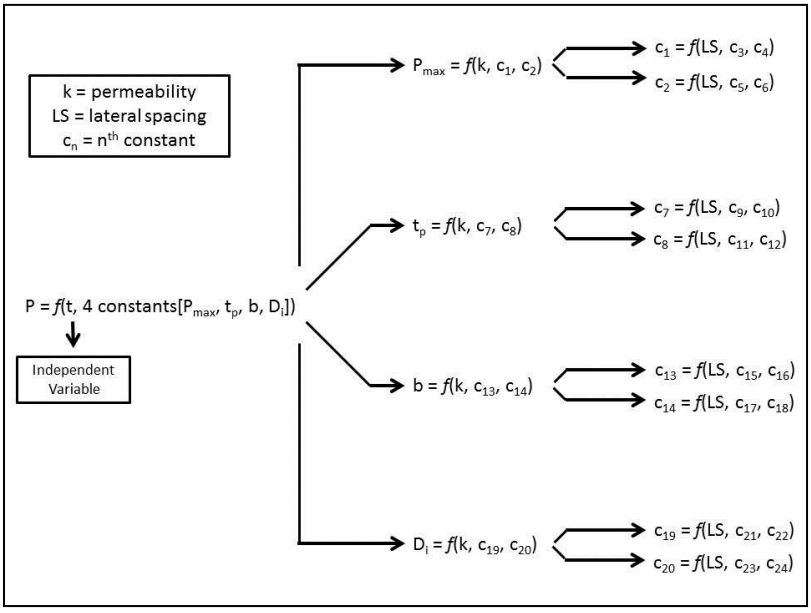

Figure 5-19: Methodology for linking equation inputs to permeability and lateral spacing

1. P_{max} values were plotted against permeability (k) for each varied level of lateral spacing. This yields a graph with an x-axis of permeability and a y-axis of P_{max}. Four separate curves exist, one for each level of lateral spacing.

2. The resulting shapes of the curves from plotting P_{max} versus permeability were analyzed. It was determined that a logarithmic function in the form of Equation 5.16 best fit the relationship. Four separate trend-lines in the form of Equation 5.16 were fit to the *k* vs. P_{max} plots, one for each level of lateral spacing.

$$P_{max} = c_1 \ln(k) + c_2 \quad \text{(Equation 5.16)}$$

3. The new equation constants, c_1 and c_2 associated with the four trend-lines are plotted against lateral spacing. Both relationships (c_1 vs. lateral spacing and c_2 vs. lateral spacing) were found to be linear, in accordance with Equations 5.17 and 5.18. Trend-lines in the form of Equations 5.17 and 5.18 are fit to the lateral spacing vs. c_1 and lateral spacing vs. c_2 plots, resulting in linear functions which relate c_1 and c_2 to lateral spacing.

$$c_1 = c_3(LS) + c_4 \quad \text{(Equation 5.17)}$$
$$c_2 = c_5(LS) + c_6 \quad \text{(Equation 5.18)}$$

4. In calculating P_{max} as a function of lateral spacing and permeability, c_1 and c_2 are first calculated as functions of lateral spacing and constants c_3, c_4, c_5, and c_6. c_1 and c_2 are no longer truly constants, but are functions of lateral spacing, c_3, c_4, c_5, and c_6. The obtained values of c_1 and c_2 are then used to calculate P_{max} in accordance with Equation 5.16.

The above steps outline the methodology in determining P_{max}. Equations 5.19 through 5.27 outline the functional forms of the equations associated with linking t_p, b, and D_i to permeability and lateral spacing.

Table 5-7 contains the constants in Equations 5.20, 5.21, 5.23, 5.24, 5.26, and 5.27. Similar to the case of determining P_{max}, c_7, c_8, c_{13}, c_{14}, c_{19}, and c_{20} are not truly constants but functions of other constants and lateral spacing.

$$t_p = c_7 \ln(k) + c_8 \quad \text{(Equation 5.19)}$$
$$c_7 = c_9(LS) + c_{10} \quad \text{(Equation 5.20)}$$
$$c_8 = c_{11}(LS) + c_{12} \quad \text{(Equation 5.21)}$$
$$b = c_{13} \ln(k) + c_{14} \quad \text{(Equation 5.22)}$$
$$c_{13} = c_{15}(LS) + c_{16} \quad \text{(Equation 5.23)}$$
$$c_{14} = c_{17}(LS) + c_{18} \quad \text{(Equation 5.24)}$$
$$D_i = c_{19} k^{c_{20}} \quad \text{(Equation 5.25)}$$
$$c_{19} = c_{21}(LS) + c_{22} \quad \text{(Equation 5.26)}$$
$$c_{20} = c_{23}(LS) + c_{24} \quad \text{(Equation 5.27)}$$

Table 5-7: Constants Corresponding with Equations 5.19 through 5.27

Constant	Value	Constant	Value
C_3	-0.027	C_{15}	1.00E-04
C_4	341	C_{16}	-0.18
C_5	-0.85	C_{17}	3.00E-04
C_6	1681	C_{18}	0.72
C_9	-5.00E-04	C_{21}	4.00E-05
C_{10}	1.50	C_{22}	0.23
C_{11}	-0.0036	C_{23}	-2.00E-04
C_{12}	6.66	C_{24}	-0.095

Using the constants in Table 5-7 and Equations 5.19 through 5.27, production rates were predicted for the 16 combinations of levels of permeability and lateral spacing. Comparing the reservoir modeling output to the analytical model output, the coefficient of determination was computed. Table 5-8 compares the coefficient of determination for the analytical model to best-fit curve coefficient of determination from Section 5.3.2.

Table 5-8: Comparison of Coefficients of Determination of Analytical Model (left) to Best Fit Curve (middle) to percent difference of best fit to analytical model(right)

	Permeability, md			
Lateral Spacing (ft)	0.2	0.7	2.5	8
200	0.93/0.99/-7%	0.99/0.99/-1%	0.98/0.98/0%	0.98/0.98/0%
400	0.97/0.97/0%	0.82/0.96/-14%	0.96/0.99/-3%	0.98/0.99/-1%
600	0.94/0.98/-5%	0.85/0.97/-13%	0.91/0.97/-6%	0.99/0.99/-1%
800	0.86/0.98/-12%	0.92/0.97/-5%	0.95/0.97/-2%	0.99/0.99/0%

As delineated in Table 5-8, the analytical model matches the coefficient of determination of the best-fit curve in in the 8-md case for the 600- and 800-ft lateral spacing scenarios. The coefficient of determination is also matched in all 200-ft lateral spacing models with the exception of the 0.2 md permeability case. The analytical model does not accurately match simulated production data in the 400- and 600-ft lateral spacing models coupled with permeability values of 0.7 md. The same holds true for the 800-ft lateral spacing model with a permeability of 0.2 md. Still, the ability of Equation 5.14 to act as an analytical model is proven.

Re-analyzing the functional forms in Equations 5.16 through 5.27 could result in a more consistently accurate analytical model across the entire span of permeability and lateral spacing values.

Additional geologic parameters could be linked to the analytical model by expanding the formula tree displayed in Figure 5-19. As additional parameters are introduced and the formula tree in Figure 5-19 expands, the accuracy of the analytical model with respect to simulation output will decrease. A practical limit exists where it is more beneficial to run a 3-dimensional reservoir simulation with advanced modeling software as opposed to deriving an analytical model.

5.4. Conclusions

Standard decline equations, including the hyperbolic, harmonic and exponential decline curves only provide an analysis of production data following production peaks. Coalbed methane wells require dewatering to initiate the flow of gas. During the dewatering phase, gas production rates rises to a peak value. Following the peak value, standard decline equations can accurately describe the decline period.

A modified version of the Morse Potential equation was presented to describe the early producing period of coalbed methane wells. This curve uses similar equation inputs as the hyperbolic decline equation and does not introduce additional constants. The MMP curve holds accurate to represent production rates up to and immediately following a well's peak production rate. The applicability of MMP curve to real world production was verified through sample data from a well-developed coalbed methane field in the Central Appalachian Basin.

Merging the MMP curve with the hyperbolic decline curve was accomplished through an arctangent weighting function. Each curve is multiplied by a weighting factor and the curves are summed. A high weighting factor is placed on the MMP curve for coalbed methane wells' early production period. The weight shifts to the hyperbolic decline equation following the peak production value. The final equation which merges the MMP and hyperbolic decline curves is represented below in Equation 5-28.

$$P = W_{MMP} * \left[-P_{max}\left(1 - e^{D_i(t_p - t)}\right)^2 + P_{max}\right] + W_{Hyp}\left[P_{max}\left(1 + bD_i\left(t - t_p\right)\right)^{-1/b}\right]$$

(Equation 5.28)

The merged MMP and hyperbolic model was used to analyze 50 producing wells near Pineville, WV. While additional geologic and operating parameters largely influence production, expected trends were noted with respect to equation inputs. Based on the favorable results from this study, idealistic production data was generated through advanced reservoir modeling software for analysis and to determine the curve's effectiveness in fitting production data over various levels of geological parameters and well geometry. Horizontal drilling density, initial reservoir pressure, initial gas content, seam thickness, and permeability were varied. The curve was fit to a total of 832 production datasets through a Microsoft Excel-based algorithm. Results show that the curve fits best in low- to moderate-seam thicknesses with moderate- to high-gas contents.

Finally, the curve was transformed to an analytical model by expressing equation constants in terms of horizontal lateral spacing and permeability. Reservoir pressure, initial gas content, and seam thickness were held constant to represent a generalized model of the Qinshui Basin, where significant gas reserve development is underway. This analytical model serves as a predictive tool to determine the production capability of untapped reserves in the Qinshui Basin.

Chapter 5 References

Arps, J. 1944. Analysis of decline curves. AIME Meeting, May 1944. Houston, TX.

Gentzis, T. and Bolen, D. 2008. The use of numerical simulation in predicting coalbed methane producibility from the Gates coals, Alberta inner Foothills, Canada: Comparison with Mannville coal CBM production in the Alberta Syncline. International Journal of Coal Geology. 74. 215-236.

Hook, M., Soderbergh, B., Aleklett, K. 2009. Future Danish Oil and Gas Export. Energy. 34(11). 1826-1834.

Keim, S., Luxbacher, K., Karmis, M. 2011. A numerical study on optimization of multilateral horizontal wellbore patterns for coalbed methane production in Southern Shanxi Province, China. International Journal of Coal Geology. 86(4). 306-317.

Koederitz, L., Harvey, A., Honarpour, M. 1989. Introduction to Petroleum Reservoir Analysis. published by Gulf Publishing Company, Houston, TX.

Li, K., Horne, R. 2003. A decline curve analysis model based on fluid flow mechanisms. SPE 83470.

Markes, M. 2010. A new approach to estimating reserves in a Shale. Oil and Gas Evaluation Report.

Pashin, J. 2007. Hydrodynamics of coalbed methane reservoirs in the Black Warrior Basin: Key to understanding reservoir performance and environmental issues. Applied Geochemistry. 22. 2257-2272.

Sang, S., Liu, H., Li, Y., Li, M., Li, L. 2009. Geological controls over coal-bed methane well production in southern Qinshui Basin. Procedia Earth and Planetary Sciences. 1. 917-922.

Su, X., Lin, X., Liu, S., Zhao, M., Song, Y. 2005. Geology of coalbed methane reservoirs in the Southeast Qinshui Basin of China. International Journal of Coal Geology. 62. 197-210.

West Virginia Department of Environmental Protection. Oil and Gas Database. <http:www.dep.wv.gov/oil-and-gas/databaseinfo/Pages/OGD.aspx>

West Virginia Geological and Environmental Survey. File Repositories. <http://www.wvgs.wvnet.edu/pipe2/filerepository.aspx>

Yang, S., Kang, Y., Zhao, Q., Wang, H., Li, J. 2008. Method for predicting economic peak yield for a single well of coalbed methane. Journal of China University of Mining and Technology. 18. 521-526.

Chapter 6. CONCLUSIONS

The structural geology, coal seam thicknesses, and gas contents of the Qinshui Basin provide favorable conditions for commercial-scale coalbed methane operations. Permeability represents a key factor in the design of coalbed methane well layouts and varies significantly throughout the basin. Although success has been noted in coalbed methane production from hydraulically stimulated vertical fracture wells, horizontal well drainage techniques will be necessary in targeting the lower permeability areas of the Qinshui Basin.

The close proximity of horizontal laterals rapidly depressurizes coal seams, increasing methane recovery rates. The relative importance of horizontal lateral spacing increases as seam permeability decreases. High drilling density horizontal patterns decrease the spatial variability of methane contents in a coal seam, minimizing localized zones of high methane contents prior to mining. This serves as an important analytical method, as raw gas recovery values which report average gas recovery over a drainage area can be skewed with high methane concentrations away from the producing wellbore. In comparison to hydraulically stimulated vertical fracture wells, multilaterally drilled Pinnate-style wellbores recover substantially more methane on a per-unit-area basis.

Over a 20-year period, Pinnate-style wells can recover upwards of 90 percent of methane from coals in the Qinshui Basin. Modeling shows that vertically fractured wells only recover approximately 40 percent of methane when analyzed over the same time period. Pinnate-style wells exhibit a minimum recovery value of 70 percent in their respective drainage area, while certain zones within the vertical style well's drainage area show less than 10-percent recovery. The high fluctuations in gas content associated with vertical fracture wells could cause gas-offs,

lower mining productivity, and higher risks for explosive methane concentrations in the mine air. While Pinnate-style multilaterally drilled horizontal wells require a high level of technology and operator skill for successful development, closely spaced single lateral and dual lateral wells can achieve the same recovery results. Still, maximizing coal seam exposure from a single well offers the most economically viable option for gas operators.

Greenhouse gas emission reductions associated with degasification ahead of mining operations are directly proportional to the volume of recovered methane. Therefore, maximizing gas recoveries maximizes emission reductions. Again, multilaterally drilled horizontal well patterns offer the best option for reducing greenhouse gas emissions through effective degasification. Specific to the Qinshui Basin, degasification can result in a greenhouse gas emission reduction equivalent to 15-million metric tons of carbon dioxide when analyzed over a 20-year mining period. This requires 80- to 90-percent recovery of gas which can only be obtained over a 20-year period with a Pinnate-style horizontal well. Careful planning is required to achieve a significant decrease in greenhouse gas emission reductions, as alternative wellbore patterns reach significantly lower recovery values over a 20-year period.

Reservoir and financial modeling concludes that high drilling density horizontal wells offer the most economically feasible coalbed methane drainage option in the Qinshui Basin. Alternative horizontal patterns result in acceptable investment internal rates of return, but Monte Carlo simulations show a high likelihood of unattractive benefit-to-cost ratios and net present values for lower drilling density wellbore patterns. Although Pinnate-style horizontal well patterns with individual laterals spaced at intervals of 600 ft require a nearly 2-million-dollar capital investment compared to a 400-thousand-dollar investment for vertical wells, financial

modeling shows Pinnate wells provide for a 100-percent rate of return compared to an 18-percent rate of return for vertical wells.

Pinnate-style horizontal wellbore patterns can also be optimized to produce ample volumes of methane in lower permeability reservoirs. A Pinnate-style well with laterals spaced at distances of 600 ft in a 2.0 md reservoir produces a similar production rate profile as that of a Pinnate-style well with laterals spaced 200 ft apart in a 0.5 md reservoir. A Pitchfork-style well, designed to drain similar areas as a Pinnate well, offers advantages in reservoirs exhibiting directional permeability. Pinnate wells are less sensitive to directional permeability, exhibiting an 8-percent difference in cumulative production over a 10-year period depending on orientation with respect to face cleat and butt cleat fractures. Under the same reservoir conditions, Pitchfork patterns can gain a nearly 20-percent increase in cumulative production over a 10-year period when oriented properly. Individual laterals should be designed to intersect the face cleat direction whenever possible, taking advantage of the higher permeability value.

Pitchfork patterns also offer an advantage in reservoirs with highly fractured, weak coals. Multiple millions of dollars can be lost due to wellbore failure, effectively ruining newly developed wells. This risk can be mitigated through horizontal well pattern design. Gas production from the side lateral branches associated with Pinnate-style wells are dependent on the structural integrity of the well's main lateral. A single borehole collapse can ruin an entire Pinnate well. Contrarily, the laterals of a Pitchfork-style well operate independently. As applied to a 250-acre drainage area, the maximum lost length of lateral from a single borehole collapse for a Pitchfork-style well is 3,300 feet.

A new production equation was derived to represent production rate as a function of time over the entire producing life of a coalbed methane well. The equation is based upon the same inputs as the common hyperbolic decline equation and incorporates the hyperbolic decline curve in the later production period. The applicability of the curve to real world data was verified through a sample of 50 multilaterally drilled horizontal wells in the Central Appalachian Basin. Curve-fitting accurately described multiple expected trends according to drilling density. After applying the curve to simulated production data from a multitude of geological parameters, it was determined that the curve is most applicable in under saturated coal seams up to 10 feet thick. The curve also proved more accurate in higher gas content seams. The curve was transformed to an analytical model, applicable to geology similar to that of the Qinshui Basin. The analytical model serves as a predictive tool of gas production rates based on coal seam permeability and horizontal lateral spacing in multilaterally drilled wells.

In summary, despite the minimal numbers of horizontal coalbed methane wells in the Qinshui Basin, modeling concludes that they outperform hydraulically stimulated vertical fracture wells. Despite higher capital costs which likely deter horizontal completions, long-term financial analysis of investment return proves their benefit. Horizontals offer the best recovery option in low permeability coals as found in the Qinshui Basin.

The presented research includes multiple significant contributions to the scientific and engineering fields. First, through detailed reservoir modeling, a strong case has been developed for the feasibility of economic development of gas production in low permeability coals in the Qinshui Basin. This in-depth study encourages the development of additional gas resources in the region. Second, through the use of readily available reservoir modeling software, the methodology associated with quantitatively analyzing the benefits of coal degasification has

been documented and presented. This represents a novel approach in simultaneously determining environmental, safety, and economic benefits of coal degasification. Although the results presented in this dissertation are specific to coalbed methane basins exhibiting geological features consistent with those of the Qinshui Basin, the presented methodology is applicable on a global scale.

The utilized COMET3 reservoir modeling software incorporates well-understood theoretical relationships to predict the production capabilities of coalbed methane reservoirs. An additional significant contribution of this research includes an empirical relationship between lateral spacing and permeability in multilaterally drilled horizontal coalbed methane wells. This relationship, developed through the use of COMET3 reservoir simulation models, serves as a tool for coalbed methane developers concerned with the economic feasibility of gas production from low permeability coal seams. Finally, an improved gas production rate model has been presented which accurately describes the entire producing period of coalbed methane wells as opposed to past models which only analyze the decline portion of production curves. This functions as a baseline foundation model for the scientific community which can be expanded upon and related to geologic parameters. Any past research associated with the Arps decline models is applicable to the newly presented model, as the new function is based upon the same input parameters as the Arps hyperbolic model.

Additional research is needed to further classify and analyze the production potential of coalbed methane wells in the Qinshui Basin. As more coalbed methane development occurs in the region and more production data becomes publically available, the discussed models can be further calibrated and analyzed. The presented work serves as a baseline study for entities with interest in developing the methane-bearing coals of the Qinshui Basin. Despite anticipated low

permeability values, modeling concludes strong potential exists for sustained, economic coalbed methane production in the region.

Appendix A:

Pinnacle Well Production Data

Well No.	1	2	3	4	5	6	7	8	9	10
In Seam Drilling Length (ft)	17474	9916	16820	11511	27149	13346	26788	15232	27224	14604
Average P3 Seam Thickness (ft)	5.1	5.1	4.8	5.2	5	5.3	5.3	5.4	4.6	5.3
Average Drainage Area (acres)	277.6	155.7	263.6	162.5	381	177	345.9	195.2	344.9	173.6
Drilling Density (ft/acre)	62.9	63.7	63.8	70.8	71.3	75.4	77.4	78	78.9	84.1
Month	Production Rate (mcf/month)									
1	3885	1427	354	8252	21038	993	2470	1050	0	4679
2	32066	5384	63338	36154	12408	13129	10908	14340	0	51004
3	37146	14000	63507	33407	9058	31699	22018	46246	28637	56328
4	40173	18474	64635	35833	9049	28981	32262	39801	28301	57310
5	35071	16305	63310	32778	33765	31725	25568	36848	25677	42909
6	34814	15308	60860	30886	32201	31574	26096	32996	27164	35827
7	30800	14118	54025	20027	26914	30173	26050	25938	23347	30976
8	27697	14775	48605	23862	25637	21263	28172	22232	18962	23889
9	26338	13484	41446	19565	21556	16687	26279	17808	21822	23424
10	22237	12718	33123	17877	21879	13992	23269	15896	21135	19086
11	20957	12257	31225	15228	20237	9709	17323	11687	19037	16116
12	18808	10457	26323	13314	17756	7839	18447	6411	15314	14664
13	15645	9467	25724	13328	19008	6201	21518	7520	15485	13732
14	16422	8420	22498	12941	16660	6802	17805	9000	14360	12249
15	14274	6999	23277	12959	21065	6522	17243	7694	13378	11730
16	13651	7244	21252	11529	12022	6292	9082	6793	13572	11287
17	12391	6709	19298	10742	12614	5876	17993	6138	12081	9775
18	11819	6673	19441	10864	14090	5789	16412	5318	15912	9625
19	10025	5945	16728	9817	11199	4970	12882	4474	12946	9472
20	8012	5774	19047	11146	13009	4584	15867	5355	10999	8876
21	7971	5375	13630	9587	12081	4443	7559	4030	12406	11453
22	7439	4758	13967	12064	11697	4333	11127	2897	11031	10287
23	7498	4496	14808	10880	11251	4390	9595	4308	13095	13014
24	7566	4302	10828	10957	10093	4765	10837	3214	12678	12370
25	6975	4289	13797	6443	9121	4592	11958	3659	12866	13403
26	7507	4219	12802	10009	7875	5108	12278	2596	12562	8219
27	7336	3484	12175	10115	7273	5065	10862	2398	11500	12523
28	5185	3567	11681	8064	7176	4235	7402	1928	12247	12639
29	7577	3413	10474	9291	6540	5335	5293	2094	11004	10417
30	7058	2141	11066	6591	5943	5104	6769	1289	10334	11589
31	3575	2469	10121	5590	5496	3069	8241	1613	10561	8935
32	1487	2301	10161	5380	5886	1468	10137	1627	9501	7480
33	2849	1699	9556	5238	5306	2706	8486	1558	8056	7666
34	8495	747	9461	5404	5522	6746	5445	1711	7988	6780
35	9754	1289	9472	4847	5347	8456	5771	1537	8013	6802
36	7621	2060	8423	3970	6229	6658	2638	1201	7477	6267
37	5631	1490	9116	4463	6042	5123	2887	1484	8087	5665
38	6747	3196	7752	2480	5572	6248	1343	1221	7835	6288
39	4765	3948	8166	2727	7726	4755	2054	433	7189	11401
40	6341	4804	7890	2216	6913	5879	495	200	6295	5128
41	6265	3493	7252	1863	6188	5397	703	100	6557	5581
42	6295	4388	7796	2071	6958	5345	1539		6425	7561
43	5825	4141	7309	1906	6197	5326	403		6090	3572
44	5232	4021			6116	4878	2321		6283	
45	5588	3934			5314	5172	2847		7137	
46	4274	3553			5286	4973	4230		6416	
47	4382	3927			5208	4852	2173		7291	
48	4851	3919			5219	4921	3413		6372	
49	4250	3719			4232	4708	4726		6825	
50	4694	3779			3931	4874	4423		6740	
51	4447	3688			4070	4572	3383		6244	
52	4539	3872			3971	4731	1831		5650	
53	4012	3495			3527	4453	1060		5528	
54	3566	3403			3262	4426	594		3918	
55	3371	2811			3333	4126	673		4655	
56	3654	3258			2830	3845	0		4743	
57	3759	2961			2566	4055	1494		3609	
58	3731	2976			2617	3892	2250		5111	
59	3393	3286			2940	3839	1559		4946	
60	3258	3075			2932	3687	1111		4544	
61	2623	2847			1891	3313	1250		5000	
62	2725	2724			1597	3377	791		5083	
63	3078	2615			1412	3454	2505		5207	
64	3547	2434				3733	2373		5113	
65	2923	2664				3393	810		4863	
66	3458	2921				3394			6473	
67	3572	2385				3596				
68	3475	2533				3368				
69	3612	2814				3278				
70	2539	2485				2957				
71	2907	2625				2858				
72	2026	3161				2104				
73	2648	2710				2898				
74	2680	2158				2666				
75	3184	2069				2514				
76	3402	2361				2423				
77	3136	1738				2218				
78	2395	2607				2103				
79	1977	2060				2211				
80	2714	1782				2258				
81	3745	1639				2161				
82	2691	2073				1929				
83	3785	2963				2066				
84		2729								
85		2686								

Well No.	11	12	13	14	15	16	17	18	19	20
In Seam Drilling Length (ft)	16974	13857	18648	15730	16185	14921	16741	13565	17633	24089
Average P3 Seam Thickness (ft)	4.9	4.8	4.7	4.5	4.9	5	5.2	4.7	4.4	4.7
Average Drainage Area (acres)	201	163.3	216.9	181.1	185.7	169	174.5	137.6	165.1	225.3
Drilling Density (ft/acre)	84.4	84.9	86	86.8	87.2	88.3	95.9	98.6	106.8	106.9
Month	Production Rate (mcf/month)									
1	1577	10398	17369	4722	1571	46999	0	3909	7361	9660
2	38381	38358	85454	32698	9515	47946	0	21564	68447	56297
3	40056	38337	110604	54159	46011	47271	32082	22973	67846	70428
4	36629	37165	95138	66355	68730	48746	26071	21605	58109	76487
5	37591	43359	81351	55901	54577	39051	23500	16685	53291	67944
6	20424	38713	57413	49154	71914	32152	19660	14886	50261	64192
7	27100	31193	51872	39756	65735	28543	17238	14284	48475	55126
8	2363	25774	40956	34622	51368	22413	14408	12280	39998	53937
9	967	22784	34075	28916	44410	19702	12591	12428	41869	45499
10	13338	20499	23725	22733	42255	13664	11491	9394	30328	42064
11	12371	19371	22666	16312	37325	17586	9383	8893	23577	40062
12	10211	16922	20764	14969	28017	13980	7969	6933	26819	37605
13	6719	15405	18269	15466	23764	12805	4428	6976	21977	37428
14	10008	14113	17940	14655	19712	11780	3368	6579	17115	33606
15	9934	13122	16156	12250	14953	10628	4033	6353	14485	30969
16	9250	12349	15849	12986	17141	10006	2978	5194	13527	28311
17	9682	10110	14801	11770	14109	8584	3042	4974	11749	22624
18	8615	9887	12420	11216	13034	9358	1986	5015	11286	23061
19	9131	8985	12632	9820	11251	8616	1533	4500	9876	20671
20	8622	7848	11640	9613	8959	7397	1762	4654	8814	19011
21	8327	7640	11349	8416	9713	7455	2158	3931	9036	19531
22	8041	6174	9015	4926	9102	7087	1935	3664	8457	17234
23	7544	7000	8543	4651	9017	8050	1317	3697	8052	15206
24	6916	6075	8066	4238	6216	7781	1757	3042	6170	13635
25	5478	5949	7693	3887	4433	7999	456	3598	5639	14086
26	5240	3852	8004	4370	3986	4792	950	3363	4983	12640
27	5268	5978	7715	3969	4924	7704	1326	3431	4834	11266
28	5396	6092	7833	4683	6192	8019	1596	3310	4890	10318
29	3086	4812	7766	3965	7430	6648	1835	3280	5093	9440
30	5044	5572	6877	4177	8288	6425	1181	3025	5274	10146
31	5962	3565	7086	3613	8529	5753	1181	2244	5803	8778
32	5481	2969	6647	3037	7782	4899	743	2212	5134	8310
33	5528	2351	7088	2170	8796	4809	848	1976	5404	6982
34	3604	2465	6006	2935	7976	4367	1162	1884	5045	6776
35	5609	2378	6305	2805	8484	4140	493	1431	5716	6486
36	5853	2295	6275	2848	7389	2785	231	1312	5179	6555
37	5120	1909	5451	3323	7880	2836	244	1405	6171	5856
38	6549	1899	4915	2354	7445	4429	172	1495	5879	4930
39	4744	1606	4671	2244	6727	3189		2026	5463	4717
40	4115	1826	5407	2253	6999	5140		1426	5989	4931
41	4396	1633	4769	1334	6139	3712		1866	5448	4274
42	4065	1672	3986	728	7658	3409		1500	6830	4414
43	3971	1755	4735	1964	6520	3439		659	5737	3667
44										3046
45										3235
46										3373
47										2220
48										2962
49										2872
50										2155
51										3310
52										2778
53										1472
54										2619
55										2634
56										2152
57										1768
58										2813
59										2741
60										1981
61										2001
62										51
63										
64										
65										
66										
67										
68										
69										
70										
71										
72										
73										
74										
75										
76										
77										
78										
79										
80										
81										
82										
83										
84										
85										

Well No.	21	22	23	24	25	26	27	28	29	30
In Seam Drilling Length (ft)	18800	15496	15885	21885	17248	19864	16778	16699	14215	21948
Average P3 Seam Thickness (ft)	4.7	4.4	5.1	4.4	4.7	4.7	4.8	4.1	3.9	4.6
Average Drainage Area (acres)	175.3	141.8	143.1	196.1	144.4	164.2	137.8	135.8	115.3	177.6
Drilling Density (ft/acre)	107.3	109.3	111	111.6	119.5	120.9	121.8	123	123.3	123.6
Month	Production Rate (mcf/month)									
1	7171	4321	422	7830	6490	8390	27634	9747	1169	1374
2	34860	33309	19235	8369	20285	34066	38679	23645	31642	45633
3	41267	42698	66639	9025	21805	38683	37368	27592	32046	63435
4	30606	39337	65434	9347	23513	37066	36003	24897	24819	58473
5	34521	23800	54803	9287	21720	31328	29222	22369	17278	41028
6	30409	23462	49517	8142	17234	28973	24492	17463	18958	39239
7	25720	20345	45636	7615	16209	19102	18132	16917	22111	31012
8	25203	14721	46047	7342	10669	17598	16910	13494	17033	26044
9	15824	12368	37934	6413	10233	16833	13936	10576	14311	16186
10	15651	9431	39042	5489	8707	13563	12256	10363	12383	10963
11	14047	7977	32362	4830	8849	11577	11344	8455	9078	8413
12	14022	8242	28184	5404	8306	11495	11000	7268	7835	8725
13	13743	8433	23381	4960	6667	11373	10044	6004	6832	8054
14	13808	9483	21914	4703	4473	7420	8895	5674	6184	7005
15	14051	9644	18722	4923	4139	11265	8244	5154	5246	7698
16	13619	10790	17242	4574	4103	9296	6549	4048	4494	7447
17	13165	10502	16668	4488	4238	6765	6462	4102	3381	5820
18	11758	10013	14572	4074	3860	5953	5435	2985	3513	5003
19	9708	8662	14236	3660	3485	5821	5104	2987	3381	4029
20	9887	8599	12030	3120	3084	5331	2848	2959	4316	3843
21	9192	7997	10465	2842	3565	4707	4252	2408	3513	3357
22	9513	6870	10984	2797	3042	4017	4207	2282	2674	3230
23	9269	5208	9836	2277	2822	4458	3367	2009	2256	2680
24	9124	4719	9738	1889	2656	3788	3011	406	2059	1159
25	8600	5271	5917	1747	2518	3851	3209		1137	2517
26	7441	4768	2806	1952	2252	2860	2280		1402	1877
27	7327	4248	2694	1812	2135	2530	2558		1261	4049
28	6693	4583	3522	1722	2086	2547	1091		75	3752
29	6126	4126	4675	1820	1391	2583	2213			3340
30	6056	4147	6614	1628	1393	2243	2253			3505
31	5976	3731	7952	1443	566	2468	2034			2779
32	5944	3470	8281	931	858	2866	2486			2521
33	5153	3032	7286	1713	1531	2097	2399			1748
34	5590	2721	6838	1474	1355	1821	2419			2290
35	4950	2559	7035	686	1425	972	787			1798
36	5112	2082	7597	2256	1141	1819				2000
37	4749	1567	6702	565	1476	1790				1318
38	4670	1788	7585		1198	1153				1684
39	4560	1400	6722		1130	811				1335
40	3757	1745	6009		820	894				1209
41	3995	1437	5887	1374		1442				1035
42	4152	1324	5073	1448	471	1350				714
43	3215	772	4937	1723	838	1168				1013
44	3233									
45	3349									
46	3570									
47	3448									
48	3608									
49	2156									
50	3455									
51	2769									
52	1225									
53	3656									
54	2243									
55	1956									
56	3404									
57	1585									
58	1413									
59										
60										
61										
62										
63										
64										
65										
66										
67										
68										
69										
70										
71										
72										
73										
74										
75										
76										
77										
78										
79										
80										
81										
82										
83										
84										
85										

Well No.	31	32	33	34	35	36	37	38	39	40
In Seam Drilling Length (ft)	15652	16631	13575	16346	17673	14648	15552	15256	23645	15398
Average P3 Seam Thickness (ft)	4.4	5	4.3	4.2	4.2	4.3	4.5	4.6	4.8	4.3
Average Drainage Area (acres)	126.4	132.9	106.5	127.3	135.4	111.3	117.3	114.6	172.6	112.2
Drilling Density (ft/acre)	123.8	125.1	127.5	128.4	130.5	131.6	132.5	133.1	137	137.2
Month	Production Rate (mcf/month)									
1	10484	22964	4984	13986	2418	28087	4266	416	3234	21586
2	30972	32874	27655	27387	37249	39774	32470	38072	24752	33301
3	32918	33519	32957	30860	5871	37857	32082	45758	32105	29738
4	34139	27306	32016	28006	8421	31897	24913	41357	31511	30444
5	29320	22662	27825	23744	22003	19131	19954	32952	27715	26892
6	23151	17827	21240	19188	61419	22517	12465	27310	24259	22306
7	17776	15919	18062	15794	53947	16320	11362	20104	15888	18372
8	8015	13890	16308	13698	34808	13090	9495	7530	15291	15245
9	4628	11754	13164	11093	17517	8839	7979	4748	13007	13832
10	13161	9937	11666	9918	14058	8517	4031	4414	11746	10677
11	8775	8249	9607	7714	28356	7297	5332	4387	11026	8827
12	7141	8191	8112	7408	42051	5777	4148	4162	10815	7672
13	4185	7310	7218	6936	36660	4999	2166	3876	9951	6300
14	3464	6322	5753	5276	32299	2551	1934	3482	8504	5033
15	2519	5227	4360	4852	24770	3016	2018	3604	8989	3563
16	2509	5059	2669	4407	23224	3217	1610	3078	7015	4350
17	2206	3712	2134	4004	21640	2323	1377	2626	4482	3873
18	1904	3524	2749	3570	17276	2303	1646	2812	4442	2843
19	2063	3822	2472	3314	13986	2139	841	2448	4288	1289
20	2167	3574	2485	2828	15356	1416	1755	2089	4229	
21	2001	3093	2454	2860	15135	1605	2171	2163	3206	1630
22	2219	2692	2278	2438	13489	1510	1212	2142	3118	1711
23	1677	3045	2067	2497	11466	1089	1316	1921	3425	1097
24	696	2957	2002	2301	9015	817	799	5943	3071	959
25	899	2552	1743	2204	8584	467		1627	3226	912
26	320	1778	1400	2354	9205				2612	204
27		2018	1191	2209	7596				1838	
28		1786	901	1737	8655				2260	
29		1749	434		8943				1686	
30		1357	243		7870				1985	
31		1214			7745				2205	
32					6950				640	
33					6660				1720	
34					6117				1369	
35					5966				1490	
36					6478				1385	
37					5911				1371	
38					5970				911	
39					6453				902	
40					5797				1169	
41					5786				969	
42					5266				1128	
43					6588				613	
44										
45										
46										
47										
48										
49										
50										
51										
52										
53										
54										
55										
56										
57										
58										
59										
60										
61										
62										
63										
64										
65										
66										
67										
68										
69										
70										
71										
72										
73										
74										
75										
76										
77										
78										
79										
80										
81										
82										
83										
84										
85										

Well No.	41	42	43	44	45	46	47	48	49	50
In Seam Drilling Length (ft)	24555	16396	9070	14162	14473	16237	19143	19158	15400	16518
Average P3 Seam Thickness (ft)	5.1	4.6	4.2	4.2	4.3	4.1	4	4.2	4.3	4.3
Average Drainage Area (acres)	178.4	118.8	65.5	102.1	103.8	115.7	136.4	135.8	105.8	104.2
Drilling Density (ft/acre)	137.7	138	138.4	138.8	139.4	140.3	140.3	141	145.6	158.5
Month	Production Rate (mcf/month)									
1	2949	4070	15386	3820	7694	8730	20345	18624	17480	15683
2	22871	25515	12101	30666	27172	32256	39030	30725	34716	27285
3	25248	31426	18877	28933	28361	33859	34920	25898	33170	32287
4	29574	31405	11868	26167	26927	33289	33616	22165	22696	24284
5	30209	27583	6613	23071	20676	23584	27467	18351	16059	19228
6	28990	27892	3939	19324	18255	22089	22987	14846	15535	14915
7	25716	22726	3909	13899	14892	15949	20004	13924	13132	11263
8	23942	19341	3368	12926	12475	12212	17259	11982	10399	12571
9	21409	15512	2878	10218	9978	7793	14706	9033	8133	10604
10	17731	13015	2935	8603	8959	6329	12030	7710	7429	10264
11	16751	11511	1779	6911	8068	5785	10444	6560	5397	8312
12	13009	10034		6438	6757	4644	8134	6763	3146	7758
13	13060	9005		5730	6357	4032	7628	4877	2691	6789
14	10680	7547		4551	5083	3272	6171		2349	5650
15	10185	5764		4238	4673	2987	5450		1464	5067
16	9089	4802		2961	4038	1341	5372			4600
17	8912	4274		2399	3114	1290	4828			4156
18	8310	3247		2187	2826	1166	4181			3536
19	7241	2092		1665	3307	1071	4532			3251
20	6944	3657		1123	2969	1013	4480			1290
21	6005	2289		1435	2997	976	4160			2178
22	5225	2845		946	2732	1023	2655			1959
23	5532	3048		731	2293	738	2747			647
24	5167			576	2443	109	3036			1809
25	5439			829	2429		2760			1133
26	4171			210	2299		3017			
27	4014			223	2343		2294			
28	3827				2082		2682			
29	3700				1839		2667			
30	3367				2127		2370			
31	3199				1850		2343			
32	3320				1899		2279			
33	2680				1893					
34	2971				1832					
35	2797				1460					
36	2558				1297					
37	2580				772					
38	2234									
39	2349									
40	2347									
41	2443									
42	1628									
43	571									
44										
45										
46										
47										
48										
49										
50										
51										
52										
53										
54										
55										
56										
57										
58										
59										
60										
61										
62										
63										
64										
65										
66										
67										
68										
69										
70										
71										
72										
73										
74										
75										
76										
77										
78										
79										
80										
81										
82										
83										
84										
85										

Well No.	1	2	3	4	5	6	7	8	9	10
In Seam Drilling Length (ft)	17474	9916	16820	11511	27149	13346	26788	15232	27224	14604
Average P3 Seam Thickness (ft)	5.1	5.1	4.8	5.2	5	5.3	5.3	5.4	4.6	5.3
Average Drainage Area (acres)	277.6	155.7	263.6	162.5	381	177	345.9	195.2	344.9	173.6
Drilling Density (ft/acre)	62.9	63.7	63.8	70.8	71.3	75.4	77.4	78	78.9	84.1
Month	Adjusted Production Rate (mcf/month)/(acre*ft)									
1	2.73	1.81	0.28	9.82	11.14	1.05	1.35	1	0	5.11
2	22.53	6.83	50.44	43.02	6.57	13.91	5.97	13.62	0	55.72
3	26.1	17.76	50.57	39.75	4.8	33.58	12.05	43.92	17.94	61.54
4	28.23	23.44	51.47	42.63	4.79	30.7	17.66	37.8	17.73	62.61
5	24.64	20.69	50.41	39	17.87	33.6	13.99	35	16.08	46.88
6	24.46	19.42	48.46	36.75	17.05	33.44	14.28	31.34	17.01	39.14
7	21.64	17.91	43.02	23.83	14.25	31.96	14.26	24.63	14.62	33.84
8	19.46	18.75	38.7	28.39	13.57	22.52	15.42	21.11	11.88	26.1
9	18.51	17.11	33	23.28	11.41	17.68	14.38	16.91	13.67	25.59
10	15.63	16.14	26.38	21.27	11.58	14.82	12.73	15.1	13.24	20.85
11	14.73	15.55	24.86	18.12	10.71	10.28	9.48	11.1	11.92	17.61
12	13.22	13.27	20.96	15.84	9.4	8.3	10.09	6.09	9.59	16.02
13	10.99	12.01	20.48	15.86	10.06	6.57	11.78	7.14	9.7	15
14	11.54	10.68	17.91	15.4	8.82	7.21	9.74	8.55	8.99	13.38
15	10.03	8.88	18.54	15.42	11.15	6.91	9.44	7.31	8.38	12.81
16	9.59	9.19	16.92	13.72	6.36	6.66	4.97	6.45	8.5	12.33
17	8.71	8.51	15.37	12.78	6.68	6.22	9.85	5.83	7.57	10.68
18	8.31	8.47	15.48	12.93	7.46	6.13	8.98	5.05	9.97	10.51
19	7.04	7.54	13.32	11.68	5.93	5.26	7.05	4.25	8.11	10.35
20	5.63	7.33	15.17	13.26	6.89	4.86	8.68	5.09	6.89	9.7
21	5.6	6.82	10.85	11.41	6.4	4.71	4.14	3.83	7.77	12.51
22	5.23	6.04	11.12	14.35	6.19	4.59	6.09	2.75	6.91	11.24
23	5.27	5.7	11.79	12.94	5.96	4.65	5.25	4.09	8.2	14.22
24	5.32	5.46	8.62	13.04	5.34	5.05	5.93	3.05	7.94	13.51
25	4.9	5.44	10.99	7.67	4.83	4.86	6.54	3.48	8.06	14.64
26	5.28	5.35	10.19	11.91	4.17	5.41	6.72	2.47	7.87	8.98
27	5.16	4.42	9.69	12.03	3.85	5.37	5.94	2.28	7.2	13.68
28	3.64	4.53	9.3	9.59	3.8	4.49	4.05	1.83	7.67	13.81
29	5.32	4.33	8.34	11.05	3.46	5.65	2.9	1.99	6.89	11.38
30	4.96	2.72	8.81	7.84	3.15	5.41	3.7	1.22	6.47	12.66
31	2.51	3.13	8.06	6.65	2.91	3.25	4.51	1.53	6.61	9.76
32	1.04	2.92	8.09	6.4	3.12	1.55	5.55	1.55	5.95	8.17
33	2	2.16	7.61	6.23	2.81	2.87	4.64	1.48	5.05	8.37
34	5.97	0.95	7.53	6.43	2.92	7.15	2.98	1.63	5	7.41
35	6.85	1.64	7.54	5.77	2.83	8.96	3.16	1.46	5.02	7.43
36	5.36	2.61	6.71	4.72	3.3	7.05	1.44	1.14	4.68	6.85
37	3.96	1.89	7.26	5.31	3.2	5.43	1.58	1.41	5.07	6.19
38	4.74	4.06	6.17	2.95	2.95	6.62	0.73	1.16	4.91	6.87
39	3.35	5.01	6.5	3.24	4.09	5.04	1.12	0.41	4.5	12.46
40	4.46	6.1	6.28	2.64	3.66	6.23	0.27	0.19	3.94	5.6
41	4.4	4.43	5.77	2.22	3.28	5.72	0.38	0.09	4.11	6.1
42	4.42	5.57	6.21	2.46	3.68	5.66	0.84		4.02	8.26
43	4.09	5.25	5.82	2.27	3.28	5.64	0.22		3.81	3.9
44	3.68	5.1			3.24	5.17	1.27		3.94	
45	3.93	4.99			2.81	5.48	1.56		4.47	
46	3	4.51			2.8	5.27	2.31		4.02	
47	3.08	4.98			2.76	5.14	1.19		4.57	
48	3.41	4.97			2.76	5.21	1.87		3.99	
49	2.99	4.72			2.24	4.99	2.59		4.27	
50	3.3	4.79			2.08	5.16	2.42		4.22	
51	3.12	4.68			2.15	4.84	1.85		3.91	
52	3.19	4.91			2.1	5.01	1		3.54	
53	2.82	4.43			1.87	4.72	0.58		3.46	
54	2.51	4.32			1.73	4.69	0.33		2.45	
55	2.37	3.57			1.76	4.37	0.37		2.92	
56	2.57	4.13			1.5	4.07	0		2.97	
57	2.64	3.76			1.36	4.3	0.82		2.26	
58	2.62	3.78			1.39	4.12	1.23		3.2	
59	2.38	4.17			1.56	4.07	0.85		3.1	
60	2.29	3.9			1.55	3.91	0.61		2.85	
61	1.84	3.61			1	3.51	0.68		3.13	
62	1.91	3.46			0.85	3.58	0.43		3.18	
63	2.16	3.32			0.75	3.66	1.37		3.26	
64	2.49	3.09				3.95	1.3		3.2	
65	2.05	3.38				3.59	0.44		3.05	
66	2.43	3.71				3.6			4.05	
67	2.51	3.03				3.81				
68	2.44	3.21				3.57				
69	2.54	3.57				3.47				
70	1.78	3.15				3.13				
71	2.04	3.33				3.03				
72	1.42	4.01				2.23				
73	1.86	3.44				3.07				
74	1.88	2.74				2.82				
75	2.24	2.63				2.66				
76	2.39	3				2.57				
77	2.2	2.21				2.35				
78	1.68	3.31				2.23				
79	1.39	2.61				2.34				
80	1.91	2.26				2.39				
81	2.63	2.08				2.29				
82	1.89	2.63				2.04				
83	2.66	3.76				2.19				
84		3.46								
85		3.41								

Well No.	11	12	13	14	15	16	17	18	19	20
In Seam Drilling Length (ft)	16974	13857	18648	15730	16185	14921	16741	13565	17633	24089
Average P3 Seam Thickness (ft)	4.9	4.8	4.7	4.5	4.9	5	5.2	4.7	4.4	4.7
Average Drainage Area (acres)	201	163.3	216.9	181.1	185.7	169	174.5	137.6	165.1	225.3
Drilling Density (ft/acre)	84.4	84.9	86	86.8	87.2	88.3	95.9	98.6	106.8	106.9
Month	Adjusted Production Rate (mcf/month)/(acre*ft)									
1	1.59	13.26	11.28	5.79	1.01	55.9	0	6.06	5.53	5.44
2	38.72	48.92	55.48	40.08	6.11	57.03	0	33.45	51.44	31.7
3	40.41	48.9	71.81	66.39	29.56	56.22	35.1	35.64	50.98	39.66
4	36.95	47.4	61.77	81.34	44.15	57.98	28.52	33.51	43.67	43.07
5	37.93	55.3	52.82	68.52	35.06	46.45	25.71	25.88	40.05	38.26
6	20.61	49.38	37.28	60.25	46.2	38.24	21.51	23.09	37.77	36.15
7	27.34	39.79	33.68	48.73	42.23	33.95	18.86	22.16	36.43	31.04
8	2.38	32.87	26.59	42.44	33	26.66	15.76	19.05	30.06	30.37
9	0.98	29.06	22.12	35.44	28.53	23.43	13.78	19.28	31.46	25.62
10	13.46	26.15	15.4	27.87	27.14	16.25	12.57	14.57	22.79	23.69
11	12.48	24.71	14.72	19.99	23.98	20.92	10.27	13.79	17.72	22.56
12	10.3	21.58	13.48	18.35	18	16.63	8.72	10.75	20.15	21.18
13	6.78	19.65	11.86	18.96	15.27	15.23	4.84	10.82	16.51	21.08
14	10.1	18	11.65	17.96	12.66	14.01	3.69	10.21	12.86	18.92
15	10.02	16.74	10.49	15.02	9.61	12.64	4.41	9.85	10.88	17.44
16	9.33	15.75	10.29	15.92	11.01	11.9	3.26	8.06	10.17	15.94
17	9.77	12.9	9.61	14.43	9.06	10.21	3.33	7.72	8.83	12.74
18	8.69	12.61	8.06	13.75	8.37	11.13	2.17	7.78	8.48	12.99
19	9.21	11.46	8.2	12.04	7.23	10.25	1.68	6.98	7.42	11.64
20	8.7	10.01	7.56	11.78	5.75	8.8	1.93	7.22	6.62	10.71
21	8.4	9.74	7.37	10.32	6.24	8.87	2.36	6.1	6.79	11
22	8.11	7.87	5.85	6.04	5.85	8.43	2.12	5.68	6.36	9.71
23	7.61	8.93	5.55	5.7	5.79	9.57	1.44	5.73	6.05	8.56
24	6.98	7.75	5.24	5.19	3.99	9.25	1.92	4.72	4.64	7.68
25	5.53	7.59	4.99	4.76	2.85	9.51	0.5	5.58	4.24	7.93
26	5.29	4.91	5.2	5.36	2.56	5.7	1.04	5.22	3.74	7.12
27	5.31	7.62	5.01	4.87	3.16	9.16	1.45	5.32	3.63	6.34
28	5.44	7.77	5.09	5.74	3.98	9.54	1.75	5.13	3.67	5.81
29	3.11	6.14	5.04	4.86	4.77	7.91	2.01	5.09	3.83	5.32
30	5.09	7.11	4.47	5.12	5.32	7.64	1.29	4.69	3.96	5.71
31	6.02	4.55	4.6	4.43	5.48	6.84	1.29	3.48	4.36	4.94
32	5.53	3.79	4.32	3.72	5	5.83	0.81	3.43	3.86	4.68
33	5.58	3	4.6	2.66	5.65	5.72	0.93	3.07	4.06	3.93
34	3.64	3.14	3.9	3.6	5.12	5.19	1.27	2.92	3.79	3.82
35	5.66	3.03	4.09	3.44	5.45	4.92	0.54	2.22	4.3	3.65
36	5.91	2.93	4.07	3.49	4.75	3.31	0.25	2.04	3.89	3.69
37	5.17	2.43	3.54	4.07	5.06	3.37	0.27	2.18	4.64	3.3
38	6.61	2.42	3.19	2.89	4.78	5.27	0.19	2.32	4.42	2.78
39	4.79	2.05	3.03	2.75	4.32	3.79		3.14	4.11	2.66
40	4.15	2.33	3.51	2.76	4.5	6.11		2.21	4.5	2.78
41	4.44	2.08	3.1	1.64	3.94	4.42		2.89	4.09	2.41
42	4.1	2.13	2.59	0.89	4.92	4.05		2.33	5.13	2.49
43	4.01	2.24	3.07	2.41	4.19	4.09		1.02	4.31	2.07
44										1.72
45										1.82
46										1.9
47										1.25
48										1.67
49										1.62
50										1.21
51										1.86
52										1.56
53										0.83
54										1.47
55										1.48
56										1.21
57										1
58										1.58
59										1.54
60										1.12
61										1.13
62										0.03
63										
64										
65										
66										
67										
68										
69										
70										
71										
72										
73										
74										
75										
76										
77										
78										
79										
80										
81										
82										
83										
84										
85										

Well No.	21	22	23	24	25	26	27	28	29	30
In Seam Drilling Length (ft)	18800	15496	15885	21885	17248	19864	16778	16699	14215	21948
Average P3 Seam Thickness (ft)	4.7	4.4	5.1	4.4	4.7	4.7	4.8	4.1	3.9	4.6
Average Drainage Area (acres)	175.3	141.8	143.1	196.1	144.4	164.2	137.8	135.8	115.3	177.6
Drilling Density (ft/acre)	107.3	109.3	111	111.6	119.5	120.9	121.8	123	123.3	123.6
Month	Adjusted Production Rate (mcf/month)/(acre*ft)									
1	7.16	6.88	0.29	9.15	9.66	10.91	41.62	17.64	2.57	1.69
2	34.82	53.06	13.08	9.78	30.2	44.29	58.26	42.8	69.65	56.02
3	41.22	68.02	45.3	10.55	32.46	50.29	56.28	49.94	70.53	77.87
4	30.57	62.67	44.48	10.92	35	48.19	54.23	45.06	54.63	71.78
5	34.48	37.91	37.26	10.85	32.33	40.73	44.01	40.49	38.03	50.37
6	30.38	37.38	33.66	9.51	25.66	37.67	36.89	31.61	41.73	48.17
7	25.69	32.41	31.02	8.9	24.13	24.84	27.31	30.62	48.67	38.07
8	25.18	23.45	31.3	8.58	15.88	22.88	25.47	24.42	37.49	31.97
9	15.81	19.7	25.79	7.49	15.23	21.89	20.99	19.14	31.5	19.87
10	15.63	15.02	26.54	6.41	12.96	17.63	18.46	18.76	27.26	13.46
11	14.03	12.71	22	5.64	13.17	15.05	17.09	15.3	19.98	10.33
12	14.01	13.13	19.16	6.32	12.36	14.95	16.57	13.15	17.25	10.71
13	13.73	13.43	15.89	5.8	9.92	14.79	15.13	10.87	15.04	9.89
14	13.79	15.11	14.9	5.5	6.66	9.65	13.4	10.27	13.61	8.6
15	14.04	15.36	12.73	5.75	6.16	14.65	12.42	9.33	11.55	9.45
16	13.6	17.19	11.72	5.35	6.11	12.09	9.86	7.33	9.89	9.14
17	13.15	16.73	11.33	5.24	6.31	8.8	9.73	7.42	7.44	7.14
18	11.75	15.95	9.91	4.76	5.75	7.74	8.19	5.4	7.73	6.14
19	9.7	13.8	9.68	4.28	5.19	7.57	7.69	5.41	7.44	4.95
20	9.88	13.7	8.18	3.65	4.59	6.93	4.29	5.36	9.5	4.72
21	9.18	12.74	7.11	3.32	5.31	6.12	6.4	4.36	7.73	4.12
22	9.5	10.94	7.47	3.27	4.53	5.22	6.34	4.13	5.89	3.97
23	9.26	8.3	6.69	2.66	4.2	5.8	5.07	3.64	4.97	3.29
24	9.11	7.52	6.62	2.21	3.95	4.93	4.54	0.73	4.53	1.42
25	8.59	8.4	4.02	2.04	3.75	5.01	4.83		2.5	3.09
26	7.43	7.6	1.91	2.28	3.35	3.72	3.43		3.09	2.3
27	7.32	6.77	1.83	2.12	3.18	3.29	3.85		2.78	4.97
28	6.69	7.3	2.39	2.01	3.11	3.31	1.64		0.17	4.61
29	6.12	6.57	3.18	2.13	2.07	3.36	3.33			4.1
30	6.05	6.61	4.5	1.9	2.07	2.92	3.39			4.3
31	5.97	5.94	5.41	1.69	0.84	3.21	3.06			3.41
32	5.94	5.53	5.63	1.09	1.28	3.73	3.74			3.09
33	5.15	4.83	4.95	2	2.28	2.73	3.61			2.15
34	5.58	4.33	4.65	1.72	2.02	2.37	3.64			2.81
35	4.94	4.08	4.78	0.8	2.12	1.26	1.19			2.21
36	5.11	3.32	5.16	2.64	1.7	2.36				2.46
37	4.74	2.5	4.56	0.66	2.2	2.33				1.62
38	4.66	2.85	5.16		1.78	1.5				2.07
39	4.56	2.23	4.57		1.68	1.05				1.64
40	3.75	2.78	4.08		1.22	1.16				1.48
41	3.99	2.29	4	1.61		1.87				1.27
42	4.15	2.11	3.45	1.69	0.7	1.76				0.88
43	3.21	1.23	3.36	2.01	1.25	1.52				1.24
44	3.23									
45	3.35									
46	3.57									
47	3.44									
48	3.6									
49	2.15									
50	3.45									
51	2.77									
52	1.22									
53	3.65									
54	2.24									
55	1.95									
56	3.4									
57	1.58									
58	1.41									
59										
60										
61										
62										
63										
64										
65										
66										
67										
68										
69										
70										
71										
72										
73										
74										
75										
76										
77										
78										
79										
80										
81										
82										
83										
84										
85										

Well No.	31	32	33	34	35	36	37	38	39	40
In Seam Drilling Length (ft)	15652	16631	13575	16346	17673	14648	15552	15256	23645	15398
Average P3 Seam Thickness (ft)	4.4	5	4.3	4.2	4.2	4.3	4.5	4.6	4.8	4.3
Average Drainage Area (acres)	126.4	132.9	106.5	127.3	135.4	111.3	117.3	114.6	172.6	112.2
Drilling Density (ft/acre)	123.8	125.1	127.5	128.4	130.5	131.6	132.5	133.1	137	137.2
Month	Adjusted Production Rate (mcf/month)/(acre*ft)									
1	18.9	34.39	10.86	26.39	2.36	58.6	8.09	0.79	3.92	44.53
2	55.85	49.22	60.26	51.68	36.42	82.99	61.57	72.04	30.01	68.69
3	59.35	50.19	71.81	58.23	5.74	78.99	60.84	86.59	38.92	61.34
4	61.56	40.89	69.76	52.85	8.23	66.55	47.24	78.26	38.2	62.8
5	52.87	33.93	60.63	44.81	21.52	39.92	37.84	62.36	33.6	55.47
6	41.74	26.69	46.28	36.21	60.06	46.98	23.64	51.68	29.41	46.01
7	32.05	23.84	39.36	29.8	52.75	34.05	21.55	38.04	19.26	37.9
8	14.45	20.8	35.53	25.85	34.04	27.31	18.01	14.25	18.54	31.45
9	8.34	17.6	28.68	20.93	17.13	18.44	15.13	8.98	15.77	28.53
10	23.73	14.88	25.42	18.72	13.75	17.77	7.64	8.35	14.24	22.02
11	15.82	12.35	20.93	14.56	27.73	15.23	10.11	8.3	13.37	18.21
12	12.88	12.26	17.68	13.98	41.12	12.05	7.87	7.88	13.11	15.82
13	7.55	10.95	15.73	13.09	35.85	10.43	4.11	7.33	12.06	12.99
14	6.25	9.47	12.54	9.96	31.58	5.32	3.67	6.59	10.31	10.38
15	4.54	7.83	9.5	9.16	24.22	6.29	3.83	6.82	10.9	7.35
16	4.52	7.58	5.82	8.32	22.71	6.71	3.05	5.82	8.5	8.97
17	3.98	5.56	4.65	7.56	21.16	4.85	2.61	4.97	5.43	7.99
18	3.43	5.28	5.99	6.74	16.89	4.81	3.12	5.32	5.39	5.86
19	3.72	5.72	5.39	6.25	13.68	4.46	1.59	4.63	5.2	2.66
20	3.91	5.35	5.41	5.34	15.02	2.95	3.33	3.95	5.13	
21	3.61	4.63	5.35	5.4	14.8	3.35	4.12	4.09	3.89	3.36
22	4	4.03	4.96	4.6	13.19	3.15	2.3	4.05	3.78	3.53
23	3.02	4.56	4.5	4.71	11.21	2.27	2.5	3.64	4.15	2.26
24	1.25	4.43	4.36	4.34	8.82	1.7	1.52	11.25	3.72	1.98
25	1.62	3.82	3.8	4.16	8.39	0.97		3.08	3.91	1.88
26	0.58	2.66	3.05	4.44	9				3.17	0.42
27		3.02	2.6	4.17	7.43				2.23	
28		2.67	1.96	3.28	8.46				2.74	
29		2.62	0.95		8.74				2.04	
30		2.03	0.53		7.7				2.41	
31		1.82			7.57				2.67	
32					6.8				0.78	
33					6.51				2.09	
34					5.98				1.66	
35					5.83				1.81	
36					6.33				1.68	
37					5.78				1.66	
38					5.84				1.1	
39					6.31				1.09	
40					5.67				1.42	
41					5.66				1.17	
42					5.15				1.37	
43					6.44				0.74	
44										
45										
46										
47										
48										
49										
50										
51										
52										
53										
54										
55										
56										
57										
58										
59										
60										
61										
62										
63										
64										
65										
66										
67										
68										
69										
70										
71										
72										
73										
74										
75										
76										
77										
78										
79										
80										
81										
82										
83										
84										
85										

Well No.	41	42	43	44	45	46	47	48	49	50
In Seam Drilling Length (ft)	24555	16396	9070	14162	14473	16237	19143	19158	15400	16518
Average P3 Seam Thickness (ft)	5.1	4.6	4.2	4.2	4.3	4.1	4	4.2	4.3	4.3
Average Drainage Area (acres)	178.4	118.8	65.5	102.1	103.8	115.7	136.4	135.8	105.8	104.2
Drilling Density (ft/acre)	137.7	138	138.4	138.8	139.4	140.3	140.3	141	145.6	158.5
Month	Adjusted Production Rate (mcf/month)/(acre*ft)									
1	3.27	7.43	55.3	8.99	17.22	18.26	37.66	32.84	38.74	34.83
2	25.39	46.56	43.5	72.16	60.81	67.47	72.25	54.18	76.93	60.6
3	28.03	57.35	67.85	68.08	63.47	70.82	64.64	45.67	73.51	71.71
4	32.83	57.31	42.66	61.57	60.26	69.63	62.23	39.09	50.29	53.94
5	33.53	50.34	23.77	54.29	46.27	49.33	50.85	32.36	35.59	42.71
6	32.18	50.9	14.16	45.47	40.86	46.2	42.55	26.18	34.43	33.13
7	28.55	41.47	14.05	32.7	33.33	33.36	37.03	24.56	29.1	25.02
8	26.58	35.3	12.11	30.41	27.92	25.54	31.95	21.13	23.04	27.92
9	23.76	28.31	10.34	24.04	22.33	16.3	27.22	15.93	18.02	23.55
10	19.68	23.75	10.55	20.24	20.05	13.24	22.27	13.6	16.46	22.8
11	18.59	21.01	6.39	16.26	18.06	12.1	19.33	11.57	11.96	18.46
12	14.44	18.31		15.15	15.12	9.71	15.06	11.93	6.97	17.23
13	14.5	16.43		13.48	14.23	8.43	14.12	8.6	5.96	15.08
14	11.86	13.77		10.71	11.38	6.84	11.42		5.21	12.55
15	11.31	10.52		9.97	10.46	6.25	10.09		3.24	11.25
16	10.09	8.76		6.97	9.04	2.8	9.94			10.22
17	9.89	7.8		5.64	6.97	2.7	8.94			9.23
18	9.22	5.93		5.15	6.32	2.44	7.74			7.85
19	8.04	3.82		3.92	7.4	2.24	8.39			7.22
20	7.71	6.67		2.64	6.64	2.12	8.29			2.87
21	6.67	4.18		3.38	6.71	2.04	7.7			4.84
22	5.8	5.19		2.23	6.11	2.14	4.91			4.35
23	6.14	5.56		1.72	5.13	1.54	5.09			1.44
24	5.74			1.36	5.47	0.23	5.62			4.02
25	6.04			1.95	5.44		5.11			2.52
26	4.63			0.49	5.15		5.58			
27	4.46			0.52	5.24		4.25			
28	4.25				4.66		4.96			
29	4.11				4.12		4.94			
30	3.74				4.76		4.39			
31	3.55				4.14		4.34			
32	3.69				4.25		4.22			
33	2.97				4.24					
34	3.3				4.1					
35	3.1				3.27					
36	2.84				2.9					
37	2.86				1.73					
38	2.48									
39	2.61									
40	2.61									
41	2.71									
42	1.81									
43	0.63									
44										
45										
46										
47										
48										
49										
50										
51										
52										
53										
54										
55										
56										
57										
58										
59										
60										
61										
62										
63										
64										
65										
66										
67										
68										
69										
70										
71										
72										
73										
74										
75										
76										
77										
78										
79										
80										
81										
82										
83										
84										
85										

Appendix B:

Best Fit Curves for Pinnacle Wells and Error Charts

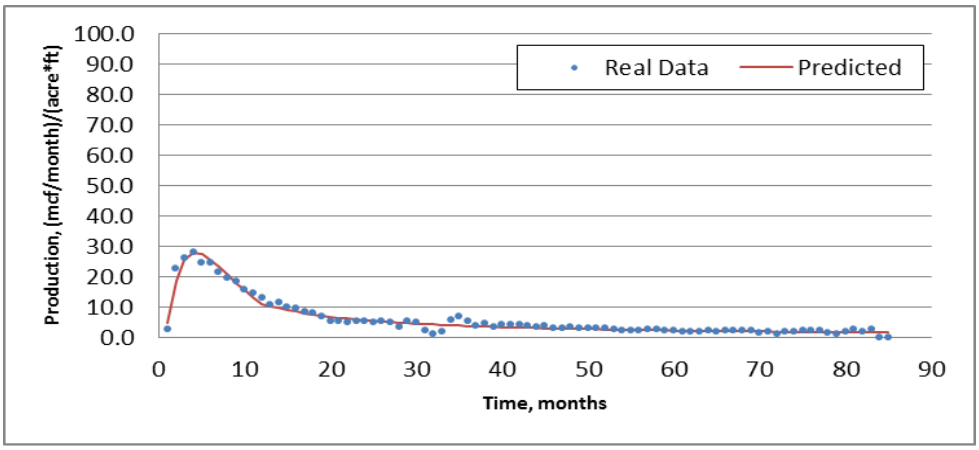

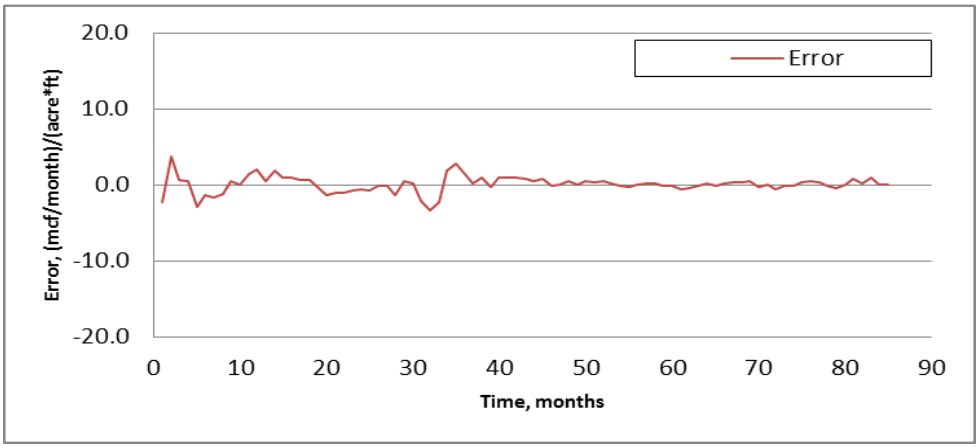

Well No.	1
Starting (Actual) Pmax (mcf/month)/(acre*ft)	28.2
Starting (Actual) Tp (months)	4
Starting di	0.5
Starting b	0.5
Best Fit Pmax (mcf/month)/(acre*ft)	27.89
Best Fit Tp (months)	4.33
Best Fit Di (1/month)	0.1937
Best Fit b	1
SSQ	98
R^2	0.97

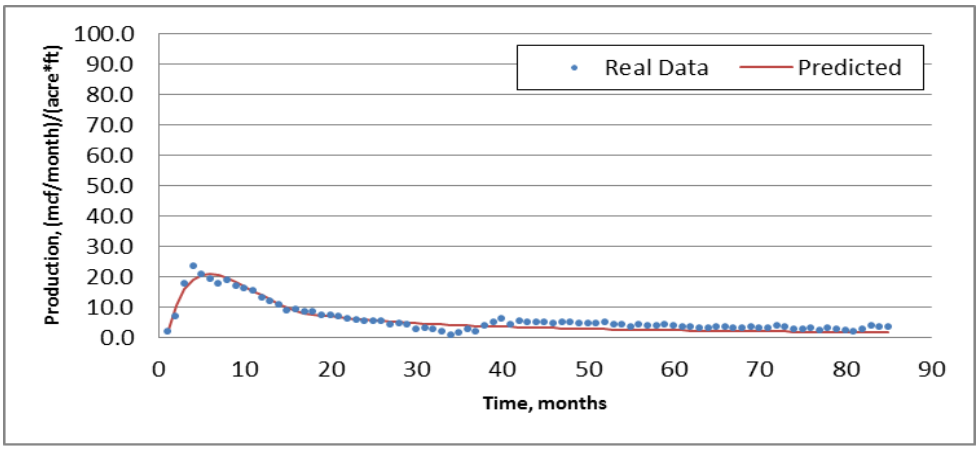

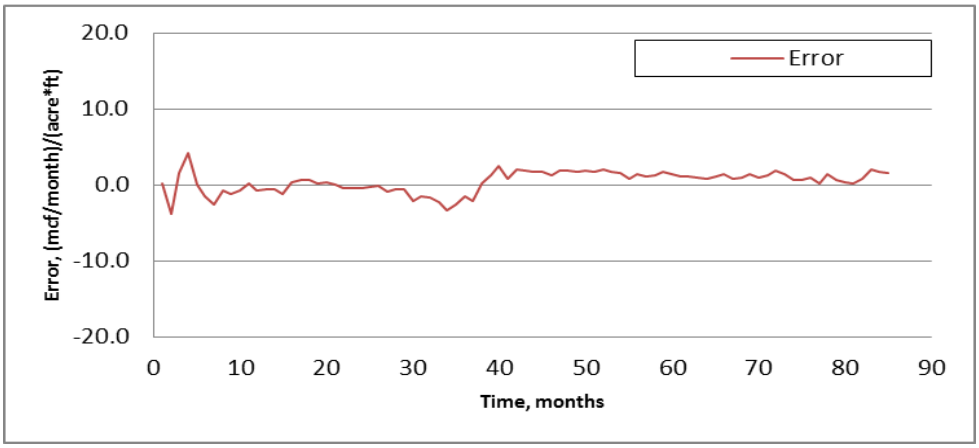

Well No.	2
Starting (Actual) Pmax (mcf/month)/(acre*ft)	23.4
Starting (Actual) Tp (months)	4
Starting di	0.5
Starting b	0.5
Best Fit Pmax (mcf/month)/(acre*ft)	20.98
Best Fit Tp (months)	5.81
Best Fit Di (1/month)	0.1401
Best Fit b	1
SSQ	187
R^2	0.93

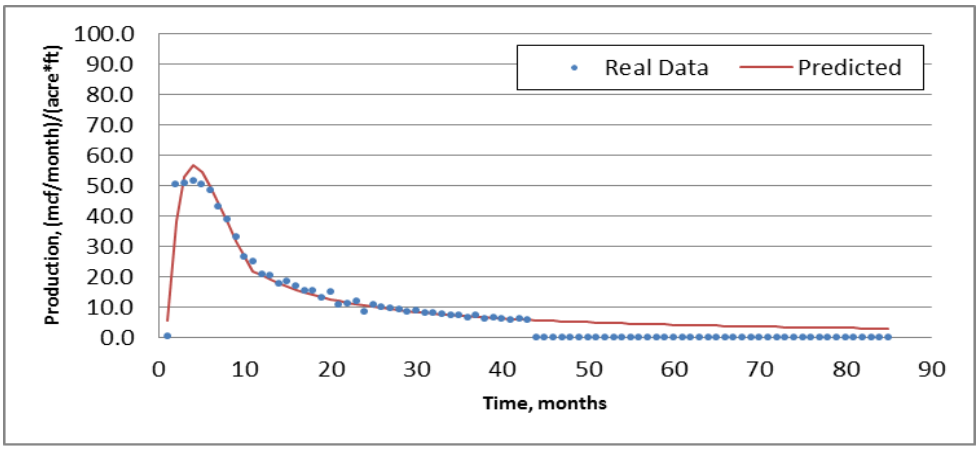

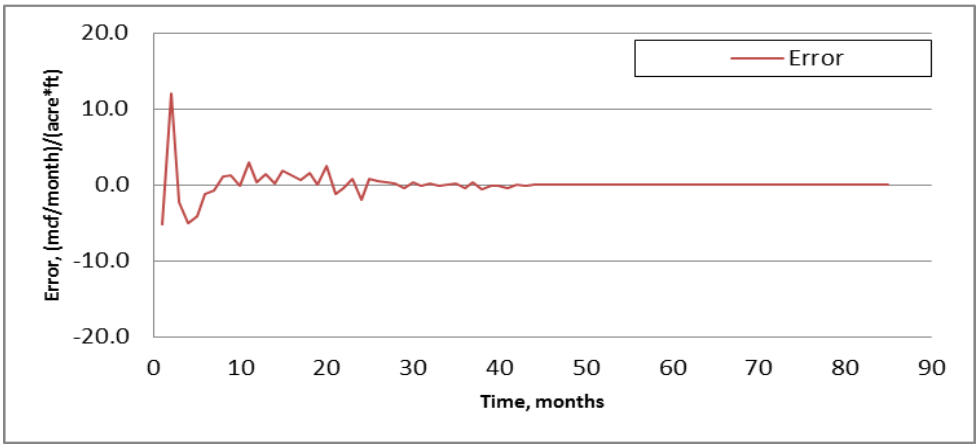

Well No.	3
Starting (Actual) Pmax (mcf/month)/(acre*ft)	51.5
Starting (Actual) Tp (months)	4
Starting di	0.5
Starting b	0.5
Best Fit Pmax (mcf/month)/(acre*ft)	56.53
Best Fit Tp (months)	4.05
Best Fit Di (1/month)	0.2192
Best Fit b	1
SSQ	258
R^2	0.97

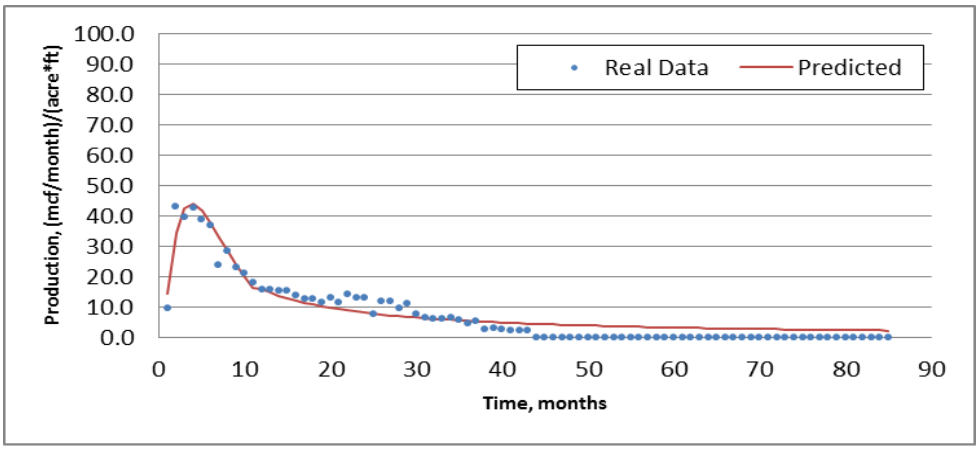

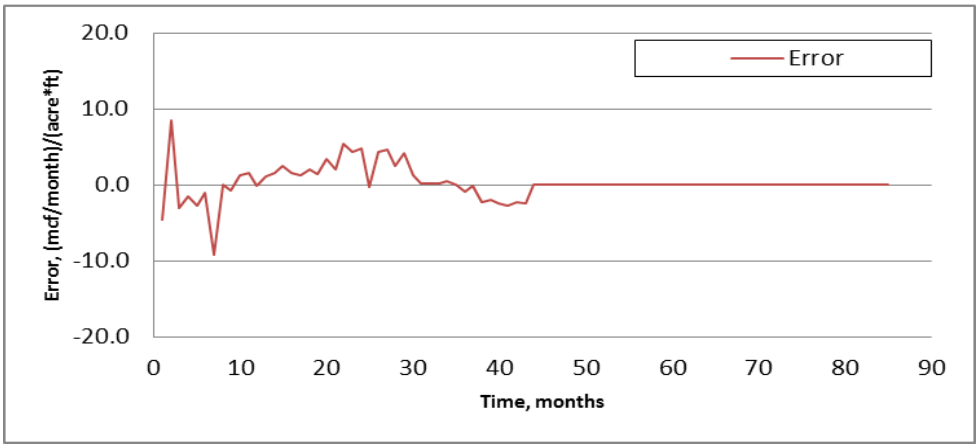

Well No.	4
Starting (Actual) Pmax (mcf/month)/(acre*ft)	43
Starting (Actual) Tp (months)	2
Starting di	0.5
Starting b	0.5
Best Fit Pmax (mcf/month)/(acre*ft)	44.14
Best Fit Tp (months)	3.77
Best Fit Di (1/month)	0.2161
Best Fit b	1
SSQ	410
R^2	0.93

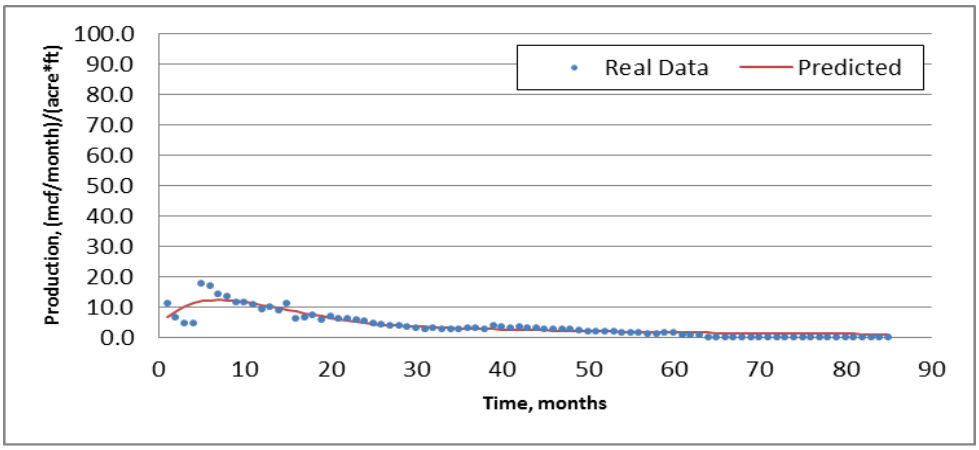

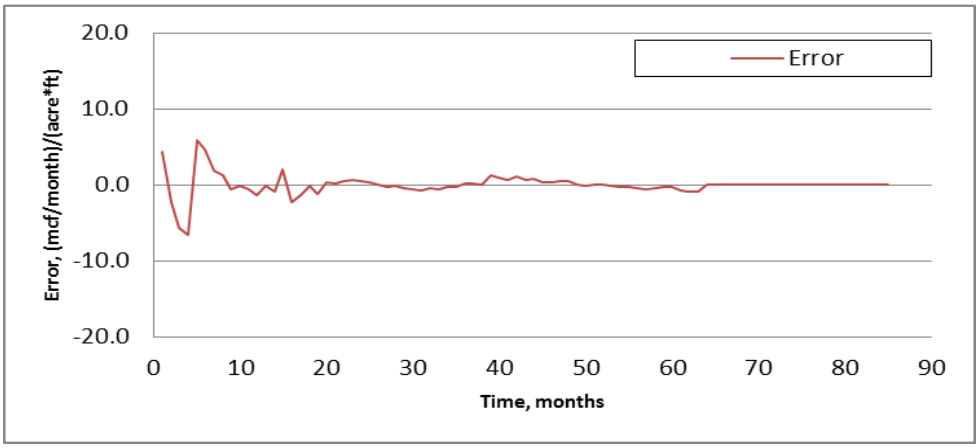

Well No.	5
Starting (Actual) Pmax (mcf/month)/(acre*ft)	17.9
Starting (Actual) Tp (months)	5
Starting di	0.5
Starting b	0.5
Best Fit Pmax (mcf/month)/(acre*ft)	12.39
Best Fit Tp (months)	6.86
Best Fit Di (1/month)	0.0881
Best Fit b	0.7928
SSQ	188
R^2	0.81

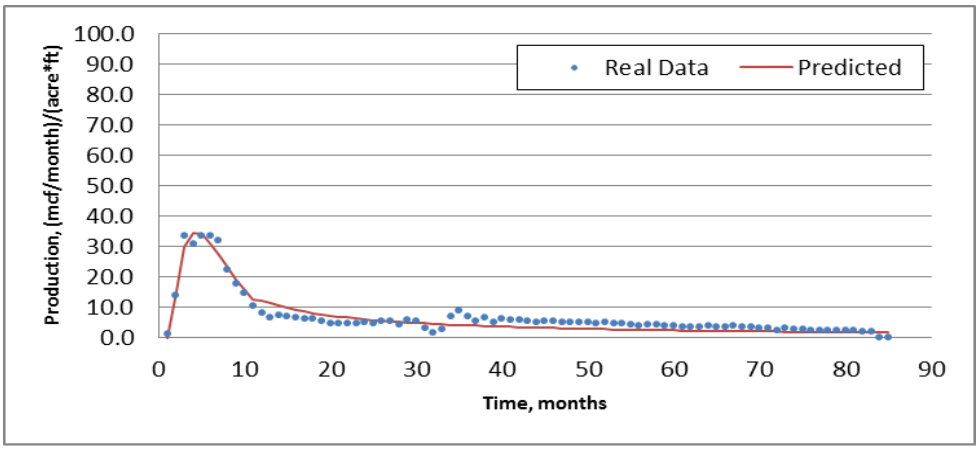

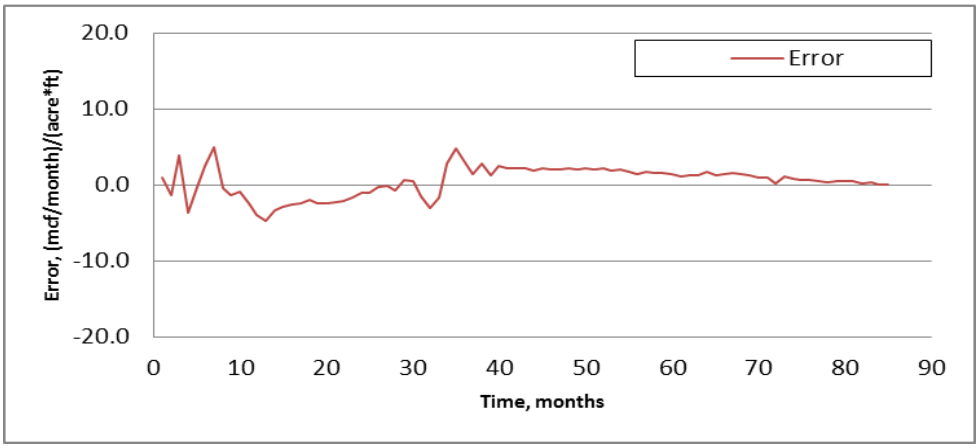

Well No.	6
Starting (Actual) Pmax (mcf/month)/(acre*ft)	33.6
Starting (Actual) Tp (months)	5
Starting di	0.5
Starting b	0.5
Best Fit Pmax (mcf/month)/(acre*ft)	34.59
Best Fit Tp (months)	4.34
Best Fit Di (1/month)	0.2385
Best Fit b	1
SSQ	345
R^2	0.93

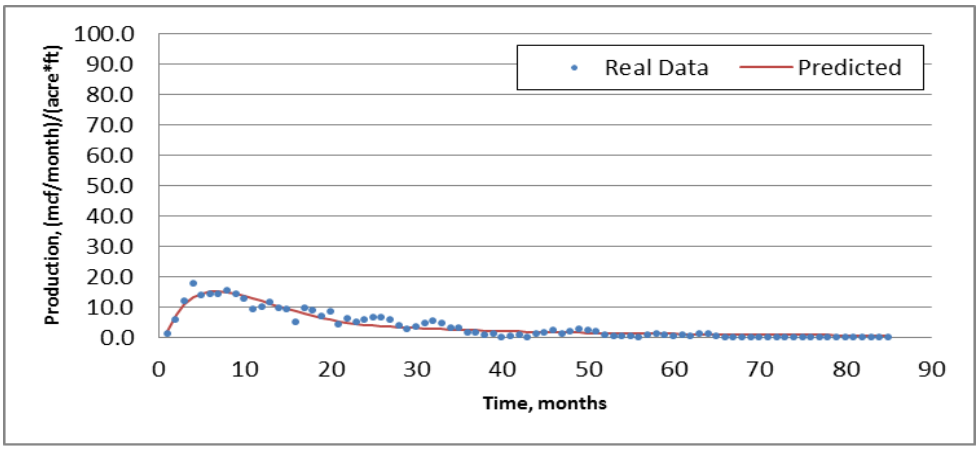

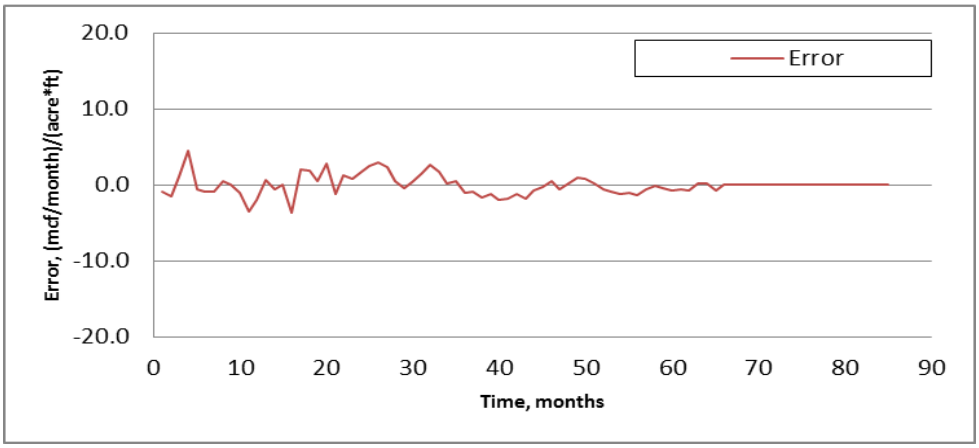

Well No.	7
Starting (Actual) Pmax (mcf/month)/(acre*ft)	17.7
Starting (Actual) Tp (months)	4
Starting di	0.5
Starting b	0.5
Best Fit Pmax (mcf/month)/(acre*ft)	15.2
Best Fit Tp (months)	6.69
Best Fit Di (1/month)	0.1152
Best Fit b	0.6379
SSQ	140
R^2	0.9

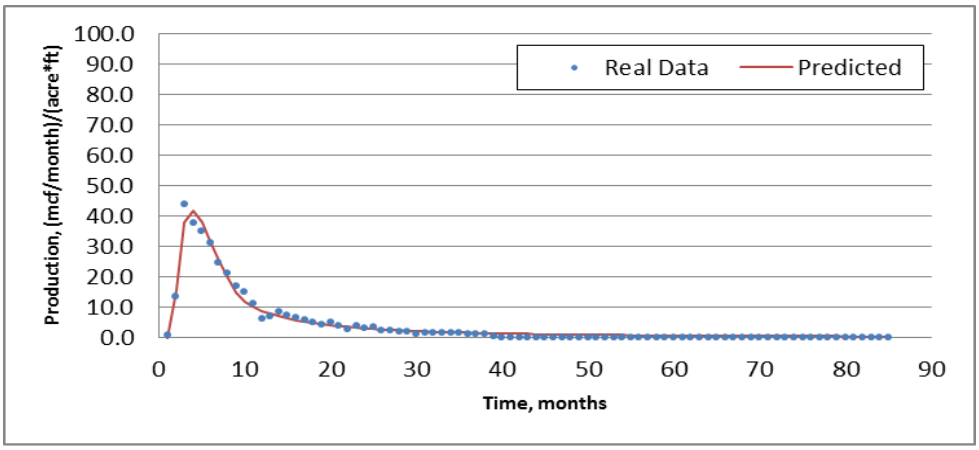

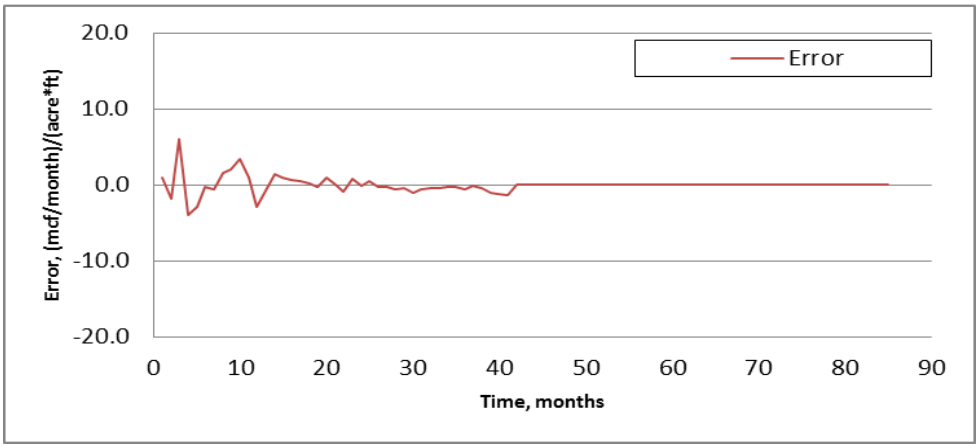

Well No.	8
Starting (Actual) Pmax (mcf/month)/(acre*ft)	43.9
Starting (Actual) Tp (months)	3
Starting di	0.5
Starting b	0.5
Best Fit Pmax (mcf/month)/(acre*ft)	41.81
Best Fit Tp (months)	3.85
Best Fit Di (1/month)	0.3161
Best Fit b	0.6099
SSQ	107
R^2	0.98

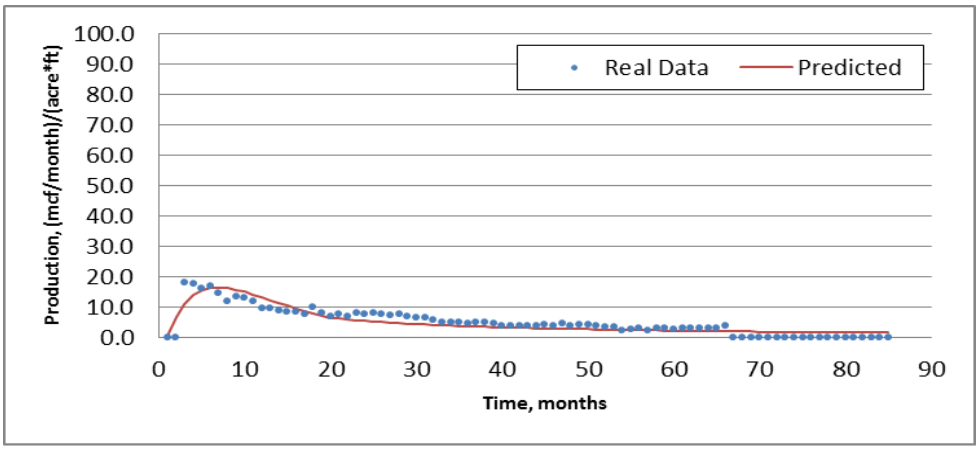

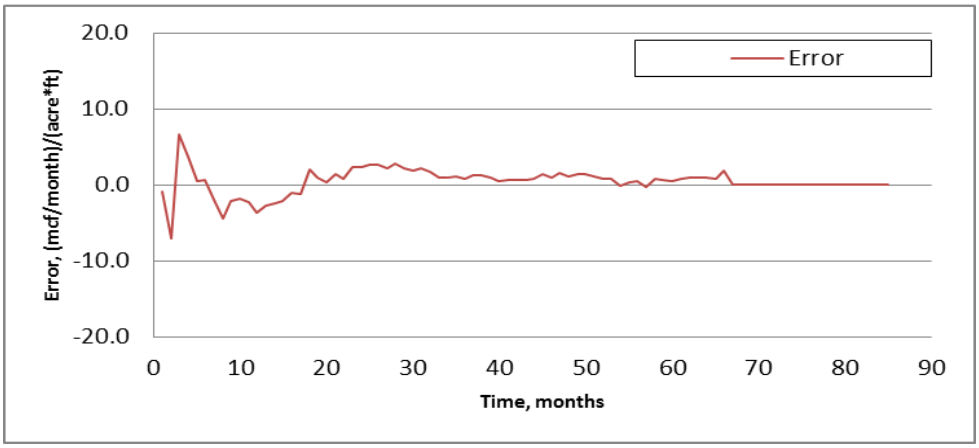

Well No.	9
Starting (Actual) Pmax (mcf/month)/(acre*ft)	17.9
Starting (Actual) Tp (months)	3
Starting di	0.5
Starting b	0.5
Best Fit Pmax (mcf/month)/(acre*ft)	16.55
Best Fit Tp (months)	6.9
Best Fit Di (1/month)	0.1154
Best Fit b	1
SSQ	278
R^2	0.8

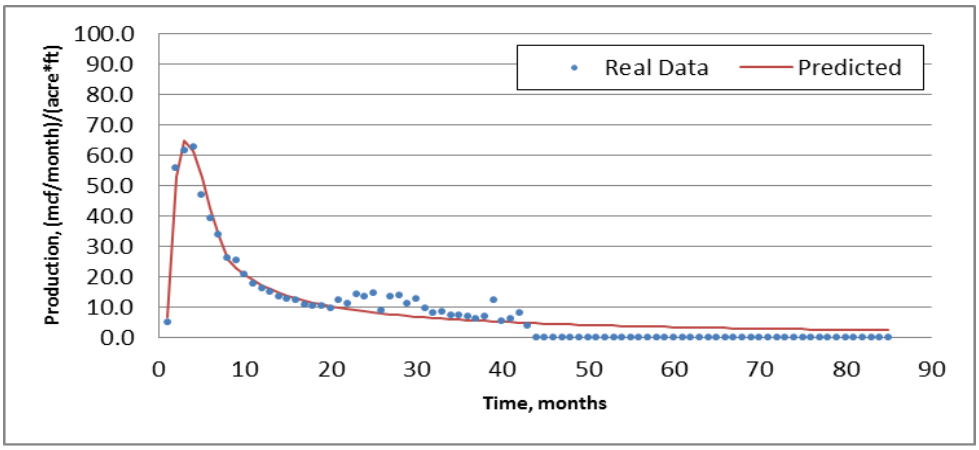

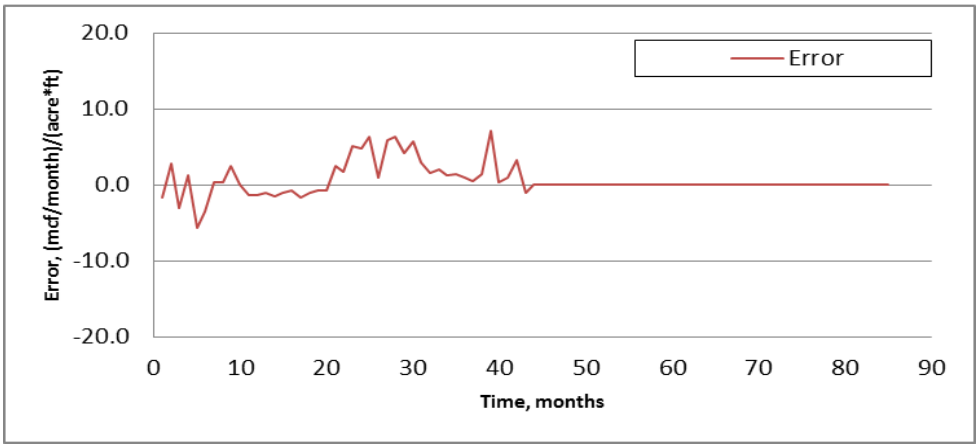

Well No.	10
Starting (Actual) Pmax (mcf/month)/(acre*ft)	62.6
Starting (Actual) Tp (months)	4
Starting di	0.5
Starting b	0.5
Best Fit Pmax (mcf/month)/(acre*ft)	64.73
Best Fit Tp (months)	3.15
Best Fit Di (1/month)	0.3091
Best Fit b	1
SSQ	397
R^2	0.97

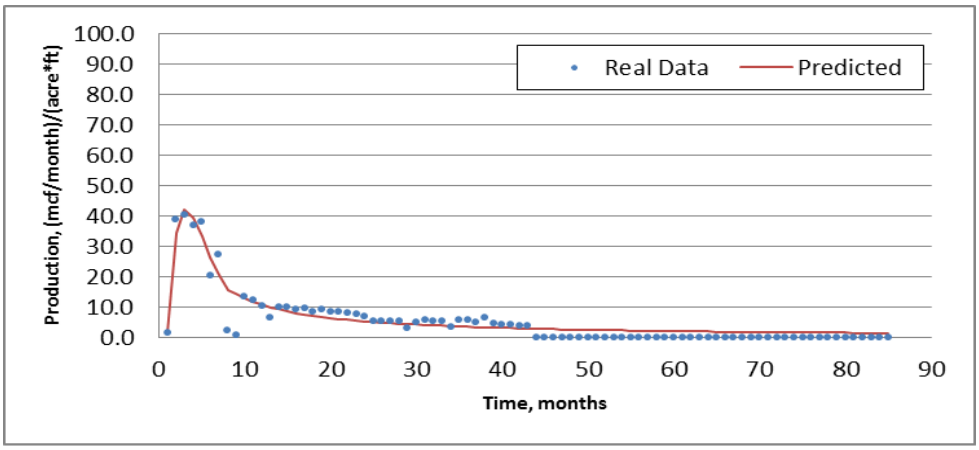

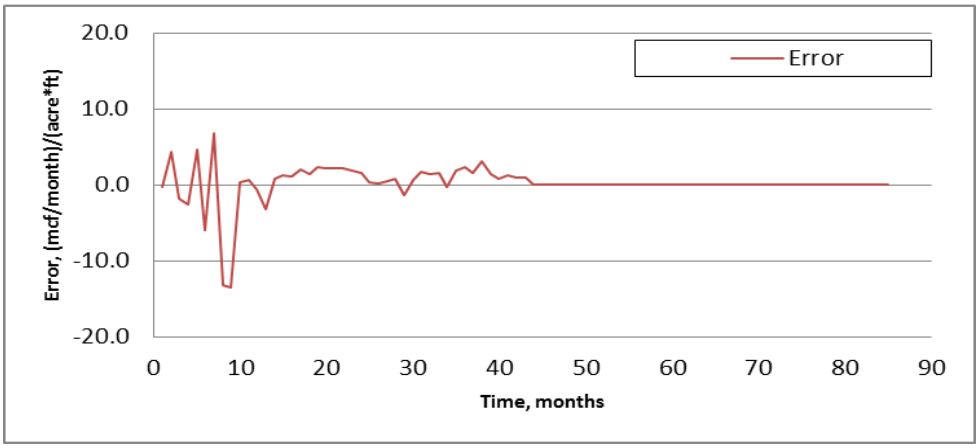

Well No.	11
Starting (Actual) Pmax (mcf/month)/(acre*ft)	40.4
Starting (Actual) Tp (months)	3
Starting di	0.5
Starting b	0.5
Best Fit Pmax (mcf/month)/(acre*ft)	42.16
Best Fit Tp (months)	3.1
Best Fit Di (1/month)	0.3244
Best Fit b	1
SSQ	574
R^2	0.87

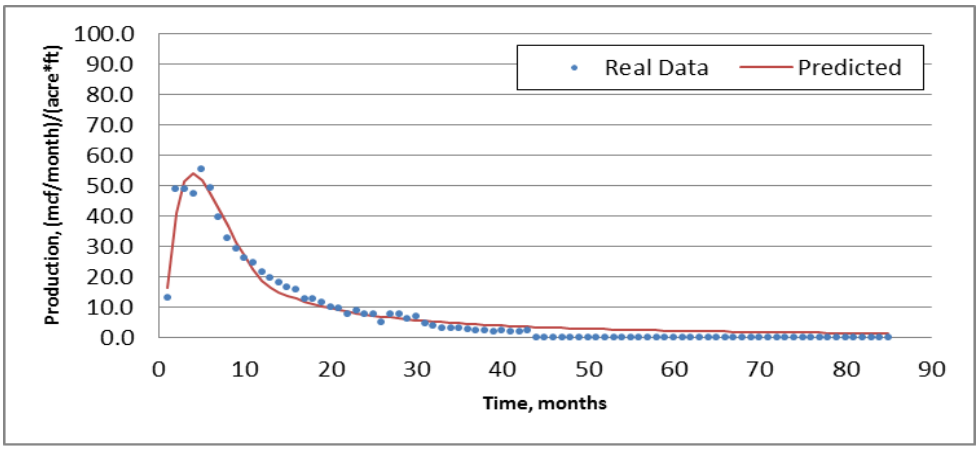

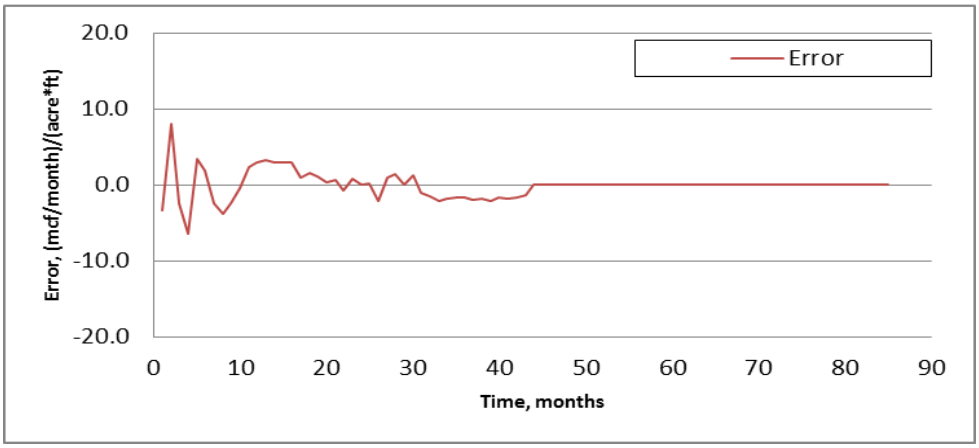

Well No.	12
Starting (Actual) Pmax (mcf/month)/(acre*ft)	55.3
Starting (Actual) Tp (months)	5
Starting di	0.5
Starting b	0.5
Best Fit Pmax (mcf/month)/(acre*ft)	53.84
Best Fit Tp (months)	3.95
Best Fit Di (1/month)	0.2053
Best Fit b	0.695
SSQ	271
R^2	0.97

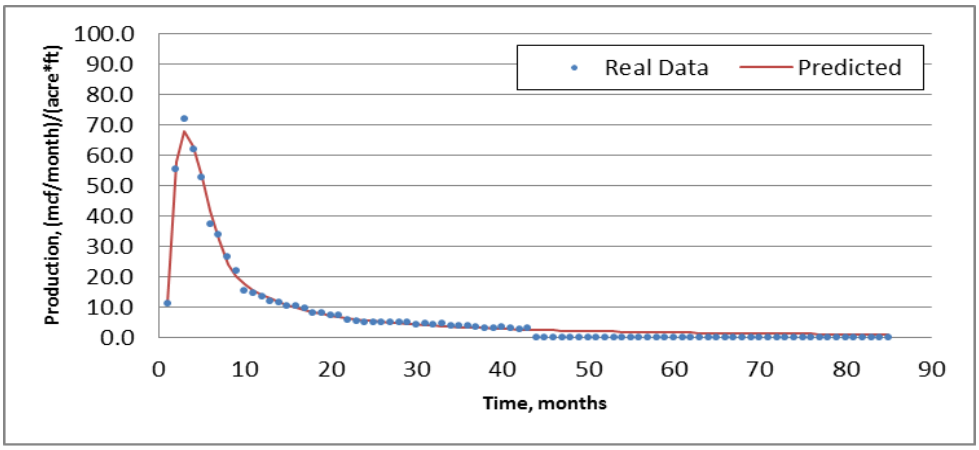

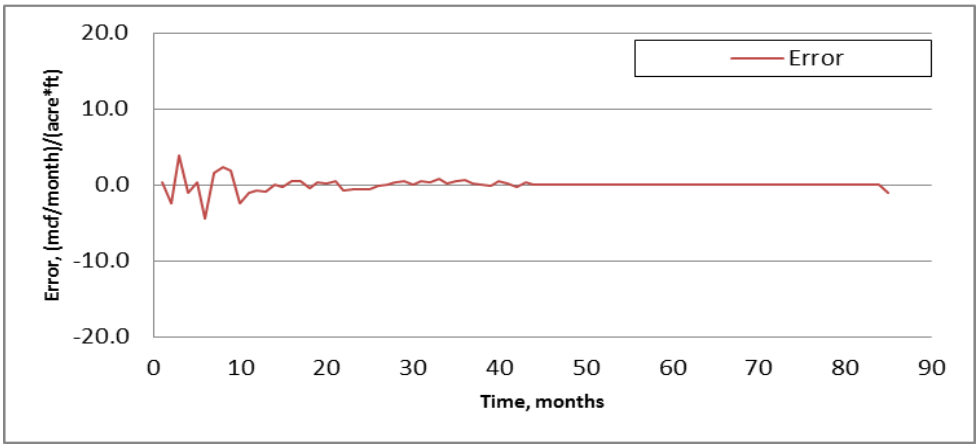

Well No.	13
Starting (Actual) Pmax (mcf/month)/(acre*ft)	71.8
Starting (Actual) Tp (months)	3
Starting di	0.5
Starting b	0.5
Best Fit Pmax (mcf/month)/(acre*ft)	67.91
Best Fit Tp (months)	3
Best Fit Di (1/month)	0.3247
Best Fit b	0.7245
SSQ	66
R^2	0.99

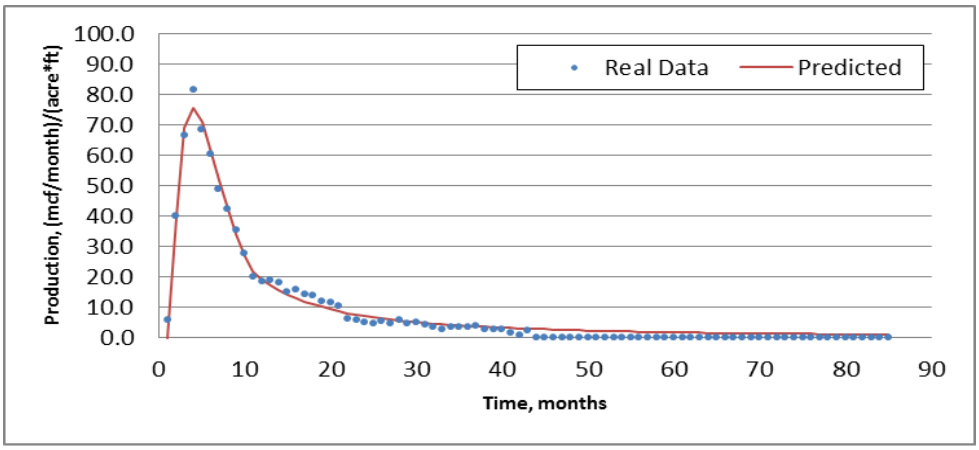

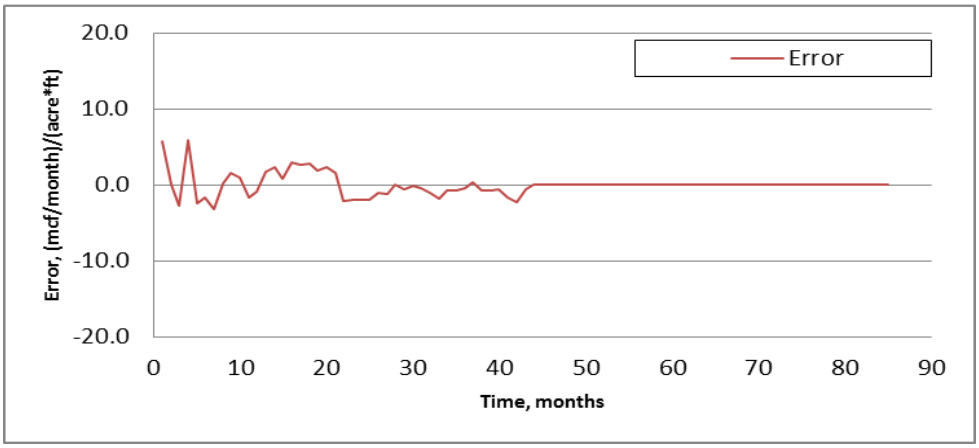

Well No.	14
Starting (Actual) Pmax (mcf/month)/(acre*ft)	81.3
Starting (Actual) Tp (months)	4
Starting di	0.5
Starting b	0.5
Best Fit Pmax (mcf/month)/(acre*ft)	75.39
Best Fit Tp (months)	3.95
Best Fit Di (1/month)	0.2682
Best Fit b	0.6261
SSQ	180
R^2	0.99

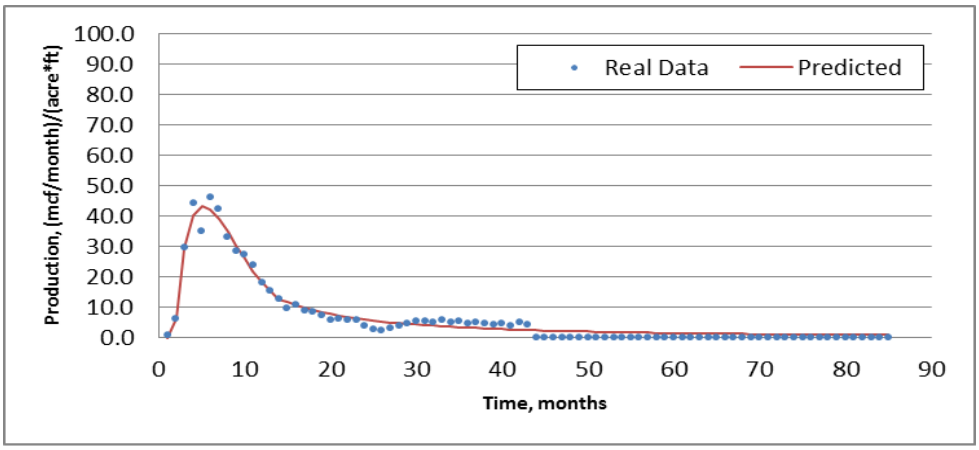

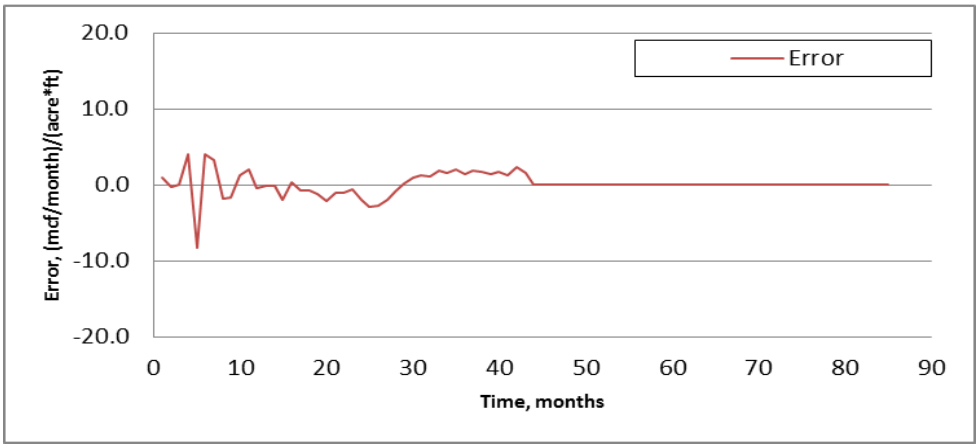

Well No.	15
Starting (Actual) Pmax (mcf/month)/(acre*ft)	46.2
Starting (Actual) Tp (months)	6
Starting di	0.5
Starting b	0.5
Best Fit Pmax (mcf/month)/(acre*ft)	43.33
Best Fit Tp (months)	5.15
Best Fit Di (1/month)	0.2076
Best Fit b	0.625
SSQ	197
R^2	0.97

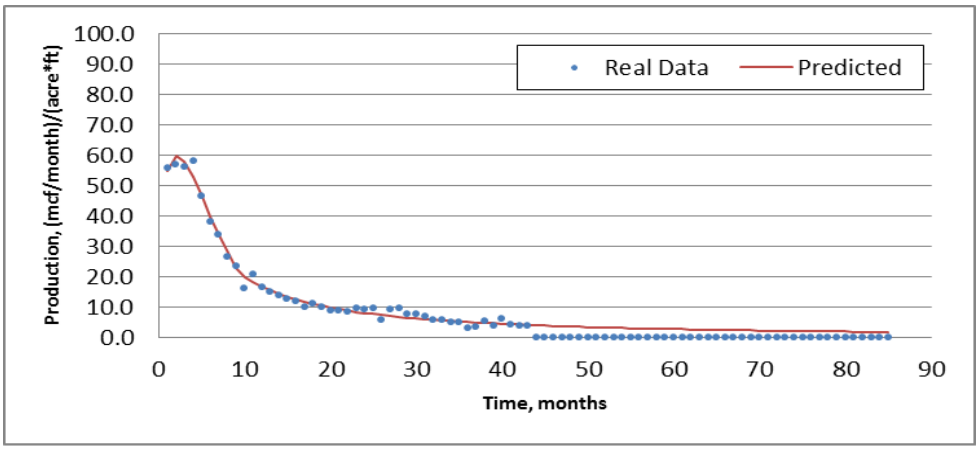

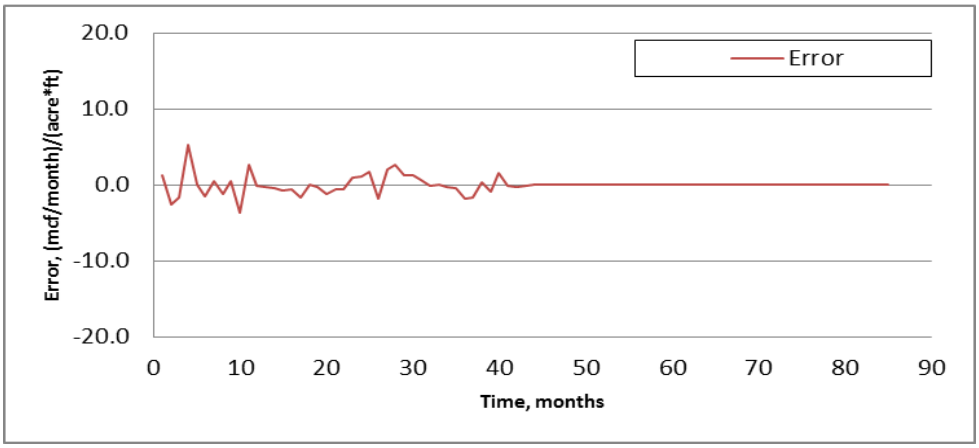

Well No.	16
Starting (Actual) Pmax (mcf/month)/(acre*ft)	58
Starting (Actual) Tp (months)	4
Starting di	0.5
Starting b	0.5
Best Fit Pmax (mcf/month)/(acre*ft)	59.66
Best Fit Tp (months)	2.14
Best Fit Di (1/month)	0.2235
Best Fit b	0.7965
SSQ	102
R^2	0.99

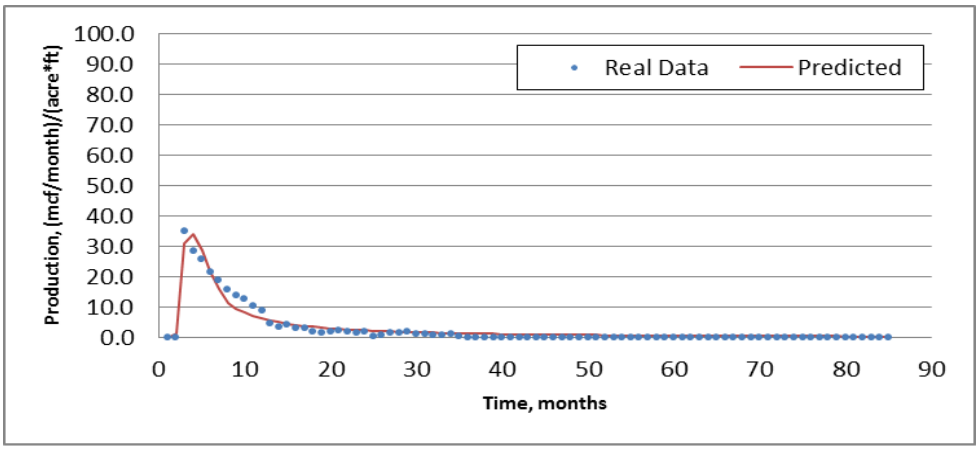

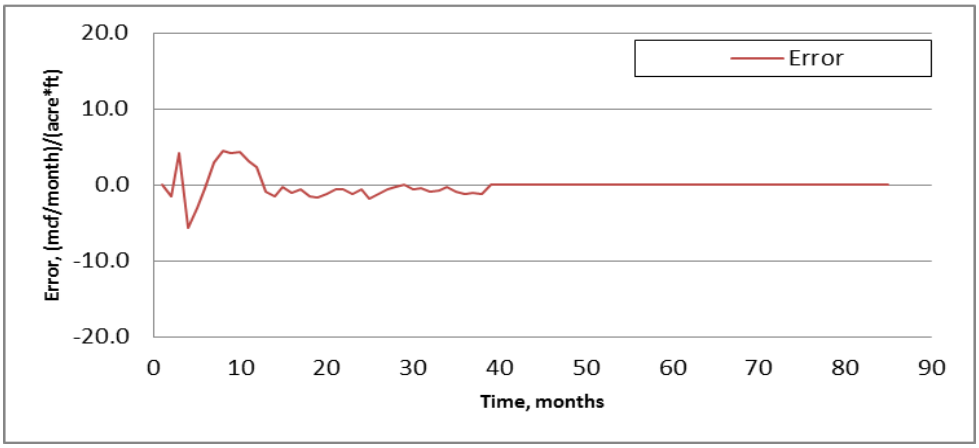

Well No.	17
Starting (Actual) Pmax (mcf/month)/(acre*ft)	35.1
Starting (Actual) Tp (months)	3
Starting di	0.5
Starting b	0.5
Best Fit Pmax (mcf/month)/(acre*ft)	34.54
Best Fit Tp (months)	3.69
Best Fit Di (1/month)	0.4029
Best Fit b	0.7322
SSQ	165
R^2	0.94

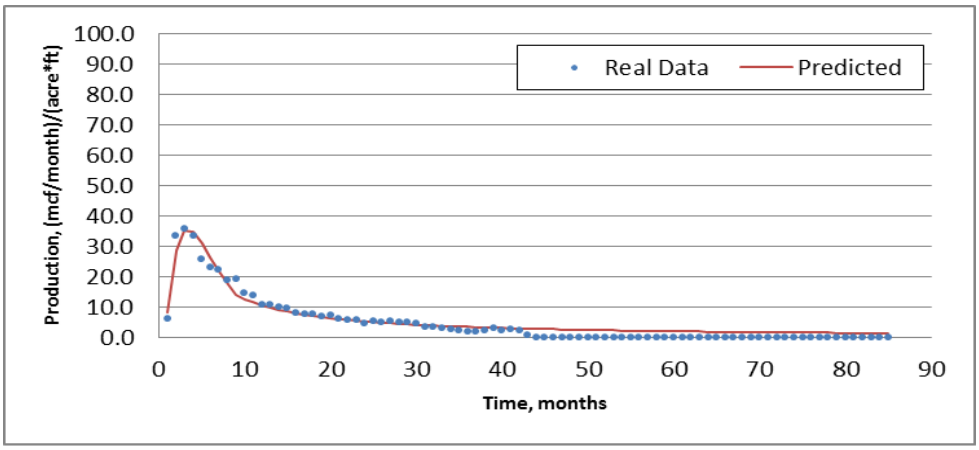

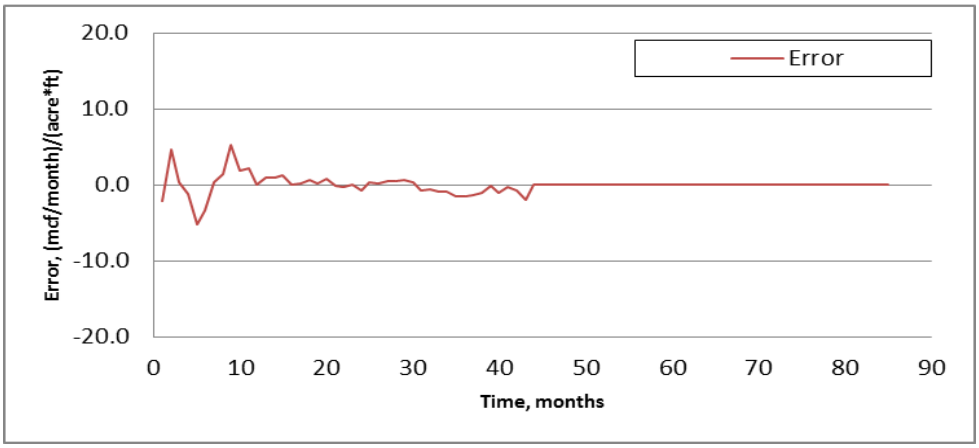

Well No.	18
Starting (Actual) Pmax (mcf/month)/(acre*ft)	35.6
Starting (Actual) Tp (months)	3
Starting di	0.5
Starting b	0.5
Best Fit Pmax (mcf/month)/(acre*ft)	35.63
Best Fit Tp (months)	3.35
Best Fit Di (1/month)	0.2675
Best Fit b	0.9825
SSQ	126
R^2	0.96

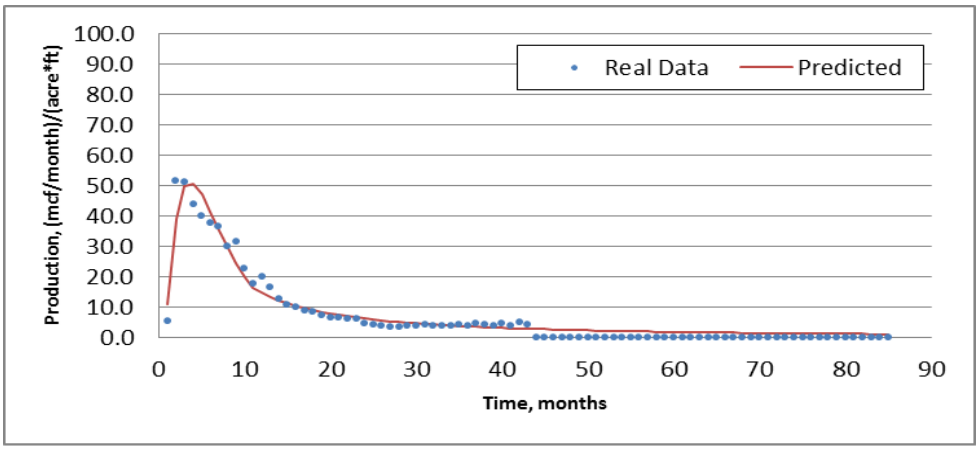

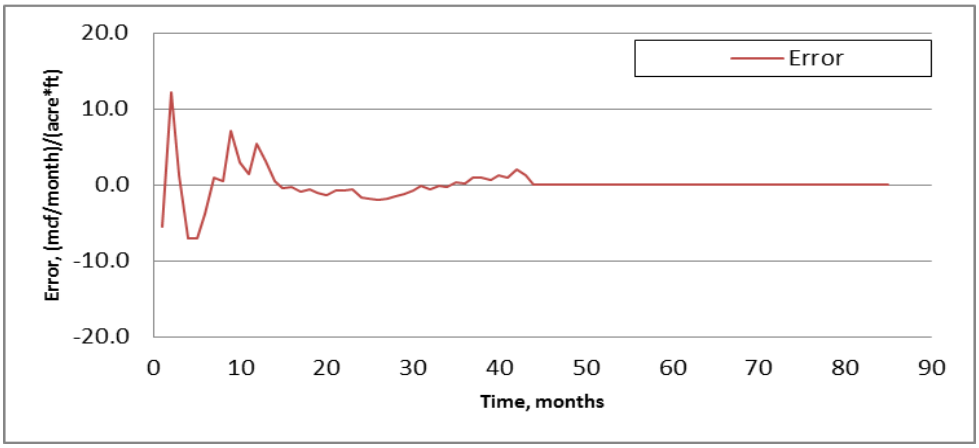

Well No.	19
Starting (Actual) Pmax (mcf/month)/(acre*ft)	51.4
Starting (Actual) Tp (months)	2
Starting di	0.5
Starting b	0.5
Best Fit Pmax (mcf/month)/(acre*ft)	51.04
Best Fit Tp (months)	3.64
Best Fit Di (1/month)	0.2403
Best Fit b	0.721
SSQ	433
R^2	0.95

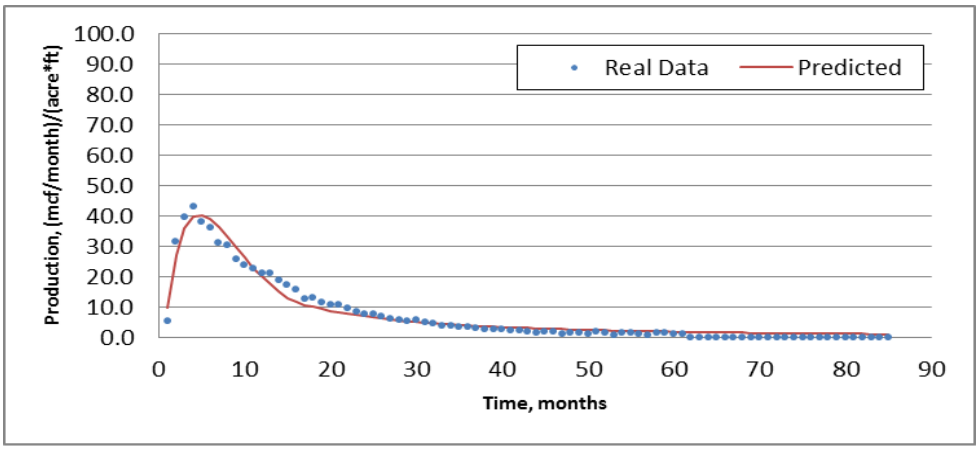

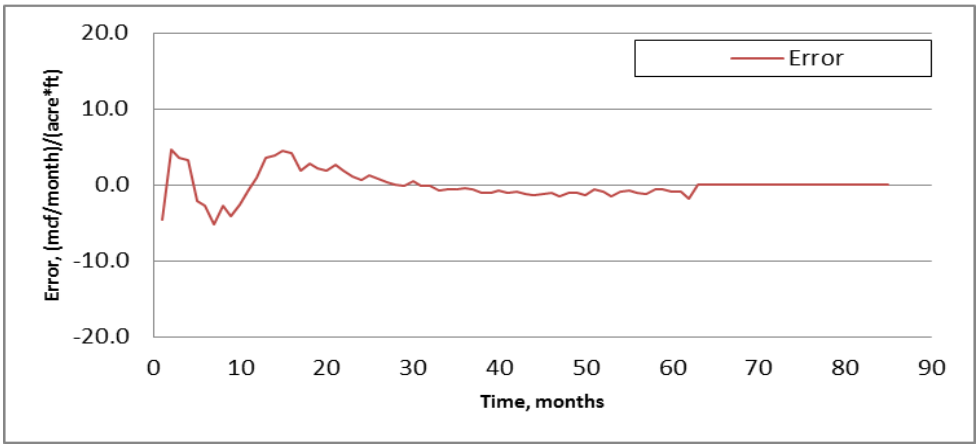

Well No.	20
Starting (Actual) Pmax (mcf/month)/(acre*ft)	43.1
Starting (Actual) Tp (months)	4
Starting di	0.5
Starting b	0.5
Best Fit Pmax (mcf/month)/(acre*ft)	40.47
Best Fit Tp (months)	4.7
Best Fit Di (1/month)	0.169
Best Fit b	0.6453
SSQ	270
R^2	0.97

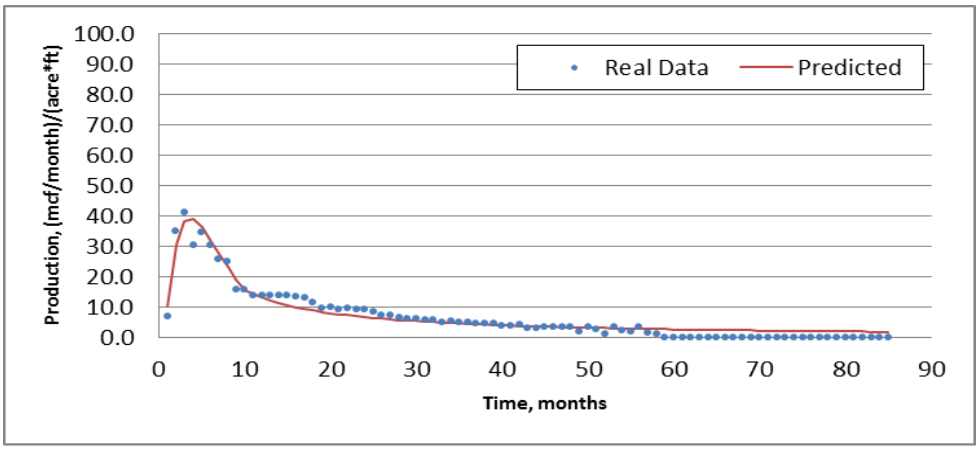

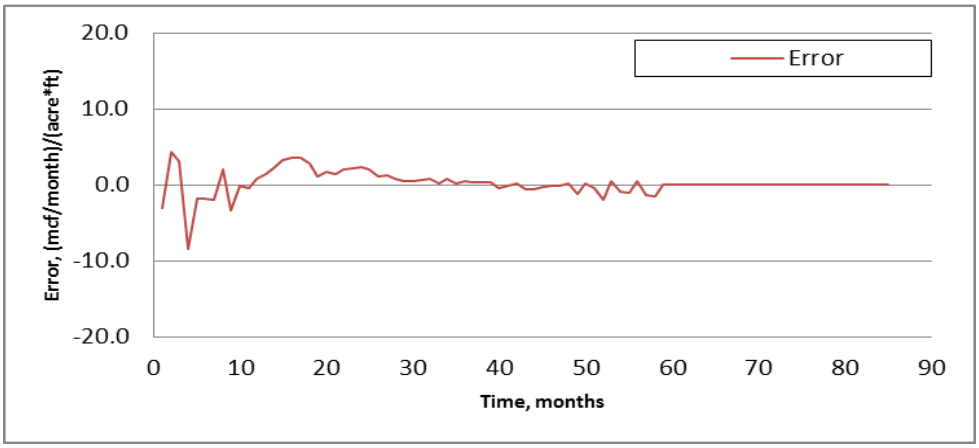

Well No.	21
Starting (Actual) Pmax (mcf/month)/(acre*ft)	41.2
Starting (Actual) Tp (months)	3
Starting di	0.5
Starting b	0.5
Best Fit Pmax (mcf/month)/(acre*ft)	39.17
Best Fit Tp (months)	3.65
Best Fit Di (1/month)	0.2345
Best Fit b	1
SSQ	231
R^2	0.96

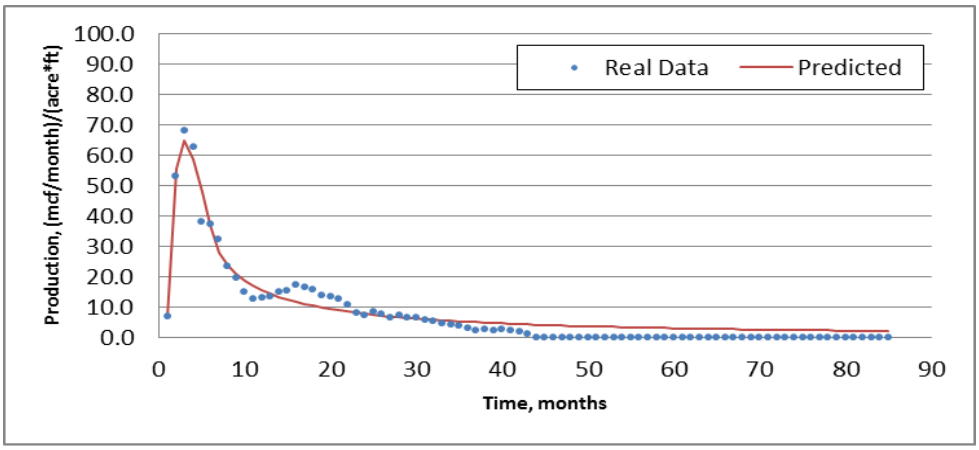

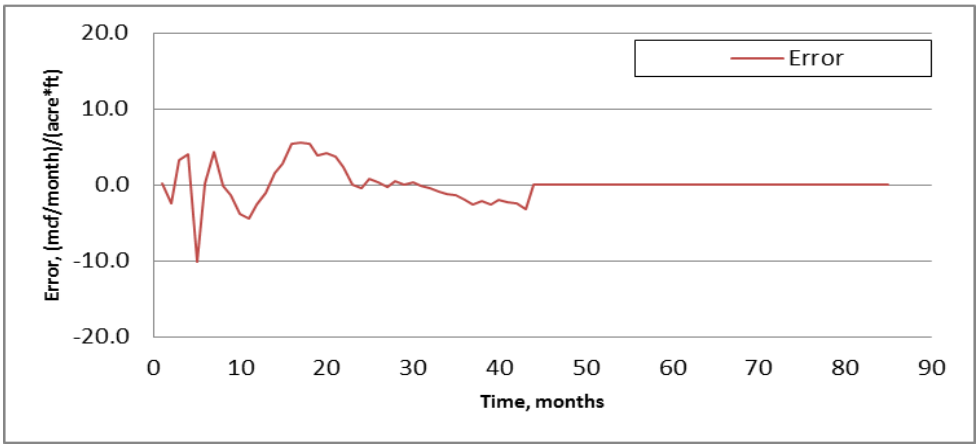

Well No.	22
Starting (Actual) Pmax (mcf/month)/(acre*ft)	68
Starting (Actual) Tp (months)	3
Starting di	0.5
Starting b	0.5
Best Fit Pmax (mcf/month)/(acre*ft)	64.81
Best Fit Tp (months)	2.93
Best Fit Di (1/month)	0.3447
Best Fit b	1
SSQ	404
R^2	0.96

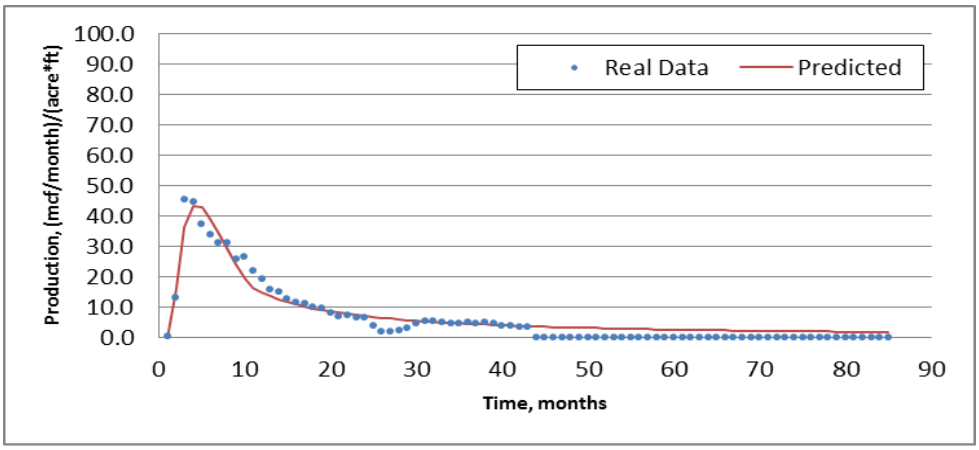

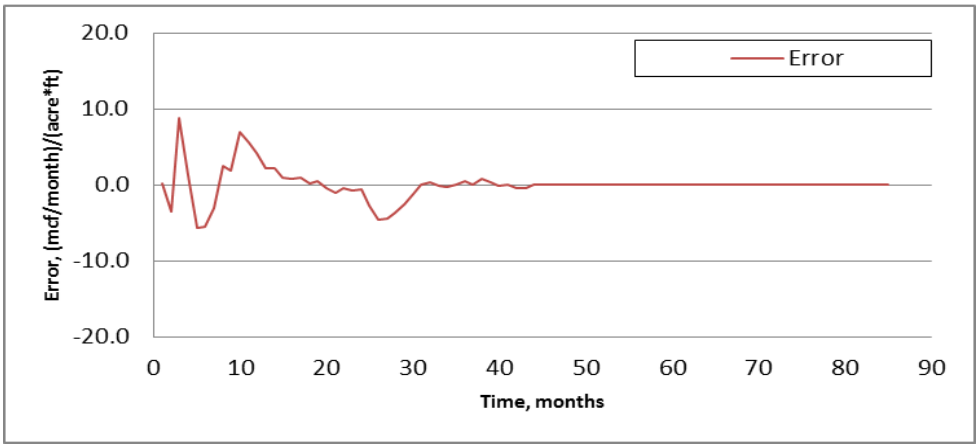

Well No.	23
Starting (Actual) Pmax (mcf/month)/(acre*ft)	45.3
Starting (Actual) Tp (months)	3
Starting di	0.5
Starting b	0.5
Best Fit Pmax (mcf/month)/(acre*ft)	43.61
Best Fit Tp (months)	4.4
Best Fit Di (1/month)	0.2425
Best Fit b	0.9324
SSQ	355
R^2	0.94

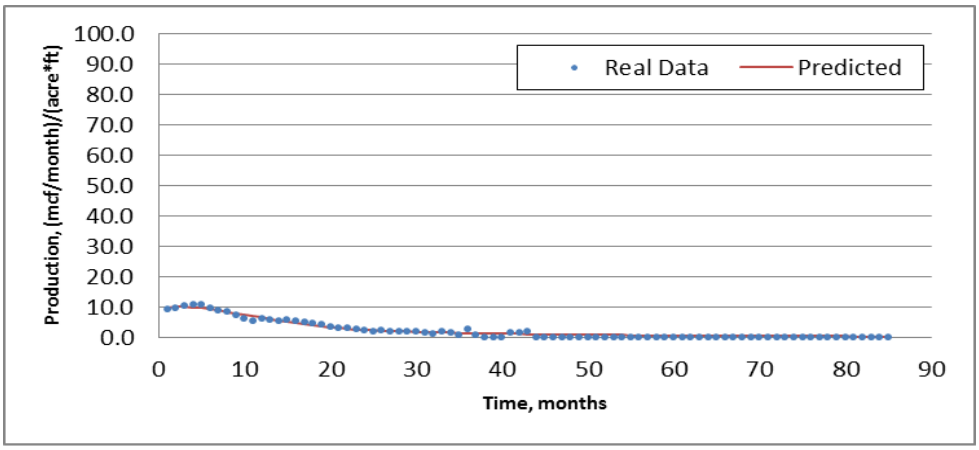

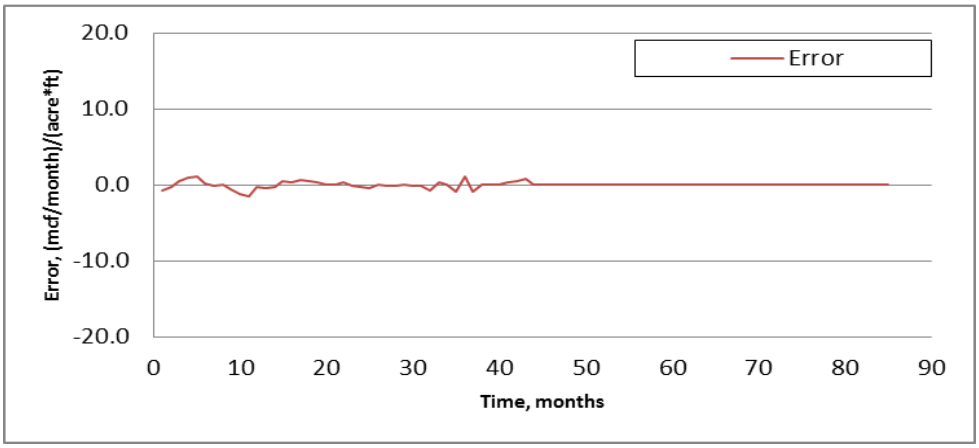

Well No.	24
Starting (Actual) Pmax (mcf/month)/(acre*ft)	10.9
Starting (Actual) Tp (months)	4
Starting di	0.5
Starting b	0.5
Best Fit Pmax (mcf/month)/(acre*ft)	10.1
Best Fit Tp (months)	2.66
Best Fit Di (1/month)	0.0949
Best Fit b	0.5039
SSQ	13
R^2	0.97

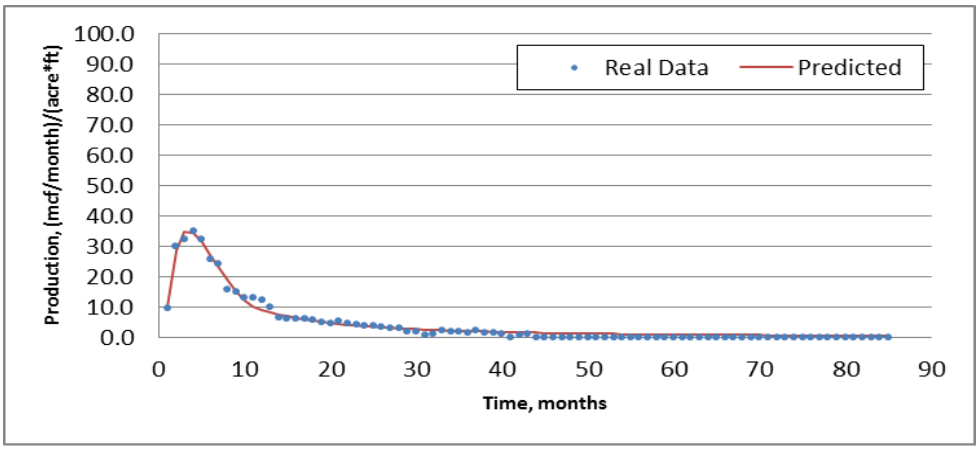

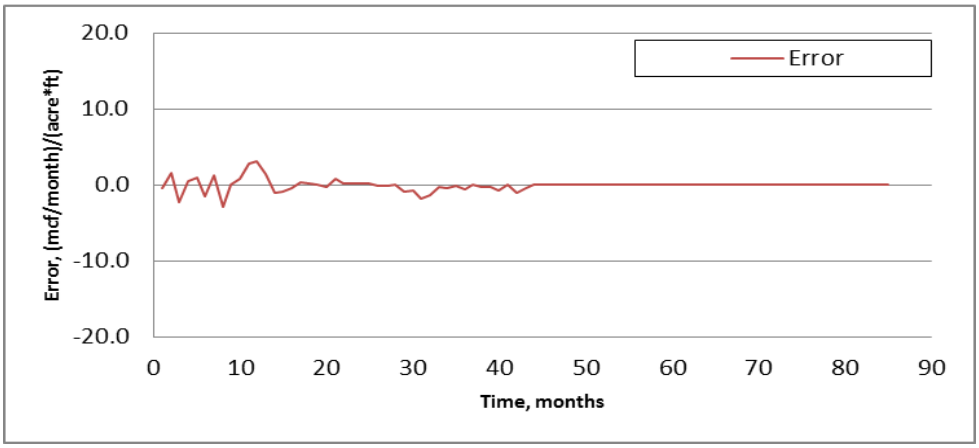

Well No.	25
Starting (Actual) Pmax (mcf/month)/(acre*ft)	35
Starting (Actual) Tp (months)	4
Starting di	0.5
Starting b	0.5
Best Fit Pmax (mcf/month)/(acre*ft)	35.16
Best Fit Tp (months)	3.43
Best Fit Di (1/month)	0.2519
Best Fit b	0.6751
SSQ	53
R^2	0.99

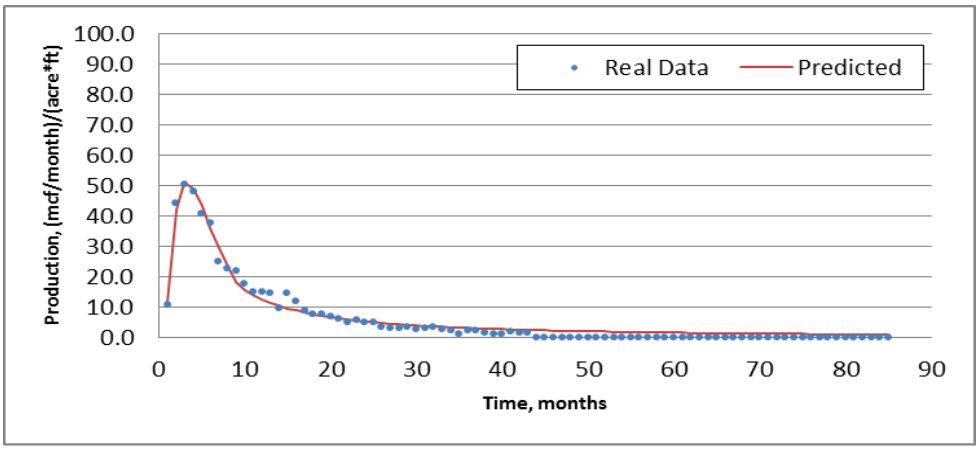

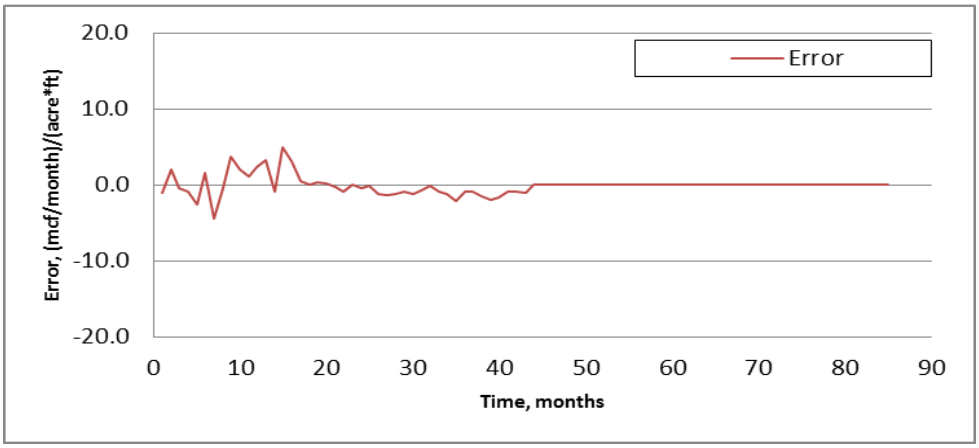

Well No.	26
Starting (Actual) Pmax (mcf/month)/(acre*ft)	50.3
Starting (Actual) Tp (months)	3
Starting di	0.5
Starting b	0.5
Best Fit Pmax (mcf/month)/(acre*ft)	50.98
Best Fit Tp (months)	3.24
Best Fit Di (1/month)	0.281
Best Fit b	0.748
SSQ	133
R^2	0.98

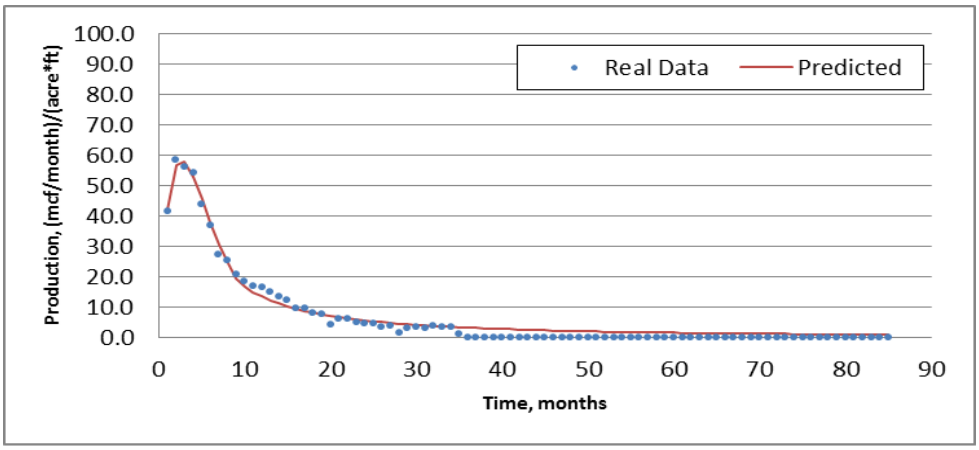

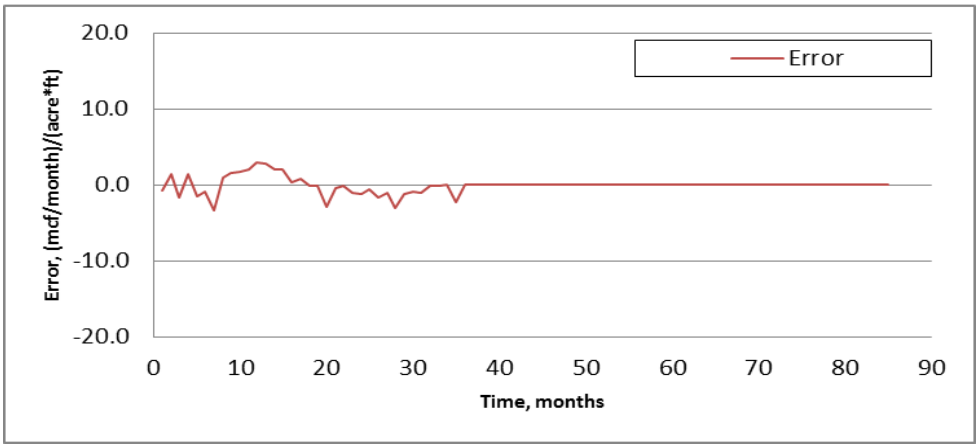

Well No.	27
Starting (Actual) Pmax (mcf/month)/(acre*ft)	58.3
Starting (Actual) Tp (months)	2
Starting di	0.5
Starting b	0.5
Best Fit Pmax (mcf/month)/(acre*ft)	58.5
Best Fit Tp (months)	2.59
Best Fit Di (1/month)	0.2659
Best Fit b	0.6793
SSQ	90
R^2	0.99

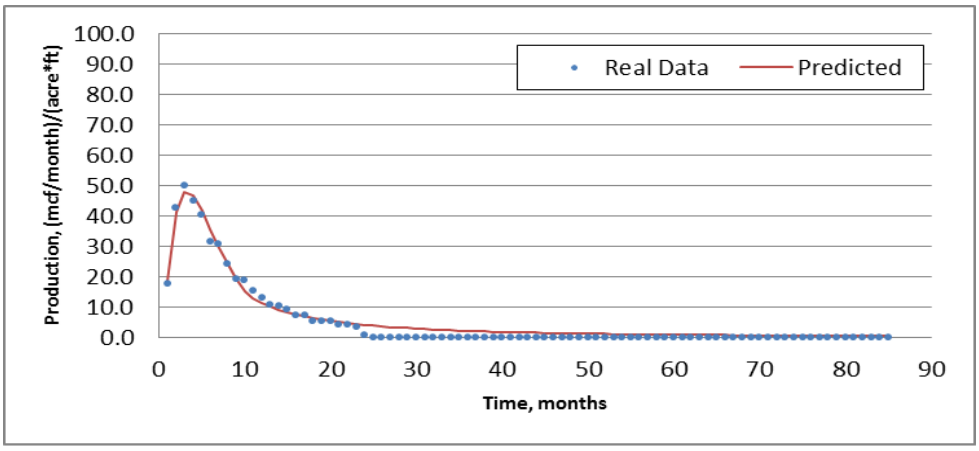

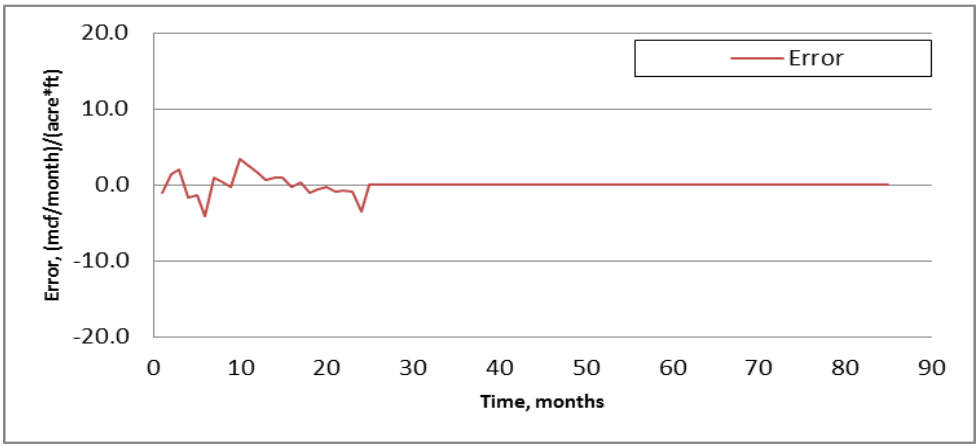

Well No.	28
Starting (Actual) Pmax (mcf/month)/(acre*ft)	49.9
Starting (Actual) Tp (months)	3
Starting di	0.5
Starting b	0.5
Best Fit Pmax (mcf/month)/(acre*ft)	48.14
Best Fit Tp (months)	3.24
Best Fit Di (1/month)	0.2581
Best Fit b	0.5808
SSQ	68
R^2	0.99

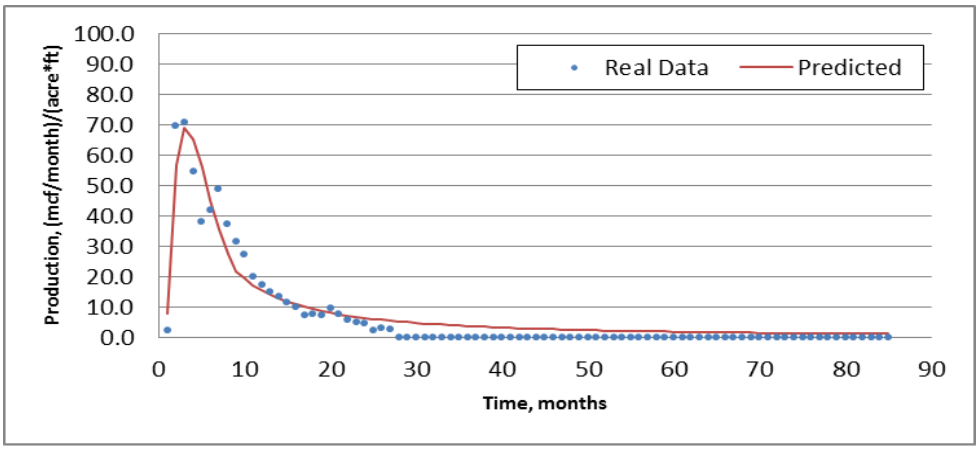

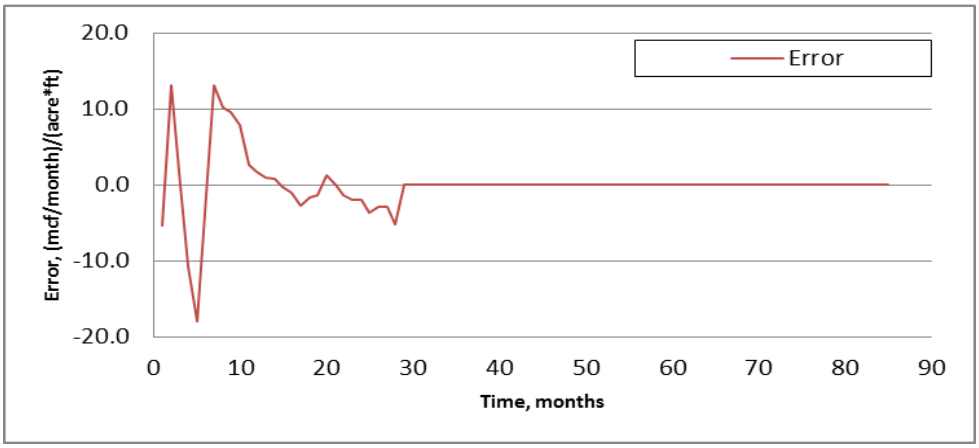

Well No.	29
Starting (Actual) Pmax (mcf/month)/(acre*ft)	70.5
Starting (Actual) Tp (months)	3
Starting di	0.5
Starting b	0.5
Best Fit Pmax (mcf/month)/(acre*ft)	68.98
Best Fit Tp (months)	3.15
Best Fit Di (1/month)	0.3092
Best Fit b	0.7442
SSQ	1168
R^2	0.9

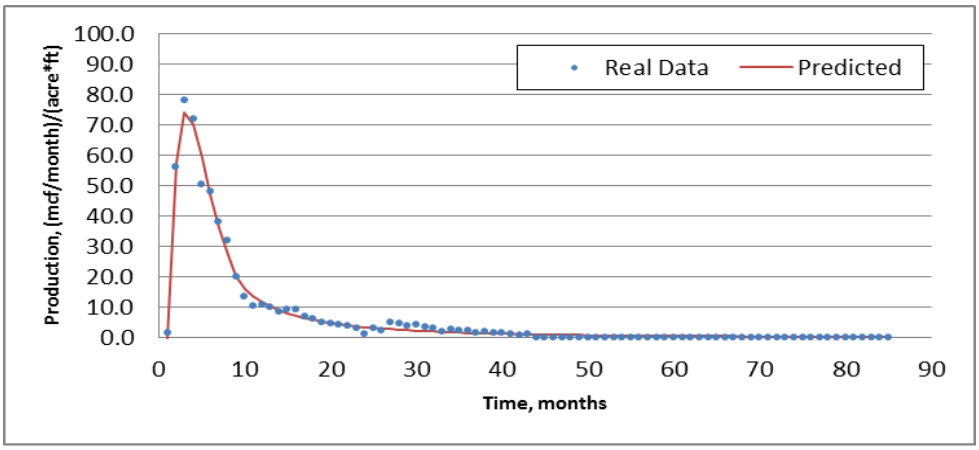

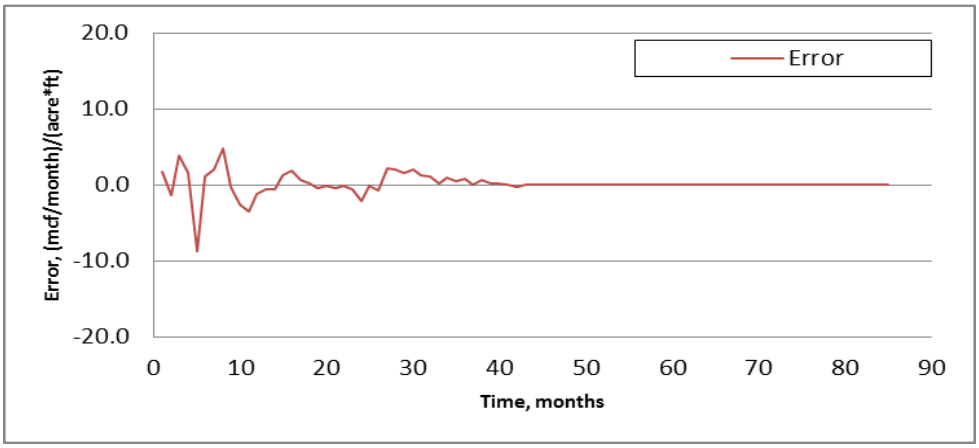

Well No.	30
Starting (Actual) Pmax (mcf/month)/(acre*ft)	77.9
Starting (Actual) Tp (months)	3
Starting di	0.5
Starting b	0.5
Best Fit Pmax (mcf/month)/(acre*ft)	74.29
Best Fit Tp (months)	3.18
Best Fit Di (1/month)	0.3308
Best Fit b	0.474
SSQ	180
R^2	0.99

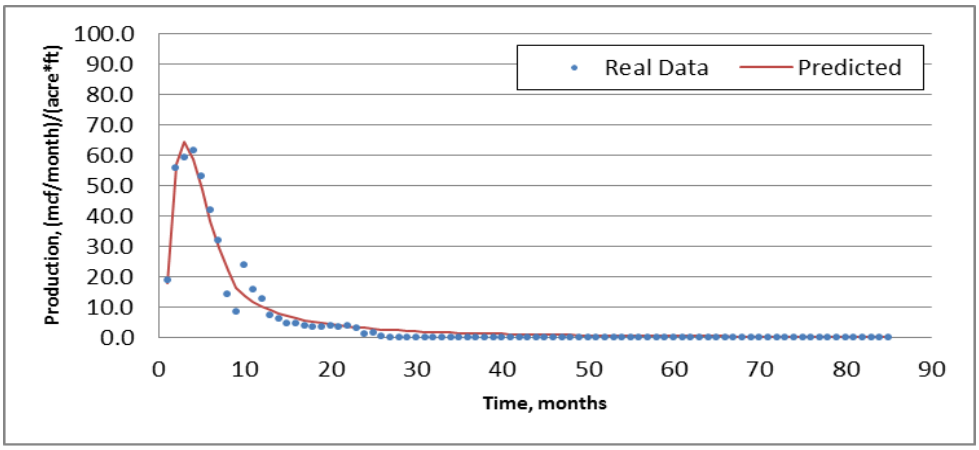

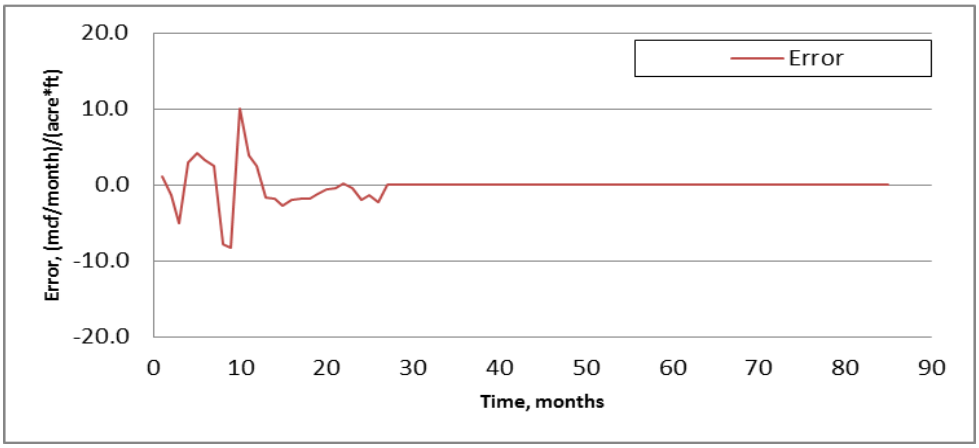

Well No.	31
Starting (Actual) Pmax (mcf/month)/(acre*ft)	61.6
Starting (Actual) Tp (months)	4
Starting di	0.5
Starting b	0.5
Best Fit Pmax (mcf/month)/(acre*ft)	64.46
Best Fit Tp (months)	2.89
Best Fit Di (1/month)	0.3249
Best Fit b	0.489
SSQ	356
R^2	0.97

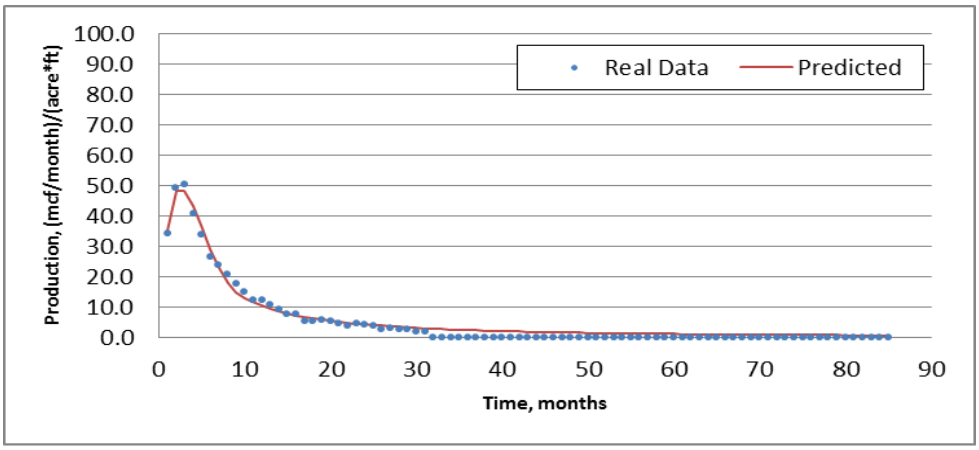

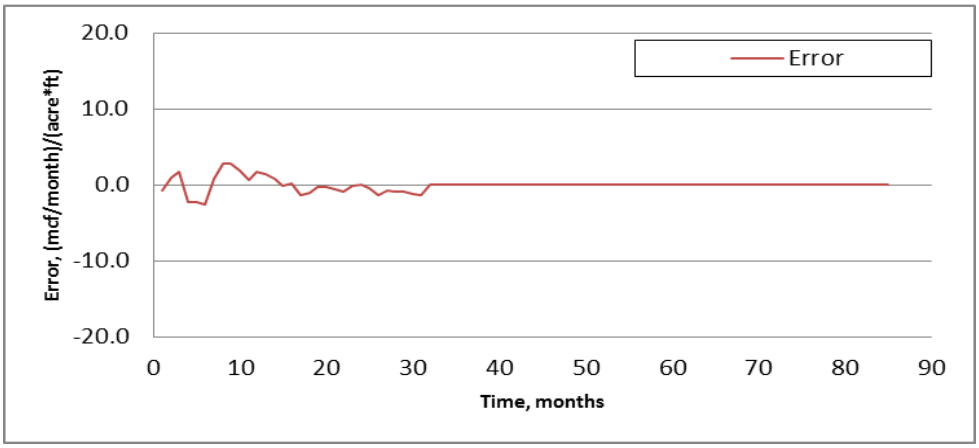

Well No.	32
Starting (Actual) Pmax (mcf/month)/(acre*ft)	50.2
Starting (Actual) Tp (months)	3
Starting di	0.5
Starting b	0.5
Best Fit Pmax (mcf/month)/(acre*ft)	49.33
Best Fit Tp (months)	2.48
Best Fit Di (1/month)	0.2897
Best Fit b	0.6864
SSQ	58
R^2	0.99

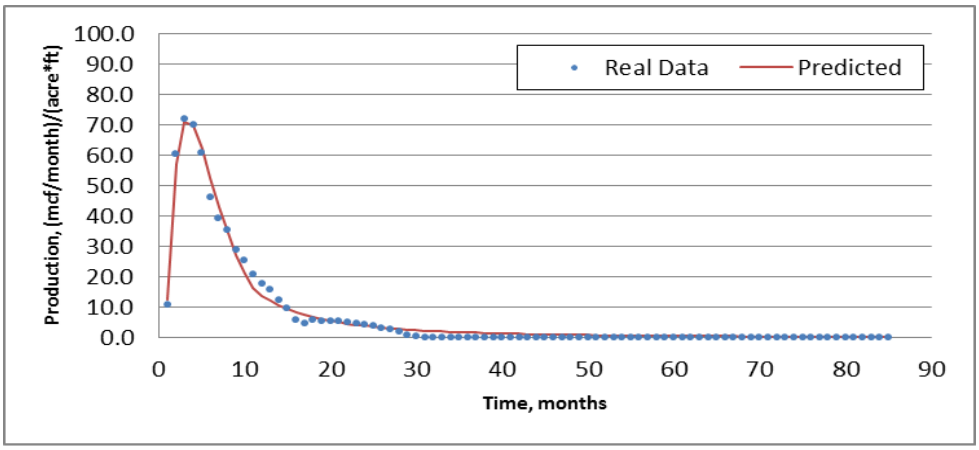

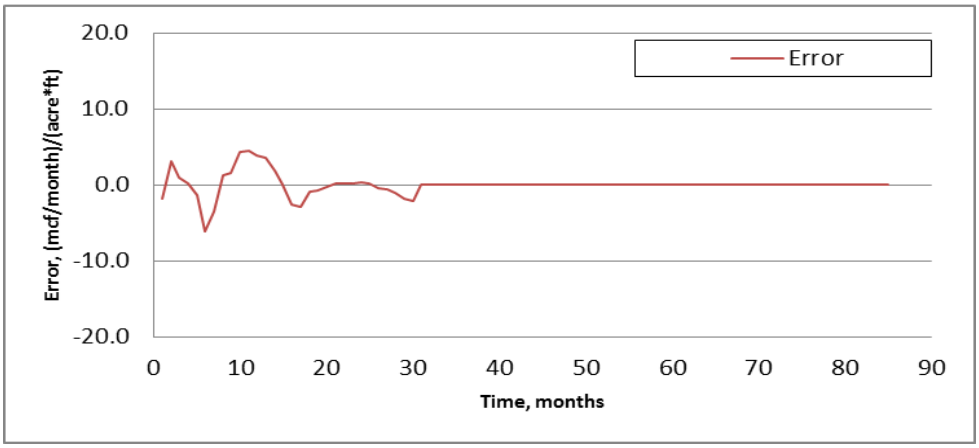

Well No.	33
Starting (Actual) Pmax (mcf/month)/(acre*ft)	71.8
Starting (Actual) Tp (months)	3
Starting di	0.5
Starting b	0.5
Best Fit Pmax (mcf/month)/(acre*ft)	71.52
Best Fit Tp (months)	3.35
Best Fit Di (1/month)	0.2751
Best Fit b	0.4231
SSQ	166
R^2	0.99

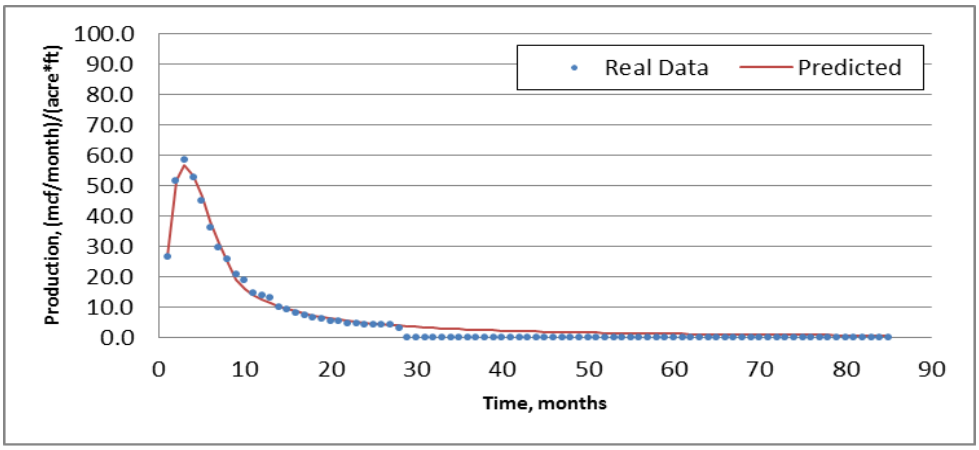

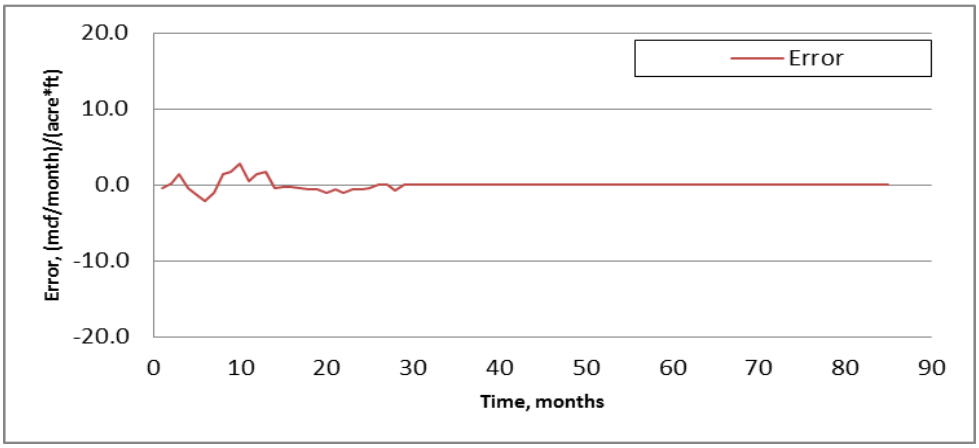

Well No.	34
Starting (Actual) Pmax (mcf/month)/(acre*ft)	58.2
Starting (Actual) Tp (months)	3
Starting di	0.5
Starting b	0.5
Best Fit Pmax (mcf/month)/(acre*ft)	56.86
Best Fit Tp (months)	2.96
Best Fit Di (1/month)	0.2791
Best Fit b	0.6323
SSQ	32
R^2	1

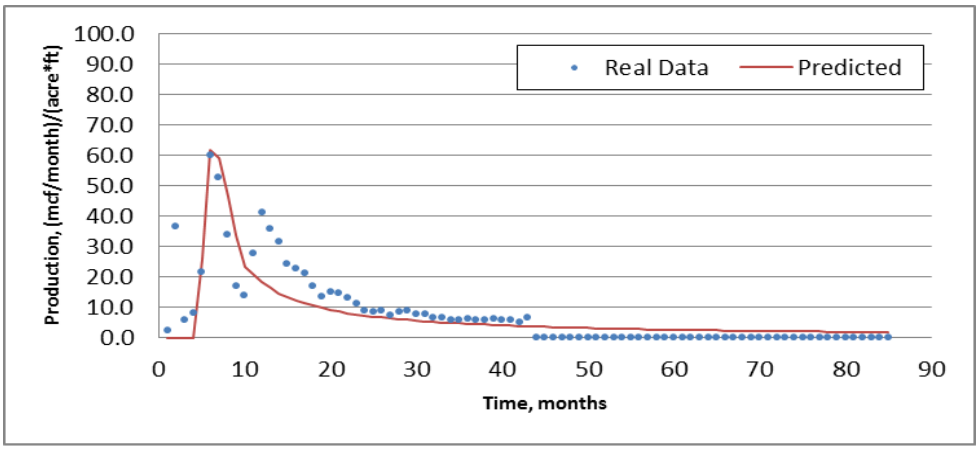

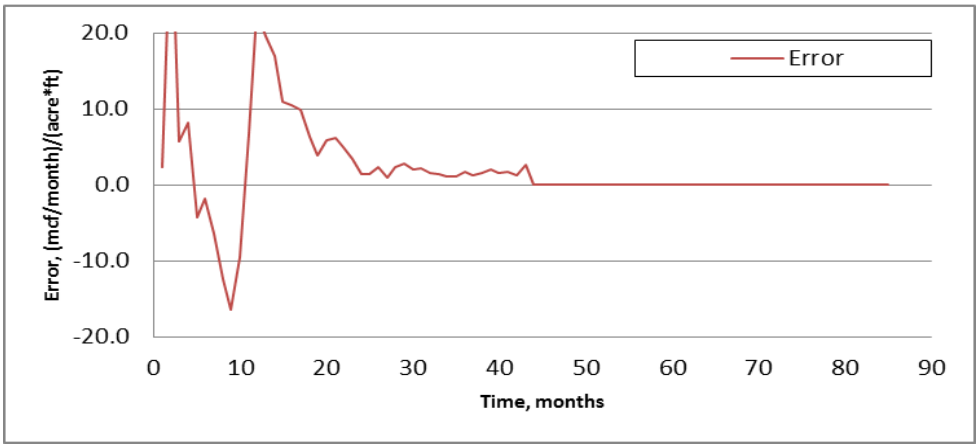

Well No.	35
Starting (Actual) Pmax (mcf/month)/(acre*ft)	60.1
Starting (Actual) Tp (months)	6
Starting di	0.5
Starting b	0.5
Best Fit Pmax (mcf/month)/(acre*ft)	63.26
Best Fit Tp (months)	6.32
Best Fit Di (1/month)	0.4319
Best Fit b	1
SSQ	3803
R^2	0.65

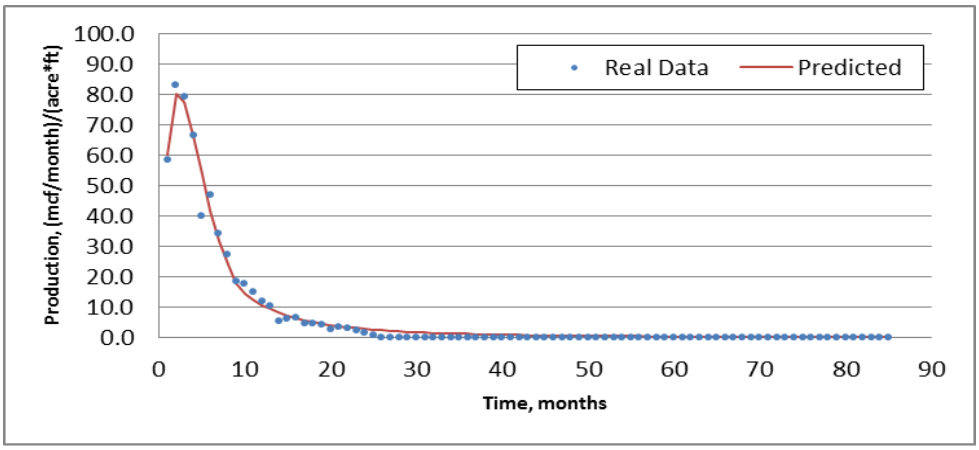

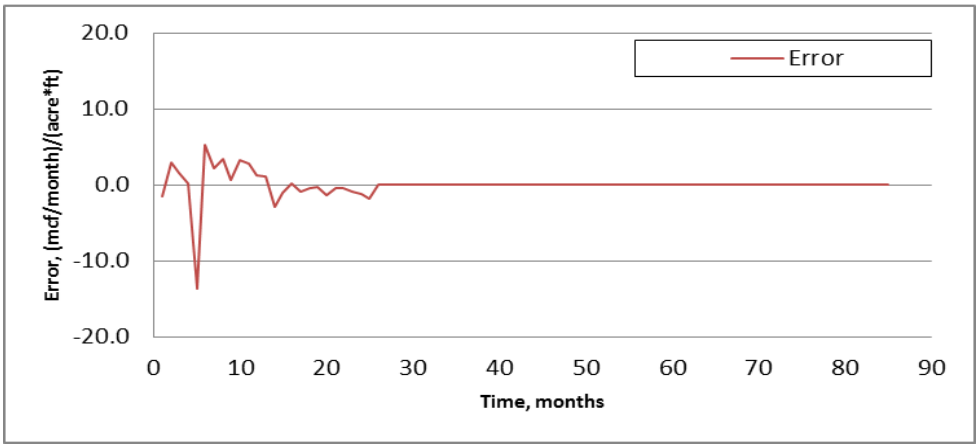

Well No.	36
Starting (Actual) Pmax (mcf/month)/(acre*ft)	83
Starting (Actual) Tp (months)	2
Starting di	0.5
Starting b	0.5
Best Fit Pmax (mcf/month)/(acre*ft)	80.75
Best Fit Tp (months)	2.28
Best Fit Di (1/month)	0.3196
Best Fit b	0.4008
SSQ	283
R^2	0.98

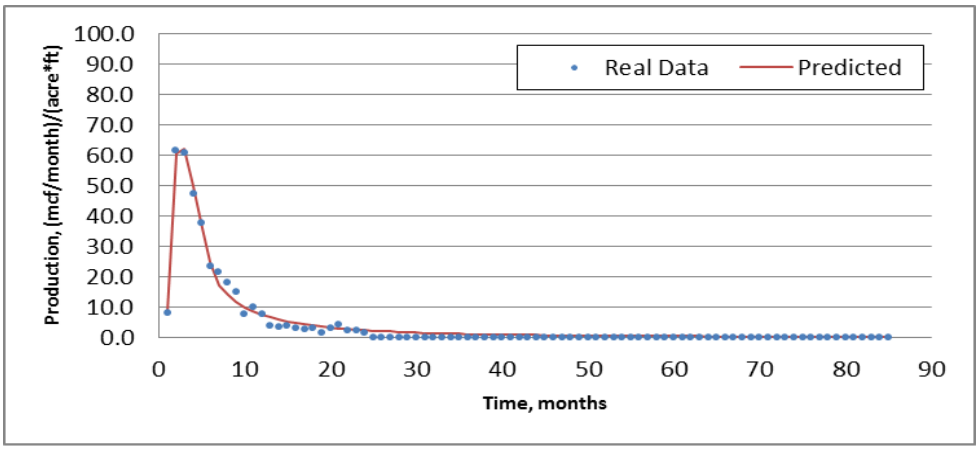

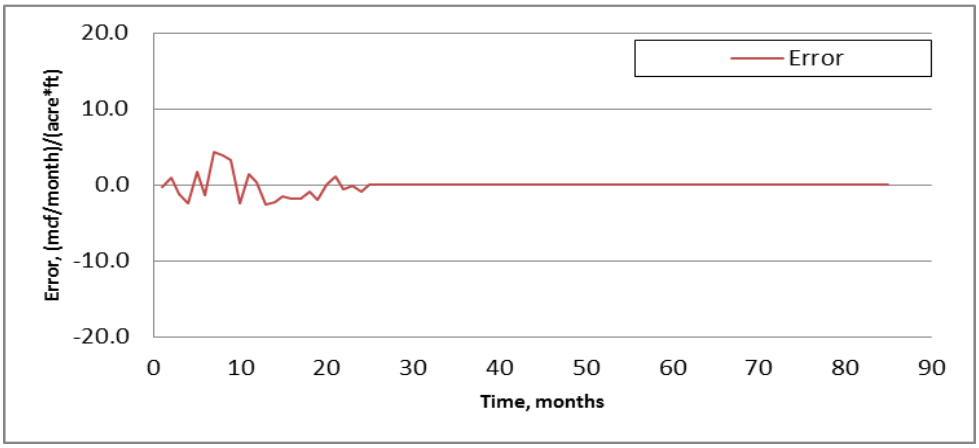

Well No.	37
Starting (Actual) Pmax (mcf/month)/(acre*ft)	61.6
Starting (Actual) Tp (months)	2
Starting di	0.5
Starting b	0.5
Best Fit Pmax (mcf/month)/(acre*ft)	64.47
Best Fit Tp (months)	2.51
Best Fit Di (1/month)	0.4376
Best Fit b	0.5611
SSQ	94
R^2	0.99

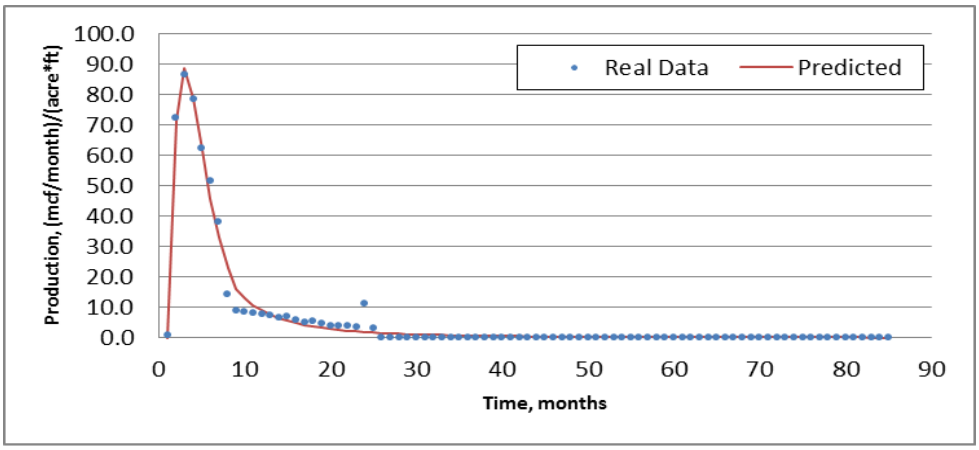

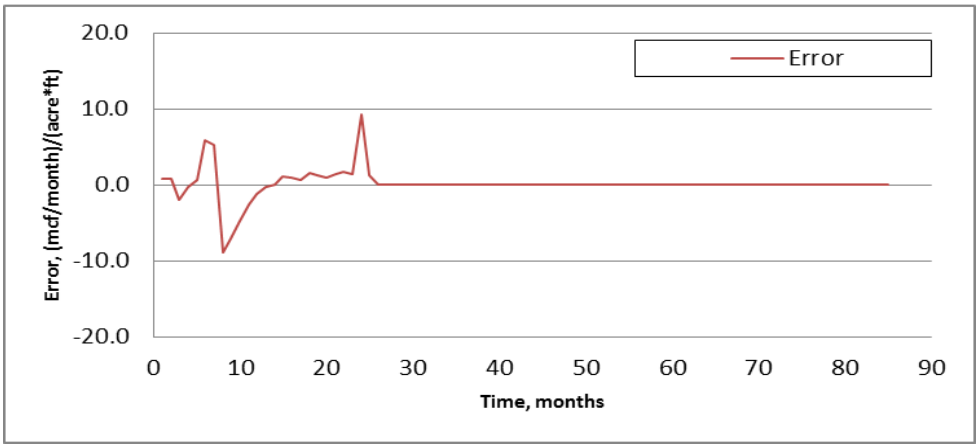

Well No.	38
Starting (Actual) Pmax (mcf/month)/(acre*ft)	86.6
Starting (Actual) Tp (months)	3
Starting di	0.5
Starting b	0.5
Best Fit Pmax (mcf/month)/(acre*ft)	88.62
Best Fit Tp (months)	2.94
Best Fit Di (1/month)	0.3894
Best Fit b	0.356
SSQ	329
R^2	0.98

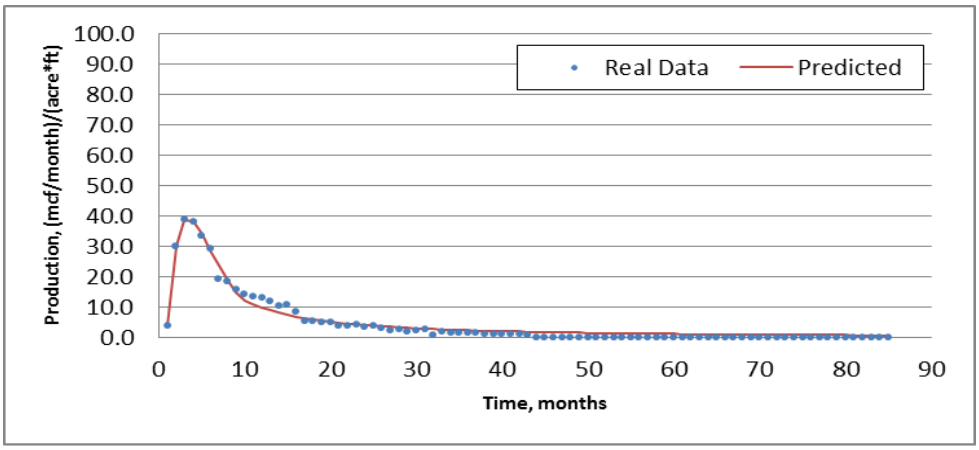

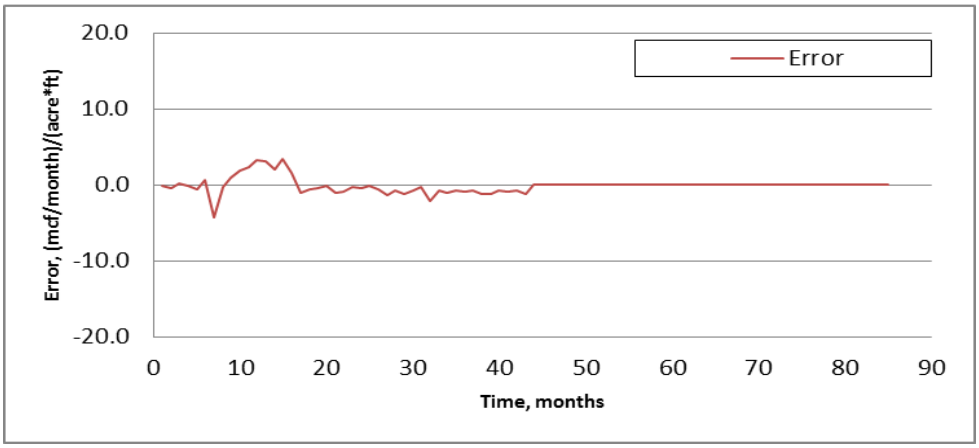

Well No.	39
Starting (Actual) Pmax (mcf/month)/(acre*ft)	38.9
Starting (Actual) Tp (months)	3
Starting di	0.5
Starting b	0.5
Best Fit Pmax (mcf/month)/(acre*ft)	39.22
Best Fit Tp (months)	3.4
Best Fit Di (1/month)	0.2783
Best Fit b	0.7366
SSQ	90
R^2	0.98

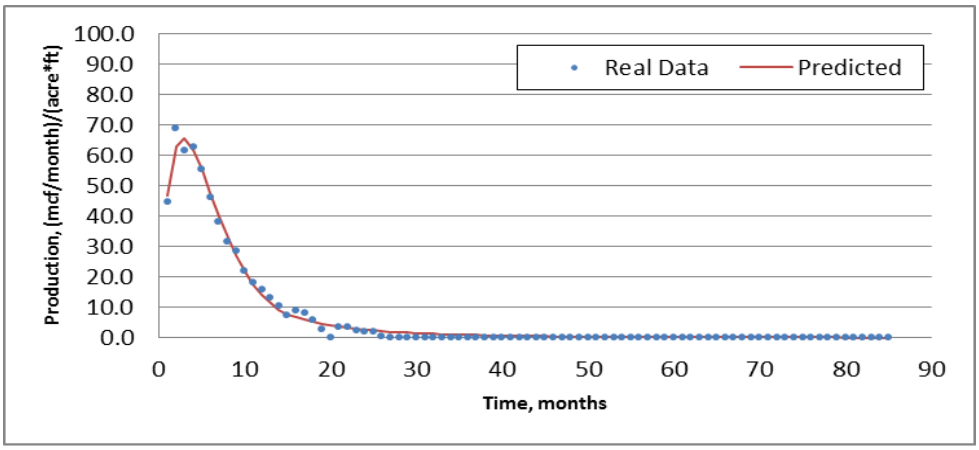

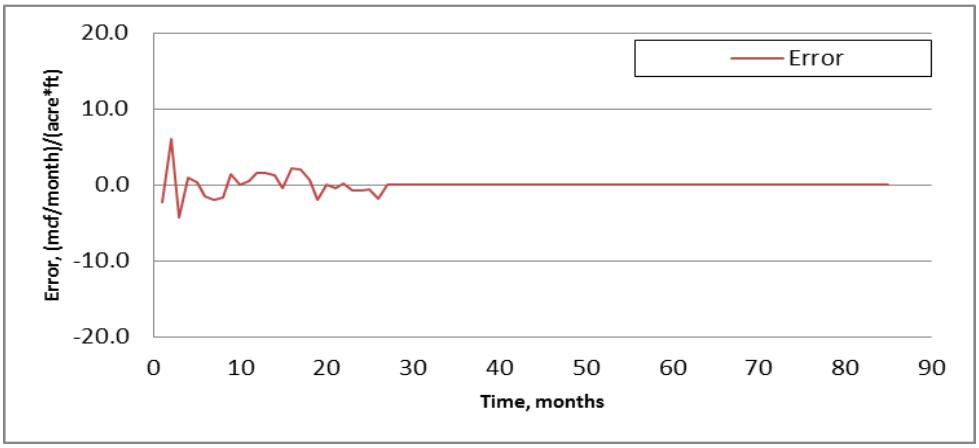

Well No.	40
Starting (Actual) Pmax (mcf/month)/(acre*ft)	68.7
Starting (Actual) Tp (months)	2
Starting di	0.5
Starting b	0.5
Best Fit Pmax (mcf/month)/(acre*ft)	65.64
Best Fit Tp (months)	2.82
Best Fit Di (1/month)	0.2357
Best Fit b	0.2599
SSQ	96
R^2	0.99

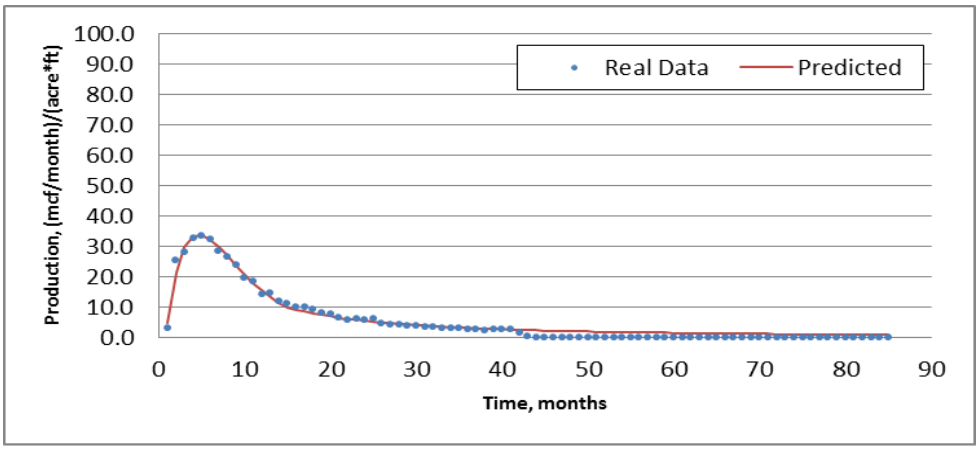

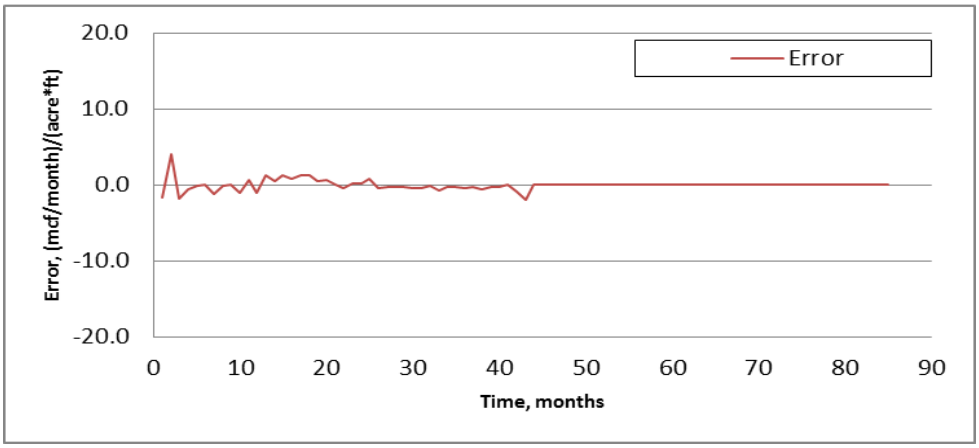

Well No.	41
Starting (Actual) Pmax (mcf/month)/(acre*ft)	33.5
Starting (Actual) Tp (months)	5
Starting di	0.5
Starting b	0.5
Best Fit Pmax (mcf/month)/(acre*ft)	33.78
Best Fit Tp (months)	4.62
Best Fit Di (1/month)	0.1808
Best Fit b	0.6666
SSQ	42
R^2	0.99

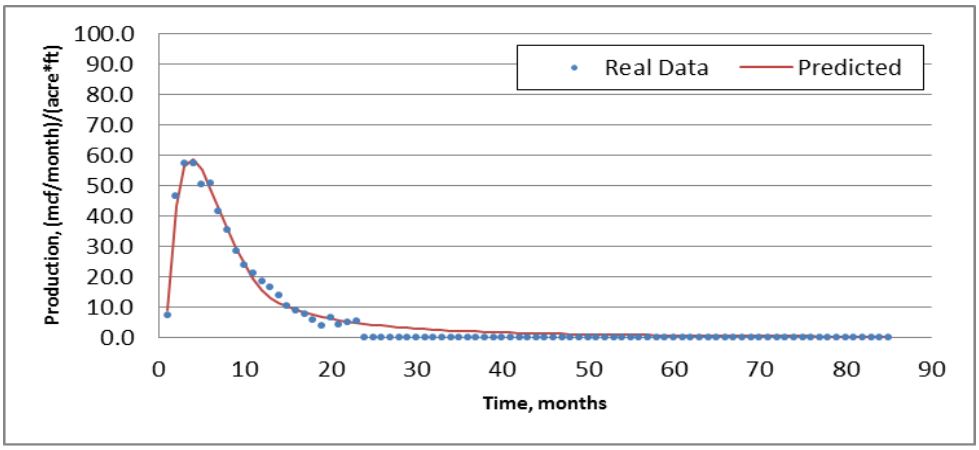

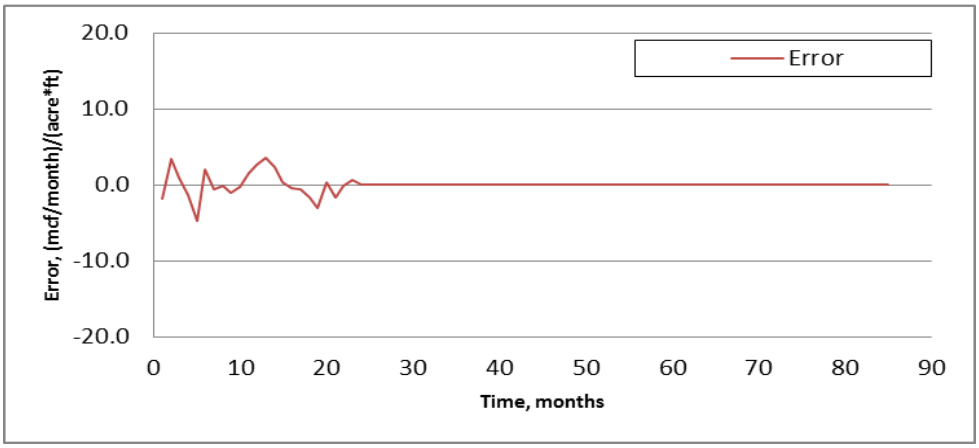

Well No.	42
Starting (Actual) Pmax (mcf/month)/(acre*ft)	57.4
Starting (Actual) Tp (months)	3
Starting di	0.5
Starting b	0.5
Best Fit Pmax (mcf/month)/(acre*ft)	58.72
Best Fit Tp (months)	3.77
Best Fit Di (1/month)	0.2355
Best Fit b	0.4452
SSQ	88
R^2	0.99

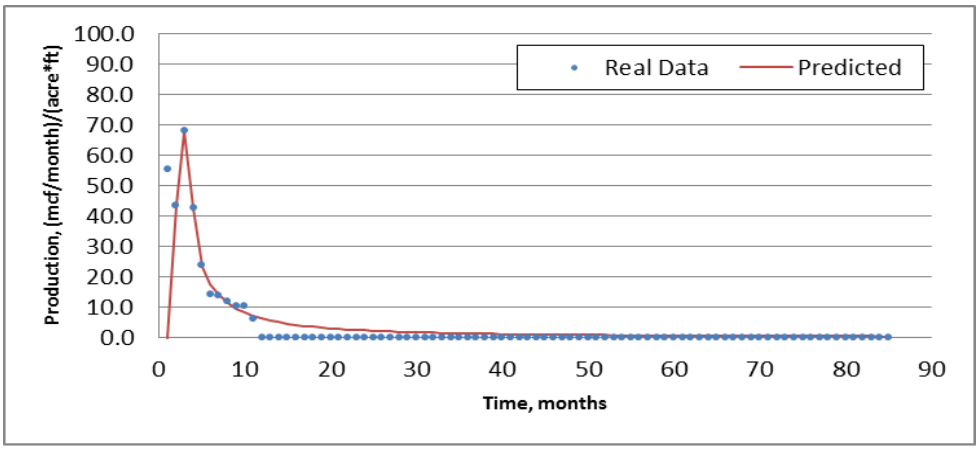

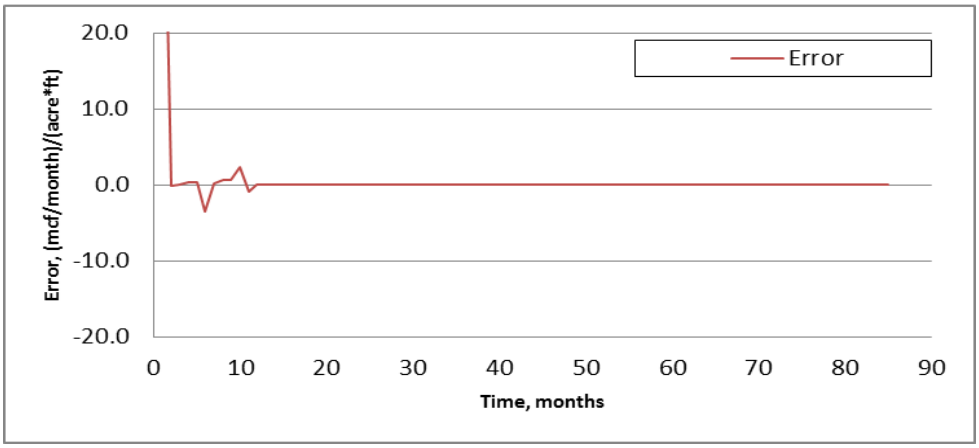

Well No.	43
Starting (Actual) Pmax (mcf/month)/(acre*ft)	67.9
Starting (Actual) Tp (months)	3
Starting di	0.5
Starting b	0.5
Best Fit Pmax (mcf/month)/(acre*ft)	71.74
Best Fit Tp (months)	2.65
Best Fit Di (1/month)	0.755
Best Fit b	0.7676
SSQ	3078
R^2	0.46

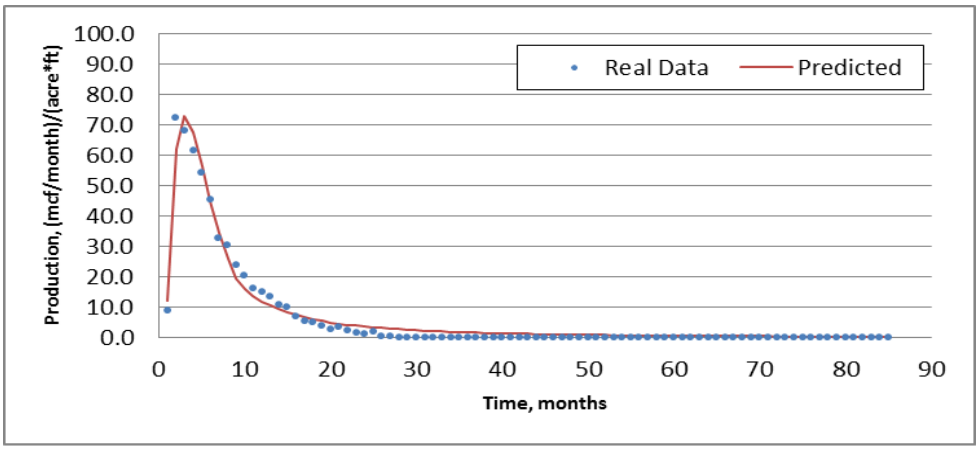

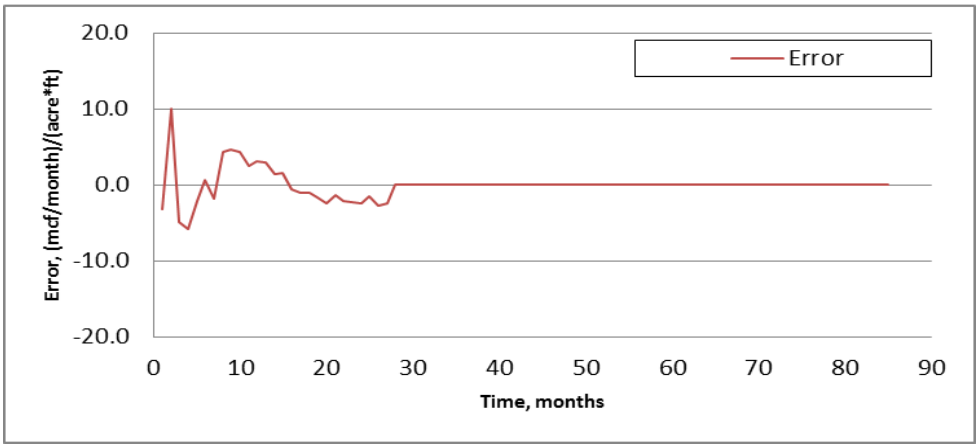

Well No.	44
Starting (Actual) Pmax (mcf/month)/(acre*ft)	72.2
Starting (Actual) Tp (months)	2
Starting di	0.5
Starting b	0.5
Best Fit Pmax (mcf/month)/(acre*ft)	72.91
Best Fit Tp (months)	3
Best Fit Di (1/month)	0.3237
Best Fit b	0.4908
SSQ	307
R^2	0.98

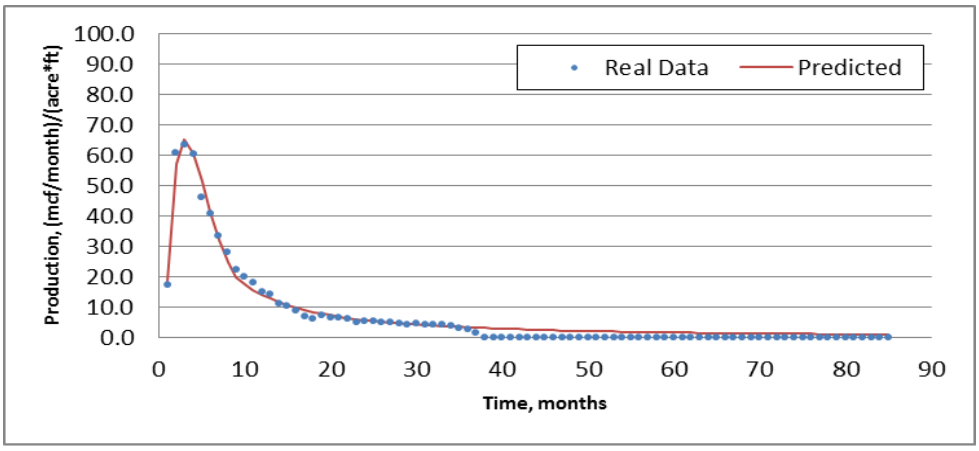

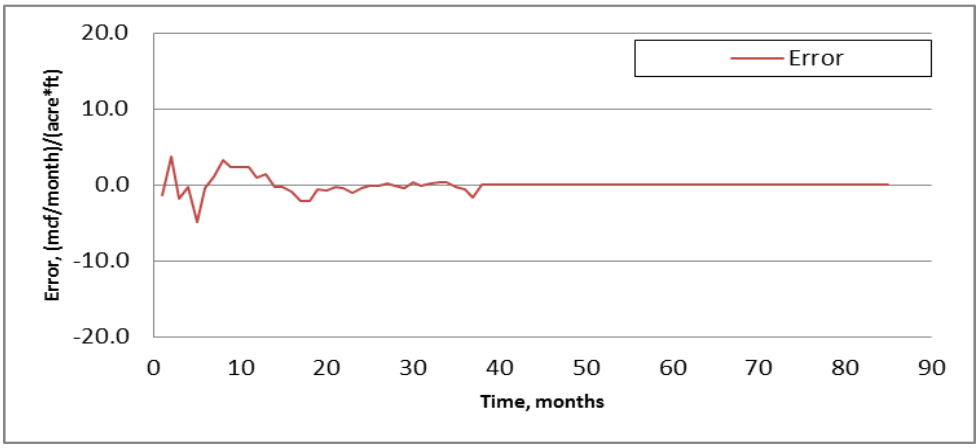

Well No.	45
Starting (Actual) Pmax (mcf/month)/(acre*ft)	63.5
Starting (Actual) Tp (months)	3
Starting di	0.5
Starting b	0.5
Best Fit Pmax (mcf/month)/(acre*ft)	65.24
Best Fit Tp (months)	2.98
Best Fit Di (1/month)	0.3095
Best Fit b	0.7186
SSQ	91
R^2	0.99

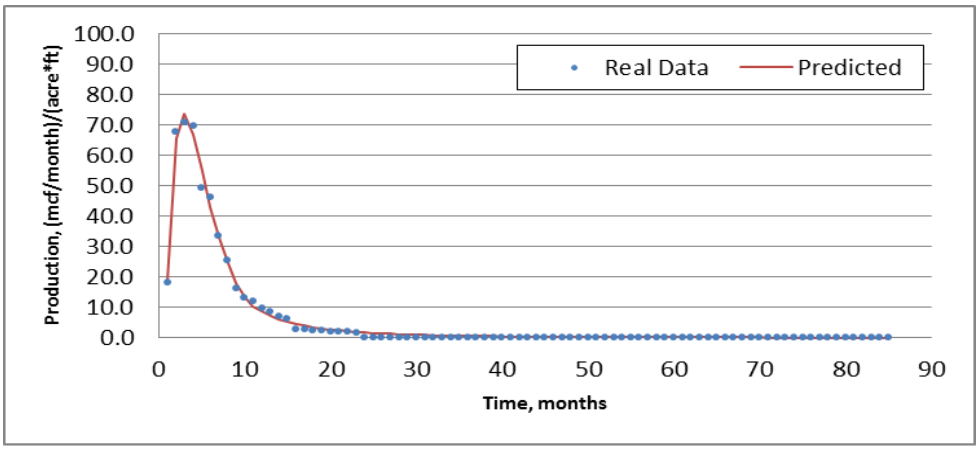

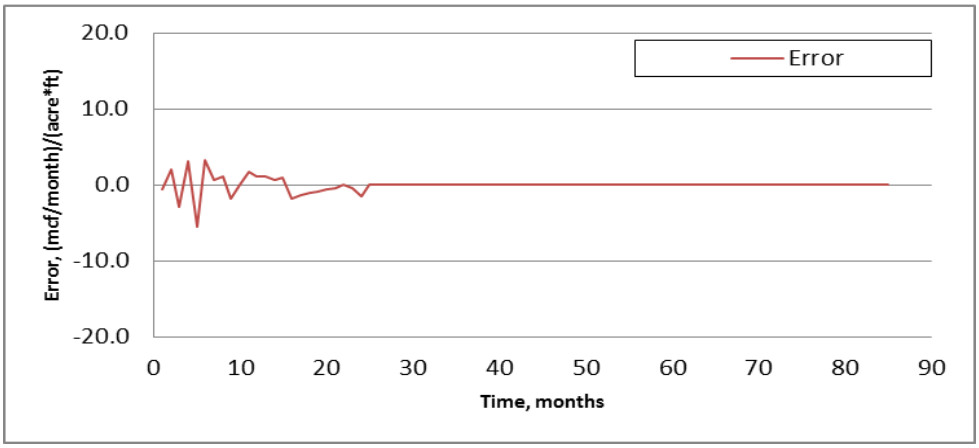

Well No.	46
Starting (Actual) Pmax (mcf/month)/(acre*ft)	70.8
Starting (Actual) Tp (months)	3
Starting di	0.5
Starting b	0.5
Best Fit Pmax (mcf/month)/(acre*ft)	73.74
Best Fit Tp (months)	2.87
Best Fit Di (1/month)	0.3321
Best Fit b	0.3036
SSQ	84
R^2	0.99

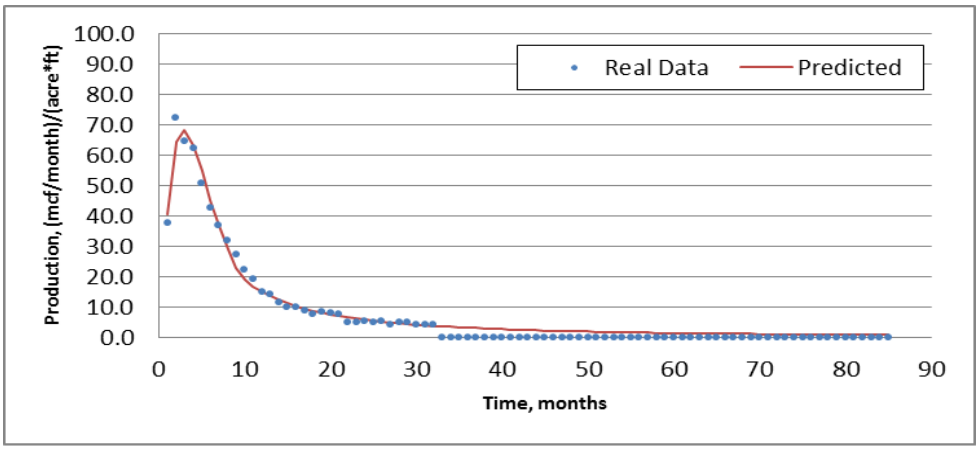

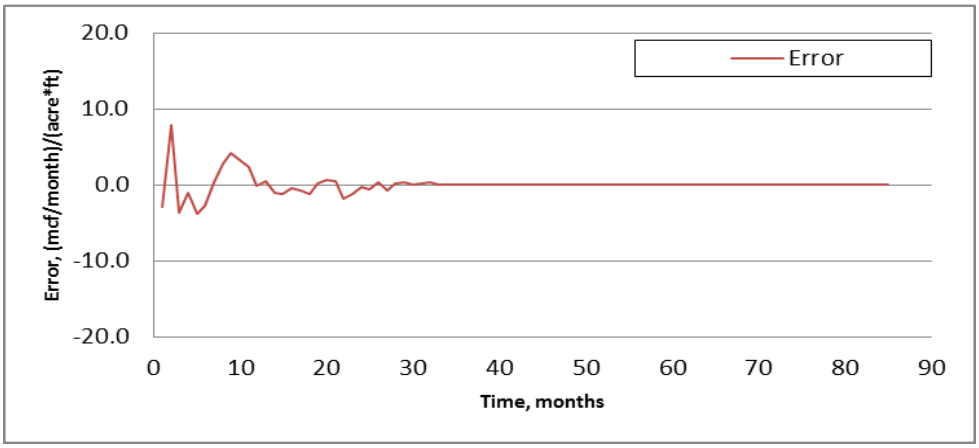

Well No.	47
Starting (Actual) Pmax (mcf/month)/(acre*ft)	72.2
Starting (Actual) Tp (months)	2
Starting di	0.5
Starting b	0.5
Best Fit Pmax (mcf/month)/(acre*ft)	68.46
Best Fit Tp (months)	2.81
Best Fit Di (1/month)	0.2729
Best Fit b	0.6246
SSQ	162
R^2	0.99

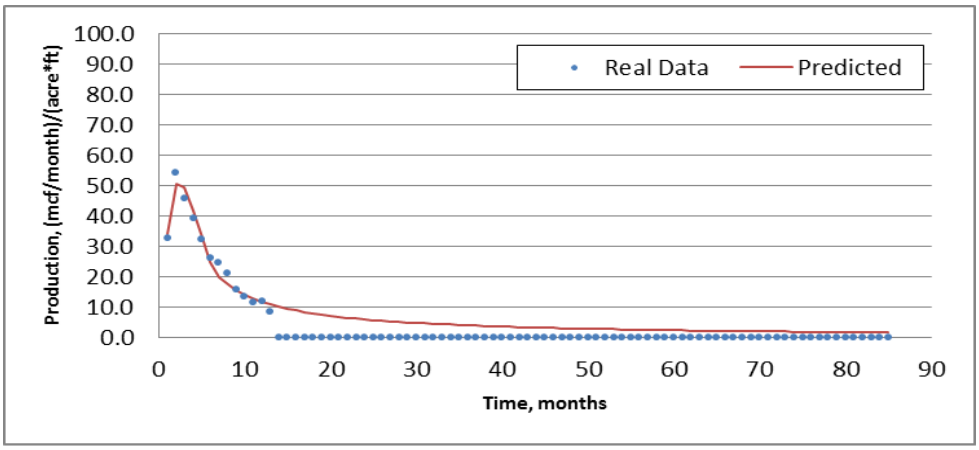

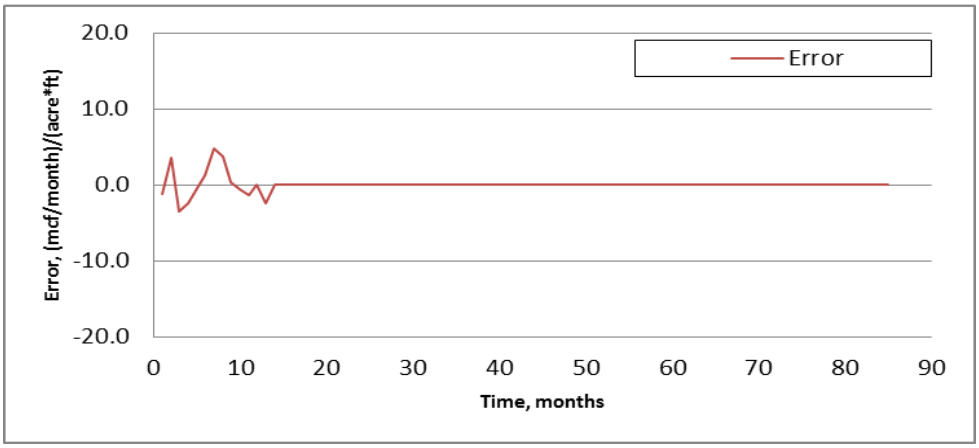

Well No.	48
Starting (Actual) Pmax (mcf/month)/(acre*ft)	54.2
Starting (Actual) Tp (months)	2
Starting di	0.5
Starting b	0.5
Best Fit Pmax (mcf/month)/(acre*ft)	51.4
Best Fit Tp (months)	2.33
Best Fit Di (1/month)	0.345
Best Fit b	1
SSQ	80
R^2	0.97

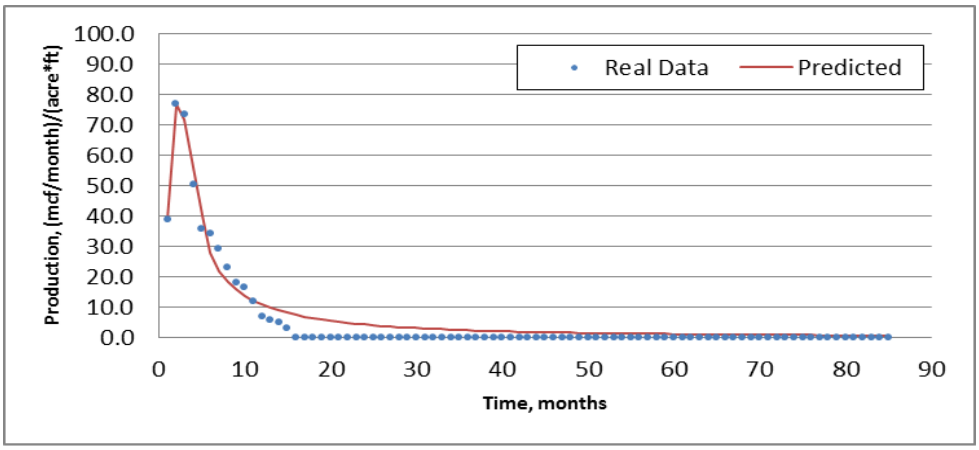

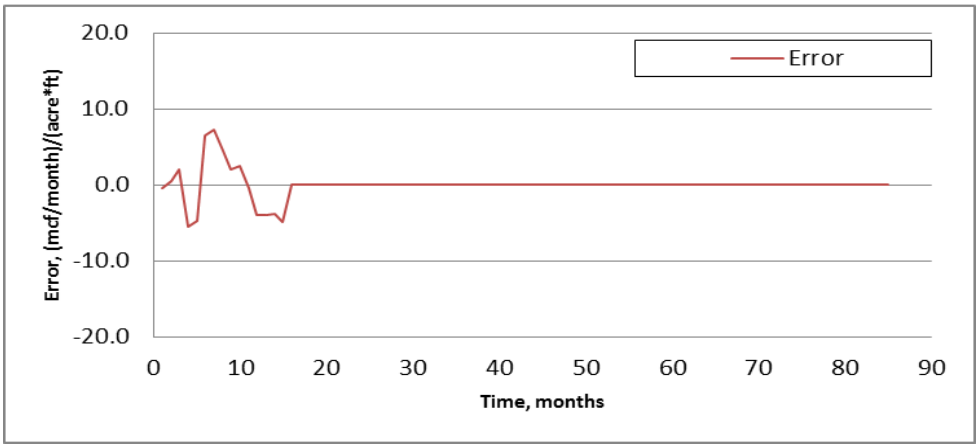

Well No.	49
Starting (Actual) Pmax (mcf/month)/(acre*ft)	76.9
Starting (Actual) Tp (months)	2
Starting di	0.5
Starting b	0.5
Best Fit Pmax (mcf/month)/(acre*ft)	77.4
Best Fit Tp (months)	2.24
Best Fit Di (1/month)	0.4278
Best Fit b	0.6978
SSQ	254
R^2	0.97

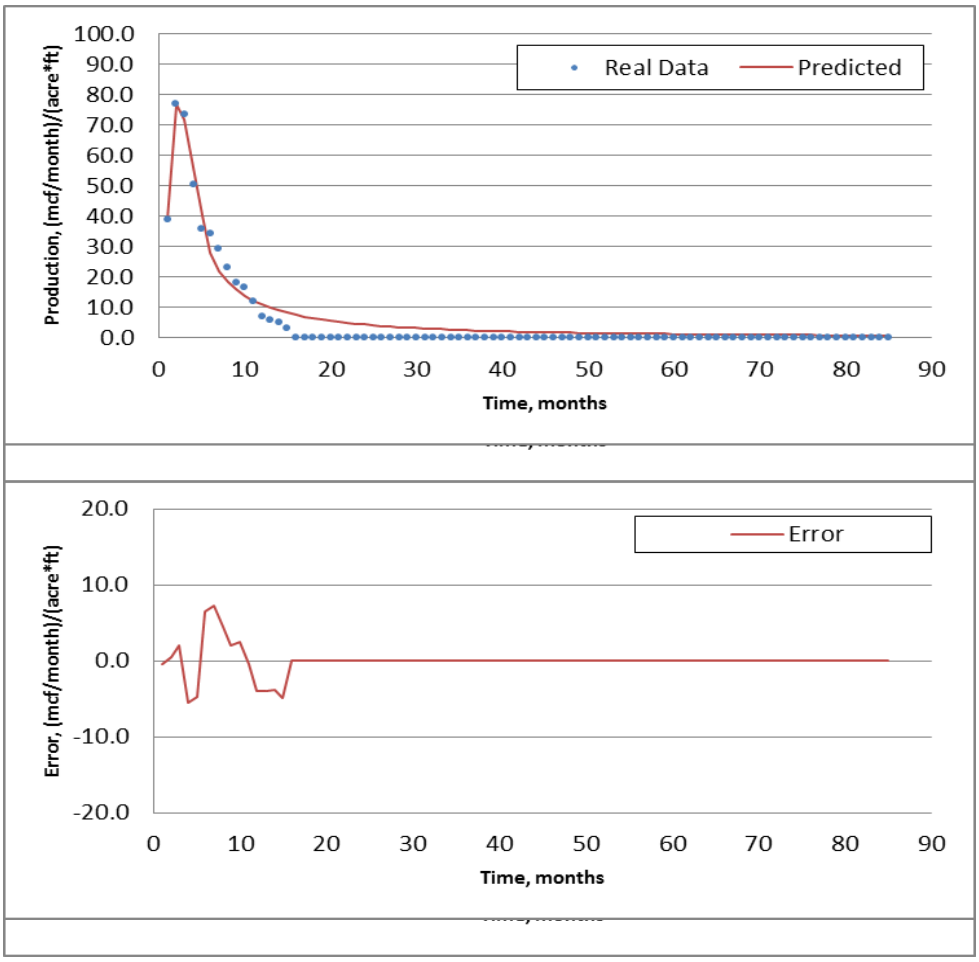

Well No.	50
Starting (Actual) Pmax (mcf/month)/(acre*ft)	71.7
Starting (Actual) Tp (months)	3
Starting di	0.5
Starting b	0.5
Best Fit Pmax (mcf/month)/(acre*ft)	67.65
Best Fit Tp (months)	2.54
Best Fit Di (1/month)	0.3468
Best Fit b	0.8571
SSQ	270
R^2	0.97

Appendix C:

Best Fit Curve Parameters for Simulated Data

Seam Thickness (ft)	Permeability (md)	Reservoir Pressure (psi)	Gas Content (scf/ton)	Horizontal Lateral Spacing (ft)	Actual P_{max} (mcf/month)	Actual T_{max} (months)	Best Fit P_{max} (mcf/month)	Best Fit T_{max} (months)	Best Fit b	Best Fit d_i	SSQ	R^2
24.3	8	50	100	600	309792	4	130683	8.0	1.00	0.03	1.38E+11	0.42
24.3	8	500	100	600	342643	5	145594	8.2	1.00	0.03	1.57E+11	0.45
24.3	8	1000	100	600	373450	5	165721	9.3	1.00	0.03	1.79E+11	0.49
24.3	8	50	100	800	279765	4	116760	6.4	1.00	0.03	8.49E+10	0.49
24.3	8	500	100	800	308101	4	130268	7.2	1.00	0.03	9.81E+10	0.51
24.3	8	1000	100	800	341060	4	144592	7.6	1.00	0.03	1.16E+11	0.53
24.3	8	1500	100	800	365912	4	167921	0.0	1.00	0.03	1.33E+11	0.55
16.6	8	1000	100	600	309188	3	169759	6.8	1.00	0.07	1.10E+11	0.60
16.6	8	1500	100	800	318446	3	153745	0.0	1.00	0.05	7.61E+10	0.62
24.3	0.7	500	433	800	1523574	4	854536	8.4	1.00	0.07	2.48E+12	0.63
16.6	8	1000	100	800	290973	3	136702	6.1	1.00	0.06	6.59E+10	0.63
24.3	0.7	500	433	600	1697052	5	1093075	8.9	1.00	0.08	3.86E+12	0.63
24.3	0.7	1000	433	600	1740206	5	1121003	8.9	1.00	0.08	3.95E+12	0.64
24.3	0.7	1000	433	800	1560712	4	911019	8.3	1.00	0.08	2.54E+12	0.65
24.3	0.7	1500	433	600	1785507	5	1156456	8.9	1.00	0.08	4.04E+12	0.66
24.3	8	50	100	400	358994	6	220668	12.4	1.00	0.06	1.57E+11	0.67
24.3	0.7	1500	433	800	1603447	4	964549	8.1	1.00	0.09	2.59E+12	0.68
24.3	8	1500	100	600	385800	5	256884	9.8	1.00	0.08	1.80E+11	0.69
16.6	8	1500	100	600	335683	4	228027	6.7	1.00	0.11	1.18E+11	0.71
24.3	0.7	500	600	600	2508290	11	1417791	17.8	0.00	0.03	6.95E+12	0.73
24.3	8	500	100	400	363062	6	243880	12.6	1.00	0.06	1.46E+11	0.74
8.91	2.5	1000	268	800	692790	2	404678	0.0	1.00	0.09	2.48E+11	0.74
24.3	0.7	500	433	400	1828029	6	1330302	11.5	1.00	0.07	3.93E+12	0.75
24.3	0.7	1500	600	600	2596966	11	1508647	18.0	0.00	0.03	7.44E+12	0.75
24.3	0.7	1000	433	400	1825078	6	1335968	11.8	1.00	0.07	3.82E+12	0.76
8.91	2.5	500	268	800	675440	2	392092	0.0	1.00	0.09	2.18E+11	0.76
16.6	8	1000	100	400	378319	5	263970	7.5	1.00	0.11	1.21E+11	0.77
24.3	0.2	1500	600	400	2537186	5	2206556	7.0	1.00	0.18	9.52E+12	0.77
24.3	0.7	1500	433	400	1823740	6	1391203	11.6	1.00	0.07	3.70E+12	0.78
8.91	0.7	500	600	800	1498727	2	943939	0.0	1.00	0.08	1.13E+12	0.78
24.3	0.2	1000	600	400	2529079	5	2217962	6.9	1.00	0.18	9.16E+12	0.78
24.3	0.2	500	600	400	2509993	5	2212426	6.8	1.00	0.19	8.81E+12	0.79
24.3	0.2	1500	600	600	1937312	4	1668726	5.8	1.00	0.19	4.95E+12	0.80
16.6	8	500	100	800	261708	3	197441	4.5	1.00	0.19	6.05E+10	0.80
16.6	8	50	100	400	350954	4	300538	5.3	1.00	0.21	1.10E+11	0.80
16.6	8	500	100	400	357570	4	317304	5.6	1.00	0.19	1.21E+11	0.80
24.3	2.5	500	100	400	261061	6	239811	7.2	1.00	0.18	8.39E+10	0.80
24.3	2.5	50	100	400	236801	6	222083	7.2	1.00	0.19	6.87E+10	0.81
16.6	8	1500	100	400	395683	5	287852	7.9	1.00	0.11	1.18E+11	0.81
24.3	2.5	1500	100	400	322394	6	294719	7.1	1.00	0.18	1.30E+11	0.81
16.6	2.5	500	268	800	905404	3	628041	6.1	1.00	0.12	6.04E+11	0.81
24.3	0.2	1000	600	600	1913026	4	1660696	5.7	1.00	0.19	4.67E+12	0.81
24.3	2.5	1000	100	400	290501	6	270813	7.1	1.00	0.19	1.05E+11	0.81
24.3	2.5	500	433	800	1792197	12	1270589	16.7	0.00	0.04	4.08E+12	0.81
24.3	8	1000	100	400	367543	6	280531	12.4	1.00	0.06	1.26E+11	0.82
24.3	2.5	500	268	800	909476	4	731387	8.7	1.00	0.09	9.04E+11	0.82
16.6	0.7	1500	433	400	1823501	5	1509416	6.5	1.00	0.15	2.93E+12	0.82
16.6	2.5	1000	268	800	916039	3	658260	6.1	1.00	0.12	6.29E+11	0.82
24.3	0.2	500	600	600	1886138	4	1648094	5.6	1.00	0.19	4.41E+12	0.82
16.6	0.7	1500	433	800	1378576	3	1036253	4.7	1.00	0.18	1.45E+12	0.83
16.6	2.5	500	268	600	934893	4	746712	6.7	1.00	0.12	7.65E+11	0.83
16.6	0.7	1000	433	400	1811135	4	1538632	6.2	1.00	0.16	2.88E+12	0.83
16.6	2.5	1500	268	800	918999	3	689642	6.2	1.00	0.12	6.56E+11	0.83
24.3	2.5	1000	268	800	911220	4	755195	8.8	1.00	0.09	9.14E+11	0.83
16.6	0.7	500	433	400	1813379	4	1540880	6.0	1.00	0.17	2.84E+12	0.83
16.6	8	50	100	800	238465	3	195153	4.0	1.00	0.23	5.05E+10	0.84
16.6	2.5	1000	268	600	949326	4	771586	6.8	1.00	0.12	7.74E+11	0.84
24.3	0.7	1000	600	600	2557225	11	1777080	14.0	1.00	0.05	4.46E+12	0.84
16.6	0.7	1000	433	800	1341622	3	1031972	4.6	1.00	0.19	1.37E+12	0.84
24.3	2.5	1500	268	800	910893	4	778845	8.9	1.00	0.09	9.27E+11	0.84
24.3	0.7	500	600	800	1993817	8	1636555	10.8	1.00	0.07	4.08E+12	0.84
24.3	0.7	1000	600	800	2071711	8	1669688	10.8	1.00	0.07	4.16E+12	0.85
24.3	2.5	500	268	600	896174	5	814298	10.3	1.00	0.07	9.81E+11	0.85
24.3	0.7	1500	600	800	2151661	8	1704343	10.9	1.00	0.07	4.26E+12	0.85
24.3	2.5	50	100	800	147120	5	140916	6.2	1.00	0.20	2.06E+10	0.85
24.3	2.5	1000	268	600	899753	5	827726	10.6	1.00	0.07	9.91E+11	0.85
16.6	8	50	100	600	284221	3	269860	4.2	1.00	0.30	8.54E+10	0.85
16.6	2.5	1500	268	600	964449	4	796017	6.9	1.00	0.12	7.79E+11	0.85
24.3	2.5	1000	100	800	178594	5	166500	5.9	1.00	0.19	3.14E+10	0.85
24.3	2.5	50	100	600	176821	5	171018	6.4	1.00	0.20	2.90E+10	0.85
24.3	2.5	500	100	800	161886	5	153799	6.0	1.00	0.20	2.51E+10	0.85
8.91	2.5	1500	268	800	702992	2	564891	3.6	1.00	0.24	2.89E+11	0.85
24.3	0.7	1500	268	400	1023890	5	942615	7.1	1.00	0.18	1.18E+12	0.85

Seam Thickness (ft)	Permeability (md)	Reservoir Pressure (psi)	Gas Content (scf/ton)	Horizontal Lateral Spacing (ft)	Actual P_{max} (mcf/month)	Actual T_{max} (months)	Best Fit P_{max} (mcf/month)	Best Fit T_{max} (months)	Best Fit b	Best Fit d_i	SSQ	R^2
16.6	8	500	100	600	300075	3	293092	4.3	1.00	0.29	1.00E+11	0.86
24.3	2.5	1500	268	600	904394	5	853707	10.7	1.00	0.07	1.00E+12	0.86
16.6	2.5	50	100	400	213155	4	198621	5.3	1.00	0.24	3.54E+10	0.86
24.3	2.5	1500	100	800	196249	5	185314	5.8	1.00	0.19	3.93E+10	0.86
24.3	2.5	500	100	600	197295	5	189995	6.2	1.00	0.21	3.53E+10	0.86
8.91	8	1500	100	400	329439	3	259850	3.8	1.00	0.25	4.63E+10	0.86
16.6	0.7	1000	433	600	1537248	3	1415219	4.6	1.00	0.24	2.39E+12	0.86
16.6	0.7	500	433	600	1534331	3	1390366	4.5	1.00	0.24	2.30E+12	0.86
24.3	0.7	1000	268	400	997446	5	916215	7.0	1.00	0.18	1.09E+12	0.86
16.6	0.7	500	433	800	1309653	3	1042408	4.4	1.00	0.20	1.30E+12	0.86
24.3	0.2	1500	600	800	1606787	4	1460789	5.2	1.00	0.21	2.86E+12	0.86
8.91	0.7	1000	600	800	1516399	2	1229233	3.9	1.00	0.20	1.41E+12	0.86
16.6	2.5	500	100	400	237563	4	216657	5.2	1.00	0.24	4.26E+10	0.86
16.6	0.7	1500	433	600	1521198	3	1443924	4.7	1.00	0.24	2.46E+12	0.86
24.3	0.7	500	268	400	965081	5	888380	7.0	1.00	0.18	1.00E+12	0.86
24.3	2.5	1000	100	600	220499	5	212492	6.1	1.00	0.21	4.47E+10	0.86
16.6	0.7	1500	600	600	1930366	7	1763057	8.0	1.00	0.10	3.34E+12	0.86
16.6	2.5	1000	100	400	266067	4	240387	5.2	1.00	0.24	5.24E+10	0.87
16.6	0.7	1000	600	600	1867886	6	1768604	7.8	1.00	0.10	3.27E+12	0.87
8.91	2.5	1000	268	600	732013	2	658905	3.7	1.00	0.24	3.51E+11	0.87
16.6	0.7	500	600	600	1811722	6	1720392	7.7	1.00	0.10	3.16E+12	0.87
24.3	2.5	1500	100	600	244470	5	236333	6.1	1.00	0.21	5.65E+10	0.87
24.3	2.5	1500	268	200	1368806	23	1167301	19.6	0.52	0.09	1.73E+12	0.87
8.91	0.7	500	600	600	1603525	2	1471817	4.0	1.00	0.21	1.70E+12	0.87
24.3	8	1500	100	400	371406	6	305123	12.9	1.00	0.06	1.05E+11	0.87
16.6	0.7	1500	600	800	1763360	4	1610013	6.7	1.00	0.12	3.06E+12	0.87
8.91	2.5	1500	268	600	696329	2	645026	3.9	1.00	0.22	3.36E+11	0.87
24.3	0.2	1000	600	800	1576927	4	1481714	5.1	1.00	0.22	2.78E+12	0.87
8.91	2.5	500	268	600	743065	2	673442	3.4	1.00	0.27	3.52E+11	0.87
8.91	8	1000	100	400	295951	3	252551	3.5	1.00	0.28	3.87E+10	0.87
16.6	0.2	1500	600	400	2318666	4	1964398	5.1	1.00	0.23	4.12E+12	0.87
16.6	0.7	1000	600	800	1737914	4	1574990	6.6	1.00	0.12	2.94E+12	0.88
16.6	2.5	1500	100	400	295414	4	268766	5.2	1.00	0.25	6.41E+10	0.88
16.6	0.7	500	600	800	1707915	4	1543372	6.5	1.00	0.12	2.84E+12	0.88
24.3	0.2	500	600	800	1550053	4	1477109	5.0	1.00	0.23	2.69E+12	0.88
8.91	0.7	1500	600	800	1508645	2	1315953	3.8	1.00	0.23	1.43E+12	0.88
8.91	0.7	1000	600	600	1537419	3	1500246	4.0	1.00	0.21	1.63E+12	0.88
16.6	0.2	1000	600	400	2278283	4	1956849	5.1	1.00	0.23	3.94E+12	0.88
8.91	8	500	100	400	264547	3	238665	3.3	1.00	0.31	3.28E+10	0.88
24.3	0.2	1500	433	400	1312155	6	1204387	7.3	1.00	0.17	1.48E+12	0.89
24.3	0.2	1000	433	400	1280134	6	1173953	7.3	1.00	0.17	1.39E+12	0.89
24.3	0.7	1000	268	600	742483	5	704026	6.0	1.00	0.19	5.07E+11	0.89
24.3	0.7	500	268	600	717500	5	676733	6.0	1.00	0.19	4.64E+11	0.89
24.3	0.2	500	433	400	1249335	6	1147741	7.4	1.00	0.17	1.31E+12	0.89
8.91	8	50	100	400	240877	3	225765	3.1	1.00	0.33	2.85E+10	0.89
16.6	0.2	500	600	400	2240076	4	1944671	5.0	1.00	0.23	3.78E+12	0.89
24.3	0.7	1500	268	600	769916	5	737223	6.0	1.00	0.20	5.53E+11	0.89
16.6	2.5	50	100	600	159672	4	154650	4.7	1.00	0.26	1.43E+10	0.89
24.3	2.5	1000	268	200	1326831	23	976683	17.6	0.38	0.06	1.25E+12	0.89
8.91	2.5	50	100	400	165922	3	151174	3.3	1.00	0.33	1.13E+10	0.90
16.6	2.5	50	100	800	130339	4	130091	4.5	1.00	0.27	1.03E+10	0.90
8.91	0.7	1500	600	600	1604569	3	1511541	4.1	1.00	0.21	1.50E+12	0.90
16.6	0.2	1500	600	800	1433909	3	1200413	4.1	1.00	0.23	1.29E+12	0.90
8.91	2.5	500	268	400	923345	3	744869	4.4	1.00	0.20	3.02E+11	0.90
24.3	2.5	500	268	200	1280548	23	953056	17.5	0.38	0.06	1.15E+12	0.90
16.6	0.7	1500	268	400	954564	4	819735	5.2	1.00	0.22	5.78E+11	0.90
8.91	2.5	500	100	400	180985	3	162796	3.3	1.00	0.32	1.33E+10	0.90
16.6	2.5	500	100	800	141547	4	143725	4.4	1.00	0.27	1.28E+10	0.90
16.6	2.5	500	100	600	174412	4	172638	4.6	1.00	0.27	1.77E+10	0.90
8.91	2.5	1000	268	400	942343	3	765740	4.5	1.00	0.19	3.01E+11	0.90
8.91	2.5	1500	268	400	959322	3	766709	4.7	1.00	0.18	3.01E+11	0.90
16.6	0.2	1000	600	800	1408664	3	1193121	4.0	1.00	0.23	1.22E+12	0.90
24.3	0.7	1000	268	800	644395	4	588502	5.6	1.00	0.19	3.43E+11	0.90
16.6	0.7	1000	268	400	921902	4	799227	5.2	1.00	0.22	5.30E+11	0.91
16.6	2.5	1000	100	800	157328	3	159782	4.3	1.00	0.28	1.63E+10	0.91
8.91	2.5	1000	100	400	199881	3	177727	3.3	1.00	0.32	1.59E+10	0.91
24.3	0.7	1500	268	800	668161	4	610774	5.5	1.00	0.20	3.72E+11	0.91
8.91	8	1500	100	600	228407	2	235485	3.0	1.00	0.34	3.79E+10	0.91
16.6	2.5	1000	100	600	192368	4	193130	4.5	1.00	0.28	2.25E+10	0.91
16.6	0.7	500	268	400	890565	4	776894	5.2	1.00	0.22	4.89E+11	0.91
24.3	0.7	500	268	800	621112	4	572371	5.5	1.00	0.20	3.16E+11	0.91
8.91	2.5	1500	100	400	220562	3	192582	3.4	1.00	0.31	1.90E+10	0.91
16.6	2.5	1500	100	800	177156	3	176745	4.3	1.00	0.28	2.05E+10	0.91

Seam Thickness (ft)	Permeability (md)	Reservoir Pressure (psi)	Gas Content (scf/ton)	Horizontal Lateral Spacing (ft)	Actual P_{max} (mcf/month)	Actual T_{max} (months)	Best Fit P_{max} (mcf/month)	Best Fit T_{max} (months)	Best Fit b	Best Fit d_i	SSQ	R^2
16.6	0.2	500	600	800	1385082	3	1183551	4.0	1.00	0.24	1.16E+12	0.91
8.91	0.7	1500	433	400	1450069	3	1253003	3.5	1.00	0.27	8.68E+11	0.91
16.6	2.5	1500	100	600	211909	4	214303	4.5	1.00	0.28	2.82E+10	0.91
1.21	2.5	50	100	400	41516	1	43145	1.4	1.00	0.76	3.46E+08	0.91
16.6	0.2	500	600	600	1663008	3	1596448	4.2	1.00	0.29	2.15E+12	0.91
16.6	0.2	1000	600	600	1683181	3	1632589	4.2	1.00	0.29	2.26E+12	0.92
16.6	0.2	1500	600	600	1699115	3	1675332	4.2	1.00	0.30	2.37E+12	0.92
8.91	8	50	100	600	204907	2	197691	2.6	1.00	0.43	2.43E+10	0.92
16.6	0.7	1000	268	800	571592	3	507142	4.3	1.00	0.24	1.83E+11	0.92
8.91	8	1500	100	800	222116	2	215305	2.7	1.00	0.40	2.90E+10	0.92
24.3	0.7	1000	600	400	2941804	17	2648890	17.1	0.91	0.07	5.02E+12	0.92
16.6	0.7	500	268	800	552111	3	489750	4.3	1.00	0.23	1.69E+11	0.92
16.6	0.2	1500	433	400	1169066	4	1054429	5.5	1.00	0.21	7.47E+11	0.92
24.3	0.2	1500	433	800	812368	5	772884	6.3	1.00	0.19	4.48E+11	0.92
16.6	0.2	1000	433	400	1140378	4	1028174	5.5	1.00	0.21	7.02E+11	0.92
24.3	0.2	1000	433	800	791852	5	754816	6.4	1.00	0.19	4.26E+11	0.92
8.91	8	50	100	800	170503	2	159852	2.5	1.00	0.42	1.62E+10	0.92
8.91	8	1000	100	600	226746	2	229616	2.8	1.00	0.39	3.32E+10	0.92
16.6	0.7	1500	268	800	591367	3	530230	4.3	1.00	0.24	1.99E+11	0.92
8.91	0.7	1000	433	400	1404354	3	1257959	3.4	1.00	0.29	8.30E+11	0.92
24.3	0.2	500	433	800	771454	5	737733	6.4	1.00	0.19	4.05E+11	0.92
16.6	0.2	500	433	400	1111046	4	1007107	5.5	1.00	0.21	6.61E+11	0.92
1.21	2.5	50	100	800	26974	1	27375	1.3	1.00	0.77	1.24E+08	0.92
1.21	2.5	500	100	400	44676	1	46105	1.3	1.00	0.73	3.93E+08	0.92
24.3	8	1500	600	200	2889349	42	2755530	28.8	0.25	0.04	8.69E+12	0.92
8.91	8	500	100	800	186203	2	177761	2.6	1.00	0.42	1.95E+10	0.92
8.91	8	1000	100	800	205441	2	198169	2.6	1.00	0.42	2.40E+10	0.92
24.3	0.7	1500	600	400	2980908	17	2608492	17.1	0.84	0.07	4.83E+12	0.92
8.91	2.5	50	100	600	118354	3	121096	2.9	1.00	0.37	4.75E+09	0.92
1.21	2.5	50	100	600	32072	1	32766	1.3	1.00	0.77	1.70E+08	0.92
24.3	0.2	500	433	600	919507	5	893913	6.6	1.00	0.19	5.55E+11	0.92
8.91	8	500	100	600	218364	2	218069	2.6	1.00	0.43	2.85E+10	0.92
8.91	0.7	500	433	400	1368277	3	1254698	3.4	1.00	0.30	8.01E+11	0.92
24.3	0.2	1000	433	600	946512	5	918768	6.5	1.00	0.19	5.84E+11	0.92
24.3	0.2	1500	433	600	973239	5	942850	6.5	1.00	0.20	6.14E+11	0.92
24.3	0.7	500	600	400	2910768	16	2325741	16.8	0.75	0.06	4.21E+12	0.92
24.3	2.5	500	600	600	4147538	24	3564538	21.0	0.55	0.08	9.44E+12	0.92
8.91	2.5	50	100	800	98459	2	102989	2.8	1.00	0.38	3.36E+09	0.93
1.21	2.5	1000	100	400	47905	1	49390	1.3	1.00	0.71	4.39E+08	0.93
24.3	2.5	1000	600	600	4210240	24	3505467	20.8	0.51	0.07	9.36E+12	0.93
24.3	8	1000	600	200	2829990	44	2732288	28.6	0.25	0.04	7.94E+12	0.93
8.91	2.5	500	433	800	1116591	3	1083276	4.4	1.00	0.18	5.53E+11	0.93
16.6	2.5	500	268	400	927508	5	873585	8.8	1.00	0.10	4.08E+11	0.93
16.6	0.7	500	600	200	2920469	15	2833775	12.9	0.68	0.17	3.57E+12	0.93
24.3	2.5	1500	600	600	4275083	24	3563578	20.8	0.50	0.07	9.51E+12	0.93
8.91	2.5	500	100	600	128254	3	134235	2.9	1.00	0.38	5.78E+09	0.93
24.3	8	500	433	600	3218974	29	2821480	23.1	0.34	0.07	6.26E+12	0.93
24.3	8	1000	433	600	3267940	29	2870352	23.1	0.33	0.07	6.40E+12	0.93
8.91	2.5	500	100	800	111141	2	113945	2.8	1.00	0.39	4.14E+09	0.93
24.3	8	500	600	200	2775063	45	2710315	28.5	0.26	0.04	7.23E+12	0.93
24.3	8	1500	100	200	432115	20	336700	15.6	0.33	0.07	8.80E+10	0.93
8.91	0.7	1500	100	400	101379	5	99800	5.9	0.91	0.22	3.23E+09	0.93
1.21	2.5	1500	100	400	50772	1	52277	1.3	1.00	0.66	4.91E+08	0.93
1.21	2.5	500	100	800	29962	1	29698	1.2	1.00	0.74	1.33E+08	0.93
1.21	2.5	1000	100	600	38280	1	38185	1.2	1.00	0.73	2.25E+08	0.93
8.91	2.5	1000	433	800	1149413	3	1137773	4.4	1.00	0.19	5.66E+11	0.93
1.21	2.5	500	100	600	35083	1	35402	1.3	1.00	0.76	1.75E+08	0.93
16.6	2.5	500	433	800	1676128	7	1356611	8.3	1.00	0.10	9.69E+11	0.93
24.3	2.5	1000	433	800	1805781	12	1563387	13.1	1.00	0.06	1.38E+12	0.93
24.3	8	1500	433	600	3318543	29	2991259	23.4	0.35	0.08	6.41E+12	0.93
8.91	0.7	1500	100	800	61838	5	61011	5.6	0.93	0.21	1.19E+09	0.93
24.3	8	1000	433	800	2868884	27	2355435	20.7	0.38	0.06	4.29E+12	0.93
16.6	8	500	433	600	2837863	18	2521618	15.5	0.44	0.10	3.72E+12	0.93
8.91	0.7	1500	100	600	75004	5	73971	5.8	0.92	0.21	1.73E+09	0.93
16.6	2.5	1000	268	400	933108	5	894573	9.0	1.00	0.09	3.89E+11	0.93
16.6	0.7	500	268	600	635934	3	639934	4.4	1.00	0.27	2.44E+11	0.93
16.6	0.7	1000	268	600	657220	3	662888	4.4	1.00	0.28	2.65E+11	0.93
24.3	8	1500	433	800	2923246	27	2456259	21.0	0.40	0.06	4.46E+12	0.93
16.6	0.7	1500	268	600	675323	3	687406	4.4	1.00	0.28	2.86E+11	0.93
24.3	8	500	433	800	2810818	27	2316930	20.6	0.39	0.06	4.07E+12	0.93
8.91	2.5	1000	100	600	140732	3	148780	2.9	1.00	0.38	7.10E+09	0.93
16.6	8	1000	433	600	2887854	18	2569157	15.6	0.44	0.10	3.75E+12	0.94
8.91	0.7	500	433	800	952822	2	890616	2.7	1.00	0.38	4.41E+11	0.94

Seam Thickness (ft)	Permeability (md)	Reservoir Pressure (psi)	Gas Content (scf/ton)	Horizontal Lateral Spacing (ft)	Actual P_{max} (mcf/month)	Actual T_{max} (months)	Best Fit P_{max} (mcf/month)	Best Fit T_{max} (months)	Best Fit b	Best Fit d_i	SSQ	R^2
24.3	8	1500	268	400	1915428	28	1585949	22.0	0.31	0.06	1.89E+12	0.94
16.6	2.5	1000	433	800	1716479	7	1404022	8.4	1.00	0.10	9.87E+11	0.94
24.3	2.5	1500	433	800	1822230	13	1600656	13.2	1.00	0.06	1.37E+12	0.94
8.91	0.7	1000	433	800	973640	2	917653	2.7	1.00	0.38	4.63E+11	0.94
8.91	2.5	1000	100	800	124687	2	126618	2.8	1.00	0.40	5.14E+09	0.94
8.91	2.5	1500	433	800	1184826	4	1172222	4.4	1.00	0.19	5.61E+11	0.94
24.3	8	1000	268	400	1872976	28	1546970	21.9	0.31	0.06	1.76E+12	0.94
8.91	0.7	1000	100	800	56765	5	55065	6.1	0.87	0.20	9.48E+08	0.94
8.91	2.5	500	433	600	1333539	4	1239224	4.9	1.00	0.17	5.28E+11	0.94
8.91	0.7	1000	100	600	68658	5	67147	6.1	0.88	0.21	1.36E+09	0.94
24.3	2.5	500	268	400	1037917	16	905927	14.7	1.00	0.06	4.53E+11	0.94
24.3	8	500	268	400	1825598	28	1509135	21.9	0.32	0.06	1.64E+12	0.94
16.6	2.5	1500	433	800	1757102	7	1447118	8.4	1.00	0.10	1.00E+12	0.94
8.91	0.7	1500	433	800	995713	2	950447	2.7	1.00	0.39	4.84E+11	0.94
24.3	2.5	1000	268	400	1099781	16	930246	14.9	0.98	0.05	4.77E+11	0.94
16.6	8	1500	433	600	2951864	19	2519590	15.3	0.39	0.10	3.60E+12	0.94
8.91	0.7	1000	100	400	92217	5	89349	6.2	0.84	0.20	2.41E+09	0.94
8.91	0.7	1500	433	600	1108382	2	1114372	2.9	1.00	0.37	7.07E+11	0.94
8.91	2.5	1000	433	600	1370026	4	1258979	5.0	1.00	0.17	5.20E+11	0.94
16.6	2.5	1500	268	400	940453	5	922687	9.1	1.00	0.09	3.72E+11	0.94
24.3	8	500	433	400	3472511	30	3283483	24.2	0.23	0.08	7.10E+12	0.94
24.3	2.5	1500	268	400	1152084	16	959190	15.2	0.96	0.05	5.03E+11	0.94
24.3	8	1000	433	400	3519408	30	3333925	24.2	0.23	0.08	7.23E+12	0.94
8.91	2.5	1500	100	600	154503	3	162153	2.9	1.00	0.38	8.62E+09	0.94
8.91	0.7	1000	433	600	1132060	2	1123658	2.8	1.00	0.39	6.97E+11	0.94
1.21	2.5	1000	100	800	33119	1	32554	1.2	1.00	0.74	1.36E+08	0.94
24.3	8	1500	433	400	3567442	30	3385871	24.2	0.22	0.08	7.37E+12	0.94
16.6	0.7	1500	100	800	71555	8	69009	9.7	0.98	0.14	1.73E+09	0.94
16.6	0.7	1000	600	200	2958390	15	2754686	12.7	0.63	0.15	2.90E+12	0.94
8.91	0.7	500	433	600	1130540	2	1114495	2.7	1.00	0.40	6.76E+11	0.94
24.3	0.2	1500	433	200	1643850	8	1542225	9.9	1.00	0.18	1.13E+12	0.94
16.6	0.7	1500	100	400	115733	8	111247	10.0	0.91	0.13	4.60E+09	0.94
16.6	0.7	1500	100	600	86358	8	82860	9.8	0.93	0.13	2.53E+09	0.94
24.3	0.2	1000	433	200	1610332	8	1507539	9.9	1.00	0.18	1.09E+12	0.94
24.3	0.2	500	433	200	1574198	8	1473114	9.9	1.00	0.18	1.05E+12	0.94
1.21	2.5	1500	100	600	41605	1	41063	1.2	1.00	0.68	2.39E+08	0.94
8.91	2.5	1500	100	800	137401	2	139487	2.7	1.00	0.40	6.30E+09	0.94
24.3	8	500	268	200	1390355	30	1352346	21.9	0.40	0.08	1.07E+12	0.94
8.91	2.5	1500	433	600	1402931	4	1276137	5.1	1.00	0.17	5.11E+11	0.94
24.3	8	1000	268	200	1412437	30	1377330	21.9	0.41	0.08	1.11E+12	0.94
24.3	8	1500	268	200	1434728	29	1402789	22.0	0.41	0.08	1.15E+12	0.94
24.3	8	500	600	800	4812085	27	4475485	22.9	0.34	0.08	1.17E+13	0.94
1.21	2.5	1500	100	800	36481	1	36849	0.9	1.00	0.70	1.61E+08	0.94
16.6	8	500	600	800	4360922	18	4057940	15.6	0.44	0.12	7.39E+12	0.94
24.3	8	1000	600	800	4868338	27	4671716	23.2	0.36	0.09	1.20E+13	0.94
8.91	0.7	500	600	400	1829702	3	1707562	5.0	1.00	0.17	8.67E+11	0.94
16.6	0.7	1500	600	200	2995308	15	2795934	12.7	0.63	0.15	2.82E+12	0.95
8.91	0.2	1500	600	400	1590133	3	1457019	3.3	1.00	0.31	1.05E+12	0.95
24.3	2.5	1500	100	200	382129	10	356218	10.1	1.00	0.18	4.23E+10	0.95
24.3	2.5	1000	100	200	352045	10	330658	10.0	1.00	0.18	3.70E+10	0.95
24.3	2.5	500	100	200	313756	10	303454	9.9	1.00	0.19	3.20E+10	0.95
24.3	2.5	50	100	200	291674	8	278661	9.8	1.00	0.19	2.77E+10	0.95
24.3	8	1000	100	200	391040	20	316367	15.2	0.35	0.08	5.87E+10	0.95
16.6	8	1000	600	800	4421230	18	4122079	15.6	0.44	0.12	7.36E+12	0.95
8.91	0.7	1500	268	400	680812	3	616353	3.3	1.00	0.30	1.59E+11	0.95
24.3	8	1500	600	800	4925817	27	4741458	23.2	0.36	0.09	1.19E+13	0.95
1.21	8	50	100	600	38024	1	41906	0.0	1.00	0.43	2.42E+08	0.95
24.3	0.7	1500	268	200	1056018	11	1039107	10.7	1.00	0.15	3.91E+11	0.95
8.91	0.2	1000	600	400	1553466	3	1449981	3.2	1.00	0.31	1.02E+12	0.95
24.3	0.7	1000	268	200	1039930	11	1020075	10.6	1.00	0.16	3.80E+11	0.95
8.91	0.7	1000	600	400	1845758	4	1729515	5.1	1.00	0.17	8.47E+11	0.95
24.3	0.7	500	268	200	1019627	11	1000089	10.5	1.00	0.16	3.68E+11	0.95
16.6	2.5	1000	268	200	1169669	15	924041	11.7	0.00	0.09	5.09E+11	0.95
16.6	8	500	268	200	1348853	19	1297061	14.8	0.45	0.12	6.96E+11	0.95
24.3	0.2	500	600	200	2179427	10	2083510	11.6	1.00	0.11	1.53E+12	0.95
8.91	0.2	1500	433	400	911301	3	808456	3.5	1.00	0.28	2.25E+11	0.95
16.6	8	1000	268	200	1372321	19	1322955	14.9	0.45	0.12	7.21E+11	0.95
16.6	8	1500	600	800	4483622	18	4189368	15.6	0.43	0.12	7.28E+12	0.95
8.91	0.7	1500	600	400	1901375	4	1751811	5.2	1.00	0.17	8.59E+11	0.95
8.91	0.7	1000	268	400	657124	3	603383	3.3	1.00	0.31	1.48E+11	0.95
16.6	8	1500	268	200	1396401	19	1349150	14.9	0.45	0.12	7.45E+11	0.95
8.91	0.7	500	100	800	50787	5	49132	6.5	0.81	0.19	6.42E+08	0.95
1.21	8	50	100	400	48794	1	53963	0.0	1.00	0.41	2.64E+08	0.95

Seam Thickness (ft)	Permeability (md)	Reservoir Pressure (psi)	Gas Content (scf/ton)	Horizontal Lateral Spacing (ft)	Actual P_{max} (mcf/month)	Actual T_{max} (months)	Best Fit P_{max} (mcf/month)	Best Fit T_{max} (months)	Best Fit b	Best Fit d_i	SSQ	R^2
8.91	0.2	1000	433	400	891345	3	794853	3.5	1.00	0.29	2.12E+11	0.95
8.91	0.2	500	433	400	873232	3	779742	3.5	1.00	0.28	2.01E+11	0.95
16.6	2.5	500	433	600	1803079	10	1482595	10.1	0.99	0.08	8.90E+11	0.95
8.91	0.7	500	100	600	60847	5	59110	6.6	0.79	0.19	9.25E+08	0.95
8.91	0.7	500	268	400	636216	3	589302	3.3	1.00	0.31	1.39E+11	0.95
8.91	0.2	500	600	400	1522479	3	1446613	3.2	1.00	0.32	9.91E+11	0.95
16.6	0.2	1500	433	800	721471	4	710668	4.7	1.00	0.25	2.17E+11	0.95
8.91	0.7	500	100	400	80867	5	78465	6.7	0.75	0.19	1.63E+09	0.95
16.6	0.2	1000	433	800	706205	4	693711	4.7	1.00	0.25	2.06E+11	0.95
16.6	0.2	1000	600	200	2326727	7	2203773	7.5	1.00	0.21	1.14E+12	0.95
1.21	0.7	500	268	400	160491	1	161545	1.3	1.00	0.61	3.50E+09	0.95
16.6	0.2	500	433	800	691855	4	677218	4.8	1.00	0.25	1.95E+11	0.95
16.6	8	500	433	400	3205525	20	2984755	16.4	0.30	0.11	3.80E+12	0.95
16.6	0.2	500	600	200	2300023	7	2222914	7.3	1.00	0.22	1.13E+12	0.95
16.6	2.5	1500	268	200	1200236	15	964206	11.7	0.45	0.10	4.09E+11	0.95
8.91	2.5	500	433	200	1884355	8	1813620	7.6	0.59	0.24	7.44E+11	0.95
16.6	2.5	1500	600	400	4295312	18	4102364	15.2	0.51	0.13	6.09E+12	0.95
16.6	2.5	1000	433	600	1832383	10	1525676	10.1	0.96	0.09	8.80E+11	0.95
16.6	0.2	1500	600	200	2350578	7	2210052	7.6	1.00	0.20	1.12E+12	0.95
24.3	0.2	1000	600	200	2170119	10	2079675	11.8	1.00	0.11	1.42E+12	0.95
24.3	2.5	500	600	400	4643423	27	4369526	22.3	0.42	0.09	8.88E+12	0.95
1.21	0.7	1000	268	400	164012	1	164638	1.2	1.00	0.59	3.57E+09	0.95
24.3	0.2	1500	268	800	260106	10	246294	11.6	1.00	0.11	2.27E+10	0.95
16.6	8	1000	433	400	3251973	20	3014246	16.5	0.00	0.11	4.18E+12	0.95
16.6	0.2	500	433	600	841837	4	809000	4.9	1.00	0.24	2.63E+11	0.95
16.6	0.2	1000	433	600	860895	4	829488	4.9	1.00	0.25	2.76E+11	0.95
16.6	2.5	1500	433	400	2390136	15	2172140	13.3	0.68	0.10	1.75E+12	0.95
16.6	8	1500	433	400	3299767	20	3065974	16.5	0.00	0.11	4.24E+12	0.95
24.3	0.2	1500	268	600	312202	10	295546	11.6	1.00	0.11	3.13E+10	0.95
16.6	0.2	1500	433	600	880862	4	849800	4.8	1.00	0.25	2.91E+11	0.95
24.3	2.5	1000	600	400	4703781	27	4431683	22.3	0.41	0.09	8.89E+12	0.95
16.6	0.2	1500	268	800	241635	6	235168	8.3	1.00	0.15	1.76E+10	0.95
24.3	0.2	1500	268	200	530944	11	500216	12.6	1.00	0.11	1.30E+11	0.95
24.3	0.2	1500	268	400	415039	10	396634	11.8	1.00	0.11	5.43E+10	0.95
24.3	0.2	1000	268	200	509964	11	478382	12.8	1.00	0.10	1.17E+11	0.95
24.3	2.5	500	433	400	2678673	24	2317952	20.1	0.56	0.07	2.51E+12	0.95
24.3	2.5	1000	433	400	2750936	24	2358283	20.1	0.55	0.07	2.60E+12	0.95
24.3	2.5	1500	433	400	2817718	24	2400515	20.2	0.54	0.07	2.71E+12	0.95
16.6	0.2	1500	268	600	291089	7	284391	8.3	1.00	0.15	2.48E+10	0.95
1.21	8	50	100	800	32244	1	36067	0.0	1.00	0.44	1.63E+08	0.95
8.91	2.5	1000	433	200	1910927	8	1844202	7.6	0.59	0.24	7.28E+11	0.95
1.21	0.2	500	433	400	233624	1	246345	1.4	1.00	0.64	6.48E+09	0.95
24.3	0.2	1000	268	800	246075	10	234548	11.9	1.00	0.11	1.93E+10	0.95
1.21	0.7	1500	268	400	168026	1	168007	1.2	1.00	0.58	3.58E+09	0.96
16.6	0.2	1500	268	400	392808	7	382056	8.5	1.00	0.15	4.27E+10	0.96
24.3	0.2	500	268	200	488267	11	458628	13.0	1.00	0.10	1.05E+11	0.96
24.3	0.7	500	600	200	3139483	22	3041968	18.7	0.60	0.11	3.38E+12	0.96
24.3	2.5	1500	600	400	4765757	27	4495605	22.3	0.41	0.09	8.87E+12	0.96
16.6	0.2	1000	268	800	233828	7	226023	8.5	1.00	0.15	1.54E+10	0.96
1.21	0.2	1000	433	400	239329	1	250063	1.4	1.00	0.64	6.63E+09	0.96
24.3	8	500	433	200	2076796	30	2114715	23.9	0.55	0.06	2.19E+12	0.96
16.6	2.5	500	433	400	2290753	15	2019934	13.1	0.65	0.10	1.50E+12	0.96
24.3	8	500	268	800	1244001	17	1028244	15.3	0.85	0.06	4.43E+11	0.96
16.6	2.5	1500	433	600	1858371	10	1558513	10.2	1.00	0.09	8.64E+11	0.96
8.91	0.7	500	600	200	2337413	7	2130620	6.6	0.66	0.23	9.51E+11	0.96
8.91	8	500	268	800	861787	4	757662	4.8	1.00	0.18	1.39E+11	0.96
1.21	0.7	500	268	600	125676	1	124484	1.2	1.00	0.62	1.76E+09	0.96
16.6	0.7	1000	100	800	63096	8	61055	10.5	0.85	0.12	1.09E+09	0.96
24.3	8	1000	433	200	2093198	29	2133485	24.0	0.54	0.06	2.19E+12	0.96
16.6	2.5	500	268	200	1136356	15	916952	11.5	0.46	0.10	3.29E+11	0.96
1.21	0.2	1500	433	400	245695	1	253878	1.4	1.00	0.64	6.73E+09	0.96
24.3	0.7	1000	600	200	3165998	22	3081533	18.7	0.60	0.11	3.33E+12	0.96
8.91	2.5	1500	433	200	1938069	8	1875405	7.6	0.59	0.24	7.13E+11	0.96
16.6	2.5	1000	433	400	2342902	15	2058357	13.1	0.64	0.10	1.53E+12	0.96
24.3	8	500	100	200	352462	19	293715	14.9	0.00	0.08	4.38E+10	0.96
16.6	8	1000	268	400	1620616	17	1369981	14.7	0.00	0.09	9.80E+11	0.96
24.3	8	1500	433	200	2111617	29	2152497	24.1	0.54	0.06	2.18E+12	0.96
24.3	0.2	1000	268	600	296400	11	285726	11.9	1.00	0.11	2.65E+10	0.96
16.6	0.7	1000	100	600	75459	8	73518	10.6	0.83	0.12	1.56E+09	0.96
8.91	0.2	1000	268	400	333404	4	316773	5.2	1.00	0.23	1.97E+10	0.96
24.3	0.2	1500	600	200	2161472	10	2100302	12.0	1.00	0.11	1.30E+12	0.96
16.6	2.5	500	433	200	2154444	17	2122449	14.1	0.51	0.13	1.40E+12	0.96
8.91	0.2	1500	268	800	211877	4	209517	4.8	1.00	0.24	8.89E+09	0.96

Seam Thickness (ft)	Permeability (md)	Reservoir Pressure (psi)	Gas Content (scf/ton)	Horizontal Lateral Spacing (ft)	Actual P_{max} (mcf/month)	Actual T_{max} (months)	Best Fit P_{max} (mcf/month)	Best Fit T_{max} (months)	Best Fit b	Best Fit d_i	SSQ	R^2
8.91	0.2	1500	268	400	346169	4	335160	5.0	1.00	0.24	2.19E+10	0.96
24.3	8	1500	268	600	1503547	23	1258132	19.1	0.49	0.06	7.36E+11	0.96
8.91	8	1000	268	800	894569	4	783112	4.8	1.00	0.18	1.41E+11	0.96
16.6	0.2	1000	268	600	282512	7	275693	8.5	1.00	0.15	2.14E+10	0.96
24.3	8	1000	268	800	1266745	17	1057407	15.4	0.85	0.06	4.54E+11	0.96
8.91	0.2	1500	268	600	257046	4	251535	4.9	1.00	0.24	1.25E+10	0.96
16.6	0.7	1000	100	400	101335	10	98338	10.7	0.80	0.12	2.79E+09	0.96
8.91	8	500	268	200	1211072	10	1140584	8.0	0.51	0.22	2.77E+11	0.96
16.6	8	1500	268	400	1675589	18	1434461	14.6	0.41	0.09	7.97E+11	0.96
16.6	8	500	433	200	2088326	18	2129159	15.9	0.56	0.10	1.62E+12	0.96
24.3	0.2	1000	268	400	398506	11	383374	12.0	1.00	0.11	4.53E+10	0.96
1.21	0.7	1000	268	600	129523	1	127879	1.1	1.00	0.61	1.78E+09	0.96
8.91	0.2	1000	268	800	206254	4	199459	5.0	1.00	0.23	7.86E+09	0.96
8.91	0.2	1000	268	600	248932	4	239073	5.1	1.00	0.23	1.11E+10	0.96
16.6	8	500	268	400	1584916	17	1363214	14.4	0.44	0.09	7.06E+11	0.96
8.91	0.2	500	268	400	320080	4	303201	5.3	1.00	0.22	1.77E+10	0.96
16.6	0.2	1000	268	400	380165	7	372501	8.6	1.00	0.15	3.66E+10	0.96
24.3	0.7	1500	600	200	3192816	22	3121542	18.7	0.59	0.11	3.26E+12	0.96
1.21	0.7	500	268	800	106870	1	105199	1.1	1.00	0.62	1.17E+09	0.96
8.91	0.7	500	268	800	424349	2	415006	2.7	1.00	0.39	5.37E+10	0.96
24.3	0.7	1500	100	200	151630	12	146395	14.2	1.00	0.10	8.99E+09	0.96
16.6	2.5	1000	433	200	2178983	17	2152472	14.1	0.51	0.13	1.40E+12	0.96
16.6	8	1000	433	200	2108170	20	2150365	16.0	0.56	0.10	1.63E+12	0.96
16.6	0.2	500	268	800	227099	7	218028	8.7	1.00	0.14	1.30E+10	0.96
8.91	8	1500	268	800	925592	4	803274	5.0	1.00	0.17	1.41E+11	0.96
8.91	0.7	1000	268	800	437629	2	428556	2.7	1.00	0.39	5.78E+10	0.96
24.3	0.2	500	268	800	238353	11	227079	12.2	1.00	0.11	1.61E+10	0.96
8.91	8	1000	268	200	1234374	10	1167143	8.0	0.52	0.22	2.82E+11	0.96
16.6	8	500	268	800	1063189	10	948701	9.3	1.00	0.09	2.65E+11	0.96
24.3	8	1000	268	600	1438127	23	1207267	18.9	0.48	0.05	6.55E+11	0.96
1.21	8	500	100	400	51422	1	56116	0.0	1.00	0.38	2.39E+08	0.96
16.6	0.2	500	268	600	273617	7	262403	8.8	1.00	0.14	1.82E+10	0.96
8.91	0.2	500	600	600	1245494	2	1235739	2.7	1.00	0.41	6.20E+11	0.96
16.6	8	1500	433	200	2129858	20	2172367	16.0	0.56	0.10	1.63E+12	0.96
8.91	0.2	1000	600	600	1256860	2	1253843	2.7	1.00	0.41	6.48E+11	0.96
16.6	2.5	1500	433	200	2204220	17	2182965	14.1	0.50	0.13	1.40E+12	0.96
24.3	2.5	500	433	200	2236427	24	2245885	20.8	0.46	0.09	1.90E+12	0.96
24.3	2.5	500	433	600	1852226	18	1676122	16.3	0.77	0.05	1.09E+12	0.96
24.3	2.5	1000	433	200	2259117	24	2234627	20.6	0.44	0.09	1.91E+12	0.96
16.6	0.2	500	268	400	366632	7	350910	8.8	1.00	0.14	3.11E+10	0.96
8.91	0.7	1500	268	800	450468	2	443074	2.7	1.00	0.39	6.19E+10	0.96
8.91	0.2	500	268	600	239823	4	228543	5.2	1.00	0.22	9.71E+09	0.96
1.21	0.7	1000	268	800	110633	1	108710	1.1	1.00	0.61	1.19E+09	0.96
1.21	0.7	1500	268	600	133883	1	131887	1.1	1.00	0.60	1.82E+09	0.96
24.3	0.7	1000	100	200	135149	13	128063	14.9	1.00	0.09	6.24E+09	0.96
8.91	0.2	1500	600	600	1257928	2	1266448	2.7	1.00	0.40	6.73E+11	0.96
8.91	0.7	500	268	600	492798	2	499648	2.8	1.00	0.39	7.38E+10	0.96
8.91	8	1500	268	200	1258060	10	1193159	8.0	0.51	0.22	2.88E+11	0.96
8.91	0.2	500	268	800	199426	4	190738	5.2	1.00	0.22	6.81E+09	0.96
24.3	8	1000	600	400	5235519	29	5375881	24.1	0.18	0.09	1.18E+13	0.96
24.3	0.2	500	268	600	287266	11	273695	12.3	1.00	0.11	2.21E+10	0.96
16.6	8	1000	268	800	1099098	10	977523	9.4	1.00	0.09	2.74E+11	0.96
8.91	0.2	500	600	800	1043804	2	1001287	2.6	1.00	0.40	3.61E+11	0.96
24.3	8	1500	268	800	1313111	18	1138045	15.7	0.87	0.06	4.52E+11	0.96
24.3	2.5	1500	433	200	2282379	24	2303865	20.8	0.46	0.09	1.94E+12	0.96
16.6	2.5	1500	100	200	353100	6	326976	7.1	1.00	0.25	1.90E+10	0.96
8.91	0.7	1000	268	600	505691	2	514412	2.8	1.00	0.39	7.92E+10	0.96
8.91	0.2	1000	600	800	1059262	2	1020391	2.6	1.00	0.40	3.76E+11	0.96
24.3	0.7	1500	433	200	1794960	20	1535296	15.5	0.57	0.07	9.07E+11	0.96
24.3	8	500	268	600	1401604	22	1177164	18.7	0.50	0.05	5.83E+11	0.96
8.91	0.7	50	100	800	45200	6	43036	7.2	0.71	0.17	4.06E+08	0.96
16.6	2.5	1000	100	200	329120	6	298839	7.0	1.00	0.25	1.60E+10	0.96
8.91	0.2	1500	600	800	1073183	2	1040187	2.7	1.00	0.40	3.90E+11	0.96
24.3	0.2	500	268	400	385259	11	366933	12.3	1.00	0.11	3.75E+10	0.96
1.21	0.2	500	433	600	181904	1	187736	1.4	1.00	0.66	2.89E+09	0.96
24.3	2.5	1000	433	600	1916934	18	1709161	16.4	0.75	0.05	1.10E+12	0.96
8.91	0.7	1000	600	200	2381100	7	2169313	6.6	0.66	0.23	8.47E+11	0.96
1.21	8	500	100	600	40312	1	40123	0.3	1.00	0.41	2.74E+08	0.96
8.91	0.7	50	100	200	89687	5	88492	6.7	0.99	0.20	1.43E+09	0.96
8.91	0.7	1500	268	600	513910	2	527507	2.8	1.00	0.39	8.44E+10	0.96
8.91	8	500	268	600	967855	5	823070	5.6	0.97	0.15	1.55E+11	0.96
8.91	0.7	50	100	600	54344	6	51791	7.2	0.69	0.17	5.75E+08	0.96
1.21	0.2	1000	433	600	188118	1	191652	1.3	1.00	0.66	2.94E+09	0.96

Seam Thickness (ft)	Permeability (md)	Reservoir Pressure (psi)	Gas Content (scf/ton)	Horizontal Lateral Spacing (ft)	Actual P_{max} (mcf/month)	Actual T_{max} (months)	Best Fit P_{max} (mcf/month)	Best Fit T_{max} (months)	Best Fit b	Best Fit d_i	SSQ	R^2
16.6	8	1500	268	800	1127743	10	1025741	9.5	1.00	0.10	2.79E+11	0.96
24.3	8	500	600	400	5189448	29	5222171	23.9	0.17	0.08	1.09E+13	0.96
24.3	2.5	1500	433	600	1960465	18	1741593	16.6	0.72	0.05	1.12E+12	0.96
8.91	0.7	50	100	400	72703	6	69273	7.2	0.67	0.17	1.02E+09	0.96
1.21	0.2	500	600	600	292264	1	293467	0.8	1.00	0.51	9.09E+09	0.96
1.21	0.2	500	433	800	153941	1	156935	1.3	1.00	0.66	1.97E+09	0.96
1.21	0.2	500	600	400	374409	1	377487	0.8	1.00	0.47	1.40E+10	0.96
1.21	0.7	1500	268	800	114697	1	112825	1.0	1.00	0.60	1.17E+09	0.96
16.6	0.7	1500	268	200	1018524	7	970922	7.4	1.00	0.22	1.81E+11	0.96
24.3	0.7	500	100	200	118042	14	112449	15.8	1.00	0.09	4.21E+09	0.96
16.6	2.5	500	100	200	299190	6	274123	6.9	1.00	0.25	1.31E+10	0.96
1.21	0.2	1500	433	600	193744	1	195240	1.3	1.00	0.66	3.03E+09	0.96
8.91	0.7	500	100	200	103081	5	100425	6.3	1.00	0.21	1.70E+09	0.96
1.21	0.2	1000	600	600	296440	1	298999	0.8	1.00	0.51	9.19E+09	0.96
1.21	0.2	1000	433	800	160155	1	160899	1.3	1.00	0.66	2.04E+09	0.96
24.3	0.7	1000	433	200	1749594	19	1510659	15.4	0.58	0.07	8.15E+11	0.96
16.6	0.7	1500	100	200	146198	8	139742	10.0	1.00	0.13	5.54E+09	0.96
24.3	0.7	1500	100	800	74658	12	71352	13.8	0.87	0.10	1.39E+09	0.96
16.6	2.5	1000	600	400	4234996	18	3891669	14.9	0.47	0.11	4.33E+12	0.96
8.91	8	1000	268	600	1001886	5	854558	5.7	0.96	0.16	1.59E+11	0.96
8.91	0.7	1500	100	200	127980	5	125384	5.9	1.00	0.23	2.61E+09	0.96
16.6	0.7	1000	268	200	988887	7	951276	7.3	1.00	0.22	1.73E+11	0.96
16.6	2.5	1500	600	600	3600490	16	2990772	13.3	0.56	0.09	2.79E+12	0.96
8.91	0.7	1000	100	200	116212	5	112790	6.1	1.00	0.22	2.09E+09	0.96
24.3	8	1500	600	400	5282226	29	5346002	23.9	0.17	0.08	1.09E+13	0.96
16.6	0.7	1000	100	200	128388	8	124019	10.5	1.00	0.13	4.14E+09	0.96
16.6	2.5	1000	600	600	3506819	16	2936763	13.3	0.56	0.09	2.66E+12	0.96
16.6	2.5	500	600	400	4177531	18	3707105	14.7	0.44	0.11	4.09E+12	0.96
1.21	0.2	1000	600	400	378630	1	383125	0.8	1.00	0.47	1.38E+10	0.96
16.6	0.7	500	268	200	958919	7	930211	7.3	1.00	0.22	1.66E+11	0.97
24.3	0.7	1500	100	600	89608	12	85694	14.0	0.83	0.10	2.00E+09	0.97
16.6	0.2	1500	433	200	1487809	6	1397884	7.0	1.00	0.24	4.77E+11	0.97
1.21	0.2	1500	600	600	301520	1	305959	0.7	1.00	0.50	9.16E+09	0.97
16.6	2.5	50	100	200	270801	6	251904	6.9	1.00	0.25	1.10E+10	0.97
1.21	0.2	1500	433	800	165128	1	164345	1.3	1.00	0.66	2.06E+09	0.97
24.3	8	500	600	600	5046777	28	4981568	23.6	0.27	0.09	8.77E+12	0.97
16.6	0.7	500	100	200	114330	10	108558	11.1	1.00	0.12	3.00E+09	0.97
16.6	0.2	1000	433	200	1451400	6	1370882	7.0	1.00	0.24	4.64E+11	0.97
24.3	0.7	1500	100	400	119382	12	114904	14.2	0.80	0.10	3.59E+09	0.97
16.6	2.5	500	600	600	3412063	16	2886692	13.2	0.57	0.09	2.51E+12	0.97
16.6	0.2	500	433	200	1416958	6	1343110	7.0	1.00	0.24	4.49E+11	0.97
1.21	8	500	100	800	34351	1	37621	0.0	1.00	0.41	1.55E+08	0.97
16.6	0.7	50	100	200	100784	10	97613	11.7	1.00	0.12	2.31E+09	0.97
8.91	2.5	1000	600	200	2756905	10	2646007	7.8	0.56	0.20	1.30E+12	0.97
24.3	8	1000	600	600	5097030	28	5044873	23.6	0.27	0.09	8.76E+12	0.97
16.6	0.2	500	268	200	462499	7	432740	9.2	1.00	0.14	5.79E+10	0.97
16.6	8	1000	600	600	4738841	18	4715737	16.3	0.36	0.13	5.84E+12	0.97
8.91	2.5	500	600	800	2046173	4	1922773	5.5	1.00	0.17	6.53E+11	0.97
8.91	8	1500	268	600	1034496	5	887448	5.8	0.95	0.16	1.61E+11	0.97
24.3	0.7	500	433	200	1717515	19	1488155	15.3	0.58	0.07	7.26E+11	0.97
24.3	8	1500	600	600	5148150	28	5109968	23.5	0.27	0.09	8.75E+12	0.97
1.21	0.2	1500	600	400	384330	1	390777	0.7	1.00	0.46	1.32E+10	0.97
8.91	0.2	1000	433	800	521064	3	547482	3.0	1.00	0.34	6.22E+10	0.97
16.6	0.7	1500	600	400	2624968	11	2122750	10.7	0.87	0.08	1.20E+12	0.97
16.6	0.2	1500	268	200	503430	7	472425	8.9	1.00	0.14	6.85E+10	0.97
8.91	0.2	1500	433	800	532669	2	560257	3.0	1.00	0.35	6.57E+10	0.97
8.91	2.5	1000	600	800	2071914	4	1965969	5.5	1.00	0.18	6.54E+11	0.97
8.91	0.7	1500	600	200	2425536	7	2209254	6.6	0.65	0.23	7.44E+11	0.97
8.91	0.2	500	433	800	512439	3	534759	3.1	1.00	0.34	5.86E+10	0.97
16.6	0.7	500	600	400	2473226	11	2030057	10.6	0.90	0.08	1.09E+12	0.97
16.6	0.7	1000	600	400	2549404	11	2068983	10.7	0.88	0.08	1.14E+12	0.97
24.3	2.5	500	600	200	2974960	25	3103519	21.6	0.55	0.07	3.03E+12	0.97
1.21	0.7	500	433	600	237381	1	264308	0.0	1.00	0.42	5.32E+09	0.97
16.6	0.2	1000	268	200	483087	7	455320	9.0	1.00	0.14	6.29E+10	0.97
24.3	2.5	1000	600	200	2988030	24	3124963	21.6	0.56	0.07	3.05E+12	0.97
8.91	2.5	1500	600	800	2113878	5	2017501	5.6	1.00	0.18	6.73E+11	0.97
24.3	2.5	1500	600	200	3006726	23	3147016	21.7	0.57	0.07	3.06E+12	0.97
8.91	0.2	500	433	600	625897	3	629331	3.1	1.00	0.33	7.75E+10	0.97
8.91	0.2	1500	600	200	1980750	4	1786956	4.3	1.00	0.32	3.41E+11	0.97
24.3	0.7	50	100	200	104758	15	100495	16.6	1.00	0.08	2.79E+09	0.97
8.91	0.2	1000	433	600	637739	3	643107	3.1	1.00	0.33	8.16E+10	0.97
24.3	2.5	1500	600	800	3416574	21	2924175	18.0	0.59	0.06	2.68E+12	0.97
8.91	0.2	1500	433	600	650850	3	655435	3.1	1.00	0.33	8.54E+10	0.97

Seam Thickness (ft)	Permeability (md)	Reservoir Pressure (psi)	Gas Content (scf/ton)	Horizontal Lateral Spacing (ft)	Actual P_{max} (mcf/month)	Actual T_{max} (months)	Best Fit P_{max} (mcf/month)	Best Fit T_{max} (months)	Best Fit b	Best Fit d_i	SSQ	R^2
16.6	8	500	600	400	4911499	19	4955897	16.6	0.24	0.12	6.11E+12	0.97
8.91	8	500	433	200	1996110	11	1997462	8.5	0.58	0.19	6.65E+11	0.97
24.3	2.5	1000	600	800	3341042	21	2876819	17.9	0.61	0.06	2.50E+12	0.97
8.91	8	1000	433	200	2017763	11	2021009	8.5	0.58	0.19	6.76E+11	0.97
16.6	8	1000	600	400	4959440	19	4997611	16.6	0.00	0.12	6.52E+12	0.97
16.6	8	500	600	600	4685784	18	4507596	16.1	0.34	0.12	4.92E+12	0.97
8.91	8	1500	433	200	2040561	11	2044931	8.5	0.58	0.19	6.87E+11	0.97
16.6	8	1500	433	800	2469246	16	2117427	13.3	0.48	0.08	1.26E+12	0.97
24.3	2.5	500	600	800	3252962	21	2830776	17.8	0.62	0.06	2.35E+12	0.97
16.6	2.5	500	600	200	2972631	17	3082153	14.6	0.57	0.12	2.13E+12	0.97
1.21	0.7	500	600	600	354832	1	353269	0.0	1.00	0.28	9.73E+09	0.97
16.6	8	1500	600	400	5008210	19	5059600	16.6	0.00	0.12	6.50E+12	0.97
16.6	2.5	1000	600	200	2994416	17	3107482	14.6	0.58	0.12	2.16E+12	0.97
1.21	0.7	1000	433	600	240748	1	267583	0.0	1.00	0.42	5.15E+09	0.97
16.6	2.5	1500	600	200	3016256	17	3131728	14.6	0.58	0.12	2.18E+12	0.97
8.91	8	50	100	200	273612	4	237468	4.7	0.77	0.27	6.93E+09	0.97
1.21	0.2	1500	268	400	119551	1	121739	1.4	0.62	0.44	1.46E+09	0.97
1.21	0.2	500	268	400	111238	2	113066	1.7	0.63	0.45	1.26E+09	0.97
8.91	0.2	1000	600	200	1936687	4	1790750	4.2	1.00	0.33	3.11E+11	0.97
16.6	8	1000	433	800	2426250	16	2078069	13.2	0.49	0.08	1.16E+12	0.97
16.6	8	1000	268	600	1198413	13	1090162	11.9	0.67	0.08	2.98E+11	0.97
16.6	8	1500	600	600	4793080	18	4632882	16.1	0.33	0.12	4.92E+12	0.97
1.21	0.2	500	268	600	82150	2	85200	1.6	0.63	0.44	7.10E+08	0.97
16.6	0.7	500	100	800	56411	10	53191	11.4	0.73	0.11	5.85E+08	0.97
1.21	0.2	500	268	800	68507	1	71289	1.5	0.64	0.44	4.88E+08	0.97
1.21	0.2	500	600	800	247833	1	248590	0.8	1.00	0.53	4.73E+09	0.97
1.21	0.2	1000	268	400	112462	1	117410	1.5	0.62	0.44	1.33E+09	0.97
1.21	0.2	1000	268	800	76990	1	76151	1.2	0.61	0.43	5.41E+08	0.97
1.21	2.5	50	100	200	46034	1	52107	1.5	0.90	0.75	1.38E+08	0.97
1.21	0.2	1000	268	600	89725	1	89939	1.3	0.61	0.43	7.69E+08	0.97
16.6	8	500	433	800	2385954	16	2040699	13.2	0.50	0.08	1.08E+12	0.97
8.91	2.5	500	600	400	3315624	8	3062168	7.8	0.63	0.20	1.37E+12	0.97
16.6	0.7	500	100	400	90544	10	85145	11.7	0.67	0.11	1.53E+09	0.97
1.21	0.2	1500	268	800	82392	1	80742	1.0	0.60	0.43	5.82E+08	0.97
16.6	0.7	500	100	600	67786	10	63914	11.5	0.71	0.11	8.36E+08	0.97
8.91	8	1500	600	800	3507134	10	3261794	8.1	0.56	0.19	1.59E+12	0.97
1.21	0.2	1000	600	800	251792	1	253784	0.8	1.00	0.53	4.77E+09	0.97
1.21	0.2	1500	268	600	95866	1	94522	1.2	0.60	0.43	8.15E+08	0.97
8.91	0.2	500	600	200	1896043	4	1789285	4.2	1.00	0.34	2.91E+11	0.97
1.21	0.7	500	600	800	301293	1	297151	0.0	1.00	0.28	8.41E+09	0.97
24.3	8	50	100	200	316588	18	280018	14.3	0.39	0.08	2.07E+10	0.97
8.91	0.2	500	268	200	398617	4	379406	5.5	1.00	0.22	2.08E+10	0.97
1.21	0.7	500	100	600	23198	2	23520	1.5	0.27	0.40	6.19E+07	0.97
1.21	0.7	500	433	800	201655	1	226910	0.0	1.00	0.44	3.27E+09	0.97
8.91	0.2	1000	268	200	416396	4	391758	5.4	1.00	0.23	2.19E+10	0.97
8.91	0.2	500	100	800	17400	17	16709	19.5	1.00	0.07	7.38E+07	0.97
1.21	0.7	1000	600	600	357535	1	356636	0.0	1.00	0.28	8.73E+09	0.97
1.21	0.2	1500	600	800	256303	1	260002	0.7	1.00	0.52	4.66E+09	0.97
8.91	0.2	1500	268	200	434123	4	404689	5.3	1.00	0.23	2.31E+10	0.97
16.6	8	500	268	600	1174680	13	1023325	11.7	0.64	0.08	2.51E+11	0.97
8.91	2.5	1000	600	400	3369563	8	3121501	7.9	0.62	0.20	1.31E+12	0.97
1.21	0.7	50	100	400	30682	2	29298	2.1	0.37	0.46	7.30E+07	0.97
1.21	8	1000	100	400	53355	1	61143	0.0	1.00	0.37	1.83E+08	0.97
8.91	8	500	433	400	2594425	11	2400910	8.6	0.42	0.18	8.58E+11	0.98
1.21	0.7	1500	433	600	244481	1	271241	0.0	1.00	0.41	4.83E+09	0.98
8.91	0.2	1500	100	800	22200	14	21174	16.7	0.75	0.07	1.01E+08	0.98
8.91	8	1000	433	400	2649924	11	2446048	8.6	0.42	0.18	8.65E+11	0.98
16.6	8	1500	268	600	1255675	14	1082330	12.0	0.60	0.08	2.73E+11	0.98
1.21	0.7	500	433	400	303256	1	335391	0.0	1.00	0.40	5.14E+09	0.98
8.91	0.2	1000	100	600	23941	15	22748	18.1	0.87	0.07	1.19E+08	0.98
8.91	8	500	268	400	1188496	7	1052037	7.2	0.60	0.15	1.74E+11	0.98
8.91	0.2	1500	100	600	26875	14	25471	16.9	0.76	0.07	1.44E+08	0.98
1.21	0.7	1000	600	800	304284	1	300559	0.0	1.00	0.28	7.79E+09	0.98
1.21	0.7	1500	100	200	47244	2	47553	1.8	0.57	0.51	1.83E+08	0.98
8.91	0.2	1000	100	800	19800	15	18767	18.2	0.77	0.07	7.88E+07	0.98
1.21	2.5	500	100	200	49294	1	56003	1.5	0.91	0.74	1.37E+08	0.98
8.91	0.2	1500	100	400	36030	14	34025	17.3	0.76	0.07	2.56E+08	0.98
8.91	8	1500	433	400	2707422	11	2492974	8.7	0.41	0.18	8.74E+11	0.98
8.91	8	500	600	600	3888339	10	3574730	8.6	0.45	0.19	1.68E+12	0.98
24.3	0.7	1000	100	800	66299	13	62835	15.0	0.74	0.09	7.70E+08	0.98
24.3	0.7	1000	100	400	106610	13	100791	15.3	0.68	0.09	2.06E+09	0.98
8.91	2.5	1500	600	400	3426046	8	3185247	7.9	0.62	0.20	1.25E+12	0.98
8.91	0.2	1000	100	400	31699	15	30083	18.7	0.77	0.07	1.99E+08	0.98

Seam Thickness (ft)	Permeability (md)	Reservoir Pressure (psi)	Gas Content (scf/ton)	Horizontal Lateral Spacing (ft)	Actual P_{max} (mcf/month)	Actual T_{max} (months)	Best Fit P_{max} (mcf/month)	Best Fit T_{max} (months)	Best Fit b	Best Fit d_i	SSQ	R^2
8.91	0.2	500	100	600	20960	17	19794	20.3	0.77	0.06	8.79E+07	0.98
8.91	0.2	50	100	600	18600	19	17819	22.1	0.89	0.06	7.20E+07	0.98
1.21	0.7	1000	433	800	205044	1	230384	0.0	1.00	0.44	3.18E+09	0.98
1.21	0.7	500	100	200	40506	2	40111	1.9	0.52	0.51	1.31E+08	0.98
24.3	0.7	1000	100	600	79798	13	75605	15.1	0.72	0.09	1.11E+09	0.98
8.91	0.2	50	100	800	15542	19	14641	22.4	0.79	0.06	4.84E+07	0.98
8.91	0.2	1500	100	200	45265	14	42896	16.7	0.76	0.08	3.80E+08	0.98
8.91	0.2	500	100	400	28044	17	26722	20.2	0.84	0.07	1.57E+08	0.98
8.91	8	1000	600	600	3948128	10	3631686	8.6	0.45	0.19	1.66E+12	0.98
8.91	0.2	500	100	200	35431	16	33681	19.1	0.86	0.07	2.40E+08	0.98
1.21	0.7	1000	100	200	43750	2	43737	1.8	0.55	0.51	1.52E+08	0.98
8.91	0.2	1000	100	200	40227	15	38075	17.9	0.77	0.07	2.98E+08	0.98
8.91	8	1000	268	400	1215111	7	1083847	7.3	0.58	0.15	1.73E+11	0.98
8.91	0.2	50	100	400	24815	19	23622	22.3	0.81	0.06	1.22E+08	0.98
1.21	0.7	1500	100	400	37951	1	38499	1.3	0.35	0.41	1.63E+08	0.98
1.21	0.7	50	100	200	37855	2	37149	2.0	0.50	0.50	1.08E+08	0.98
16.6	0.2	1500	100	800	23400	25	21985	30.8	1.00	0.04	1.10E+08	0.98
8.91	0.2	50	100	200	31187	18	29713	21.0	0.78	0.06	1.84E+08	0.98
1.21	8	1500	100	600	43904	1	47957	0.0	1.00	0.33	2.06E+08	0.98
8.91	8	1500	600	600	4010067	10	3690225	8.6	0.45	0.19	1.64E+12	0.98
8.91	8	500	100	200	281438	4	255897	4.9	0.74	0.26	6.12E+09	0.98
8.91	8	1500	268	400	1253969	8	1116404	7.3	0.57	0.15	1.78E+11	0.98
1.21	0.2	500	100	800	11646	2	11359	3.2	0.48	0.29	1.16E+07	0.98
16.6	0.2	1500	100	400	37255	27	35322	31.5	1.00	0.04	2.79E+08	0.98
1.21	8	1500	268	600	207348	2	188533	0.3	0.78	0.18	3.03E+09	0.98
16.6	0.2	1500	100	600	28002	25	26456	31.1	1.00	0.04	1.55E+08	0.98
1.21	0.7	1500	600	600	361365	1	362429	0.0	1.00	0.27	7.39E+09	0.98
1.21	0.7	1500	100	800	28316	1	31277	0.0	0.26	0.38	7.49E+07	0.98
1.21	0.2	50	100	800	10713	3	10056	4.2	0.45	0.27	9.48E+06	0.98
1.21	8	1500	100	400	54646	1	62826	0.0	1.00	0.34	1.69E+08	0.98
16.6	0.7	50	100	400	81075	11	76442	12.5	0.61	0.11	9.95E+08	0.98
1.21	0.7	1000	433	400	305883	1	339483	0.0	1.00	0.39	4.58E+09	0.98
16.6	0.2	1500	100	200	46996	25	44660	29.9	1.00	0.04	4.28E+08	0.98
24.3	0.2	1500	100	200	47512	37	45078	43.3	1.00	0.03	5.47E+08	0.98
16.6	0.7	50	100	800	50386	11	47676	12.4	0.66	0.11	3.70E+08	0.98
16.6	0.2	1000	100	800	20400	28	19354	33.5	1.00	0.04	8.37E+07	0.98
1.21	0.7	1000	100	600	27343	1	27544	0.9	0.25	0.38	8.28E+07	0.98
1.21	8	1000	100	600	42326	1	45284	0.3	1.00	0.41	2.64E+08	0.98
16.6	0.7	50	100	600	60598	11	57365	12.5	0.64	0.11	5.36E+08	0.98
1.21	8	1000	100	800	36458	1	39931	0.0	1.00	0.37	1.48E+08	0.98
1.21	0.7	1500	600	800	308183	1	305872	0.0	1.00	0.27	6.94E+09	0.98
1.21	0.7	1000	100	400	33801	2	34483	1.5	0.27	0.40	1.16E+08	0.98
16.6	0.2	1000	100	600	24600	29	23318	33.7	1.00	0.04	1.20E+08	0.98
16.6	0.2	1000	100	400	33000	29	31226	34.0	1.00	0.04	2.13E+08	0.98
16.6	0.2	1000	100	200	41474	27	39385	32.2	1.00	0.04	3.31E+08	0.98
24.3	0.2	1000	100	200	41885	39	39752	46.6	1.00	0.03	4.25E+08	0.98
1.21	0.2	50	100	600	12815	3	12086	4.2	0.45	0.27	1.30E+07	0.98
24.3	0.2	1500	100	400	37658	39	35720	45.7	1.00	0.03	3.29E+08	0.98
8.91	2.5	500	600	200	2730921	10	2814223	7.9	0.61	0.23	8.13E+11	0.98
24.3	0.2	1500	100	600	28200	38	26615	45.4	1.00	0.03	1.80E+08	0.98
1.21	0.7	50	100	800	19074	2	18204	2.1	0.36	0.45	2.15E+07	0.98
8.91	2.5	50	100	200	200815	4	192727	4.1	1.00	0.36	2.44E+09	0.98
16.6	0.2	500	100	800	18000	31	17061	36.7	1.00	0.04	6.42E+07	0.98
24.3	0.7	500	100	400	93962	14	88439	16.5	0.59	0.08	1.44E+09	0.98
1.21	0.2	50	100	400	17192	3	16172	4.2	0.45	0.27	2.28E+07	0.98
24.3	0.2	1000	100	800	20400	41	19475	48.8	0.91	0.03	1.01E+08	0.98
1.21	0.7	1500	433	800	208657	1	233992	0.0	1.00	0.43	2.99E+09	0.98
8.91	2.5	1500	600	200	2784323	10	2871339	7.9	0.61	0.23	8.28E+11	0.98
1.21	0.2	1500	268	200	146651	2	151503	1.7	0.75	0.52	1.22E+09	0.98
24.3	0.2	1500	100	800	23400	38	22208	44.9	1.00	0.03	1.22E+08	0.98
1.21	0.2	1000	100	200	25981	2	25913	3.0	0.51	0.32	4.77E+07	0.98
8.91	0.7	1500	268	200	848196	4	778230	4.4	1.00	0.34	4.25E+10	0.98
16.6	0.2	500	100	600	21600	31	20446	36.8	1.00	0.04	9.14E+07	0.98
1.21	0.2	1000	268	200	143400	2	143959	1.8	0.70	0.48	1.23E+09	0.98
16.6	2.5	500	600	800	2817965	12	2478299	11.2	0.79	0.09	9.43E+11	0.98
1.21	0.7	500	100	400	31761	2	30968	1.8	0.29	0.42	7.87E+07	0.98
1.21	0.2	500	268	200	140408	2	140290	1.8	0.70	0.48	1.17E+09	0.98
8.91	8	500	600	800	3350515	10	3014410	7.9	0.52	0.17	1.04E+12	0.98
16.6	0.2	500	100	400	28800	32	27378	36.9	1.00	0.04	1.63E+08	0.98
1.21	0.2	1500	100	200	29830	2	28115	2.8	0.50	0.32	5.42E+07	0.98
16.6	0.2	500	100	200	36547	30	34824	34.6	1.00	0.04	2.57E+08	0.98
24.3	0.7	50	100	400	83622	15	78056	17.8	0.53	0.07	1.14E+09	0.98
24.3	0.2	500	100	200	36737	44	34864	50.4	1.00	0.03	3.21E+08	0.98

Seam Thickness (ft)	Permeability (md)	Reservoir Pressure (psi)	Gas Content (scf/ton)	Horizontal Lateral Spacing (ft)	Actual P_{max} (mcf/month)	Actual T_{max} (months)	Best Fit P_{max} (mcf/month)	Best Fit T_{max} (months)	Best Fit b	Best Fit d_i	SSQ	R^2
8.91	2.5	500	600	600	2291895	6	2220388	6.7	0.78	0.16	5.55E+11	0.98
24.3	0.2	1000	100	600	24689	41	23415	49.1	1.00	0.03	1.39E+08	0.98
16.6	0.2	50	100	800	16108	34	15071	40.2	1.00	0.03	5.09E+07	0.98
16.6	8	1500	100	200	366784	13	326480	10.3	0.00	0.11	2.53E+10	0.98
8.91	2.5	1500	100	200	270610	4	252559	4.3	1.00	0.37	3.85E+09	0.98
16.6	8	1500	600	200	2666254	22	2774202	18.5	0.39	0.07	1.58E+12	0.98
8.91	8	1000	600	800	3426721	10	3064561	7.9	0.52	0.17	1.06E+12	0.98
24.3	0.2	1000	100	400	33216	41	31525	49.2	1.00	0.03	2.54E+08	0.98
8.91	2.5	500	100	200	220118	4	210166	4.1	1.00	0.36	2.72E+09	0.98
16.6	0.2	50	100	400	25781	34	24253	40.2	1.00	0.03	1.30E+08	0.98
16.6	0.2	50	100	200	32496	32	30599	37.6	1.00	0.04	2.02E+08	0.98
16.6	0.2	50	100	600	19200	34	18128	40.2	1.00	0.03	7.28E+07	0.98
1.21	0.7	1000	100	800	24034	1	26580	0.0	0.16	0.34	5.66E+07	0.98
1.21	2.5	1000	100	200	52792	2	60533	1.5	0.93	0.74	1.24E+08	0.98
24.3	0.2	50	100	200	32528	47	30714	54.2	0.86	0.03	2.54E+08	0.98
8.91	0.7	1000	268	200	819568	4	748143	4.3	1.00	0.33	3.79E+10	0.98
24.3	0.7	500	100	600	70288	14	66267	16.3	0.63	0.08	7.32E+08	0.98
24.3	0.7	500	100	800	58414	14	55203	16.2	0.65	0.08	4.96E+08	0.98
8.91	2.5	1000	100	200	244287	4	232270	4.1	1.00	0.36	3.17E+09	0.98
8.91	8	1000	433	800	1847816	6	1700611	6.6	0.78	0.16	3.16E+11	0.98
16.6	2.5	1000	600	800	2845671	12	2522277	11.3	0.78	0.09	9.28E+11	0.98
8.91	8	500	600	400	4239416	11	4201958	9.1	0.35	0.21	1.69E+12	0.98
16.6	8	1000	600	200	2653751	20	2755018	18.3	0.40	0.07	1.47E+12	0.98
1.21	8	1000	268	600	193489	2	188526	0.0	0.79	0.19	2.32E+09	0.98
16.6	2.5	1500	600	800	2876021	12	2559740	11.4	0.75	0.09	9.39E+11	0.98
8.91	8	1000	600	400	4288798	11	4259761	9.1	0.35	0.21	1.67E+12	0.98
24.3	0.2	500	100	400	29282	46	27437	53.4	1.00	0.03	1.87E+08	0.98
16.6	8	500	600	200	2643948	20	2737170	18.2	0.41	0.07	1.39E+12	0.98
24.3	0.7	50	100	600	62444	15	58543	17.7	0.56	0.08	5.74E+08	0.98
8.91	0.7	500	268	200	792729	4	727361	4.2	1.00	0.33	3.41E+10	0.98
24.3	0.2	500	100	800	18000	46	17078	52.9	1.00	0.03	7.11E+07	0.98
1.21	2.5	1000	268	600	153204	1	163810	0.0	1.00	0.33	1.63E+09	0.98
24.3	0.2	500	100	600	21600	46	20619	53.0	1.00	0.03	1.02E+08	0.98
24.3	0.7	50	100	800	51848	15	48803	17.6	0.59	0.08	3.77E+08	0.98
8.91	8	500	600	200	2655823	11	2730726	9.2	0.60	0.16	7.57E+11	0.98
8.91	8	1500	600	400	4339065	11	4319364	9.1	0.35	0.21	1.62E+12	0.98
1.21	2.5	1500	268	600	154825	1	162238	0.0	1.00	0.31	1.43E+09	0.98
1.21	0.7	1500	433	400	308774	1	336287	0.0	1.00	0.37	3.60E+09	0.98
1.21	0.2	50	100	200	21830	3	20143	4.0	0.46	0.28	2.81E+07	0.98
1.21	0.2	1000	100	400	21344	2	19372	2.9	0.43	0.27	2.65E+07	0.98
8.91	8	1500	433	600	2224713	8	1935704	7.6	0.52	0.15	4.04E+11	0.98
8.91	8	1000	600	200	2674849	11	2751378	9.2	0.60	0.16	7.40E+11	0.98
8.91	8	1500	433	800	1873244	6	1735174	6.7	0.75	0.16	2.86E+11	0.98
1.21	0.7	1500	100	600	32038	1	35593	0.0	0.21	0.36	9.44E+07	0.98
8.91	0.7	500	433	200	1384333	4	1295400	5.1	0.85	0.23	1.21E+11	0.98
1.21	2.5	500	268	600	151570	1	166067	0.0	1.00	0.36	1.71E+09	0.98
8.91	8	1000	433	600	2180225	8	1897390	7.6	0.53	0.15	3.78E+11	0.98
8.91	8	500	433	600	2135914	8	1860412	7.5	0.54	0.15	3.63E+11	0.98
1.21	0.7	50	100	600	22925	2	21877	2.1	0.36	0.45	2.37E+07	0.98
1.21	8	500	268	600	179575	2	184740	0.0	0.83	0.20	1.89E+09	0.98
8.91	0.2	500	433	200	1050357	4	1033894	4.2	1.00	0.33	8.50E+10	0.98
1.21	8	1500	433	800	380919	2	338676	2.0	0.81	0.24	7.73E+09	0.98
8.91	0.2	1000	433	200	1073180	4	1051026	4.2	1.00	0.33	8.67E+10	0.98
8.91	0.2	1500	433	200	1098423	4	1065560	4.2	1.00	0.33	8.78E+10	0.98
24.3	0.2	50	100	800	16200	50	15100	57.7	0.84	0.03	5.18E+07	0.98
8.91	8	500	433	800	1820812	6	1602559	6.5	0.73	0.15	2.48E+11	0.98
1.21	8	1500	268	800	174001	2	170136	0.0	0.91	0.20	1.40E+09	0.98
8.91	2.5	500	433	400	1712472	6	1462957	6.4	0.76	0.14	2.12E+11	0.98
24.3	0.2	50	100	400	25800	50	24299	57.8	0.84	0.02	1.32E+08	0.99
1.21	8	1500	100	800	38340	1	41557	0.0	1.00	0.34	1.42E+08	0.99
8.91	0.7	1000	433	200	1395868	4	1308113	5.2	0.84	0.23	1.15E+11	0.99
24.3	0.2	50	100	600	19200	50	18161	57.7	0.81	0.02	7.26E+07	0.99
1.21	2.5	1500	268	800	133860	1	139220	0.0	1.00	0.31	1.19E+09	0.99
8.91	8	1000	100	200	290201	4	275001	5.2	0.69	0.25	4.86E+09	0.99
1.21	2.5	1000	268	800	131245	1	139213	0.0	1.00	0.34	1.32E+09	0.99
8.91	2.5	1000	433	400	1751202	6	1503347	6.5	0.76	0.14	2.13E+11	0.99
8.91	0.7	1500	433	200	1407815	4	1312537	5.3	0.81	0.22	1.15E+11	0.99
8.91	2.5	1500	433	400	1790498	6	1547010	6.6	0.75	0.14	2.14E+11	0.99
16.6	8	1000	100	200	325875	13	306668	10.1	0.00	0.12	1.89E+10	0.99
8.91	2.5	1000	600	600	2339141	6	2182300	6.7	0.72	0.14	4.10E+11	0.99
1.21	0.2	500	100	200	23109	3	22701	3.4	0.47	0.29	2.75E+07	0.99
1.21	2.5	1500	100	200	57723	2	65198	1.5	0.94	0.73	9.86E+07	0.99
1.21	2.5	500	268	800	128960	1	140337	0.0	1.00	0.36	1.36E+09	0.99

Seam Thickness (ft)	Permeability (md)	Reservoir Pressure (psi)	Gas Content (scf/ton)	Horizontal Lateral Spacing (ft)	Actual P_{max} (mcf/month)	Actual T_{max} (months)	Best Fit P_{max} (mcf/month)	Best Fit T_{max} (months)	Best Fit b	Best Fit d_i	SSQ	R^2
1.21	8	1000	268	800	162579	2	163913	0.0	0.94	0.21	1.06E+09	0.99
1.21	0.2	500	433	200	267852	2	286821	1.6	0.88	0.57	2.30E+09	0.99
1.21	8	1000	433	800	353539	2	342746	0.0	0.61	0.17	5.65E+09	0.99
1.21	0.7	500	100	800	19750	1	20009	1.2	0.21	0.38	2.03E+07	0.99
8.91	2.5	1500	600	600	2384644	6	2331444	6.8	0.76	0.16	3.73E+11	0.99
1.21	0.2	1000	433	200	271892	2	290785	1.6	0.88	0.57	2.22E+09	0.99
1.21	8	1500	268	400	276315	2	252987	2.3	0.76	0.30	2.82E+09	0.99
1.21	0.7	500	600	400	453455	1	471571	0.0	0.97	0.29	5.83E+09	0.99
1.21	2.5	500	600	800	368105	2	385735	0.0	0.85	0.18	5.89E+09	0.99
1.21	0.2	1500	433	200	275880	2	294725	1.6	0.89	0.57	2.07E+09	0.99
1.21	8	500	268	800	150769	2	159360	0.0	0.98	0.21	8.01E+08	0.99
16.6	0.7	500	433	200	1443230	13	1470210	9.9	0.70	0.12	1.56E+11	0.99
1.21	2.5	500	268	400	193131	1	219752	0.0	1.00	0.37	8.91E+08	0.99
1.21	2.5	1000	600	800	383473	2	398568	0.0	0.83	0.19	5.72E+09	0.99
16.6	0.7	1000	433	200	1497261	13	1490974	9.9	0.69	0.12	1.58E+11	0.99
1.21	2.5	1000	268	400	192936	1	216368	0.0	1.00	0.34	8.58E+08	0.99
16.6	0.7	1500	433	200	1549594	13	1513544	10.0	0.68	0.12	1.60E+11	0.99
1.21	8	1000	268	400	256594	2	232442	2.0	0.70	0.25	2.25E+09	0.99
1.21	2.5	1500	600	800	400440	2	412861	0.0	0.80	0.19	5.79E+09	0.99
1.21	2.5	500	433	600	273241	1	291250	0.0	1.00	0.25	2.20E+09	0.99
1.21	2.5	1500	433	600	274930	1	306397	0.0	0.96	0.24	2.56E+09	0.99
1.21	8	500	433	800	329871	2	331617	0.0	0.62	0.17	4.05E+09	0.99
1.21	0.2	1000	100	600	15531	2	13857	2.3	0.33	0.23	8.34E+06	0.99
1.21	2.5	1500	268	400	191349	1	212172	0.0	1.00	0.32	8.39E+08	0.99
8.91	8	1500	100	200	303201	5	298810	5.3	0.67	0.24	3.48E+09	0.99
1.21	8	1500	433	600	453947	2	416184	2.4	0.70	0.27	6.40E+09	0.99
1.21	0.2	1500	100	800	16982	1	16099	0.0	0.28	0.22	7.14E+06	0.99
1.21	2.5	1000	433	600	274529	1	299468	0.0	1.00	0.25	2.22E+09	0.99
1.21	0.7	1000	600	400	454187	1	487038	0.0	0.98	0.30	4.90E+09	0.99
1.21	8	50	100	200	53748	1	59744	0.0	0.60	0.34	5.81E+07	0.99
8.91	2.5	1500	268	200	947903	7	878862	6.1	0.60	0.19	3.10E+10	0.99
1.21	2.5	500	600	600	443206	2	431848	0.0	0.60	0.15	5.95E+09	0.99
1.21	2.5	500	433	800	233383	1	242525	0.0	1.00	0.24	1.46E+09	0.99
1.21	8	1500	433	400	664791	2	628077	2.3	0.66	0.41	8.96E+09	0.99
1.21	8	500	268	400	238551	2	223530	1.2	0.61	0.21	1.56E+09	0.99
1.21	2.5	1500	433	800	239882	1	260544	0.0	1.00	0.24	1.30E+09	0.99
1.21	2.5	1500	600	600	484599	2	466782	0.0	0.57	0.16	6.15E+09	0.99
1.21	8	1000	433	600	421161	2	386302	2.2	0.64	0.23	4.71E+09	0.99
8.91	2.5	1000	268	200	913670	7	853371	6.0	0.60	0.19	2.64E+10	0.99
1.21	2.5	1000	433	800	236613	1	251533	0.0	1.00	0.24	1.31E+09	0.99
1.21	8	1500	600	800	713646	2	668616	2.4	0.70	0.32	1.11E+10	0.99
1.21	2.5	1000	600	600	462340	2	447722	0.0	0.59	0.16	5.49E+09	0.99
1.21	0.7	500	433	200	330053	1	338444	0.9	0.69	0.36	1.87E+09	0.99
1.21	8	1000	433	400	626472	2	594674	2.2	0.65	0.39	7.34E+09	0.99
1.21	8	1000	600	800	670291	2	618949	2.4	0.66	0.29	9.53E+09	0.99
1.21	0.7	500	268	200	176304	1	198262	1.5	0.95	0.67	4.76E+08	0.99
1.21	8	1500	600	600	916695	2	873451	2.3	0.67	0.41	1.42E+10	0.99
1.21	8	500	100	200	56400	1	62539	0.0	0.56	0.31	5.05E+07	0.99
1.21	2.5	1500	433	400	361966	2	363116	0.4	0.66	0.20	3.00E+09	0.99
1.21	0.7	1000	433	200	328715	1	334782	1.1	0.70	0.36	1.81E+09	0.99
8.91	2.5	500	268	200	879292	7	829612	6.0	0.61	0.19	2.20E+10	0.99
16.6	8	50	100	200	269997	7	277556	9.2	0.54	0.13	3.16E+09	0.99
1.21	8	1500	600	400	1216325	2	1173083	2.1	0.61	0.52	1.93E+10	0.99
1.21	0.2	1000	100	800	12654	2	11811	1.5	0.26	0.21	3.65E+06	0.99
1.21	2.5	1000	600	200	837415	2	849747	1.8	0.74	0.62	9.69E+09	0.99
1.21	0.7	1500	600	400	456434	1	474160	0.0	0.91	0.26	3.42E+09	0.99
1.21	0.2	1500	100	400	22523	2	20683	1.8	0.30	0.22	1.10E+07	0.99
16.6	8	500	100	200	295033	12	293973	9.5	0.50	0.13	3.41E+09	0.99
1.21	2.5	500	600	200	813533	2	829499	1.8	0.74	0.61	9.11E+09	0.99
1.21	8	1000	600	400	1169257	2	1128344	2.1	0.61	0.50	1.74E+10	0.99
1.21	8	500	433	400	591031	2	564485	2.2	0.64	0.36	5.98E+09	0.99
1.21	2.5	1500	600	400	712150	2	682996	2.2	0.74	0.35	8.78E+09	0.99
1.21	0.7	1500	433	200	330757	2	334093	1.3	0.71	0.38	1.59E+09	0.99
1.21	8	500	600	400	1123527	2	1084819	2.1	0.61	0.48	1.58E+10	0.99
1.21	0.7	1000	268	200	180180	2	202465	1.5	0.95	0.67	4.04E+08	0.99
1.21	8	1000	600	600	858779	2	823303	2.3	0.66	0.38	1.11E+10	0.99
1.21	8	500	600	800	632553	2	585643	2.3	0.64	0.26	7.35E+09	1.00
1.21	8	500	433	600	393812	2	369577	1.6	0.58	0.20	3.16E+09	1.00
1.21	2.5	1000	600	400	662200	2	631638	2.2	0.70	0.30	6.79E+09	1.00
1.21	2.5	500	433	400	345234	1	354559	0.0	0.68	0.19	1.97E+09	1.00
1.21	2.5	1000	433	400	340923	1	359775	0.0	0.65	0.19	1.96E+09	1.00
1.21	8	500	600	600	803236	2	766791	2.3	0.62	0.35	8.42E+09	1.00
1.21	8	1000	268	200	342808	2	347534	1.8	0.69	0.60	1.13E+09	1.00

Seam Thickness (ft)	Permeability (md)	Reservoir Pressure (psi)	Gas Content (scf/ton)	Horizontal Lateral Spacing (ft)	Actual P_{max} (mcf/month)	Actual T_{max} (months)	Best Fit P_{max} (mcf/month)	Best Fit T_{max} (months)	Best Fit b	Best Fit d_i	SSQ	R^2
1.21	8	500	268	200	328958	2	334592	1.8	0.69	0.59	1.04E+09	1.00
1.21	8	1000	100	200	58462	1	59616	1.0	0.59	0.32	3.84E+07	1.00
1.21	0.7	1500	268	200	185579	2	206740	1.5	0.95	0.66	3.05E+08	1.00
1.21	2.5	500	600	400	623119	2	593204	2.1	0.65	0.27	5.25E+09	1.00
1.21	0.2	1500	100	600	18275	1	18290	0.0	0.23	0.20	3.29E+06	1.00
1.21	2.5	1000	433	200	509985	2	515184	1.9	0.71	0.57	1.64E+09	1.00
1.21	8	1500	100	200	63662	2	63241	1.5	0.63	0.36	3.03E+07	1.00
1.21	0.2	1500	600	200	416307	1	445434	1.5	0.92	0.54	1.22E+09	1.00
1.21	2.5	500	433	200	490993	2	497721	1.8	0.71	0.55	1.46E+09	1.00
1.21	0.2	1000	600	200	413682	1	441816	1.5	0.93	0.54	1.06E+09	1.00
1.21	0.2	500	600	200	412312	1	438156	1.4	0.93	0.55	9.90E+08	1.00
1.21	0.7	1500	600	200	569414	2	571034	1.8	0.68	0.46	1.21E+09	1.00
1.21	2.5	1500	268	200	227574	2	228831	1.8	0.68	0.42	1.77E+08	1.00
1.21	2.5	1000	268	200	213810	2	216765	1.6	0.63	0.37	1.62E+08	1.00
1.21	0.7	1000	600	200	538743	2	547124	1.8	0.66	0.43	9.49E+08	1.00
1.21	0.7	500	600	200	514854	2	530548	1.7	0.65	0.41	8.92E+08	1.00
1.21	2.5	500	268	200	208356	1	211398	1.4	0.61	0.35	1.31E+08	1.00